Optimising the functionality of smart quay walls using measurement data obtained during the construction process

A case study in the port of Rotterdam: HHTT-quay

O. Schouten

TU Delft

Optimising the functionality of smart quay walls using measurement data obtained during the construction process

A case study in the port of Rotterdam: HHTT-quay

by

O. Schouten

to obtain the degree of Master of Science
at the Delft University of Technology,
to be defended publicly on Friday October 2, 2020

Thesis committee:	Dr. ir. M. Korff (Chair),	TU Delft, Geo-Engineering
	Prof. dr. ir. K. Gavin,	TU Delft, Geo-Engineering
	Prof. dr. ir. M.Z. Voorendt,	TU Delft, Hydraulic Structures
	Dr. ir. A.A. Roubos,	Port of Rotterdam
	Ir. M. Post (Daily Supervisor),	Deltares

An electronic version of this thesis is available at http://repository.tudelft.nl/.

TU Delft
Delft University of Technology

Deltares
Enabling Delta Life

Port of Rotterdam

Preface

In the past year I performed a research at Deltares with the objective to prove my worthiness as a geotechnical engineer and to obtain a Master's degree from the Delft University of Technology. Completing this research would not have been possible without the help and support that I received.

I would like to thank my graduation committee for their guidance, valuable feedback and encouragements. Mandy Korff you helped me in finding a research topic that combines geotechnical and structural engineering. Thanks to you I learned about the (soil)mechanics involved at one of the biggest quay walls in the Netherlands. Ken Gavin and Mark Voorendt your feedback during the progress meetings helped me to raise my thesis to a higher level. Alfred Roubos you helped me with your extensive knowledge on quay walls, provided me with all the measurement data that I needed and brought me into contact with engineers from practise. I really enjoyed the discussions that I had with these engineers about quay walls and the interpretation of measurement data. Mark Post from day 1 you provided me with valuable ideas on how to give direction to this research. You always found time to get together and discuss questions with me. I always enjoyed our discussions on the finite element models and the interpretation of the measurement data. And when I felt lost and struggled to maintain progress you helped me to get back on track.

Moreover, I would like to thank my family and friends who stood by my side during my studies. Thank you Marlou for your love and understanding, you have always been patient when I had to go studying again. Finally, I owe my parents a debt of gratitude for all their love and support over the years and for always believing in me. Without my parents, I would never have accomplished what I have now.

O. (Onno) Schouten
Hillegom, September 2020

Abstract

Quay walls are often designed with Finite Element models (FE models) to take into account the complex soil-structure interaction and highly non-linear soil behaviour. These are complex models that rely on many input parameters that have uncertainties. Nowadays, new quay walls are often equipped with sensors that collect information about the behaviour of the quay wall. These quay walls are known as **smart** quay walls. The measurement data of smart quay walls could be used to validate FE models and reduce parameter uncertainties. This could lead to an optimisation of the functionality of the quay walls. By means of a case study this thesis determines if measurement data obtained during the construction process has the potential to optimise the functionality of smart quay walls. The case used is the HES Hartel Tank Terminal (HHTT-quay), which is a smart quay wall in the port of Rotterdam. The HHTT-quay consists of sections with and without a relieving platform, both are considered in this thesis. In this thesis the functionality of a quay wall refers to the retaining or bearing functionality. Therefore, an optimisation of the functionality could consist of an optimisation in the retaining height or the surface loads.

Relevant aspects for optimising the functionality of a quay wall are:

- Insight into the parameter uncertainties that play an important role in the reliability of quay walls
- Measurement data of sufficient quality that provides insight into the behaviour of the quay wall
- A load on the quay wall which results in significant deformations and forces of the quay wall
- Insight into the mechanics of a quay wall and the way it is modelled in the calculation model as well as insight into the possibilities and limitations of the calculation model
- A method for updating the relevant (soil) parameters and/or reliability based on the measurement data, which in turn allows to optimise the functionality.

Uncertainties in soil parameters and soil-structure interaction have a large effect on the reliability of a quay wall [Roubos, 2019]. These uncertainties are epistemic and could be reduced when additional information becomes available. These uncertainties are also time-independent. Therefore, a reduction in the uncertainty of soil parameters and soil-structure interaction could be made early in the service life of a quay wall.

In the case evaluated the most useful measurement data proved to be the inclinometer measurements of the retaining wall and the anchor strains in the MV-piles. The inclinometer measurements quantify the relative horizontal deformations and indirectly the bending moments of the retaining wall and the anchor strains quantify the anchor forces.

A FE model was set-up to predict the deformations and forces of the quay wall during the construction process. For the parameter determination Cone Penetration Tests and triaxial tests results were used. The FE model was validated with the measurement data. A good match between the FE model results and the measurement data was found when realistic estimates of the friction angle were used. These realistic estimates are determined by taking into account the peak behaviour of the soil and the influence of plane strain conditions on the soil strength (9/8-factor). Since a good comparison was found between the FE model results and the measurement data it was not possible to update the mean values of the soil parameters.

The FE model validated for the construction process is extended to predict the behaviour of the quay wall during the Serviceability and Ultimate Limit States (SLS and ULS). In this model the peak shear strength of soil is used. In ULS the peak shear strength could be exceeded and therefore additional calculations are made to include the effect of softening behaviour. With this model it is possible to determine how relevant the construction process is compared to the SLS and ULS. The construction process introduces a significant part of the horizontal deformations and forces that occur during the SLS and ULS:

- The horizontal deformations are 50 - 65 % of the value found in SLS
- The bending moments are 50 - 65% of the value found in ULS
- The anchor forces are 25 - 45 % of the value found in ULS.

The behaviour of soil is predominantly effected by its stiffness and strength properties. With the validated FE model a sensitivity analysis is performed to gain insight into which of these soil parameters has the largest influence on the behaviour of the quay wall. During the construction process the friction angle already accounts for 60 - 70% of the deformations and forces, whereas the stiffness accounts for 30 - 40%. Since the friction angle accounts for the majority of the deformations and forces it is possible to gain insight into the friction angle based on measurement data obtained during the construction process. In the ULS phase the influence of the friction angle increases to 80%. Therefore, to better predict the behaviour of the quay wall in the ULS it is important to gain insight into the friction angle, which can be done with measurement data that is obtained during the construction process.

With the validated FE model it was then possible to determine that the bending moment in ULS is approximately 50 - 60% of the allowable value and the anchor force in ULS is approximately 55% of the allowable value. This indicates that the structural elements have capacity left and there is a large potential for increasing the retaining height or the surface load, and therefore optimising the functionality of the quay wall.

Finally the validated FE model is used to quantify how much the functionality can be optimised. This is based on the assessment of the yielding of the combined wall and the MV-piles. The water depth in front of the quay wall could be increased up to 2 metres and the surface load could be increased with 50% from 40 kPa to 60 kPa. It should be noted that other failure mechanisms, such as the bearing capacity of the bearing piles, should be assessed as well.

The case study used in this thesis shows that measurement data obtained during the construction process already provides important information that can be used to optimise the functionality of the quay wall. This indicates that for smart quay walls the construction process can act as a load test and this could reduce the necessity to perform a load test during the service life.

Contents

1 Introduction

1.1. Motivation for this research

Quay walls play an important role in the functionality of a port as they are used for the loading and unloading of ships. The functional requirements of these quay walls depend on service-level agreements between port authorities and their clients. The typical duration of such an agreement is 25 years [Roubos, 2019]. Most quay walls have a minimal lifespan of 50 years, therefore it is likely that the functional requirements of quay walls change during their lifespan. Examples of changes to the functional requirements of quay walls are increasing water depths or enhancing surface loads.

Quay walls can have complex soil-structure interaction, due to the presence of (inclined) retaining walls, anchors, relieving platforms and bearing piles. Furthermore, the behaviour of soil under primary loading conditions tends to be highly non-linear. To take this complex soil-structure interaction and the non-linear behaviour of soil into account the design of quay walls is usually performed with finite element models (FE models). These models are potentially powerful tools that can give insight into the deformations and stresses of the soil as well as the forces in the structural elements. However, FE models are also complex and often rely on many input parameters that have uncertainties. Especially soil parameters tend to have a high degree of uncertainty compared to other input parameters. The complexity of the FE model and the uncertainty in the input parameters makes it difficult to determine if it is possible to implement adjustments to a quay wall. To be able to determine if the functionality of a quay wall can be optimised the uncertainties in the input parameters should be reduced as much as possible and FE models have to be validated.

Nowadays, new quay walls are often equipped with sensors, such as fiber optic strain sensors on anchors or inclinometers that measure horizontal deformations, these are known as **smart** quay walls. In the port of Rotterdam 2% of the quay walls are smart quay walls, these are mainly new quay walls. The idea is that the measurement data obtained by a smart quay wall could be used to reduce parameter uncertainties.

The measurement data collected by the sensors can provide information about the behaviour of a smart quay walls. Potentially this measurement data can be used to reduce uncertainties of the model input parameters and validate FE model results, which could lead to an optimisation of the functionality of the quay wall. Using measurement data to reduce parameter uncertainties and to validate model results is known as a back-analysis or inverse analysis.

Ideally, such an analysis is performed with measurement data that is collected during the early service life of a quay wall, this prevents the necessity to collect measurement data for a long period. Measurement data from the construction process could already give enough information to determine if it is possible to optimise the functionality of a smart quay wall. During the construction process the soil in front of the quay wall is dredged away, this leads to the mobilisation of a permanent driving horizontal soil load on the quay wall. This permanent soil load is expected to be significant compared to the total loads on the quay wall.

1.2. Problem Definition

At the moment there is little experience with using the measurement data of smart quay walls in an inverse analysis. It is unknown if the currently collected measurement data provides sufficient information about the behaviour of the smart quay walls or if essential information is missing. The measurement data could be collected in the wrong place or at a wrong frequency. Furthermore, the reliability of some sensors is still under debate as these sensors have a relatively new design and have not been used very often. If the measurement data does not provide sufficient information the potential of an inverse analysis decreases and it might not be possible to determine if it possible to optimise the functionality of the quay walls.

Moreover, it is unknown whether measurement data obtained during the construction process can already provide insight into model parameters that are governing during the limit states (where the smart quay wall is designed for). If, for example, the behaviour of the quay wall is dominated by soil layer X during the construction process and it is dominated by soil layer Y during the limit states the measurement data obtained during the construction process provides very little insight into the behaviour of the quay wall during the limit states.

1.3. Research objective

The objective of this thesis is to determine if measurement data obtained during the construction process has the potential to optimise the functionality of smart quay walls. From the objective the following main research question is defined:

How to use the measurement data of smart quay walls obtained during the construction process to optimise their functionality?

The four main functions of a quay wall are the retaining function, bearing function, navigation function and safety function [De Gijt and Broeken, 2013]. For this study the retaining function and the bearing function are relevant. This is because these two functions have a relation to the geotechnical and mechanical behaviour of a quay wall. Therefore, in the main research question optimising the functionality relates to optimising the retaining or the bearing function of a quay wall.

To answer the main research question five sub-questions are defined.

1. What is needed to optimise the functionality of a quay wall?
2. Does the currently collected measurement data provide sufficient information about the behaviour of a quay wall, if not, what data is missing?
3. Which soil parameters have a dominant influence on the behaviour of the quay wall, and do these soil parameters have a reducible uncertainty?
4. Is the behaviour of the quay wall dominated by the same soil layers during the construction process as it is during the limit states?
5. To what extent is the validated finite element model capable of predicting the behaviour of the quay wall?

1.4. Research methodology

This thesis determines if measurement data obtained during the construction process could be used to optimise the functionality of smart quay walls. In this section the method of approach that is applied in this research is presented. The goal of each step in the approach is explained and the chapter(s) in which the step is elaborated is mentioned.

Step 1: Determine what is needed to optimise the functionality of quay walls
This step is elaborated in chapter 2. In this step information is collected that provides insight into what is needed to optimise the functionality of a quay wall. This information is used to answer research sub-question 1. Information is collected about uncertainties in geotechnical engineering and what soil parameters have a reducible uncertainty. Additional to this insight is given on current design guidelines for quay walls and the basic idea of limit states is explained. Then the different methods of performing an inverse analysis are presented and finally the different calculation methods for quay walls are shown.

Step 2: Introduction of the case
This step is elaborated in chapter 3. In this thesis a case is elaborated. The case represents a smart quay wall in the port of Rotterdam and has soil conditions that are typical for the Maasvlakte area. The analyses performed in the successive steps are based on the case. An answer to the main research question is given based on the results of the case study.

Step 3: Determine the usability of the measurement data
This step is elaborated in chapter 4. The measurement data obtained during the construction process of the case is presented and analysed. This includes a review of the measurement methods to gain insight into how the data is collected and to understand possible measurement errors. The goal is to determine what information is collected by the measurement data and which sections of the quay wall can be used in the analyses in the successive steps. The information in this step is used to answer the second research sub-question.

Step 4: Set-up and validation of the a priori model used to predict the behaviour of the quay wall during the construction process
This step is elaborated in chapters 5 and 6. Based on prior knowledge the construction process is set-up in a model. This model should take into account soil-structure interaction and non-linear soil behaviour. The a priori model is validated with measurement data to determine how well the model is capable of predicting the behaviour of the quay wall. If necessary adjustments are made to the model parameters to better fit the model with the measurement data. The outcome of this step is a model that is in line with the measurement data. This validated model can then be used in the analysis performed in the next step.

Step 5: Determine the relevance of the construction process compared to the limit states
This step is elaborated in chapter 7. In this step the validated model is extended to predict the behaviour of the quay wall during the limit states. With this model it is possible to determine how significant the forces and deformations of the construction process are compared to those of the limit states. Secondly, a sensitivity analysis is performed to determine which soil parameters are governing during the construction process and limit states. With this model it is also possible to quantify how much the functionality of the quay wall can be optimised. The information in this step is used to answer the third, fourth and fifth research sub-questions.

2

Background information

The goal of this chapter is to provide information on aspects that are relevant for optimising the functionality of a smart quay wall. In section 2.1 the functions of a quay wall and the relevant aspects for optimising the functionality of a quay wall are presented. In section 2.2 to 2.5 information is presented regarding some of these aspects. Finally, in section 2.6 the information in this chapter is summarised in a conclusion. The information in this chapter was collected by reviewing relevant literature.

2.1. Optimising the functionality of quay walls

The four main functions of a quay wall are the retaining function, bearing function, navigation function and safety function [De Gijt and Broeken, 2013]. For this study the retaining function and the bearing function are relevant. This is because these two functions have a relation to the geotechnical and mechanical behaviour of a quay wall. In this thesis an optimisation of the functionality would therefore result in an increase of the retaining height or an increase in the surface load on top of the quay wall. Relevant aspects for optimising the functionality of a quay wall are:

- Insight into the parameter uncertainties that play an important role in the reliability of quay walls
- Measurement data of sufficient quality that provides insight into the behaviour of the quay wall
- A load on the quay wall which results in significant deformations and forces of the quay wall
- Insight into the mechanics of a quay wall and the way it is modelled in the calculation model as well as insight into the possibilities and limitations of the calculation model
- A method for updating the relevant (soil) parameters and/or reliability based on the measurement data, which in turn allows to optimise the functionality.

2.2. Uncertainty in Geotechnical Engineering

Predicting the behaviour of a quay wall is complicated by the uncertainties that must be taken into consideration. Uncertainties can be divided in 2 types, inherent uncertainty and epistemic uncertainty [van Gelder, 2000]. Inherent uncertainties arise due to a randomness or variation in nature, the inherent uncertainty is not reducible as it is not possible to fully predict the randomness. An example of inherent uncertainty are low water levels, even with a lot of data about the history of the water levels one cannot fully predict the maximum and minimum water levels in the coming years.

On the other hand there are epistemic uncertainties which result from of a lack of knowledge or data. This means that the uncertainty can be reduced as more information becomes available. Examples of epistemic uncertainties are parameter uncertainties and model uncertainties. Parameter uncertainties occur due to a limited data set from which the distribution of the parameter is determined. Most applied models are not perfect as reality is complex and often not fully understood, therefore models are based on simplifications and assumptions which results in model uncertainties.

Uncertainties in soil parameters and soil-structure interaction have a large effect on the reliability of a quay wall [Roubos, 2019]. These uncertainties are epistemic and could therefore be reduced when additional information becomes available. These uncertainties are also time-independent, therefore a reduction in the uncertainty of soil parameters and soil-structure interaction could be made early in the service life of a quay wall. Important sources of uncertainty in soil parameters are:

- Spatial variability of soil
- Measurement uncertainty of in-situ tests and sample disturbance for laboratory tests
- Applied correlations for converting in-situ tests to soil parameter

2.3. Calculation methods for quay walls

According to De Gijt and Broeken [2013] there are two calculation methods that are suitable for the design of quay walls, which are the spring supported beam method and the finite element method. Another well known calculation method for retaining walls is Blum's method, which is based on the analytical concept of the beam theory [Korff, 2018]. It assumes fully active and passive soil failure on both sides of the retaining wall regardless of the displacements. Consequently, the method is not suitable to calculate deformations of the retaining wall or the surrounding soil. Blum's method is a good first approximation for the minimally required penetration depth of a retaining wall. However, it does not take into account stiffness of the soil, effects of phases during construction, complex geometries and complex soil-structure interaction. Therefore, Blum's method is not used in this thesis.

Spring supported beam method
In the spring supported beam method a retaining wall is modelled as a beam on an elastic foundation, i.e. the soil [Korff, 2018]. The behaviour of the soil is modelled by a series of elasto-plastic uncoupled springs, which have bi-linear characteristics, meaning there is an elastic and a plastic part, see Figure 2.1. By modelling the soil as a series of bi-linear springs the stresses in the soil depend on the displacement.

The active and passive effective soil stresses depends on the vertical effective stress and the coefficient of lateral earth pressure, see equation 3.1. The stiffness of the soil is described by a linear elastic relation between the changes in deformation and stresses, which is given by the horizontal coefficient of subgrade reaction k_h. The basic differential equation that is solved in the spring supported beam method is:

$$EI \cdot \frac{d^4w}{dx^4} + k(x,w) \cdot w = f(x) \tag{2.1}$$

in which EI is the rigidity of the retaining wall, w the displacement of the retaining wall, x the height of the retaining wall, k the horizontal coefficient of subgrade reaction and f the external loads on the retaining wall.

The basic differential equation is solved for multiple points along the height of the retaining wall and requires multiple iterations to converge. The main advantages of the calculation method are the relatively simple input parameters, and soil schematizing, which easily allow the users to understand the method. Furthermore, the calculation times are relatively short. Disadvantages of using this calculation method for quay walls are [De Gijt and Broeken, 2013]:

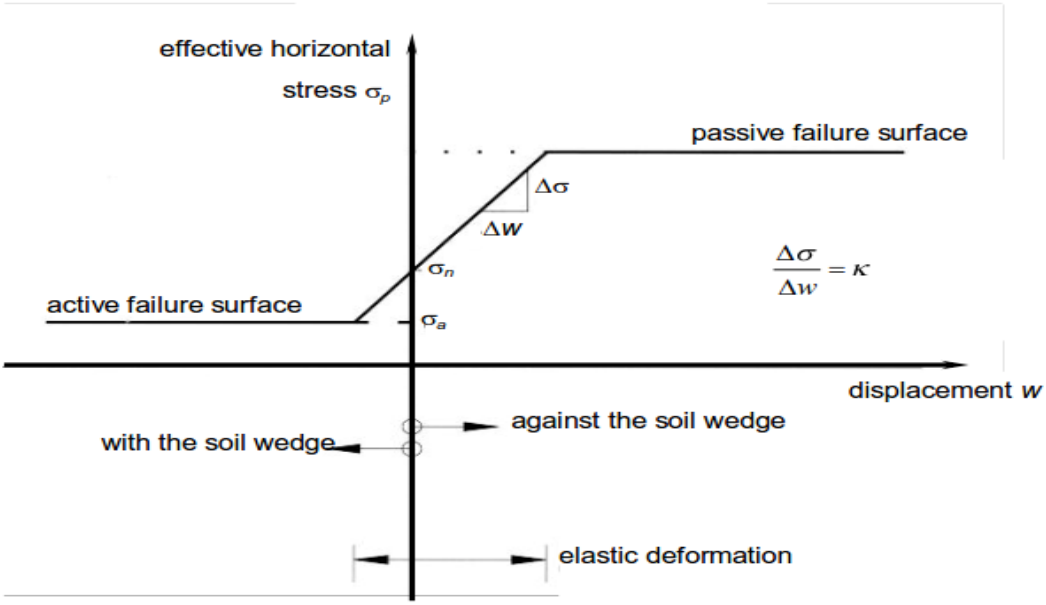

Figure 2.1: Development of horizontal soil stresses [Korff, 2018]

- doesn't cover soil-structure interaction of anchors, relieving platform etc.;
- doesn't allow for modelling of inclined retaining wall;
- failure surfaces of soil are prescribed, difficult to approach actual soil behaviour;
- deformations are only determined for the retaining wall, not for the soil next to it;
- arching in the soil is not considered because the springs are uncoupled.

Due to these disadvantages the spring supported beam method is only used to make draft designs for complex quay walls. To more accurately design a quay wall with a relieving platform more sophisticated calculation methods are necessary that also model the behaviour of the soil body and the soil-structure interaction.

Finite Element Method

The Finite Element Method (FEM) describes the soil and structural behaviour of a model by solving a series of partial differential equations. These partial differential equations do not have an exact solution and therefore cannot be solved analytically, thus they are solved numerically. To solve these equations the continuum needs to be divided in a finite number of elements, known as the finite element mesh. Each element contains a number of nodes, see Figure 2.2, and each node has a number of degree of freedom that corresponds to the number of unknowns. The unknowns in the nodes are the so-called primary variables, which have to be solved by the governing partial differential equations.

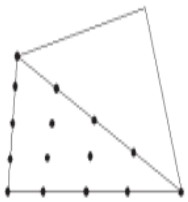

Figure 2.2: 15-node triangle element FEM

The main advantages of FEM models are:

- possible to model complex geometries
- includes soil-structure interaction in the model
- soil deformations are calculated as well
- arcing effects in the soil can be estimated

The aforementioned advantages outweigh the main disadvantages of FEM models, which are the large amount of input parameters required, relatively long calculations times and the required level of knowledge about the soil behaviour. In this thesis the software package Plaxis is used to perform FEM calculations. Plaxis has 2-Dimensional (2D) and 3-Dimensional (3D) packages in which FEM calculations can be performed. There are multiple constitutive soil models available in Plaxis. The Hardening Soil (small strain) model is considered to be the most suitable for analysing the behaviour of the quay wall [De Gijt and Broeken, 2013, Obrzud and Truty, 2018].

The Hardening Soil model (HS model) is an advanced soil model which can be used for predicting the behaviour of both soft and stiff soils [Schanz et al., 1999]. The HS model is able to simulate phenomena often observed in soil behaviour, such as stress dependent stiffness, plastic yielding and dilation. The yield surface of the HS model is equal to the Mohr coulomb yield surface, yet it is not fixed in principle stress state but can expand due to hardening plasticity. The HS model is a double hardening model, the two types of hardening mechanisms are shear hardening and cap hardening. Shear hardening occurs in the case of primary deviatoric loading, whereas compression hardening occurs under primary oedometer and isotropic loading.

The shear hardening in the HS model leads to hyperbolic behaviour in the deviatoric stress path. During primary deviatoric loading mobilisation of the friction angle results in an expansion of the shear yield surface, this process is accompanied by plastic shear strains. Due to the plastic shear strain an apparent reduction of stiffness is created, which results in a hyperbolic stress-strain curve. The mobilisation of the friction angle during primary deviatoric loading and the expansion of the shear yield surface is visualised in Figure 2.3. When the maximum friction angle of the soil is mobilised the shear yield surface is equal to the Mohr Coulomb surface and a state of failure is reached, therefore no further expansion of the shear yield surface is possible. The plastic shear strains occur during primary deviatoric loading, during unloading/reloading conditions the soil behaves fully elastically.

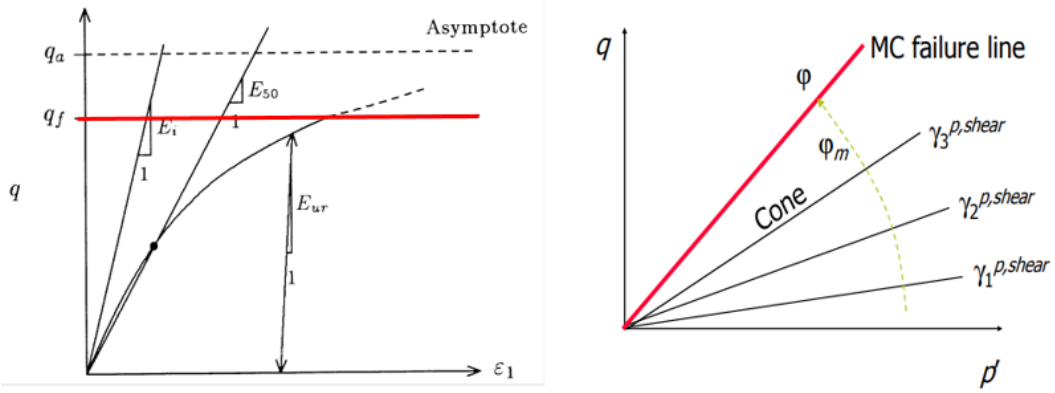

Figure 2.3: Hyperbolic behaviour HS model in deviatoric stress paths [Schanz et al., 1999]

During primary compressive loading cap hardening occurs in the HS model, which leads to plastic volumetric strains. If the mean effective stress in the model exceeds the pre-consolidation pressure the cap surface of the model extends. This is accompanied by plastic volumetric strains and these cause an apparent reduction in the primary compressive stiffness.

The stiffness modulus in the HS model are stress-dependent, the amount of stress-dependency is described by a power law. The stress-dependent stiffness modulus are described based on a reference stress level, which is equal to 100 kPa. The stress-dependency of the stiffness parameters accounts for an increasing stiffness with increasing stress levels.

Another advanced soil model in the software package Plaxis is the Hardening Soil with small-strain stiffness model (HSsmall). This model accounts for the observation that soil tends to behave very stiff under small strains and a decrease in stiffness occurs under increasing strains levels, see Figure 2.4.

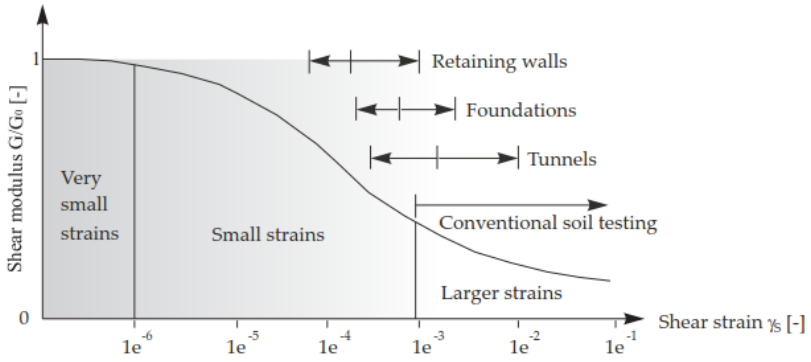

Figure 2.4: Small-strain stiffness dependency on the strain levels [Brinkgreve, 2019a]

Both the HS model and the HSsmall model do not take into account softening behaviour of soil, which means there is no distinction between peak and residual friction angles. Therefore, the input friction angles should be chosen carefully.

Table 2.1 gives an overview of the general input parameters of the Hardening Soil (small strain) model.

Parameter	Unit	Description
γ_{dry}	Kn/m^3	Dry unit weight
γ_{wet}	Kn/m^3	Saturated Unit weight
ϕ'	°	Internal friction angle
ψ	°	Dilatancy angle
c'	kPa	Drained cohesion
E_{oed}^{ref}	kPa	Tangent stiffness for primary oedometer loading
E_{50}^{ref}	kPa	Secant stiffness in standard drained triaxial test
E_{ur}^{ref}	kPa	Unloading \reloading stiffness
m	-	power for stress-level dependency of stiffness
G_0^{ref}	kPa	Reference shear modulus small strains
$\gamma_{0.7}$	-	Threshold shear strain

Table 2.1: General input parameters Hardening Soil (small strain) model

2.4. Design methods and design guidelines for quay walls

A quay wall should be designed such that it is reliable and safe to use. This means that the probability of failure should be sufficiently low. There are different methods available which can be used to calculate the reliability of a quay wall. In this section the most common methods are explained. Furthermore, guidelines which are used to design quay walls in the Netherlands are mentioned.

2.4.1. Design methods

Before the design methods are explained it is necessary to present the general concept of structural reliability. The reliability of a structure can be assessed by comparing the resistance of a structure with the loads on a structure. This is done in a so-called limit state function (2.2), in which R is the resistance and S is the load. Failure of a structure occurs when the resistance is smaller than the load (R < S), which means that Z < 0. Since failure of a structure should not occur the limit state function should result in Z ≥ 0. However, it must be noted that structures are often complex and that it is not possible to combine all loads and resistances in one function. Therefore, multiple limit state functions are often made. These limit state functions are linked to the failure mechanisms of a structure. In the case of a quay wall some of the most relevant failure mechanisms are presented in Figure 2.5. For each of the failure mechanisms a limit state function can be made. As an example the limit state function of yielding of the retaining wall is presented in equation 2.3. In this equation f_y is the yield strength of the steel, M is the bending moment in the retaining wall, W is the section modulus of the retaining wall, N is the normal force in the retaining wall and A is the sectional area of the retaining wall. The bending moment M and the normal force N should be obtained from calculations.

$$Z = R - S \tag{2.2}$$

$$Z_{STR;yield} = f_y - (\frac{M}{W} + \frac{N}{A}) \tag{2.3}$$

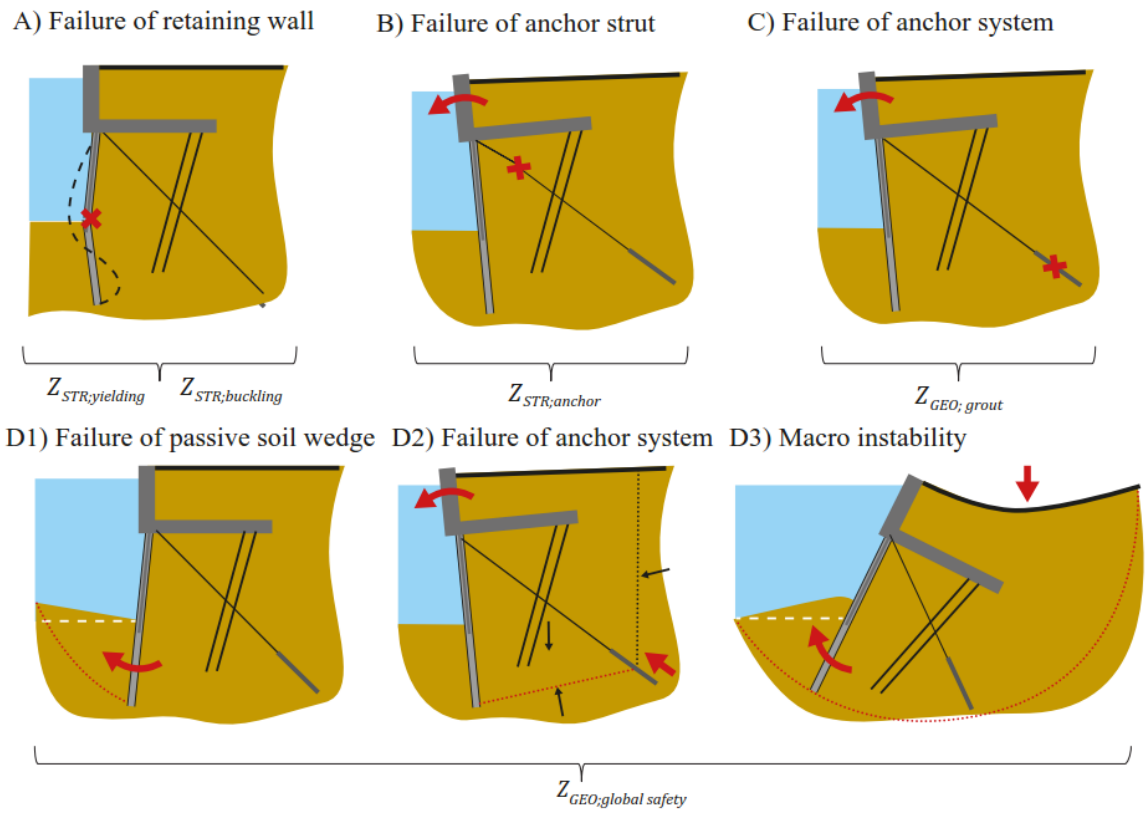

Figure 2.5: Failure mechanisms of a quay wall [Roubos, 2019]

The limit state functions can be divided into two groups, which are the: Serviceability Limit State (SLS) and the Ultimate Limit State (ULS). The Serviceability Limit State is a condition of the structure beyond which it can no longer fulfill it's function, this often refers to deformations of a structure. When the Ultimate Limit State function of a structure is exceeded failure occurs and the structure is damaged permanently.

The desired reliability of a structure depends on the consequences when failure occurs. If the consequences of failure are high a very low probability of failure is desired. The Eurocode NEN-EN 1997-1 specifies three reliability classes (RC). Each reliability class has a specified reliability index β, which is related to the probability of failure. In Table 2.2 the reliability classes and the reliability indexes are shown for quay structures with a design life of 50 years.

Description of reliability classes	**Reliability index β**	**Design life in years**	**Example**
RC1/CC1 Consequences of failure - Risk of danger to life negligible - Risk of economic damage low	3.3	50	Simple sheet pile structure, quay wall for small barges. Retaining height till 5 m
RC2/CC2 Consequences of failure - Risk of danger to life negligible - Risk of economic damage high	3.8	50	Conventional quay wall for barges and seagoing vessels. Retaining height >5m
RC3/CC3 Consequences of failure - Risk of danger to life high - Risk of economic damage high	4.3	50	Quay wall in flood defence/ LNG-plant or nuclear plant (hazardous goods)

Table 2.2: Reliability classes and indexes for quay walls, [De Gijt and Broeken, 2013]

In general there are two different methods to evaluate the reliability of a quay wall. These methods are a semi-probabilistic and probabilistic approach. There also exists a deterministic approach, however this approach is not used anymore. The two aforementioned approaches are now further explained.

Semi-probabilistic approach
In a semi-probabilistic approach the uncertainties in parameters is accounted for by using characteristic values, which are cautious estimates of the parameters. For loads this corresponds to high percentiles and for resistances to low percentiles of the statistical distribution. The characteristic values are normally chosen such that the probability of exceedance is less than 5%. The characteristic values should then be converted to design values by applying partial safety factors.

For each limit state that is evaluated there is a specific set of generalised partial safety factors. Therefore, each limit state is assessed based on an specific probability of failure and consequence. The partial safety factors are based on probabilistic calculations of general cases and can be found in guidelines. The semi-probabilistic approach is visualised in Figure 2.6. The red line indicates the distribution of a load and the green line that of resistance. For each limit state the design resistance is checked with the design loads, based on the following equation [Jonkman et al., 2017]:

$$\frac{R_k}{\gamma_R} \geq \gamma_S \cdot S_k \tag{2.4}$$

in which R_k is the characteristic resistance, γ_R the partial safety factor on resistance, γ_S the partial safety factor on the loads and S_k the characteristic load.

The applied partial safety factors depend on the reliability class of the structure, with a higher reliability class resulting in higher partial safety factors. The semi-probabilistic approach is considered as the standard design approach in the Eurocode NEN-EN 1997-1, CUR 166 and CUR211.

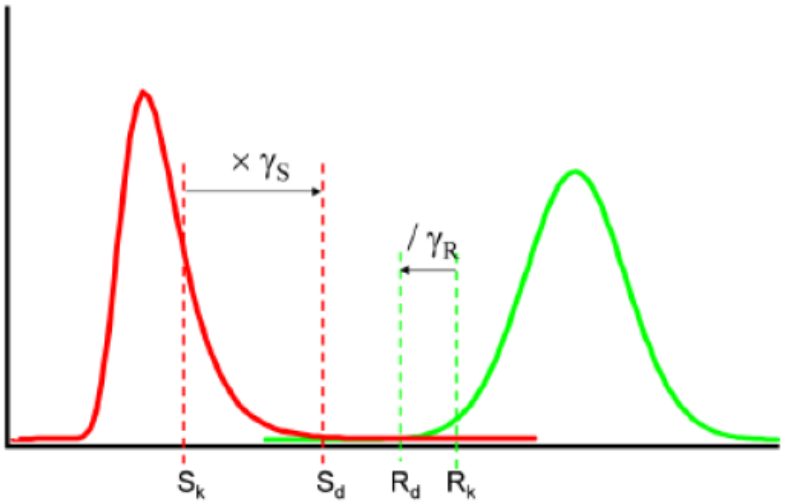

Figure 2.6: Idea of semi-probabilistic approach [Jonkman et al., 2017]

Probabilistic approach
In a probabilistic design approach there are no (partial) safety factors and characteristic values of parameters. All parameters are stochastic to fully take into account the uncertainties. The probability of failure of a structure is the probability that the limit state functions are smaller than zero (Z < 0) [Jonkman et al., 2017]:

$$P_f = P(Z < 0) \tag{2.5}$$

in which P_f is the probability of failure. The probability of failure should be lower than the target probability, which is related to the reliability index β. Since the parameters are stochastic there are many different values and combinations of values possible. Consequently, the probability of failure of any of the limit state functions can only be determined by performing a sufficient amount of iterations. The probabilistic approach can lead to more accurate values of the reliability index β compared to the semi-probabilistic approach. However, the probabilistic approach is time-consuming since many iterations must be made.

2.4.2. Design guidelines

In the Netherlands the design guidelines that describe the design process of retaining structures are the CUR166 and CUR211. Both the design guidelines are in accordance to the Eurocode NEN-EN 1997-1. The CUR166 describes aspects of the design of sheet pile walls and anchor systems. Since quay walls are often more complex structures with multiple structural elements, i.e. sheet pile wall, anchors, relieving platforms and bearing piles, an additional design guideline is made for quay walls, which is CUR211. In CUR211 the focus is on the design of retaining walls with relieving platforms.

2.5. Inverse analysis based on measurement data

With measurement data it is possible to calibrate models by performing an inverse analysis, also known as a back-analysis. The measurement data gives additional information about the behaviour of a quay wall which can be used to reduce uncertainties in the (soil) parameters. There are different ways to perform an inverse analysis.

Semi-probabilistic
An inverse analysis can be performed with semi-probabilistic calculations, in which (soil) parameters are iteratively updated until the output of the model has a good match with the measurement data. Performing an inverse analysis with semi-probabilistic calculations requires a lot of knowledge about the sensitivity of the model to be able to identify the dominant parameters. Especially in multi layer models it can be difficult to understand the influence of all parameters. Furthermore, a semi-probabilistic calculation results in the identification of 1 possible set of parameters that better fits the measurements data. It is too time consuming and complex to identify all possible parameters sets that have a good fit with the measurement data with semi-probabilistic calculations.

Probabilistic
It is also possible to perform an inverse analysis with probabilistic calculations, meaning that parameters are defined as stochastic variables in the analysis. This results in a more sophisticated update of (soil) parameters since the uncertainty in the parameter is taken into account. A well known probabilistic updating method is Bayesian updating, which allows for an update in the reliability of a quay wall.

Den Adel [2018] showed in his study that Bayesian updating could successfully be used to increase the reliability of a complex quay wall. Based on a series of artificial measurements updates of the soil parameters where made leading to a reduction in the uncertainty of the parameters. His research indicates that based on two types of measurements, horizontal deformations of the combined wall and anchor strains, a reduction in the uncertainty of the (soil) parameters can be achieved.

Büller [2019] investigated what types and amount of service domain measurement data are most effective in updating the calculated reliability of sheet pile walls. In his research he coupled a FEM-model to a Bayesian updating interface to update soil parameters based on a set of artificial measurements. In a series of analyses it was determined whether the Bayesian updating process was able to effectively converge towards a predefined set of true soil parameters. In the analyses no set of measurements was able to enforce the updating process towards the true set of soil parameters. The most accurate update was achieved with larger number of observations of different types, i.e. horizontal wall deformations, bending moments of the wall, horizontal earth pressures behind the wall, anchor forces and surface settlements. This indicates that a large number of accurate measurement data leads to a more accurate outcome of the updating process.

Advantages of performing an inverse analysis in a probabilistic framework are that the uncertainty in the (soil) parameters is updated and the most likely combination of parameters is achieved. A Downside is that a probabilistic analysis is very complex and it requires a lot of time to get the models up and running.

2.6. Conclusion

In this study the retaining function and the bearing function are relevant. This is because these two functions have a relation to the geotechnical and mechanical behaviour of a quay wall. An optimisation of the functionality would therefore result in an increase of the retaining height or an increase in the surface load on top of the quay wall. Relevant aspects for optimising the functionality of a quay wall are:

- Insight into the parameter uncertainties that play an important role in the reliability of quay walls
- Measurement data of sufficient quality that provides insight into the behaviour of the quay wall
- A load on the quay wall which results in significant deformations and forces of the quay wall
- Insight into the mechanics of a quay wall and the way it is modelled in the calculation model as well as insight into the possibilities and limitations of the calculation model
- A method for updating the relevant (soil) parameters and/or reliability based on the measurement data, which in turn allows to optimise the functionality.

In section 2.2 information is presented about parameter uncertainties that play an important role in the reliability of a quay wall. Uncertainties in soil parameters and soil-structure interaction have a large effect on the reliability of a quay wall [Roubos, 2019]. These uncertainties are epistemic and could be reduced when additional information becomes available. These uncertainties are also time-independent. Therefore, a reduction in the uncertainty of soil parameters and soil-structure interaction could be made early in the service life of a quay wall.

Insight into the different calculation methods for quay walls is obtained by reviewing the available calculation methods in section 2.3. It is concluded that the FEM allows for the calculation of complex geometries and soil-structure interaction, which are both present at quay walls. For detailed calculations of the behaviour of a quay wall the FEM is superior to other calculation methods. In this thesis FEM calculations are performed in the Plaxis software package. The Hardening Soil (small strain) constitutive model is seen as the most suitable model for quay wall design.

In section 2.4 and 2.5 information is presented about design methods and methods which can be used to update (soil) parameters and/or the reliability of a quay wall based on measurement data. Ideally the functionality of a quay wall is optimised by using a sophisticated inverse analysis method such as Bayesian updating. Recent studies of [Büller, 2019, Den Adel, 2018] showed that the Bayesian updating technique can be coupled to complex FEM calculations to optimise the functionality of complex quay walls based on measurement data. However, in both of these studies it is noted that it requires a significant amount of effort and time to couple the Bayesian updating technique with FEM calculations. Therefore, these studies used simplified cases or synthetic measurement data. This thesis determines if it is possible to optimise the functionality of a quay wall based on measurement data obtained during the construction process. The focus is on determining whether the measurement data obtained during the construction process gives sufficient insight into the behaviour of the quay wall. Therefore, in this thesis semi-probabilistic analyses are used to be able to focus on the aforementioned goal.

For the case used in this thesis the measurement data is analysed in chapter 4. This is done to determine if the collected measurement data is of sufficient quality and what information is provided by the data.

In chapter 5 and 6 a finite element model (FE model) is set-up and validated. By analysing this model insight is gained in the mechanics of a quay wall and some of the limitations of the FE model are discussed.

In this study measurement data that is obtained during the construction process is used. For this measurement data to be useful for optimising the functionality of the quay wall it is necessary to determine how significant the loads on the quay wall are during the construction process. In chapter 7 more insight is provided into the relevance of the construction process compared to the limit states.

3

Case description

This chapter introduces the case used in this thesis. The case represents typical conditions that are present in the Maasvlakte area of the port of Rotterdam.

3.1. Introduction to the case

The HES Hartel Tank Terminal (HHTT) consists of a 2200-metre-long quay wall, of which 1200 metres for large sea-going vessels and 1000 metres for smaller inland vessels. The HHTT-quay is a tank terminal for the storage and transshipment of oil products and biofuels. Next to the quay there is a 27-hectare site on which 54 tanks are constructed with a combined storage capacity of 1.3 million m^3. The project site is located on the first Maasvlakte in the port of Rotterdam area, see Figure 3.1. The construction of the HHTT-quay started in the first quarter of 2018 and was finished by the end of 2019. The dredging of the deep-sea quay took place from week 28 until week 48 in 2019. The quay is planned to be fully operational in 2021.

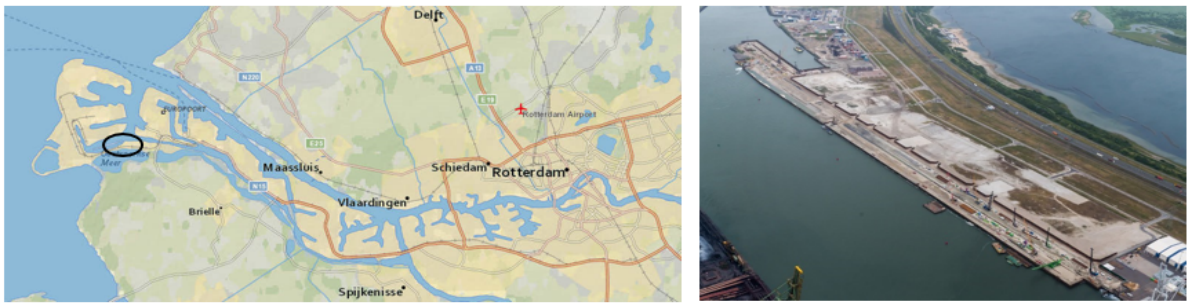

Figure 3.1: Project location HHTT-quay, www.google.nl

The deep-sea quay is equipped with sensors to monitor the behaviour of the structure, meaning it is a so-called smart quay wall. The quay wall for the smaller inland vessels is not equipped with sensors; therefore, it is not included in this thesis. When the HHTT-quay is mentioned in this thesis it refers to the deep-sea quay wall only.

The retaining height depends on the Nautical Guaranteed Depth (NGD), which is the minimum required water depth that has to be guaranteed for a ship to safely moor at a quay. The Port of Rotterdam authority defines different NGD's based on ship types. The HHTT-quay is designed for three types of ships, i.e. VLCC, Suezmax and MR2, each of these ships has its own NGD requirements. Therefore, the HHTT-quay is divided in multiple zones that are specifically designed for one of the three ship types.

In total there are six different zones along the HHTT-quay, these are: zone UB, zone A t/m D and zone TK. Zone UB is an expansion of the adjacent Brammenterminal and zone TK is the transition between the deep-sea quay and a natural underwater slope. These zones don't have sensors and are significantly different from zones A to D, therefore zones UB and TK are not considered in this thesis. Zones A to C are constructed with a relieving platform, whereas zone D is constructed with a front wall only. Each zone is constructed of multiple sections, which have a width of approximately 23 metres. In Table 3.1 some specifications of each zone are presented, all depths presented in the table are in metres relative to 'Normaal Amsterdams Peil' (NAP).

Zone	A	B	C	D
Ship type	Suezmax	VLCC	Suezmax	MR2
Ground level	+4.5 m NAP			
NGD	19	-23.6	-19	-14.6
Design depth	-20.5	-25.6	-20.5	-16.1
Retaining height	25	30.1	25	20.6
Relieving platform	yes			no
Number of sections in zone	11 (A1 to A11)	20 (B1 to B20)	11 (C1 to C11)	8 (D1 to D8)

Table 3.1: Specification of zones A t/m D

Prior to the construction of the quay wall an extensive soil investigation was performed by Wiertsema & Partners Dijkstra [2016, 2017] and Fugro Weijst [2010], consisting of Cone Penetration Tests (CPT's), boreholes and laboratory tests. Based on the borehole logs and the CPT's 12 soil layers are identified within the project area. In Table 3.2 a description of each layer is given. In Appendix F 4 representative CPT's are presented.

Layer number	Main soil type	Description
1	Fine sand	Sand fill of fine sand used to raise the surface level of the first Maasvlakte
2	Clay	Soft clay layer, locally with horizontal bands of fine sand
3	Fine sand	Sand fill of fine sand used to raise the surface level of the first Maasvlakte
4	Fine sand	Sand fill of fine sand used to raise the surface level of the first Maasvlakte, locally with horizontal bands of silt
5	Fine to moderate coarse sand	Sand fill of fine to moderate coarse sand used to raise the surface level of the first Maasvlakte
6	Fine sand	Fine sand with a lot of horizontal bands of silt and clay
7	Fine clayey sand	Fine sand layer with a lot of clay, part of the 'laag van Wijchen'
8	Clay	Moderate stiff clay layer, part of the 'laag van Wijchen'
9	Fine sand	Fine sand layer
10	Fine to moderate coarse sand	Fine to moderate coarse sand layer
11	Moderate coarse to coarse sand	Moderate coarse to coarse sand layer
12	Fine to moderate coarse sand	Fine to moderate coarse sand layer, with local clayey sand bands

Table 3.2: Description of soil layers

3.2. Applied type of quay wall

Within the port of Rotterdam different types of quay walls are constructed over the years. Which type of quay wall is applied depends on the function of a quay wall and the local conditions, e.g. soil properties, retaining height, surface load and material costs [De Gijt and Broeken, 2013]. In Figure 3.2 the type and date of construction for quay walls in the port of Rotterdam are shown.

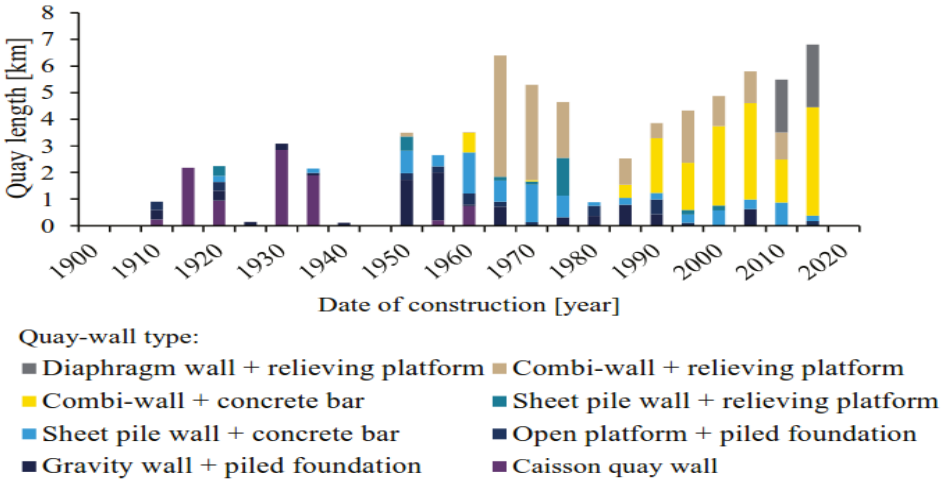

Figure 3.2: Type of quay walls in port of Rotterdam [Roubos, 2019]

The HHTT-quay wall consists of 2 types, which are a combined wall with a relieving platform (zone A to C) and a combined wall with a concrete bar (zone D). The difference between the 2 types is the presence of the relieving platform. As can be seen in Figure 3.2 these 2 types of quay walls are common in the port of Rotterdam. A description of the structural components of both types is given in the remainder of this section. For a general impression of quay walls with relieving platforms, see Figure 3.3.

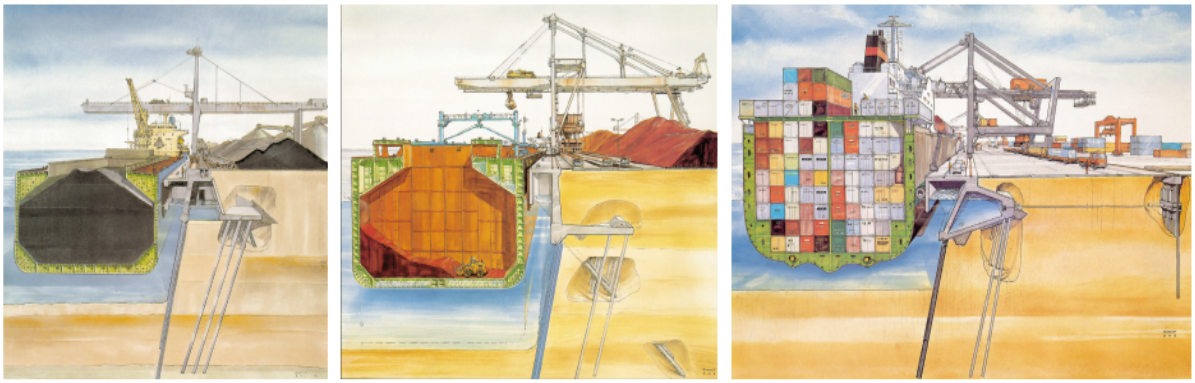

Figure 3.3: Examples quay walls with relieving platforms in the port of Rotterdam [Roubos, 2019]

Combined wall

A combined wall is a retaining wall that has a larger bending stiffness than regular sheet pile walls. Therefore, a combined wall is often applied when large retaining heights and/or high surface loads are present. It is composed of alternating tubular piles and one or more sheet piles which are connected by interlocks, see figure 3.4. The tubular piles are the primary elements and have a much higher bending stiffness than the sheet piles, which are the secondary elements. A result of the higher bending stiffness of the tubular piles is that they react much stiffer to horizontal loads than the sheet pile elements. Therefore, the horizontal loads are mainly transferred to the tubular piles. Because the tubular piles carry most of the horizontal loads soil arches occur in the soil, see Figure 3.4.

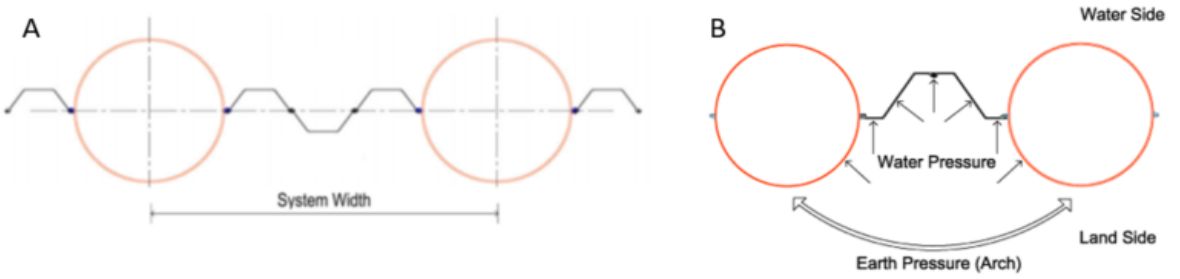

Figure 3.4: A) combined wall example, B) impression of arching effect near tubular piles

Besides the soil retaining function the combined wall has a vertical bearing function for the relieving platform as well. Therefore, a large normal force is transferred from the relieving platform to the combined wall. This normal force is eccentrically placed

The connection between the sheet pile wall and the relieving platform is often a hinge support, which has multiple advantages compared to a fully fixed support. A hinge support results in a less complex construction system since there are no bending moments in the hinge. Furthermore, the anchor forces are significantly lower compared to the situation where a fully fixed support is used [De Gijt and Broeken, 2013]. In the case of a combined wall a cast iron saddle creates the hinge support, see Figure 3.5. The cast iron saddle is placed eccentric from the centre of the tubular piles. Therefore, the normal force transferred from the relieving platform introduces a bending moment in the tubular piles. This bending moment is beneficial as it reduces the maximum field bending moment in the combined wall.

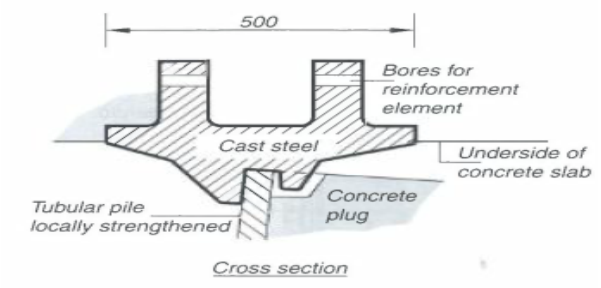

Figure 3.5: Iron saddle hinge support [De Gijt and Broeken, 2013]

MV-piles
MV-piles (Müller Verpress piles) are applied in cases where an anchor with a large tension capacity is required. A MV-pile is a steel H-beam or tubular element which is driven in place with an impact hammer, during installation an grout mixture is injected through a nozzle at the tip of the steel element. The first advantage of the grout injection is a reduction of the friction between the steel element and the soil during installation. This makes it possible to drive a MV-pile up to 70 metres in the soil. The second advantage is that any voids in the soil created during the installation of the MV-pile are filled with the pressurised grout mixture, which increases the adhesion between the MV-pile and the soil after installation. The created grout body area depends on the injection pressure of the grout and the soil properties, in Figure 3.6 the theoretical maximum and minimum area of the grout body is showed for an H-beam steel element.

relieving platform
The relieving platform is constructed of reinforced concrete and is supported by the bearing piles, anchors and the combined wall. The main function of the relieving platform, which is reducing the horizontal stresses on the combined wall, is achieved in two ways. First of all the relieving platform reduces the combined height. Secondly, the relieving platform takes a large part of the surface load and transfers it to deeper soil layers. The reduction of the horizontal stresses on the combined wall result in lower bending moments and sheet pile lengths compared to the situation without a relieving platform.

Figure 3.6: Theoretical maximum and minimum grout body around a H-beam element [Srigopal, 2018]

The reduction of the horizontal effective soil stresses on the retaining wall depends on the geometry of the relieving platform, combined wall and the ground surface as well as the soil properties. Figure 3.7 shows the vertical effective soil stresses at the combined wall and behind the relieving platform, which can be converted to horizontal effective soil stresses by multiplying it with the coefficient of lateral earth pressure K, equation 3.1.

$$\sigma'_h = K \cdot \sigma'_v \tag{3.1}$$

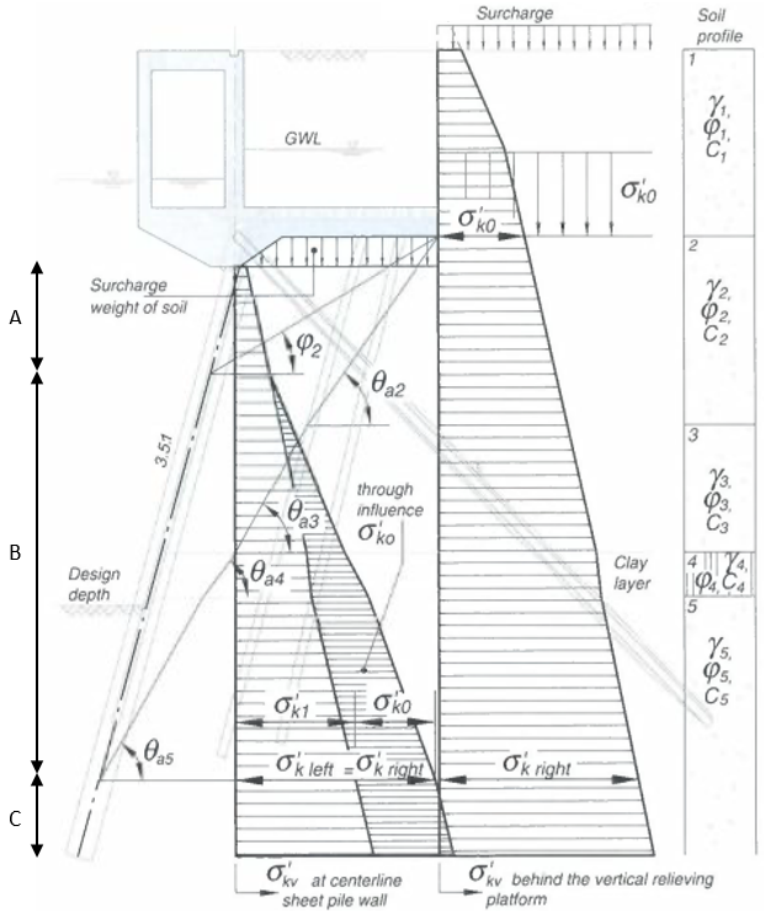

Figure 3.7: Principle of relieving platform [De Gijt and Broeken, 2013]

The maximum reduction of the vertical effective stress due to the relieving platform is equal to surface load plus the effective weight of the soil over the height of the relieving platform. The maximum reduction is denoted as σ'_{k0} in Figure 3.7. The maximum reduction of the vertical effective stress is present at the top of the retaining wall and reduces with depth. To further explain this three different zones over the height of the retaining wall are distinguished.

- zone A: The maximum reduction of the vertical effective stress is present here. The soil on top of the relieving platform and the surface load have no vertical effective stress. The vertical effective stress is equal to the effective weight of the soil below the relieving platform only. The bottom of zone A depends on the width of the relieving platform, the angle of internal friction of the soil ϕ and the inclination of the retaining wall.
- zone B: The influence of the vertical effective stress σ'_{k0} on the retaining wall increases with depth in zone B. At the bottom of zone B the vertical effective stress at the retaining wall and behind the relieving platform are equal. The bottom of zone B is determined by the sliding plane of the soil. The angle of the sliding plane θ depends on the angle of internal friction of the soil ϕ, the wall friction angle δ and the inclination of the retaining wall α
- zone C: The vertical effective stress at the retaining wall and behind the relieving platform are equal.

SI-piles

The main function of the bearing piles is creating horizontal and vertical stability for the quay wall. To guarantee vertical stability of a quay wall the relieving platform must be supported by a system of bearing piles that transfer the vertical forces to deeper sand layers which have a larger bearing capacity than the top layers. The bearing piles can be constructed of various pile types, for the HHTT-quay screwed displacement piles with a permanent steel casing are used (SI-piles). During installation a hollow steel casing is screwed to the desired depth while simultaneously grout is injected around the pile tip. The grout reduces the friction between the steel casing and the surrounding soil. Another benefit of the grout injection is the increased circumference of the pile and a better adhesion between the pile and the surrounding soil. After the hollow steel casing is installed reinforcement is placed inside and concrete is poured to fill the steel casing. An advantage of SI-piles is the large resistance to bending moments due to the presence of the hollow steel casing, see Figure 3.8 for an general impression of horizontal loads on bearing piles underneath a relieving platform.

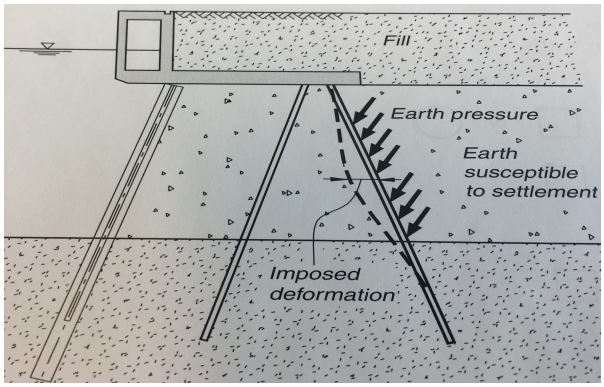

Figure 3.8: Horizontal soil deformation causes deformation of the bearing piles and induce bending moments [De Gijt and Broeken, 2013]

In figure 3.7 the effective vertical soil stresses at the retaining wall and behind the relieving platform are shown. From this figure and equation 3.1 we can conclude that the effective horizontal soil stresses are higher behind the relieving platform than at the retaining wall. Due to the difference in stresses the soil moves towards the retaining wall, and thus moves perpendicular to the bearing piles. The bearing piles are much stiffer than the soil and resist against the moving soil. Therefore, the bearing piles take up part of the effective horizontal soil stresses, this is the so-called shielding effect. In a research on the shielding effect by Qiu and Grabe [2012] soil arches where clearly visible in small scale model tests,

see Figure 3.9. Soil arches are a 3-dimensional effect in which the soil is restrained over a larger width than the width of the bearing piles itself. Although this seems favourable at first since the effective horizontal soil pressure on the retaining wall decrease, it's not because the effective horizontal soil stresses on the bearing piles are transferred through the relieving platform to the MV-piles and the retaining wall. Consequently, these structural elements are experiencing a heavier load compared to the situation when the shielding effect is absent.

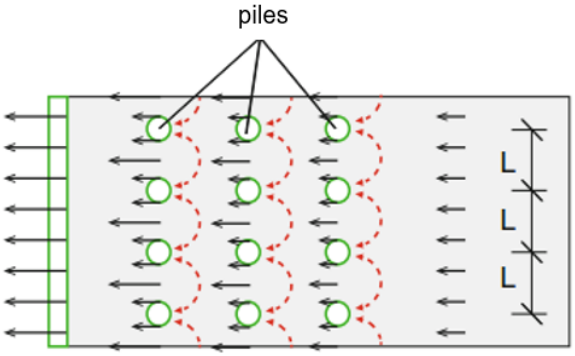

Figure 3.9: Top view of small-scale model in which soil arches develop near the bearing piles [Qiu and Grabe, 2012]

4

Usability of the measurement data

The measurement data obtained during the construction process of the case is presented and analysed. This includes a review of the measurement methods to gain insight into how the data is collected and to understand possible measurement errors. Then the measurement data is reviewed and the usability of the measurement data is determined. The goal is to determine what information is collected by the measurement data and which sections of the quay wall can be used in the analyses in the successive steps. This chapter provides information to answer the second research sub-question.

4.1. Description of the measurement methods

The measurement methods are reviewed to gain insight into how the data is collected and to understand possible measurement errors. This allows to better asses if the measurement data is of sufficient quality. In Table 4.1 an overview is presented on the used measurement methods and the data that these methods provide.

4.1.1. Fiber Bragg Grating sensors

Fiber Bragg Grating (FBG) sensors are known for their durability and high sensitivity. Therefore, they are often used for the long-term monitoring of structures where deformations are generally small. A FBG sensor consists of an optical fiber in which a bragg grating is positioned on a short segment of the fiber, the typical length of the bragg grating is in the order of 5 mm - 10 mm [Fedorov et al., 2015]. When a light signal is transmitted through the optical fiber the bragg grating reflects a particular wavelength depending on its properties, such as the refractive index and the grating period. When the FBG sensor is exposed to an external load or a temperature change the reflected wavelength of the bragg grating changes, see Figure 4.1. The change in the reflected wavelength is calculated by equation 4.1 [Kim et al., 2017].

$$\Delta\lambda = \lambda_B(1 - P_e)\Delta\epsilon + \lambda_B(\alpha + \xi)\Delta T \tag{4.1}$$

In this equation λ_B is the initial reflected wavelength, P_e the effective strain-optic constant, $\Delta\epsilon$ the change in strain, α the thermal expansion coefficient, ξ the thermo-optic coefficient and ΔT the change in temperature.

Measurements				
Desciption	**Method**	**Frequence**	**Reference measurement**	**Measurement quantity\location**
Anchor strains	FBG-sensors	Every hour from start of dredging	After installation of MV-piles, before it's connected to front wall / concrete cap	Total of 6 MV-piles; 1 pile in each of the following sections: A5, A11, B4, B14, C2 and D1
Strains in connection bearing piles and relieving platform	FBG-sensors	Every hour from start dredging	After installation of bearing-piles, before it's connected to relieving platform	2 bearing piles; both bearing piles located in section C9
Relative horizontal deformation combined wall + front wall / concrete cap	Inclinometer	4-5 times during dredging	After pouring of concrete cap / relieving platform, before the sand fill	Total of 50 tubular piles; 1 tubular pile in each section
Absolute deformation top of front wall / concete bar	XYZ-measurements	5-8 times during dredging	After pouring of concrete cap / relieving platform, before the sand fill	Total of 400 points; the corners of each section are measured, so 4 points per section
Harbour water levels	Radar	Every 10 minutes	-	1 piezometer at 1 km from the project location
Ground water levels	Piezometer	multiple times per day during the construction process	-	X piezometers at the project location
Bottom level of harbour	Bathymetric surveys	3 -6 times per week during dredging	-	Surveys is performed up to 120 m in front of the quay

Table 4.1: Overview of measurements during construction process

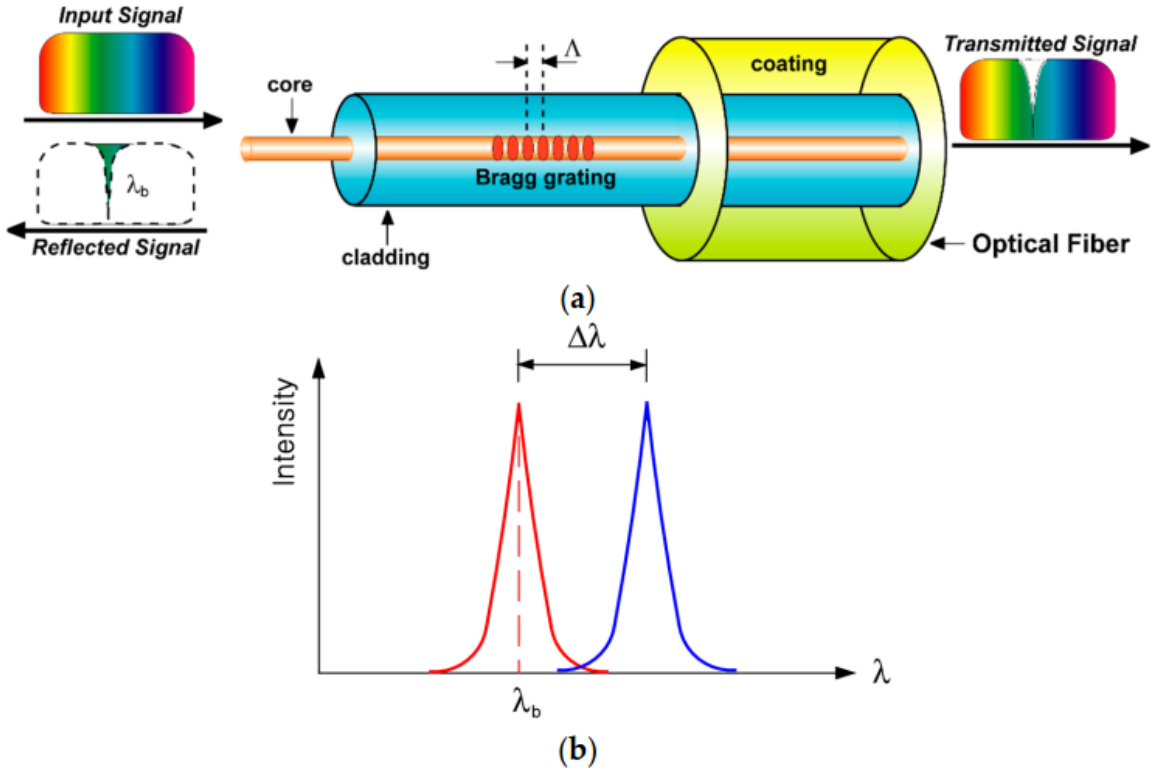

Figure 4.1: a) Principle of a FBG sensor b) wavelength shift due to external load or temperature change [Kim et al., 2017]

The initial reflected wavelength of the applied sensors is in the range of 1520 - 1580 nanometre (nm) and according to the fabricator of the FBG sensors P_e = 0.22 and ξ = 7.32*$10^{-6}\frac{m}{m}/^{\circ}C$. The FBG sensors that measure strain are fixed to the steel MV-pile or reinforcement of the bearing piles, therefore they must follow the thermal expansion of the steel and α_{steel} = $12 * 10^{-6}\frac{m}{m}/^{\circ}C$. Equation 4.1 is rewritten to equation 4.2 in which $\Delta\lambda$ is in picometre, $\Delta\mu\epsilon$ in micro-strain and ΔT in degrees Celsius. The temperature change near the MV-piles and bearing piles is measured by FBG sensors that are not fixed to these structural elements.

$$\Delta\mu\epsilon = \frac{\Delta\lambda - 30\Delta T}{1.2} \tag{4.2}$$

Anchor strains

There are 6 MV-piles equipped with sensors. These are located at sections A5, A11, B4, B14, C2 and D1. Each of the equipped MV-piles has 6 FBG sensors located in a single cross-section according to the configuration shown in Figure 4.2. The cross-section which contains the FBG sensors is located at a depth of approximately NAP -2.30 m, which is just below the bottom of the relieving platform.

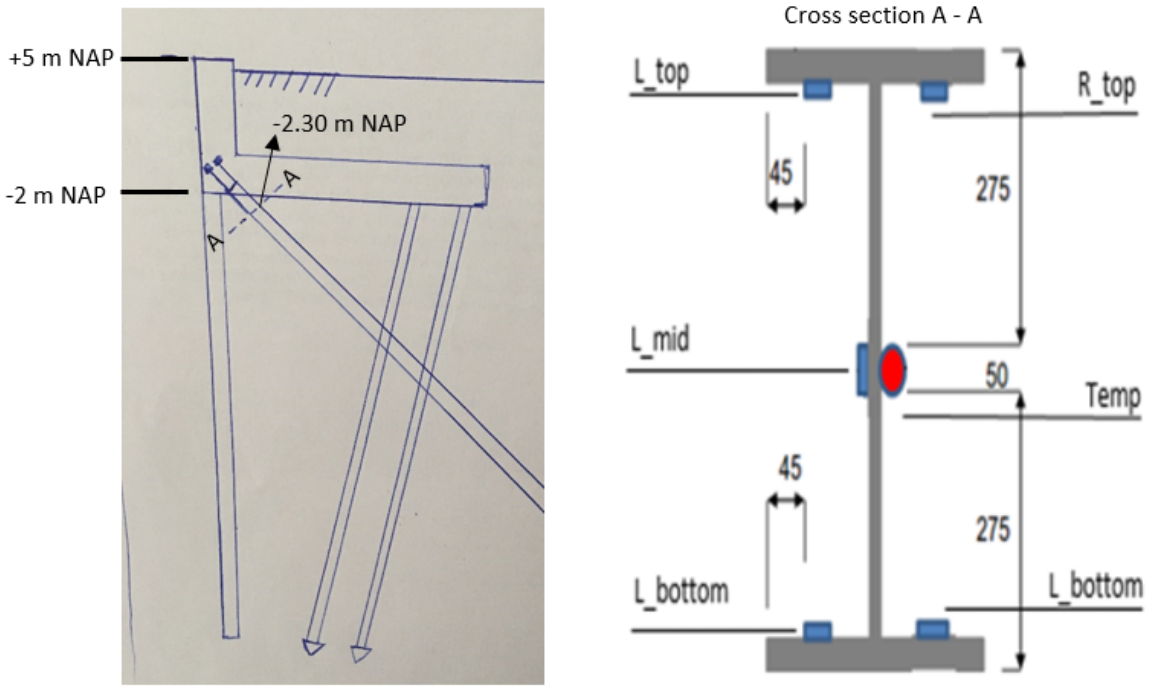

Figure 4.2: cross-section of MV-pile with FBG sensors, dimensions are in mm

The FBG sensors that measure the strains of the MV-piles are mounted to the MV-piles in 2 different ways, both mounting methods are explained below. After the installation of the FBG sensors on MV-pile A5 it was decided to switch to another mounting method.

- The FBG sensors on MV-pile A5 are mounted as follows:
  - The optical fiber containing the FBG sensor is placed in the notch of an U-shaped steel plate (S355), the dimensions of the U-shaped steel plate are shown in Figure 4.3. Under controlled conditions the FBG sensor is glued to the U-shaped steel plate with a slight pretension, this should allow the FBG sensor to measure compressive strains as well.
  - The U-shaped steel plate is bolted to the HEB600 profile with 4 corner bolts and the bottom of the plate is glued to the HEB600 profile to provide adhesion.
  - After the U-shaped steel plate is installed on the HEB600 profile a resin coating is applied to prevent moisture to reach the sensor and the steel plate

- The FBG sensors on the remaining MV-piles are mounted as following:
  - The optical fiber containing the FBG sensor is glued to a thin steel plate, this is done under controlled conditions with a slight pretension. The dimensions of the steel thin plate are 400 mm x 50 mm x 1.5 mm (l x w x h). For protection a cap is placed over the FBG sensor.
  - The thin steel plate is glued and welded to the HEB600 profile. The type of glue used between the steel plate and the steel HEB600 profile is a 2-component epoxy glue. The steel plate is welded on both sides along the first 4 centimetres of the plate, see Figure 4.4.
  - After the U-shaped steel plate is installed on the HEB600 profile a resin coating is applied to prevent moisture from reaching the sensor and the steel plate

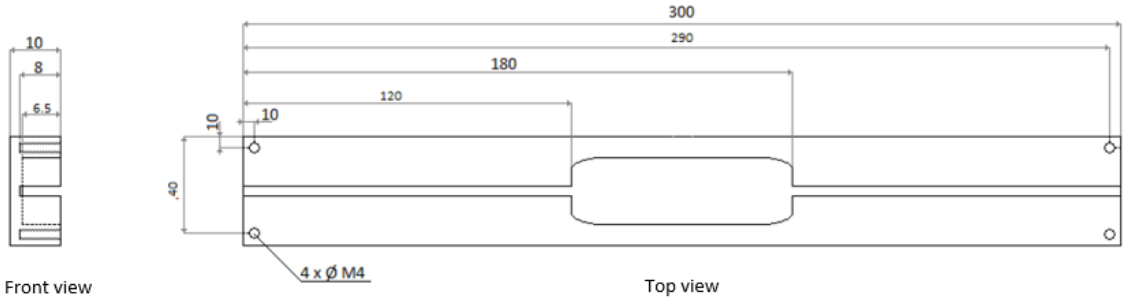

Figure 4.3: Dimensions U-shaped steel plate used for MV-pile A5

Figure 4.4: Mounted FBG sensors on MV-piles A11, B4, B14, C2 and D1

Each monitored MV-pile also has 1 FBG sensor that measures temperature near the anchor. This sensor is not fixed to the steel HEB600 profile and is therefore free to deform under temperature variations.

The FBG sensors are mounted to the MV-piles after it was installed and not yet connected to the relieving platform / concrete bar. The reference measurements of the FBG sensors on the MV-piles were taken several weeks after installation of the FBG sensors to allow the sensors to adapt to the local temperature and let the glue cure. One reference measurement is performed for each monitored MV-pile, at the time of the reference measurement the anchor was not connected to the relieving platform / concrete bar. The strains in the MV-piles are measured every hour starting from 10-07-2019.

The strains in the MV-piles are measured normal to the axis of the piles and are therefore the result of normal stresses. These normal stresses could be the result of a combination of a normal force (tension or compression), a bending moment and/or torsion. In Figure 4.5 a general impression of these forces and the corresponding normal stresses in the HEB profile are shown, T indicates a tensional stress and C a compressive stress. The shown normal stresses due to bending moments and torsion (b, c and d in figure 4.5) are only valid when the yield strength of the steel is not reached, i.e. stresses are elastic. The only force that results in normal stresses/strains in the middle of the web is an axial force, therefore the strains from the FBG sensor in the middle of the web can directly be used for the determination of the axial force. Furthermore, the normal stresses due to torsion only occur when warping of the flanges is restrained, otherwise torsion only results in shear stresses, which are not measured by the FBG sensors [Hughes et al., 2011].

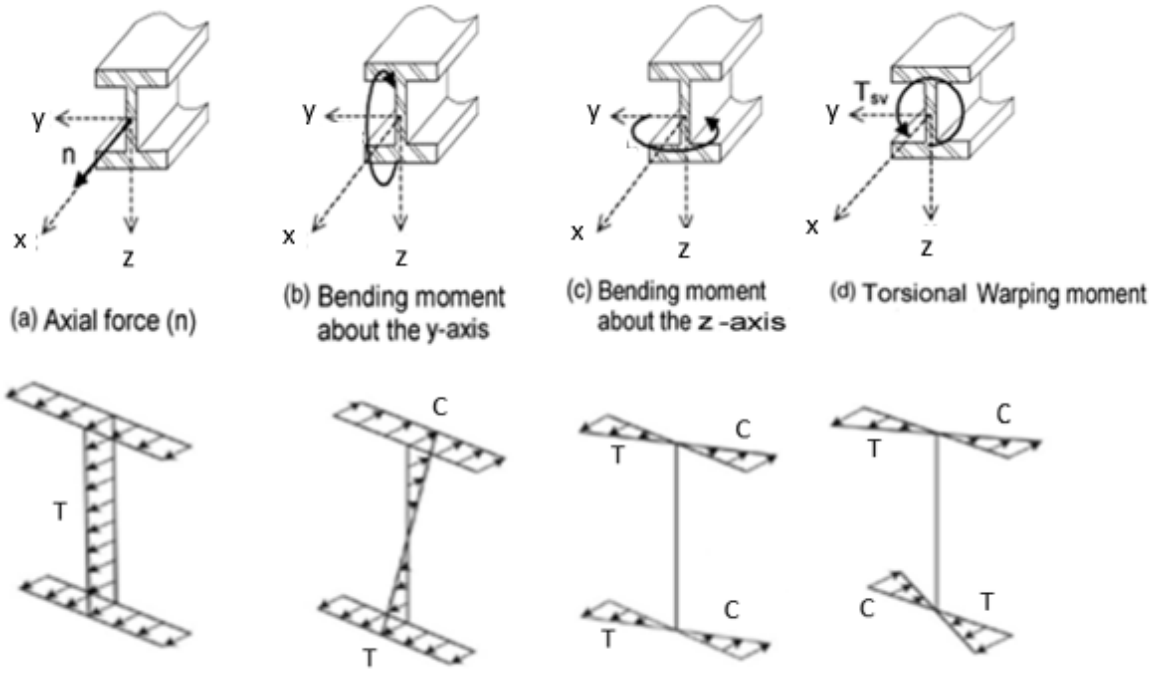

Figure 4.5: Normal stresses in a HEB profile resulting from different forces

Strains in connection bearing piles with relieving platform

There are two bearing piles that are equipped with FBG sensors to measure the strains in the connection between the bearing piles and the relieving platform. These piles are located in section C9. The optical fibers containing the FBG sensors are placed in the groove of additional steel reinforcement bars, and are glued to provide bounding between the optical fibers and the steel bars, see Figure 4.6. This process is performed under controlled conditions to increase the quality of the bound. A load test on the additional steel reinforcement bars was performed to check if the bound between the sensors and the bar was sufficient.

In each bearing pile there are 8 additional reinforcement bars which are provided with optical fibers, these bars are evenly distributed within the pile. In the optical fiber there is a FBG sensor every 25 centimetres. The distance between the top and the bottom FBG sensor is 1.75 metres. The optical fiber is placed in loops over two reinforcement bars. This improves the redundancy of the system, see Figure 4.7. An additional FBG sensor is placed close to the bearing piles to measure the temperature.

A reference measurement is performed after the installation of the bearing piles, at that moment the concrete of the relieving platform was not poured yet.

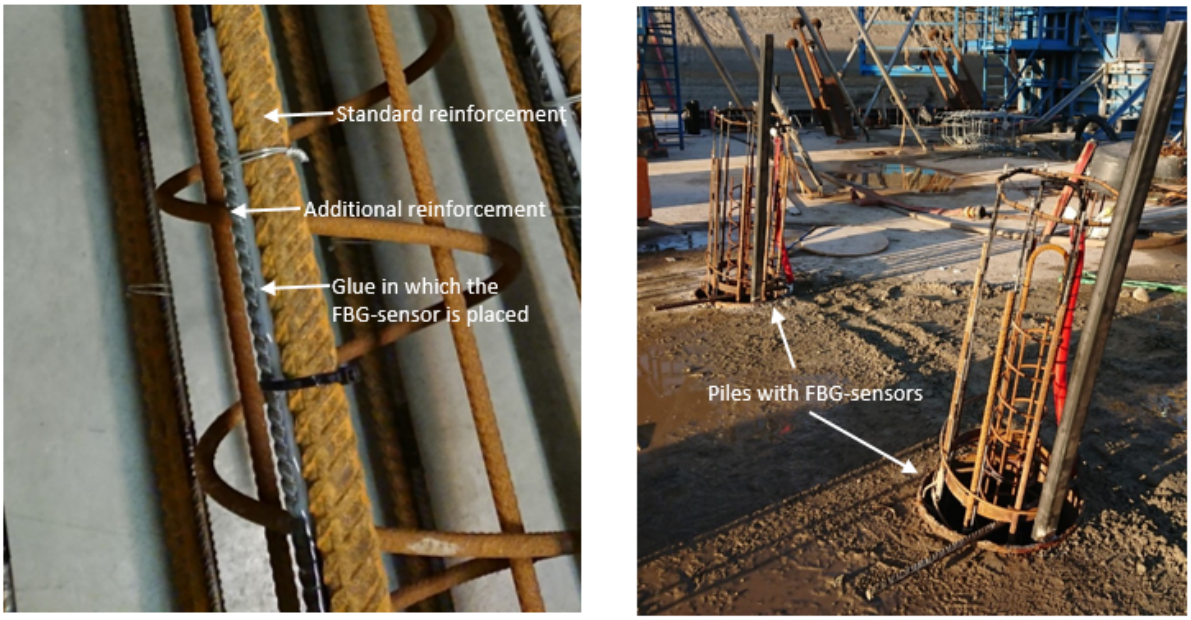

Figure 4.6: FBG sensors placed in reinforcement steel of bearing piles

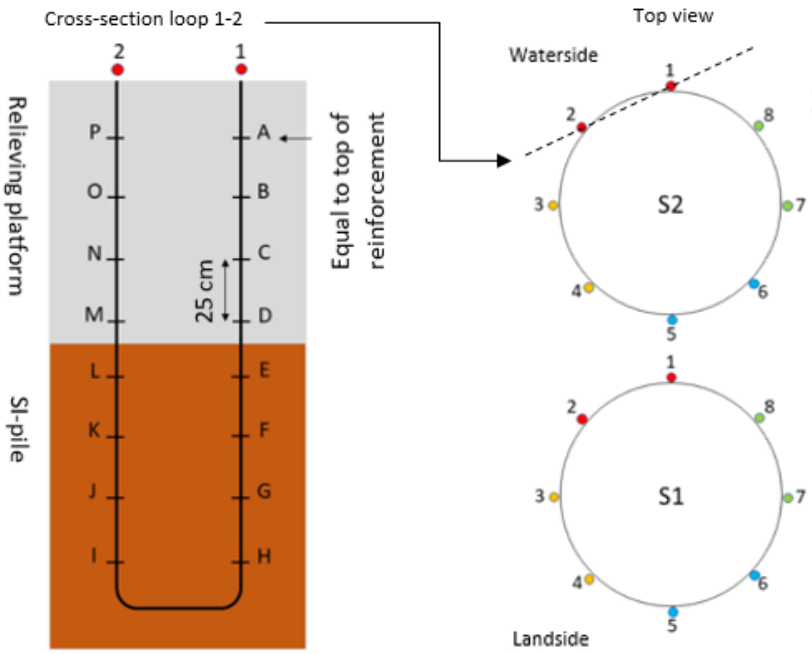

Figure 4.7: cross-section and top view of bearing piles with FBG sensors

4.1.2. Inclinometer

Inclinometers are used to determine the relative magnitude and direction of the lateral deformation of the combined wall and the concrete bar / front wall. The inclinometer measures the inclination of the casing it is passing through, in this case the casing is a hollow steel square casing and is attached to the tubular piles of the combined walls and the concrete bar / front wall. The inclination is measured by two force-balanced accelerometers in the inclinometer probe. Therefore, the inclination is measured in two planes perpendicular to the vertical plane. The orientation of the hollow square steel casing is such that the direction of the measured inclination is perpendicular and parallel to the quay wall, see Figure 4.8 A, the orientation is checked after the installation of the combined wall. Figure 4.8 B shows a general concept of the inclinometer probe inside the casing.

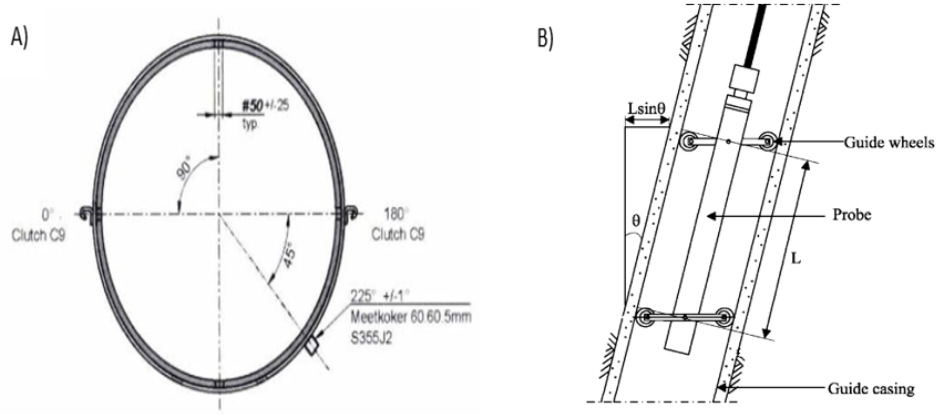

Figure 4.8: A) Orientation of hollow square steel casing B) inclinometer probe inside the casing

The measurement is started from the bottom of the casing. During the measurements subsequent readings are taken as the inclinometer probe is raised in intervals of 0.5 metre. As described in the previous section the inclinometer does not measure the horizontal deformation directly, but instead measures the inclination of the casing. The inclination of the casing must be converted to a horizontal deformation. The horizontal deformation is calculated based on equation 4.3. The relative horizontal displacement over the height of the combined wall and the concrete bar / front wall is obtained by summing the deviation of each interval, see Figure 4.9.

$$deviation = sin\theta \cdot L_{interval} \tag{4.3}$$

To increase the accuracy each measurement is carried out twice, during the second measurement the probe is rotated 180°. By averaging the results of both measurements systematic errors made during the measurements are reduced. Common types of systematic errors are the bias-shift error and rotation error [Stark, 2008]. The bias-shift error is due to a bias of the sensors, since the applied inclinometer is regularly calibrated the bias-shift error should be limited. Furthermore, the bias-shift error is reduced significantly by the double measurements. The rotation error occurs when the casing deviates significantly from the vertical plane. If the A-axis is slightly rotated towards the B-axis, a significant deviation of the vertical plane in the B-axis results in apparent deviations in the A-axis, see Figure 4.10. Since the deviations from the vertical axis are relatively small in this project the rotation error is small as well (< 1 à 2 mm over the entire height). The system accuracy depends on a combination of the systematic errors and the random errors. The manufacturer of the applied inclinometer, the DIS-500, reports a system accuracy of ±2 mm / 25 m, this might be too optimistic. Stark [2008] reports a system accuracy of ±6.5 mm / 25 m. This value is empirically determined based on different case studies. The latter seems more realistic as it is based on multiple case studies, the system accuracy is assumed to be ±6.5 mm / 25 m.

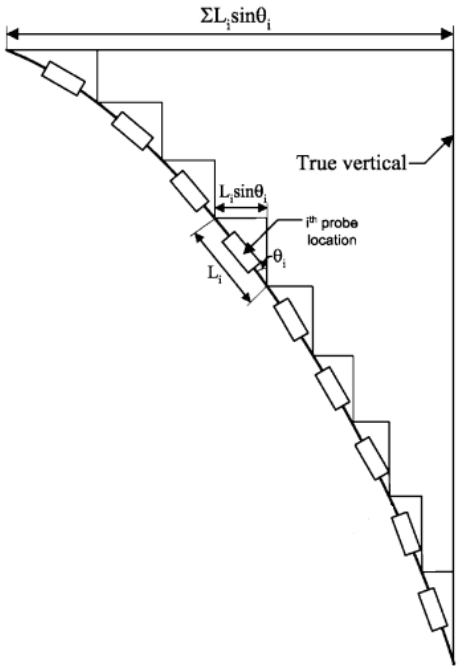

Figure 4.9: Incremental horizontal deformation of inclinometer measurement

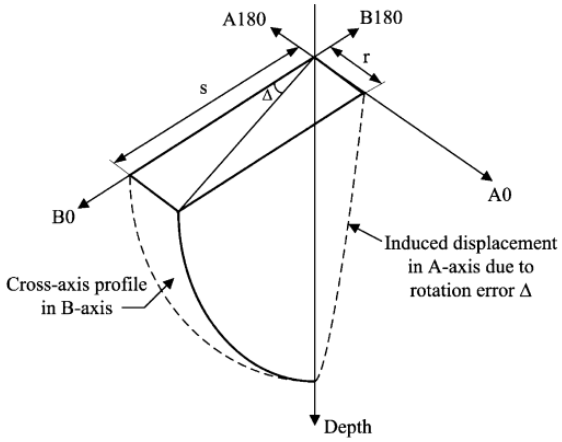

Figure 4.10: illustration of rotation error [Stark, 2008]

The aim of the inclinometer measurements is to determine the change in horizontal deformations of the combined wall. The measured horizontal deformations are therefore made relative to a reference measurement, which is taken after the concrete relieving platform / concrete bar is poured. However, the toe of the combined wall is assumed to be fixed during the inclinometer measurements. As this might not be the case, it is necessary the convert the relative horizontal deformations to absolute horizontal deformations by using the XYZ-deformation measurements of the top of the relieving platform / concrete bar. The process of converting the inclinometer measurements to absolute horizontal deformations is summarised as following:

- Each inclinometer measurement is made relative to the bottom of the measurement (bottom is assumed to be fixed).
- To determine the increase of horizontal deformation the inclinometer measurements are made relative. The reference measurement (first inclinometer measurement) is taken after the concrete of the relieving platform / concrete bar is poured.

- As the bottom of the inclinometer measurements might not be a fixed point it is necessary to convert the relative horizontal deformations to absolute horizontal deformations. The absolute horizontal deformations are determined by using the XYZ-deformation measurements of the top of the relieving platform / concrete cap.

The following remarks are made regarding the inclino measurements:

- The measured angles of the combined wall and the concrete bar / front wall are small (<2°) and therefore the vertical height of an interval is equal to the interval length ($L_{interval} = L_{height}$)
- this study assumes a system accuracy of ±6.5 mm / 25 m, which accounts for systematic and random errors

4.1.3. XYZ Deformation measurements

The horizontal and vertical deformation of each section are measured on the top 4 corners of the concrete bar / front wall. The measurement locations on the top 4 corners are indicated by the presence of so-called measurement bolts. The measurements bolts are measured with respect to reference points within the project site. The reference points are located on the corners of a bund wall (retaining wall), see Figure 4.11. This bund wall lies parallel to the quay wall and the distance between them is approximately 40 metres. The position of the bund wall is determined with respect to the 'Rijksdriehoekscoördinaten' (RD-coordinates) at the start of the project. The reference points are assumed to be fixed. Therefore, the deformations of the reference point should be minimal during the duration of the project. It is noted that construction works took place behind the bund wall, which could have resulted in deformations of the bund wall. The reference points are only measured once at the start of the project. Therefore, it is not possible to verify that the reference points can be considered as fixed points.

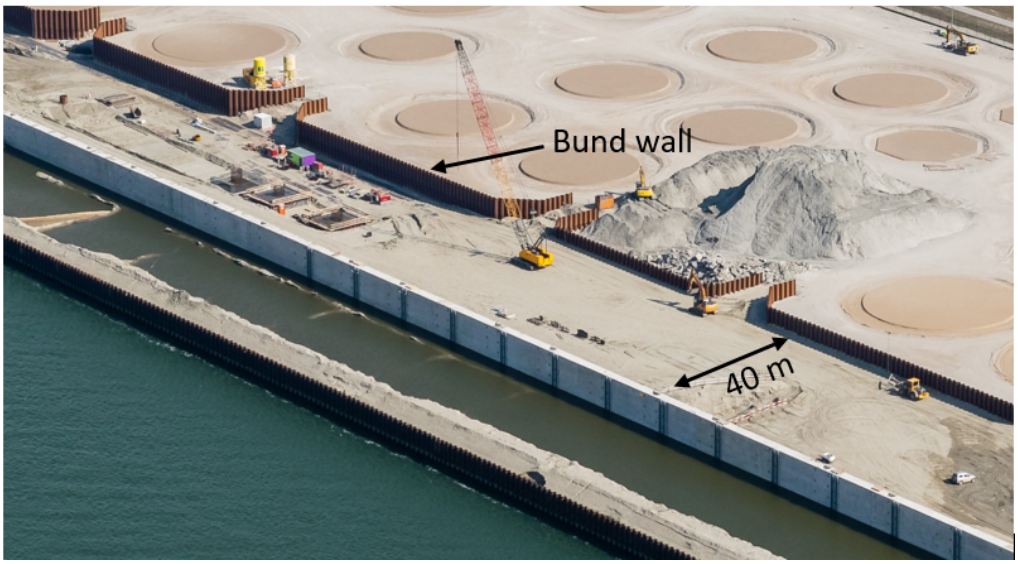

Figure 4.11: Location of the bund wall on the project site

The XYZ deformations are measured relative to a local reference system, which was linked to the RD-coordinates. The X- and Y-axis of the local reference system are respectively parallel and perpendicular to the quay wall. The Z-axis of the local reference system is equal to the vertical plane. The XYZ-deformations are measured with a total station.

4.2. Determining the usability of the measurement data

In this section the usability of the measurement data is determined. This is done by analysing the data and comparing the data to each other. The comparison of the data should reveal if there is consistency in the data. For each measurement method the available data is presented and arguments are given on why the data is usable or not.

The presented data is limited to 6 sections (A5, A11, B4, B14, C2 and D1) of the quay wall. This is because at these sections multiple types of measurement data are collected. Which potentially makes these sections suitable for an analysis in the successive chapters of this thesis.

4.2.1. Anchor strains

In **Appendix A.1** the measured strains of each MV-pile are plotted in time. These graphs also show the increasing bottom depth in front of the quay. In the analysis of the anchor strains it is assumed that the cross-section containing the FBG sensors is far enough from the load introduction, so that the forces are evenly distributed over the cross-section.

- The design of the FBG sensors is robust to ensure that the FBG sensors have a long lifespan. The downside of this robust design is that there is a lot of material between the FBG sensor and the steel HEB600 profile, e.g. steel plate, epoxy glue and welds. The effect on these materials on the strain transfer between the FBG sensor and the HEB600 profile is unknown. No load tests have been performed on the monitored MV-piles to quantify any possible strain losses between the HEB600 profile en the FBG sensors.
- The reference measurements of the MV-piles are performed only once. Therefore, no checks of the reference measurement have been performed and any errors remain unidentified. If errors during the reference measurement have caused a bias in the data this bias would still be present in the data.
- The strains presented in the graphs do not start from zero. The reference measurements of the FBG sensors are made before 10-07-2019. Strains have developed in the anchors during the construction processes prior to 10-07-2019.
- As the bottom level in front of the quay wall increases in depth it is expected that (tensional) strains develop in the anchor. The measurement data indicates that the FBG sensors react to the increasing bottom level in front of the quay wall and show an increase in tensional strains.
- Sensors L_top of anchor B14 and R_top and R_bot of anchor D1 are not included in the presented graphs because the measured strains deviate significantly from the other measurements. Furthermore, they showed a significant change in strain while the bottom level in front of the quay was constant, which indicates a drift in these FBG sensors.
- The strains in the middle of the web should be equal to the average of the strains in the top and bottom flanges. For MV-anchors A5 and B14 the measured strains in the middle of the web are respectively higher and lower than the maximum/minimum measured strains in the flanges, which is not possible from a mechanical point of view. This indicates that the middle FBG sensor or the FBG sensors in the flanges have a bias. There is no other information available from which the anchor force could be determined. Therefore, it is not possible to verify which sensors have a bias.
- It appears that there is a compressive axial force in the MV-piles A11 and C2 while the retaining height of the quay wall is fully mobilised. When the retaining height of the quay wall is fully mobilised there is a large horizontal force acting on the quay wall which is orientated such that is would result in a tensional force in the MV-piles. Therefore, it is unlikely that a compressive force is present in the aforementioned MV-piles.
- Due to the position of the FBG sensors on the cross-section of the HEB600 profile it is possible to distinguish the different types of forces from each other.
- Compared to the other MV-piles the data from MV-piles B4 and D1 seems to be most usable for an analysis, see Figure 4.12 and 4.13 The axial force in these piles is a tensional force and the strains of the middle FBG sensors are more or less the average of the strains in the flanges. However, as mentioned in the first remark there is an uncertainty in the strain transfer between the steel HEB600 profile and the FBG sensor. Therefore, it is not possible to verify the absolute values of the measured strains in MV-piles B4 and D1.

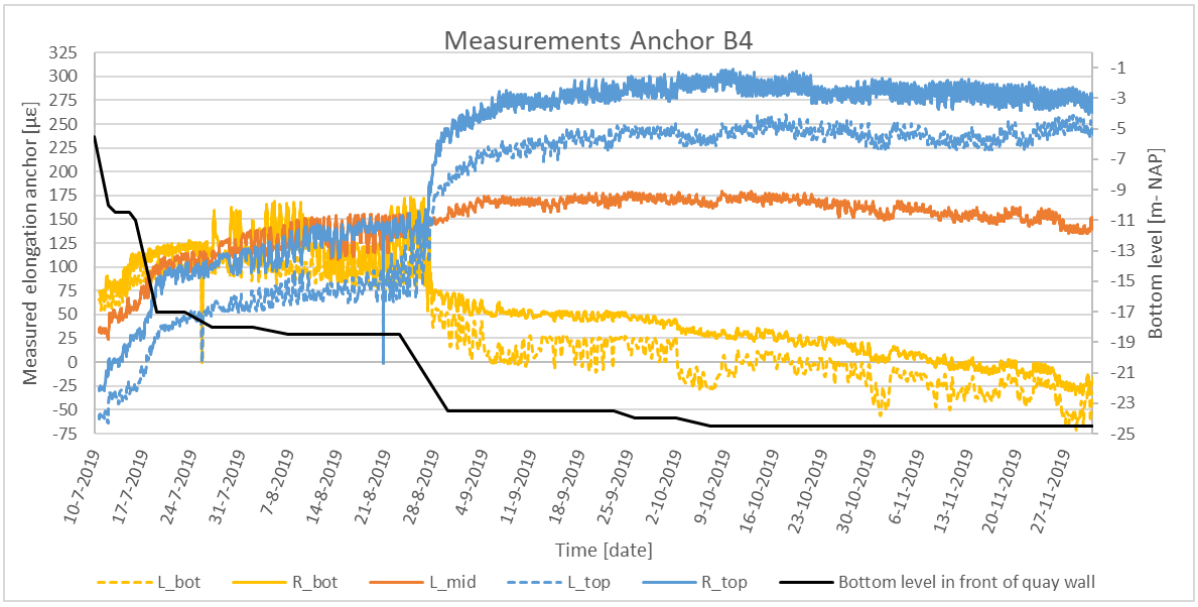

Figure 4.12: Measured elongation of MV-pile B4

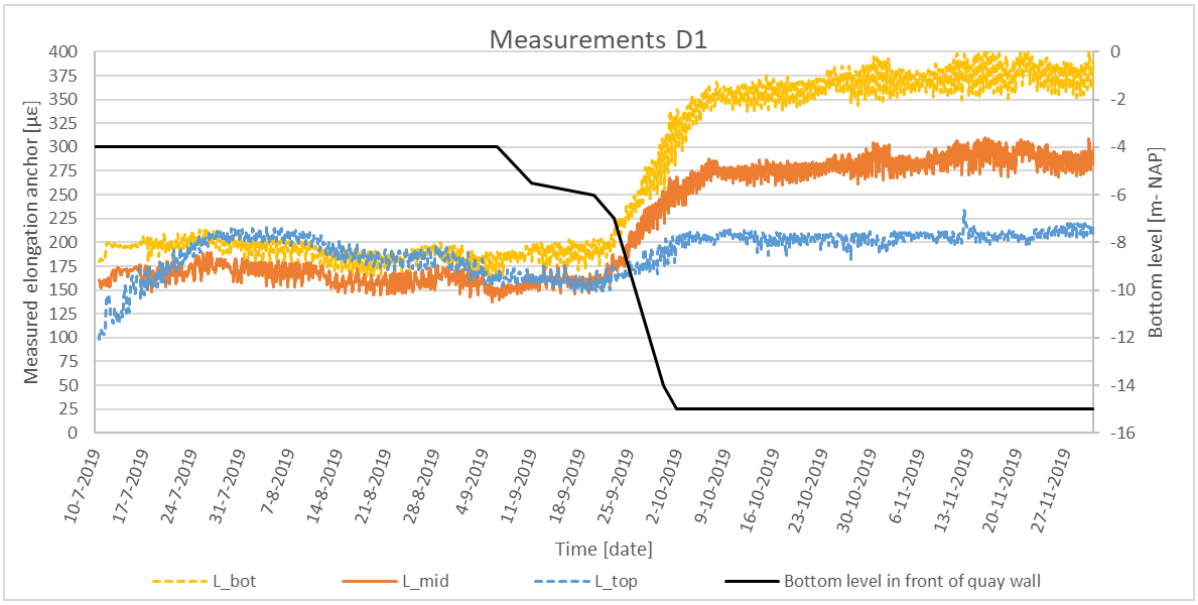

Figure 4.13: Measured elongation of MV-pile D1

Only the data from MV-piles B4 and D1 was used in the remainder of this thesis. The measured micro-strains of the middle FBG sensors are converted to a normal force with equation 4.4, in which E is Young's modulus of steel (E=200 GPa) and A is the cross-sectional area of the HEB600 profile (A=27000 mm^2). Based on the change of strain over the height of the cross-section the curvature of the cross-section is determined. From the curvature the bending moment around the y-axis is determined, see equation 4.5 and 4.6. In these equations d is the distance in metres between the top and bottom sensors on the flanges and I_y is the moment of inertia around the y-axis in m^4.

In Figures 4.14 and 4.15 the normal forces and bending moments around the y-axis of the MV-piles are presented. These graphs also show the increasing bottom level in front of the quay. The bending moment around the z-axis and the warping torsion are not considered as they do not seem to show a relation with the increasing bottom level.

$$F_{anchor} = \epsilon\mu_{middle;sensor} \cdot 10^{-6} \cdot EA \tag{4.4}$$

$$\kappa = \frac{(\epsilon\mu_{average;top} - \epsilon\mu_{average;bottom}) \cdot 10^{-6}}{d} \tag{4.5}$$

$$M_y = \kappa \cdot E \cdot I_y \tag{4.6}$$

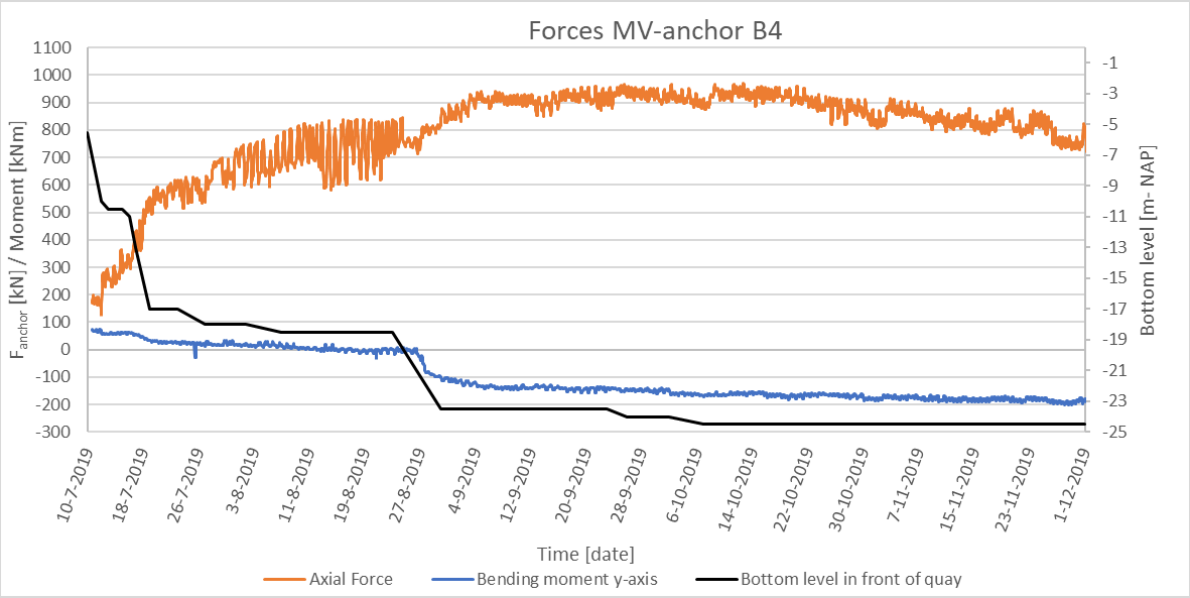

Figure 4.14: Axial force and bending moment in MV-pile B4

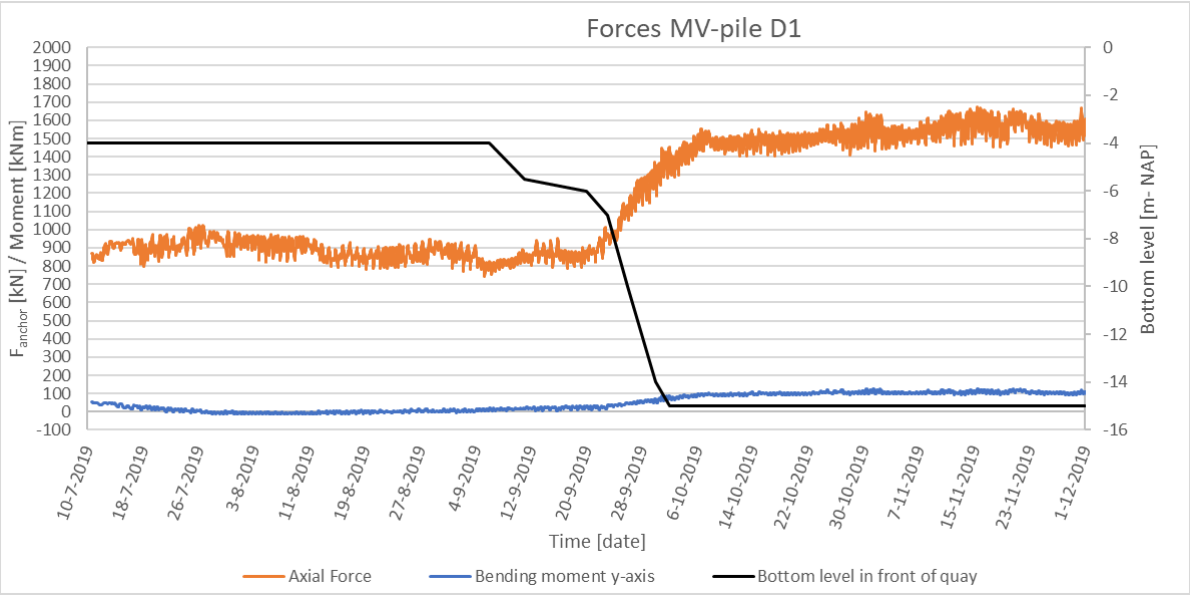

Figure 4.15: Axial force and bending moment in MV-pile D1

Distribution of stresses in the HEB600 profile
The forces are transmitted from the relieving platform / concrete bar to the MV-piles by 4 anchor rods, see Figure 4.16. These anchor rods are welded to the flanges of the MV-piles over a length of 700 millimetres. The distance between the end of the anchor rods and the cross-section containing the FBG sensors is approximately 1200 millimetres. A 3D-model of a MV-pile is made in Plaxis, in which 3 force configurations are applied to check whether the distance between the force introduction and the cross-section containing the FBG sensors is long enough for the forces to distribute evenly. The input parameters and results of the model are shown in Appendix D. The calculation results indicate that the required length for forces to distribute evenly over the height of the profile is 1.2 à 1.3 metres. Therefore, the FBG sensors are far enough from the force introduction.

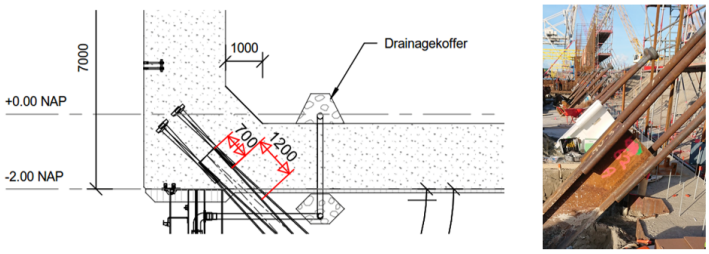

Figure 4.16: Detail of connection between the relieving platform / concrete bar and the MV-piles, distance is in millimetres

4.2.2. Strains in connection bearing piles and relieving platform

There are 2 bearing piles in section C9 which are equipped with FBG sensors to measure the strains in the connection between the bearing piles and the relieving platform. Bearing pile SI-1 is located on the land side and bearing pile SI-2 on the water side, see Figure 4.7. In **Appendix A.2** the measured strains of the bearing piles are presented. As visualised in Figure 4.6 the FBG sensors are placed every 25 centimetres on 8 reinforcement bars that are evenly distributed over the circumference of the bearing pile. The measurements presented in Appendix A.2 are based on the cross-sections shown in the aforementioned figure.

- The reference measurements of the bearing piles are performed only once. Therefore, no checks of the reference measurement have been performed and any errors remain unidentified. If errors during the reference measurement have caused a bias in the data it would still be present in the data.
- There are multiple sensors that show a significant increase in strains and deviate from the other sensors in the cross-section. These deviations are likely causes by drift in the sensors or by very local stress distributions in the pile. In both cases it is not possible to use these deviating sensors for the global pile behaviour.
- From the available data it not possible to identify a trend in the data of the bearing piles regarding the presence of a bending moment. See for example the strains in cross-section E-L, F-K and G-J of bearing pile SI-1. In cross-sections E-L and G-J the yellow line is located below the blue line, whereas in cross-section F-K the yellow line is located above the blue line. This would indicate a double change in the direction of the bending moment over a height of 50 centimetres, which is very unlikely. Therefore, it seems that the strains in the cross-sections are too close to each other to identify the presence of a bending moment. If larger bending moments develop in the future a pattern might become visible in the data.
- The strains in the sensors seem to increase with a constant rate in time. This might be caused by the creep of concrete.

4.2.3. XYZ-deformation

The horizontal deformations parallel to the axis of the quay wall are not considered as these deformations are less relevant for a 2D analysis, in general the deformations parallel to the quay wall are small (<5 mm). From here on if horizontal deformations of the quay wall are mentioned in this thesis it refers to horizontal deformations perpendicular to the axis of the quay wall.

In **Appendix A.3** two types of figures are presented in which the horizontal and vertical deformation of the quay wall are shown. In the first type of figures the horizontal and vertical deformations are presented over the length of the quay wall per zone. The presented deformations in the first type of figures are determined by averaging the results of the 2 measurement bolts located on each side of the concrete front wall.

In the second type of figures the horizontal and vertical deformations are presented for the relevant sections. The presented deformations in the second type of figures are based on the average value of the 4 measurement bolts on each corner of a section. A positive horizontal deformation indicates a displacement towards the water, a negative deformation towards the land. A positive vertical displacement is upwards, whereas negative is downwards. Based on these figures the following remarks are made:

- Each section has a total of 4 measurement bolts, one located on every corner. The measurement bolts located on the same joint should have a similar horizontal deformation as the concrete structure is very stiff. The difference of the measurement results between the two measurement bolts located on the same joint could give an estimation of the measurement error. In Figure 4.17 the difference of the horizontal deformation on each joint is visualised. This figure implies that differences of up to 5 millimetres occur.
- The reference points of the XYZ-measurements are only been measured once at the start of the project. Since many construction processes have taken place near the reference points (corners of the bundwall) deformations could have occurred resulting in errors in the XYZ-measurements.
- A horizontal deformation of 5 à 20 mm towards the landside is measured after the sand fill is in place (first measurement in the figures). This indicates a rotation of the concrete front wall due to the weight of the sand fill. A horizontal deformation towards the landside after the sand fill is in place is often observed at other quay walls in the port of Rotterdam as well (SIF-quay and Euromax-quay).
- Zone A to C (with relieving platform): During the dredging a small horizontal deformation towards the waterside is measured, however the horizontal deformation remains negative at the end of the construction process.
- Zone D (without relieving platform): The concrete front wall is fixed to the combined wall and therefore follows the rotation of the combined wall. During the dredging a horizontal deformation towards the landside is measured, which is most likely caused by a rotation of the combined wall.
- All sections show an increase in the vertical displacement during the dredging. It is likely that this is caused by heave of the soil in front of the quay wall as the bottom level depth increases.

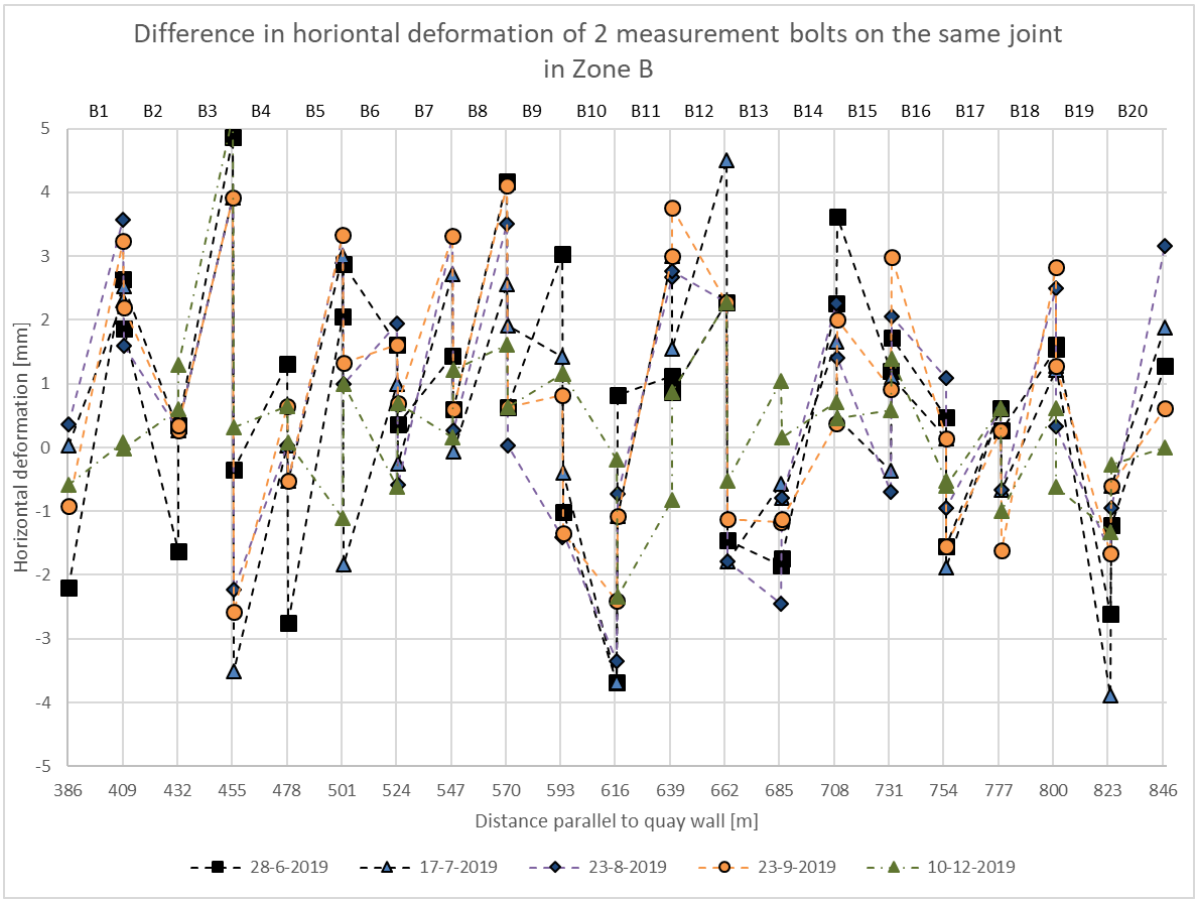

Figure 4.17: Difference in measured horizontal deformation between measurement bolts on the same joint, zone B

4.2.4. Inclinometer

In **Appendix A.4** the measured, relative and absolute horizontal deformations of the combined wall and concrete bar / relieving platform are presented. In section C2 and B14 the casing that guides the inclinometer probe was blocked. Therefore, no inclinometer measurements have been performed at these sections. The absolute deformations are determined by linking the top of the inclinometer measurement to the horizontal deformations of the XYZ-deformations measurements.

In appendix **A.5** the inclinometer results of sections B4 and D1 are compared to other inclinometer measurements in their zone. An example of this comparison is also presented in Figures 4.18 and 4.19. The comparison is made to determine whether the inclinometer results within a zone are in line with each other.

Regarding the inclinometer measurements the following remarks are made:

- The system accuracy is approximately 6.8 mm / 25 m. The height of the inclinometer measurement varies from 34.9 to 39.3 metres. The maximum system measurement error is approximately between ± 9.3 and ± 10.6 millimetres. During the initial phases of the dredging the measured horizontal deformations are small, often <5 millimetres. The possible error in the measurements is larger than the measured displacement during the initial phases. Therefore, the measurements of the initial phases are not used for the analyses.
- In general the maximum measured horizontal deformations increase as the bottom level in front of the quay wall increases.
- In all sections the absolute horizontal deformation of the toe of the combined wall becomes negative (deformation towards the land side), which is very unlikely.

- In the figures in Appendix A.5 it can be seen that the inclinometer results of section B4 and D1 are in line with the results of other sections in their zone. The difference between the inclinometer measurements within a zone have a maximum value of ± 15 mm. This difference is caused by a measurement error and differences in soil conditions.

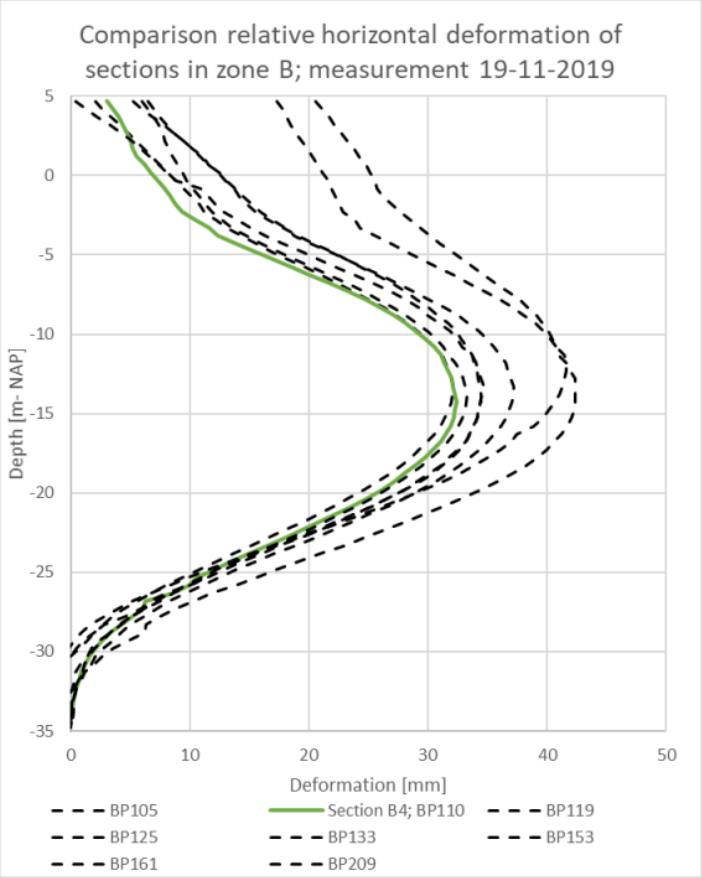

Figure 4.18: Comparison inclinometer measurements in zone B

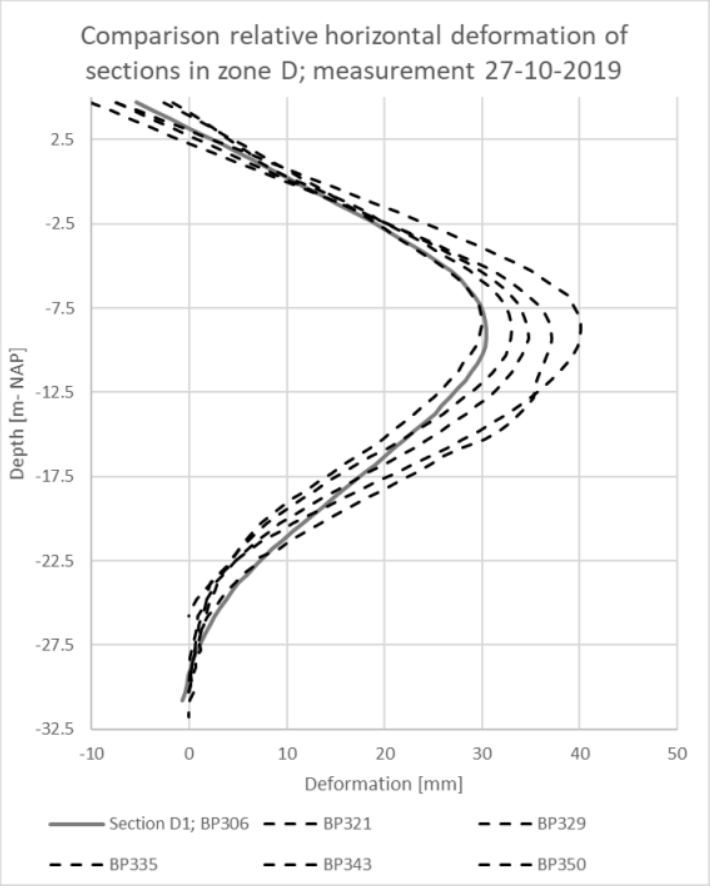

Figure 4.19: Comparison inclinometer measurements in zone D

4.2.5. Water levels

The sensors recording the water levels at the HHTT-quay started working after the completion of the construction process. As a result no direct measurements of the (ground) water levels within the project area are available. However, there are multiple locations within the port of Rotterdam at which the harbour water levels are frequently measured, one of these locations is in the Hartelhaven. The measurement location in the Hartehaven is located at approximately 1 kilometres from the project site. To determine whether the measured water levels in the Hartelhaven are representative for the HHTT-quay a comparison is made between the two. In Figure 4.20 the data is compared over a period of 10 days, from this it is concluded that the water levels from the Hartelhaven can be used for the HHTT quay.

Ground water levels are obtained during the construction process by manually measuring the water level in standpipes. During the construction process the ground water level is lowered by a series of deep wells to a depth of NAP -3 m. A drainage system is present beneath the relieving platform. From the measured water levels after the construction process it is concluded that this drainage system works well and the the ground water level follows the harbour water level, see Figure 4.21. Therefore, no significant water level differences occur during the dredging.

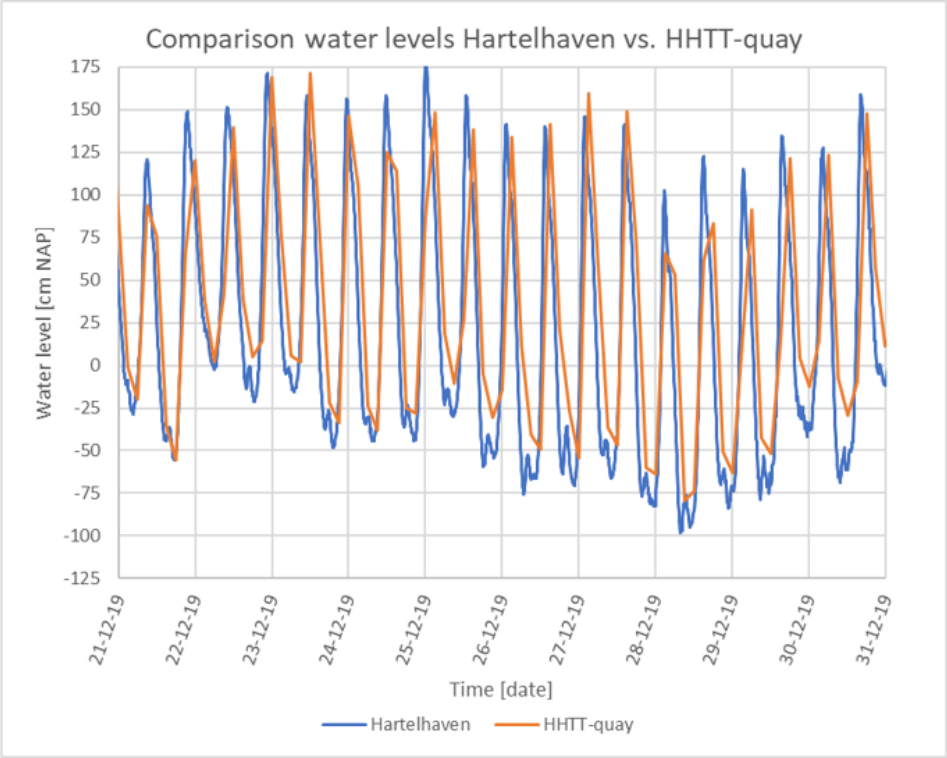

Figure 4.20: Comparison harbour water levels Hartelhaven and HHTT-quay

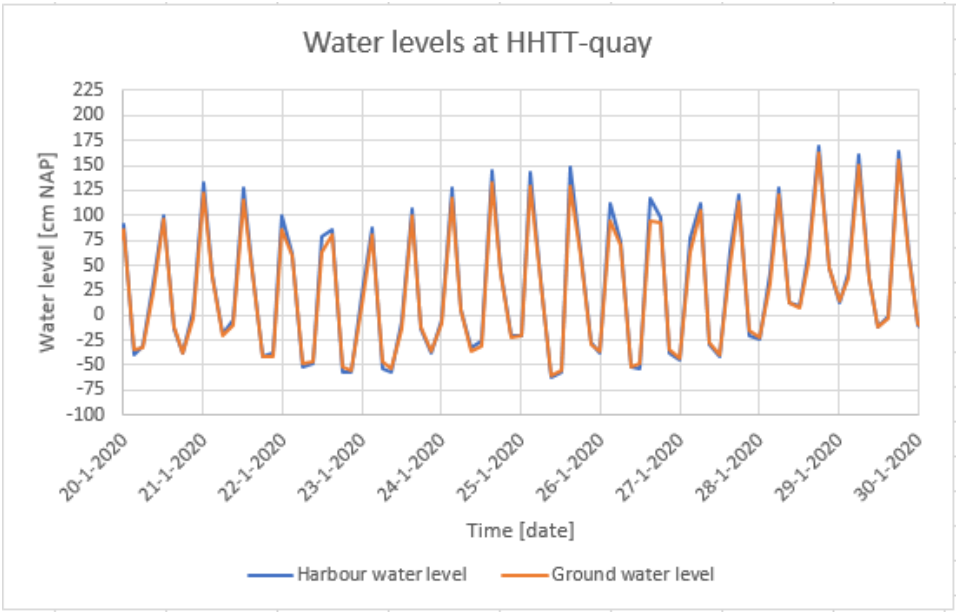

Figure 4.21: Comparison harbour water level and ground water level HHTT-quay after the construction process

4.3. Conclusion

The goal of this chapter was to determine if there is sufficient measurement data of good quality which can be used to gain insight into the behaviour of the quay wall. This seems to be the case for the HHTT-quay. A more detailed description of the available measurement data that is analysed is given below.

Anchor strains

- The design of the FBG sensors is robust to ensure that the FBG sensors have a long lifespan. The downside of this robust design is that there is a lot of material between the FBG sensor and the steel HEB600 profile, e.g. steel plate, epoxy glue and welds. The effect on these materials on the strain transfer between the FBG sensor and the HEB600 profile is unknown. No load tests have been performed on the monitored MV-piles to quantify any possible strains losses between the HEB600 profile en the FBG sensors.
- The reference measurements of the MV-piles are performed only once. Therefore, no checks of the reference measurement have been performed and any errors remain unidentified. If errors during the reference measurement have caused a bias in the data it would still be present in the data.
- Compared to the other MV-piles the data from MV-piles B4 and D1 seems to be most usable for an analysis. It is noted that it is not possible possible to verify the absolute values of the measured strains in MV-piles B4 and D1.

Strains in connection bearing piles and relieving platform

- The reference measurements of the bearing piles are performed only once. Therefore, no checks of the reference measurement have been performed and any errors remain unidentified. If errors during the reference measurement have caused a bias in the data it would still be present in the data.
- There are multiple sensors that show a significant increase in strains and deviate from the other sensors in the cross-section. These deviations might be caused by drift in the sensors or by very local stress distributions in the pile. In both cases it is not possible to use these deviating sensors for the global pile behaviour.
- From the available data it is not possible to identify a trend in the data of the bearing piles regarding the presence of a bending moment. It seems that the strains in the cross-sections are too close to each other to identify the presence of a bending moment. If larger bending moments develop in the future a pattern might become visible in the data.

XYZ-deformations

- The reference points of the XYZ-measurements are only been measured once at the start of the project. Since many construction processes have taken place near the reference points (corners of the bundwall) deformations could have occurred resulting in errors in the XYZ-measurements. It is unknown whether the reference point was a fixed point.
- The difference of the measurement results between the two measurement bolts located on the same joint could give an estimation of the measurement error. In Figure 4.17 the difference of the horizontal deformation on each joint is visualised. This figure implies that differences of up to 5 millimetres occur.
- At the end of the construction process the horizontal deformations of all sections are still negative (5 à 15 mm), meaning that the top of the quay wall has moved towards the land. This phenomena is observed at similar quay walls in the port of Rotterdam, such as the the SIF-quay and Euromax-quay.

Inclinometer

- The system accuracy is approximately 6.8 mm / 25 m. The height of the inclinometer measurement varies from 34.9 to 39.3 metres. The maximum system measurement error is approximately between ± 9.3 and ± 10.6 millimetres. During the initial phases of the dredging the measured horizontal deformations are small, often <5 millimetres. The possible error in the measurements is larger than the measured displacement during the initial phases. Therefore, the measurements of the initial phases are not used for the analyses.
- In general the maximum measured horizontal deformations increase as the bottom level in front of the quay wall increases.
- In all sections the absolute horizontal deformation of the toe of the combined wall becomes negative (deformation towards the land side), which is very unlikely.

Water levels

- The harbour water levels measured at the Hartelhaven are comparable to the harbour water levels at the HHTT-quay. Therefore, the harbour water levels from the Hartelhaven can be used in the analyses
- Due to the presence of the drainage system no significant water level differences occur at the HHTT-quay during the dredging.

The most suitable sections for an analysis in the remainder of this thesis are sections B4 and D1. This is mainly due to the results of the measured anchor strains.

5

Set-up and validation of the a priori model

In this chapter the construction process is set-up in a model. The goal is to predict the behaviour of the quay wall during the construction process as best as possible based on prior knowledge. The model is then validated with the measurement data to determine how good the model is capable of predicting the behaviour of the quay wall.

5.1. Introduction

The construction process is set-up in a model to predict the behaviour of the quay wall. This is done based on prior knowledge, meaning that the measurement data is not considered during the set-up of the model. Since this model is based on prior knowledge it is referred to as an a priori model. The analysis in this chapter are performed in a finite element model (FE model). The a priori FE model is an important step in determining the possibility of optimising the functionality of the quay wall for two main reasons. First of all the a priori FE model gives insight into the local project conditions and the mechanics of the constructed quay wall. Secondly, the a priori FE model acts as a base model from which improvements could be made if a significant difference is present between the a priori FE model results and the measurement data. In the a priori FE model three parameters sets are considered to account for the uncertainty in the input parameters. These sets represent lower bound, mean and upper bound parameter values.

In this chapter section B4 (with relieving platform) and section D1 (without relieving platform) are used. In chapter 4 it is concluded that these two sections provide the most usable measurement data. In Appendix B the cross-sections of sections B4 and D1 are shown. To approach the behaviour of the quay wall it is important to model the geometry as accurate as possible. According to the Port of Rotterdam authority there are no significant deviations between the realised construction and the design, as shown in Appendix B. Therefore, the design drawings are used to determine the structural dimensions and geometry.

5.2. Soil profile

Due to the spatial variability of soil the thickness of a layer is likely to vary, which can ultimately lead to discontinuities such as local vanishing of a layer. The spatial variability of soil can result in uncertainties regarding the soil profile. To reduce these uncertainties as much as possible the thicknesses and presence of the soil layers described in Table 3.2 are based on CPT's located close to the sections used, see Figure 5.3. For section B4 these are CPT's: DKM7, DKM27, DKM55 and DKM56, and for section D1: DKM112, DKM113, DKM212, DKM213, DKM312 and DKM313. In Table 5.1 the soil profile for both sections are shown. The dashes shown in Table 5.1 are used to indicate that a layer is not present in the CPT.

Layer number	Top side layer [m NAP]					
	Cross-section B4			Cross-section D1		
	Axis 1 (DKM7)	Axis 2 (DKM27)	Axis 3 (DKM55 +56)	Axis 1 (DKM112+113)	Axis 2 (DKM212+213)	Axis 3 (DKM312+313)
1	-	Surface level	Surface level	-	Surface level	Surface level
2	-	0.75	1	-	0.5	0.5
3	-	0	0.25	-	-1.5	-2
4	Surface level	-3	-3.5	Surface level	-3	-3
5	-7.5	-7.5	-7.5	-7.5	-7.5	-7.5
6	-12	-12.5	-13	-12.5	-13	-13
7	-18.5	-18.5	-18.5	-19	-19.5	-19.5
8	-20.5	-21	-21	-20.5	-20	-20.5
9	-21	-21.5	-	-	-	-
10	-23	-23	-22.5	-21	-22	-23
11	-30	-30	-30	-30	-30	-30
12	-44	-38	-37	-41	-40	-42

Table 5.1: Soil profile for sections B4 and D1

In Figure 5.1 it can be seen that the CPT's are located on three different axes, which are parallel to the length direction of the quay. Axis 1 is located 25 metres in front of the combined wall in the passive zone, axis 2 is located at the location of the combined wall and axes 3 is located 25 metres behind the combined wall in the active zone.

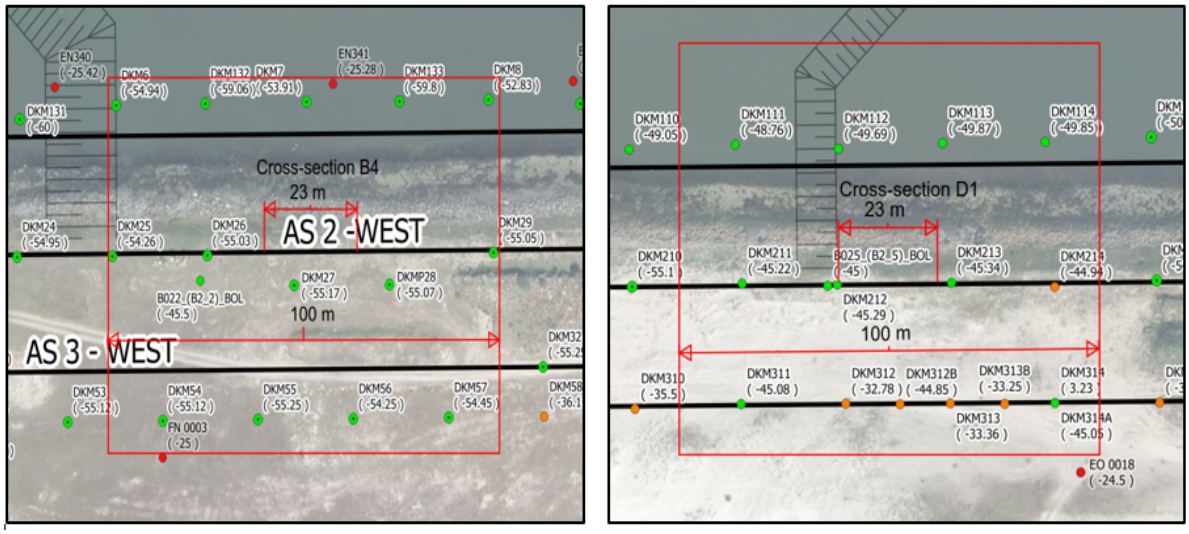

Figure 5.1: Relevant CPT's for sections B1 and D4

5.3. Soil Parameters

Soil parameter determination is a challenging task as soil properties are site specific and vary within a project location due to spatial variability. As a result soil parameters are likely to have a relatively large uncertainty compared to other parameters, such as structural parameters. Soil parameters are determined based on laboratory tests and/or in-situ tests, both have their own pros and cons.

The soil parameters for the a priori FE model are determined based on CPT results and laboratory tests from the soil investigation performed by Wiertsema & Partners Dijkstra [2016, 2017] and Fugro Weijst [2010]. The laboratory tests consisted of classification tests (visual classification, sieve analysis and volumetric weight determination) and triaxial tests.

For laboratory tests there are theoretical defined relations between the parameters and the test results. And these tests are performed under defined boundary conditions. On the other hand, only small volumes of soil are tested so there is little information about the spatial variability, especially if the amount of samples is limited. Even more important is the occurrence of sample disturbance which could significantly influence test results.

In situ-tests, such as the CPT's, rely on empirical correlations for the determination of soil parameters. In-situ tests are cheaper, quicker and easier to perform compared to laboratory tests. Other advantages are that the soil is tested under the in-situ stresses and a larger volume of soil is tested which gives more insight into the spatial variability. The empirical correlations found in literature are often based on soils from different locations to make them valid for a larger range of soil types (different types of sand for example). Therefore, soil parameters determined with empirical correlations will be an estimation as they are not based on site specific correlations.

The goal of the a priori FE model is to estimate the global behaviour of the quay wall as best as possible. The global behaviour of the quay wall is defined by deformations of the quay wall and forces in the structural components such as the MV-piles. The quay wall considered in this thesis is a stiff structure that has the capacity to redistribute forces among the different structural elements. Therefore, the global behaviour of the quay wall is determined by large volumes of soil. This means that small scale fluctuations in the value of a soil parameter average out over the large volume of soil that is responsible for the global behaviour of the quay wall.

As an example 3 data sets are presented in Figure 5.2 that show the variation of parameter c over the height (z) of a soil layer at different locations (x1, x2 and x3). For each data set a layer average is determined ($c_{av}(x)$) and from these layer average values the spatial layer average is determined (μ_C). It is now possible to determine two types of standard deviation, first of all the standard deviation of the local layer average value around the spatial layer average (σ_{av}), secondly the standard deviation of the local fluctuations within a layer around the spatial layer average (σ_f). Since the global behaviour of the quay wall is determined by large volumes of soil the local fluctuations average out and the local layer average becomes governing for its behaviour. This means that the variation of the local layer average around the spatial layer average is more interesting for the behaviour of the quay wall than the small scale fluctuations within a layer.

When determining the spatial layer average, also known as the mean of a layer, there is a certain amount of statistical uncertainty, as the spatial layer average is often determined from a limited amount of samples. To take this statistical uncertainty into account the lower and upper bounds of the spatial layer average are determined as well. The fluctuations of the local layer average values around the spatial layer average values are assumed to be normally distributed for all soil parameters. The process to determine the spatial layer average value of a soil parameter and the upper and lower bounds is explained step by step.

1. Determine local layer average for each CPT and all soil layers
2. Determine the mean of a layer μ (spatial layer average) for each layer
3. Determine the standard deviation from the variation in the local layer averages around the mean value for each layer, σ_{mean}
4. Determine the upper and lower bound of the spatial average for each layer with a 95% confidence interval with equation 5.1 [Calle et al., 2008], in which $t_{n-1}^{0.95}$ is the student t-factor which accounts for a possible statistical error in the standard deviation if the number of samples are low and n is the number of CPT's from which the mean value is determined.

$$X_{5\%} = X_{mean} \pm t_{n-1}^{0.95} \cdot \sigma_{mean} \cdot \sqrt{1 + \frac{1}{n}} \tag{5.1}$$

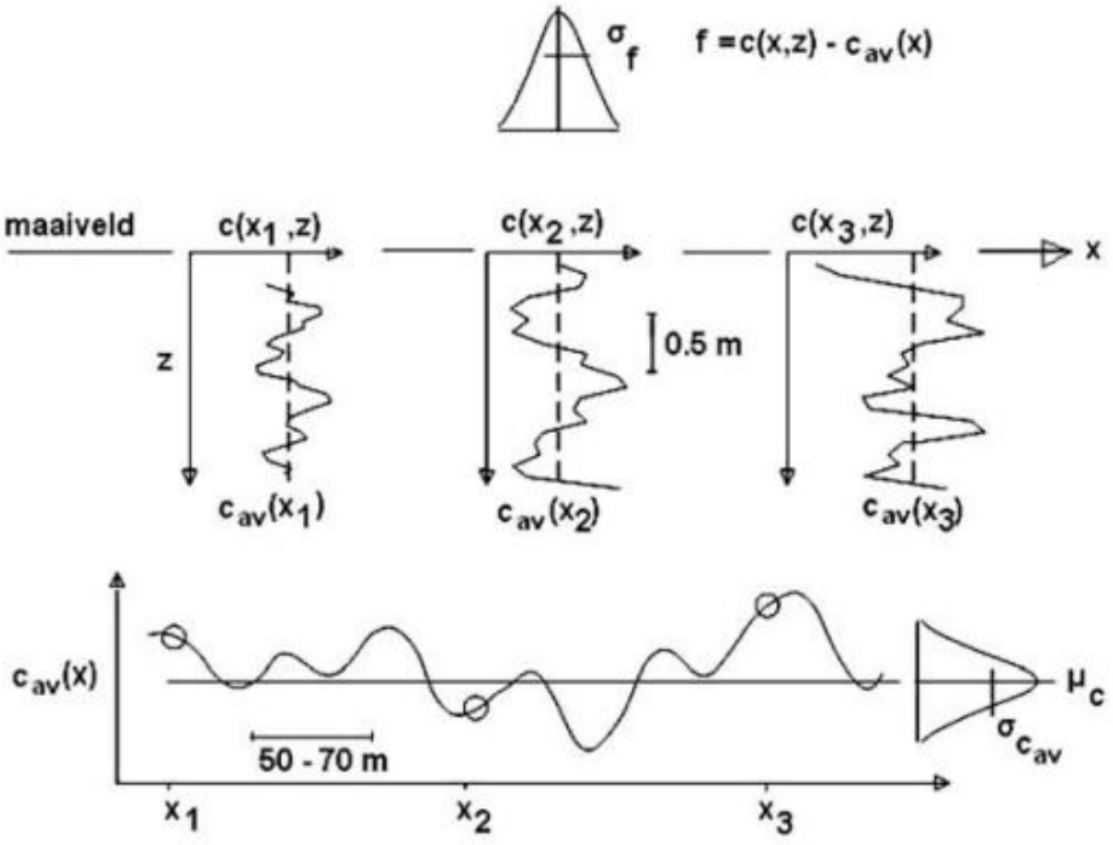

Figure 5.2: Standard deviation of spatial layer average and local fluctuations example [Calle et al., 2008]

5.3.1. Parameters from CPT correlations

In this subsection the soil parameters are determined based on empirical correlations with the cone resistance, qc-values, of the relevant CPT's, see Figure 5.1. This is done for the layers that predominantly consist of sand (layers 1, 3, 4, 5, 6, 7, 9, 10, 11 and 12). For clay layers correlations between soil properties and the cone resistance are not as widely available. Therefore, the properties of layer 2 and 8 are determined with the laboratory tests only. The qc-values of the CPT's close to section B4 and D1 are shown respectively in Figure 5.3 and 5.4.

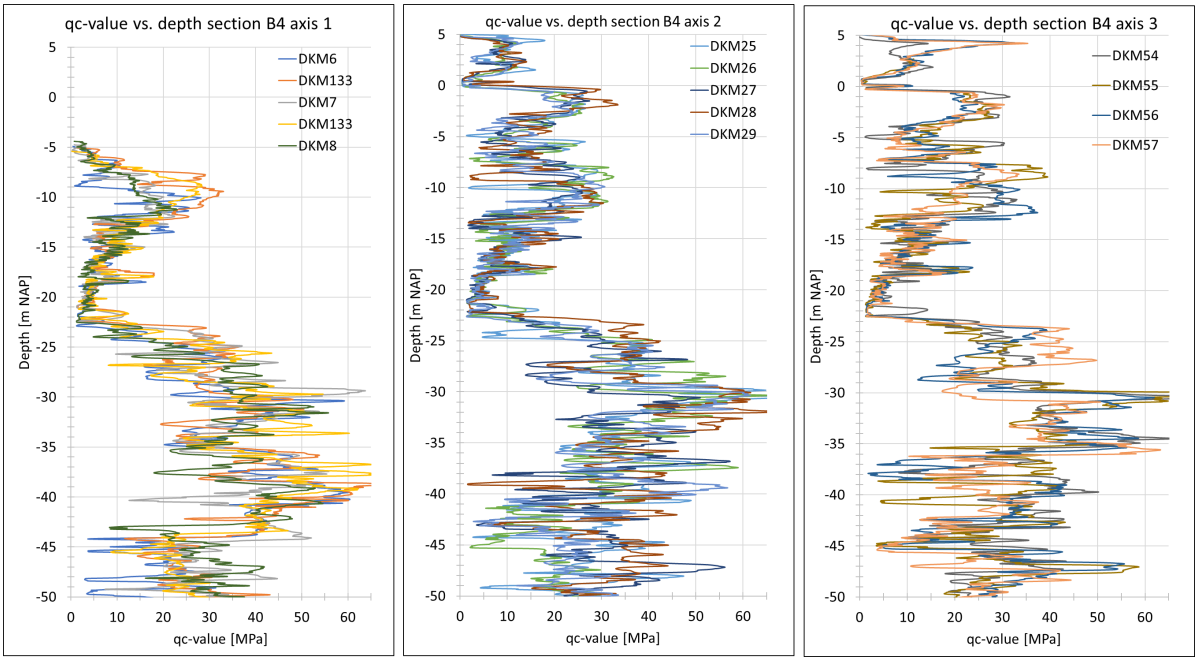

Figure 5.3: qc-value v.s depth CPT's section B4

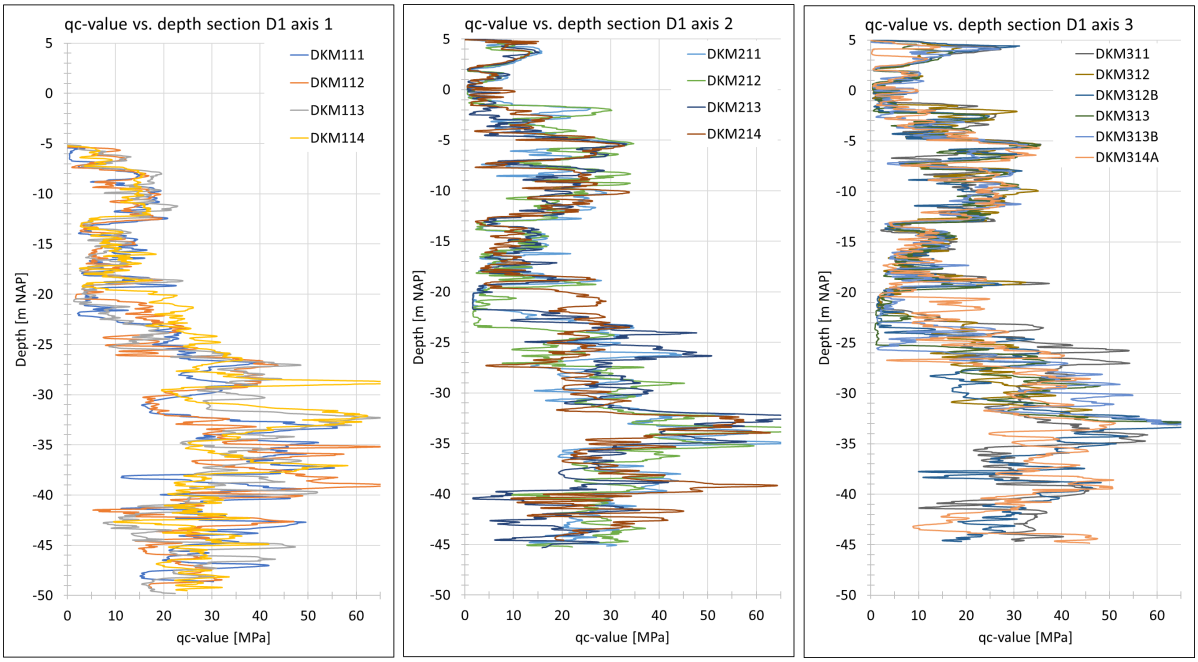

Figure 5.4: qc-value v.s depth CPT's section D1

Relative Density

The strength and stiffness of coarse grained soils, such as sand, largely depend on the in-situ density. It is common practice in geotechnical engineering to describe the in-situ density relative to the maximum and minimum density, the so-called Relative Density (RD), see equation 5.2, in which e is the in-situ void ratio, e_{max} the maximum void ratio and e_{min} the minimum void ratio. The void ratio is a ratio between the volume of the solid soil particles and the volume of the void in between the soil particles. As the RD is often used to determine the properties and parameters of coarse grained soil there are many studies that provide empirical relations between the qc-value and the RD. This thesis

uses the correlation proposed by Jamiolkowski et al. [2003], see equation 5.3, in which q_c is the cone resistance, P_a the atmospheric pressure, σ_v' the vertical effective stress in the soil and C_0, C_1 and C_2 are empirical constants. The sand layers are assumed to be normally consolidated, in that case the empirical constants are C_0 = 17.68, C_1 = 0.5 and C_2 = 3.1. The vertical effective stress is calculated assuming a dry unit weight of 17 kN/m^3 and a saturated unit weight of 20 kN/m^3. In Figure 5.5 the mean, lower and upper bound RD of the sand layers are shown.

$$RD = \frac{e_{max} - e}{e_{max} - e_{min}} \tag{5.2}$$

$$RD = \frac{1}{C_2} \cdot \frac{q_c}{C_0 \cdot P_a \cdot \left(\frac{\sigma_v'}{P_a}\right)^{C_1}} \tag{5.3}$$

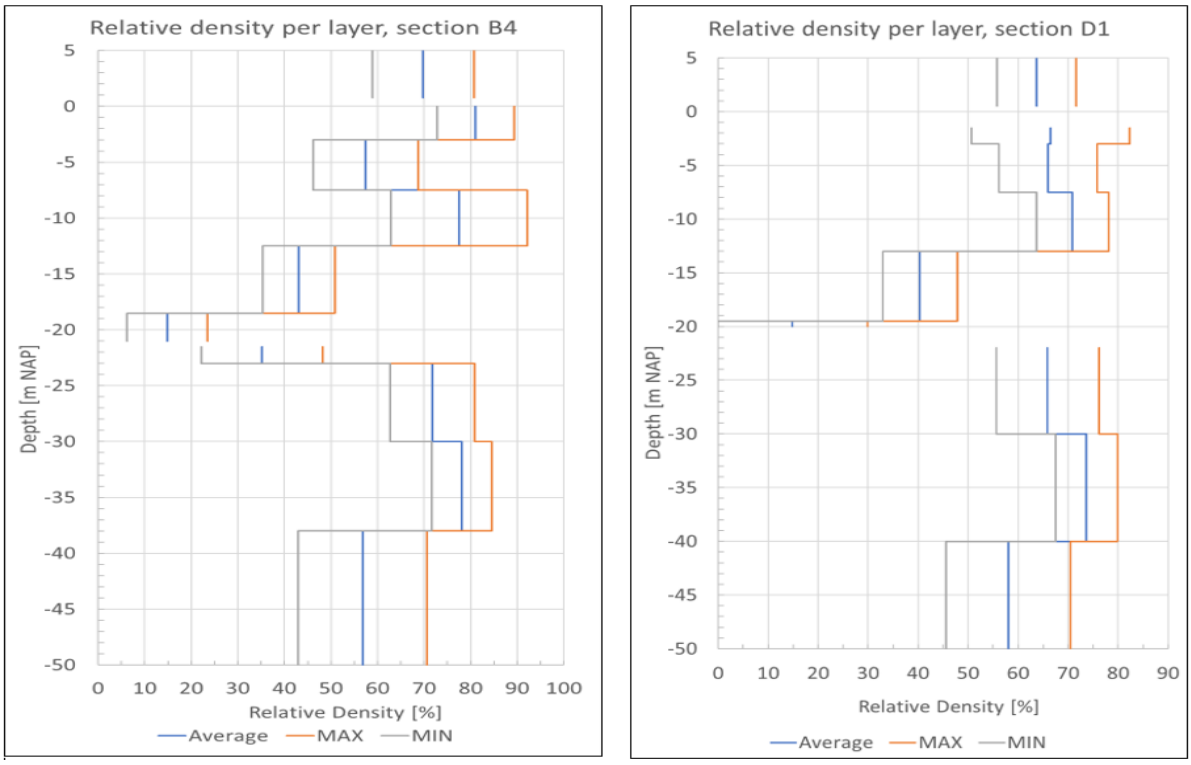

Figure 5.5: Relative Density vs. depth for both sections

Peak friction angle and dilatancy angle

Mayne and Kulhawy [1990] define a correlation between the peak friction angle and the qc-value that accounts for the non-linear normalization of qc with the effective vertical stress. This correlation is derived from data of Calibration Chamber Tests on 26 different types of clean sand. In another study Mayne [2001] showed that a good fit between the correlation and triaxial test results was acquired for a silty sand (up to 30% of fines) as well. The correlation is shown in equation 5.4, in which σ_v' is the vertical effective stress and P_a is the atmospheric pressure. In Figure 5.6 the friction angle of all sand layers are shown versus the depth for both sections. The dilatancy angle is determined from the RD based on the correlation described by Brinkgreve et al. [2010], see equation 5.5. The graphs of the dilatancy angle versus depth are shown in Appendix C.1.

$$\phi'_p = 17.6 + 11 \cdot log\left(\frac{\frac{q_c}{Pa}}{\left(\frac{\sigma'_v}{Pa}\right)^{0.5}}\right) \tag{5.4}$$

$$\psi = -2 + \frac{12.5 D_r}{100}[^\circ] \tag{5.5}$$

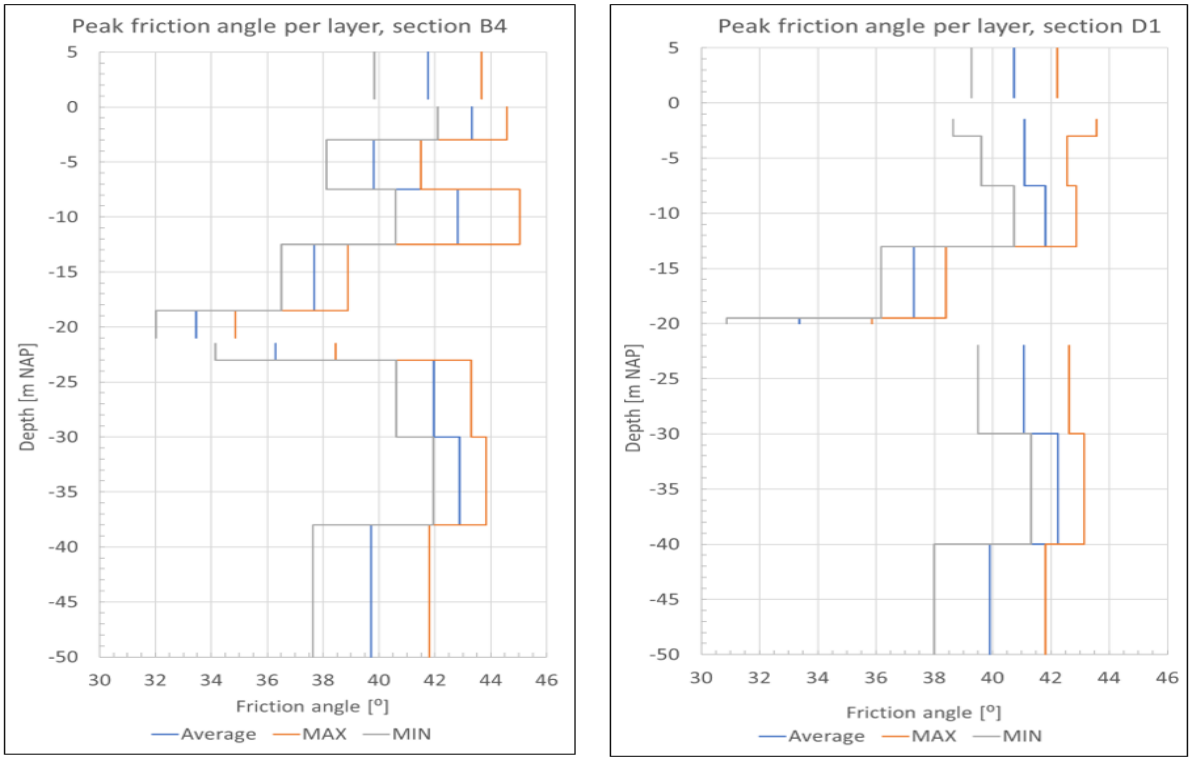

Figure 5.6: Friction angle vs. depth for both sections

Stiffness moduli

In equation 5.6 a correlation between the constrained tangent stiffness modules, E_{oed}, the qc-value and the RD in the case of normally consolidated coarse grained soils is given [Mayne and Kulhawy, 1990]. The stiffness moduli in the HS model are stress-dependent. Therefore, the input stiffness moduli are expressed relative to a reference stress level, p^{ref}, which is set to 100 kPa. In equation 5.7 the constrained tangent stiffness modulus is converted to a reference stress level, in this equation σ'_v is the vertical effective stress and m is the power function.

$$E_{oed} = q_c \cdot 10^{1.09 - 0.0075 \cdot RD} \tag{5.6}$$

$$E_{oed}^{ref} = E_{oed} / \left(\frac{\sigma'_v}{p_{ref}}\right)^m \tag{5.7}$$

The reference constrained tangent modulus, E_{oed}^{ref}, and the reference unloading/reloading stiffness modulus, E_{ur}^{ref}, for sand layers are derived from the reference constrained tangent modulus, E_{oed}^{ref}, by the following relations [Brinkgreve, 2019a, CUR, 2003, Obrzud and Truty, 2018]:

- $E_{50}^{ref} \approx E_{oed}^{ref}$
- $E_{ur}^{ref} \approx 3{*}E_{50}^{ref}$

In Appendix C.1 graphs are presented in which the reference stiffness moduli are plotted in depth for all sand layers.

Power parameter

The power parameter m, which accounts for the stress-dependency of the stiffness moduli, is based on a correlation with the RD, given by Brinkgreve et al. [2010].

$$m = 0.7 - \frac{D_r}{320}[-] \tag{5.8}$$

Statistical parameters derived from CPT correlations

In Table 5.2 an overview is presented of the derived mean value, standard deviation and coefficient of variation for each soil layer. The coefficient of variation (V) is the ratio between the standard deviation and the mean value of a parameter. The presented standard deviation and coefficient of variation are related to the variance of the mean value of the distribution.

Layer	Parameter	ϕ_p' [°]		ψ [°]		E_{oed}^{ref} [MPa]		E_{50}^{ref} [Mpa]		E_{ur}^{ref} [Mpa]		m [-]	
		B4	D1	B4	D1	B4	D1	B4	D1	B4	D1	B4	D1
1	μ	42.0	41.0	7.0	6.0	60	60	60	60	180	180	0.48	0.50
	σ_{mean}	1.1	0.5	0.6	0.5	8	8	8	8	24	25	0.02	0.03
	V_{mean}	0.03	0.01	0.08	0.09	0.13	0.14	0.13	0.14	0.13	0.14	0.04	0.05
3	μ	43.5	41.0	8.0	6.5	65	55	65	55	195	165	0.45	0.50
	σ_{mean}	0.5	1.4	0.6	0.8	5	8	5	8	16	25	0.01	0.03
	V_{mean}	0.01	0.03	0.08	0.13	0.08	0.15	0.08	0.15	0.08	0.15	0.03	0.05
4	μ	40.0	41.0	5.0	6.5	50	55	50	55	150	166	0.52	0.50
	σ_{mean}	0.8	0.8	0.9	0.5	3	3	3	3	8	8	0.02	0.01
	V_{mean}	0.02	0.02	0.17	0.08	0.05	0.05	0.05	0.05	0.05	0.05	0.04	0.03
5	μ	43.0	41.5	7.5	7.0	65	60	65	60	195	180	0.46	0.48
	σ_{mean}	1.1	0.8	1.1	0.5	8	3	8	3	24	8	0.02	0.01
	V_{mean}	0.03	0.02	0.14	0.08	0.12	0.05	0.12	0.05	0.12	0.05	0.05	0.03
6	μ	37.5	37.5	3.5	3.0	40	40	40	40	121	120	0.57	0.57
	σ_{mean}	0.8	0.5	0.4	0.5	3	3	3	3	8	8	0.01	0.01
	V_{mean}	0.02	0.01	0.12	0.18	0.06	0.07	0.06	0.07	0.06	0.07	0.02	0.02
7	μ	33.5	33.5	0.5	0.0	25	25	25	25	75	75	0.65	0.65
	σ_{mean}	0.8	1.4	0.3	0.0	3	5	3	5	8	16	0.01	0.03
	V_{mean}	0.02	0.04	0.53	-	0.11	0.22	0.11	0.22	0.11	0.22	0.02	0.04
9	μ	36.5	-	3.0	-	35	-	35	-	105	-	0.59	-
	σ_{mean}	0.8	-	0.6	-	5	-	5	-	16	-	0.02	-
	V_{mean}	0.02	-	0.20	-	0.15	-	0.15	-	0.15	-	0.04	-
10	μ	42.0	41.0	7.0	6.0	60	55	60	55	180	164	0.48	0.49
	σ_{mean}	0.6	0.8	0.6	0.8	3	3	3	3	8	9	0.02	0.02
	V_{mean}	0.01	0.02	0.09	0.14	0.04	0.05	0.04	0.05	0.04	0.05	0.03	0.04
11	μ	43.0	42.0	8.0	7.0	65	60	65	60	195	181	0.46	0.47
	σ_{mean}	0.5	0.5	0.3	0.5	3	2	3	2	8	7	0.01	0.01
	V_{mean}	0.01	0.01	0.04	0.08	0.04	0.04	0.04	0.04	0.04	0.04	0.02	0.02
12	μ	39.5	40.0	5.0	5.5	50	50	50	50	150	150	0.52	0.52
	σ_{mean}	1.3	1.1	1.0	0.8	5	5	5	5	16	16	0.02	0.02
	V_{mean}	0.03	0.03	0.19	0.15	0.11	0.11	0.11	0.11	0.11	0.11	0.04	0.04

Table 5.2: Mean values and standard deviation determined from CPT results

5.3.2. Parameters from laboratory tests

The laboratory tests consist of classification tests (visual classification, sieve analysis and volumetric weight determination) and triaxial tests. These tests are performed on soil samples which are taken from different depths along the length of the boreholes. If executed carefully it is possible to retrieve soil samples from a cohesive soil, such as clay, without significant disturbance of the in-situ compaction of the soil. Laboratory tests on cohesive soils are potentially valuable as the soil is tested close the in-situ compaction. For sand layers, where there is no cohesion, there is a method to retrieve 'undistributed' samples, however this method is rarely applied as it is quite expensive and time consuming. For the HHTT-quay the sand samples are disturbed samples, meaning that the in-situ compaction of the sand is lost. Therefore, the sand samples must be reconstructed in the laboratory, which introduces uncertainties as the in-situ compaction of the sand is difficult to determine.

For the disturbed sand samples the results of the laboratory tests are governed by the relative density of the samples. As the void ratio of each sand sample is measured prior to the test it is possible to estimate the RD of each sample. This is done by using equation 5.2 and assuming a maximum void ratio of 0.9 and a minimum void ratio of 0.45 [CUR, 2003]. The laboratory results of the sand samples can then be plotted versus the relative density of the samples. This allows for a better estimation of the parameters.

Volumetric unit weight
The unit weight of the soil layers are determined from the results of the laboratory volumetric weight tests, which can be found in the geotechnical laboratory report [Dijkstra, 2017]. From layer 2 and 8, the clay layers, undisturbed samples are taken. Thus the measurements are likely to represent the in-situ volumetric weight. The dry volumetric unit weight of the clay layers is assumed to be equal to the fully saturated unit weight. In Figure 5.7 the test results of the sand samples are plotted versus the RD, the linear regression line drawn through the results shows a good fit.

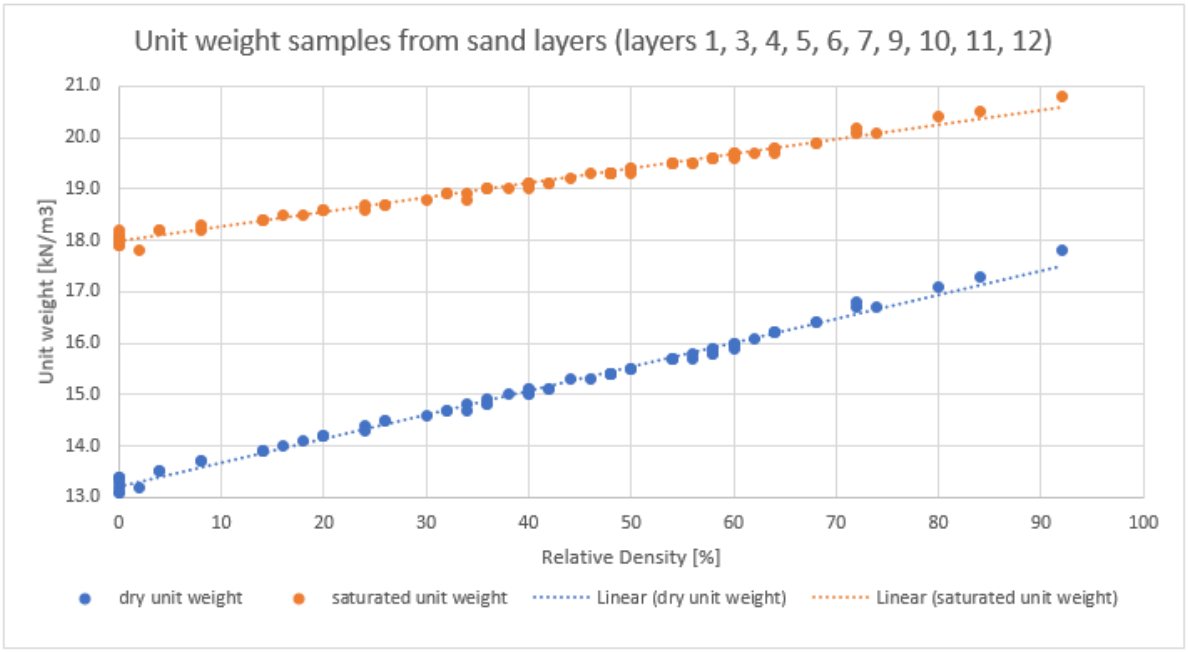

Figure 5.7: Relative Density vs. Unit weight sand layers

In table 5.3 the average unit weight of all layers are shown. For the sand layers the average unit weight is determined based on the average in-situ RD as shown in Figure 5.5. For the clay layers the average unit weight is determined from the average result of the laboratory tests. The difference in the unit weight of a layer between section B4 and D1 is small and is therefore neglected.

Layer number	1	2	3	4	5	6	7	8	9	10	11	12
γ_{dry} [kN/m^3]	16.5	15.5	17.0	16.0	17.0	15.0	14.0	16.5	15.0	16.5	17.0	16.0
γ_{sat} [kN/m3]	20.0	15.5	20.5	19.5	20.0	19.0	18.5	16.5	19.0	20.0	20.5	20.0

Table 5.3: Unit weight layers in kN/m^3

Triaxial tests

If properly executed triaxial tests can give valuable insight into the characteristics and properties of the soil. A general description of a triaxial test can be found in the guideline for laboratory tests [SBR-CUR, 2017]. Different types of triaxial test exist, which are: Consolidated Drained (CD), Consolidated Undrained (CU) and Unconsolidated Undrained (UU). The sand samples are subjected to CD triaxial test. During a CD triaxial test the excess pore water pressure is allowed to dissipate and thus a volume change of the soil sample is possible. The clay samples are subjected to CU triaxial tests, in which the dissipation of excess pore water pressure is prevented, and no volume change can occur as a result. In Appendix C.2 the triaxial tests results are presented.

The secant stiffness modulus, E_{50}, is calculated from the triaxial tests with equation 5.9 in which $q_{peak;50}$ is 50% of the total deviatoric stress at failure and $\epsilon_{1;50}$ is the corresponding vertical strain in percentage. The secant stiffness modulus of each triaxial test is converted to a reference stress level of 100 kPa with equation 5.10. In which m is the power function (assume m=0.5 for sand and m=1 for clay) and f is a correction factor for undrained behaviour, for a CD triaxial test f=1.0 and for a CU triaxial test f=0.7 [CUR, 2003].

$$E_{50} = \frac{q_{peak;50}}{\epsilon_{1;50}} \cdot 100 \tag{5.9}$$

$$E_{50}^{ref} = f \cdot E_{50} / \left(\frac{\sigma_3'}{p_{ref}} \right)^m \tag{5.10}$$

From the reference secant stiffness modulus, E_{50}^{ref}, the other reference stiffness moduli are determined based on the following relations [Brinkgreve, 2019a, CUR, 2003, Obrzud and Truty, 2018]:

- Sand layers
  - $E_{50}^{ref} \approx E_{oed}^{ref}$
  - $E_{ur}^{ref} \approx 3{*}E_{50}^{ref}$
- Clay layers
  - $E_{50}^{ref} \approx 2{*}E_{oed}^{ref}$
  - $E_{ur}^{ref} \approx 3{*}E_{50}^{ref}$

The friction angle is determined at 2% strain, 5% strain and at the peak strength. For the sand samples which where tested under consolidated drained circumstances the friction angle of each test is plotted versus the RD of the sample. The friction angle for triaxial compression conditions, ϕ_{tc}' of the sand samples is based on the mean effective stress s' and the deviatoric stress t with equation 5.13 [Head and Epps, 2014]. The effective cohesion of the sand samples are assumed to be zero.

$$s' = \frac{\sigma_1' + \sigma_3'}{2} \tag{5.11}$$

$$t = \frac{\sigma_1 - \sigma_3}{2} \tag{5.12}$$

$$\phi'_{tc} = \sin^{-1}\left(\frac{t}{s'}\right) \tag{5.13}$$

The results of the clay samples, which were tested under consolidated undrained conditions, are plotted in the s-t space, see equation 5.11 and 5.12. For each clay layer a linear regression line is fitted through the data points, which is described by y=a*s'+b. From the characteristics of the linear regression line the effective friction angle under triaxial compression conditions, ϕ'_{tc}, and effective cohesion, c', are determined with the following equations:

$$\phi'_{tc} = \sin^{-1}(a) \tag{5.14}$$

$$c' = \frac{b}{\cos(\phi')} \tag{5.15}$$

In a triaxial test the lateral stress is equal on both of the lateral planes (σ_2 = σ_3). Whereas, in plane strain conditions one of the lateral planes is confined and thus has higher stresses than the unconfined lateral plane. Consequently, the friction angle under plane strain conditions is different than under triaxial compression conditions. According to Wroth [1984] the relation between the friction angle under plane strains conditions and triaxial compression conditions can be described by equation 5.16. According to Teunissen [2016] it is valid to use the friction angle under plane strain conditions when calculations are performed in a FE model. Therefore, the friction angles determined with triaxial test results should be converted to a friction angle for plane strain conditions by equation 5.16.

$$\phi'_{ps} = \frac{9}{8} \cdot \phi'_{tc} \tag{5.16}$$

Based on the equations described in this section the triaxial test results are analysed and several graphs have been made, which are presented in Appendix C.2. From these graphs the soil parameters for each soil layer are determined. For the sand layers the average in-situ RD values are used to determine the soil parameters from the graphs presented in Appendix C.2.

For layers 1, 3, 4, 5, 9, 10, 11 and 12, which are clean sand layers, the peak friction angle occurred at approximately 4% strain. For the other layers, containing a larger amount of silt or clay, the peak friction angle occurred at strain levels larger than 5%. It is assumed that during the construction process the strain levels are between 2 and 5%. Therefore, the peak friction angle is used for layers 1, 3, 4, 5, 9, 10, 11 and 12. And the friction angle at 5% axial strain is used for the layers 2, 6, 7 and 8. This is because the peak friction angle of layers 2, 6, 7 and 8 occurs beyond 5% strain, and these strain levels are not expected to occur during the construction process.

5.3.3. Soil parameters a priori FE model

The soil parameters determined from the CPT's and laboratory tests are summarized in Appendix C.3. The parameters determined with the CPT correlations and the laboratory tests are compared, which resulted in the following remarks:

- Volumetric weight
  - For most layers the difference between the maximum and minimum volumetric weight is 1 kN/m^3 the influence of this variation is assumed to be small. Therefore, the volumetric weight of the layers is fixed to the average value.

- Peak friction angle
  - In Figure 5.8 the average peak friction angles determined with the CPT correlation, $\phi'_{p;CPT}$, and the triaxial tests, $\phi'_{p;triaxial;ps}$ are compared. The average peak friction angle of the triaxial test are already converted to plane strain conditions (so including the 9/8 factor). For the clean sand layers (1, 3, 4, 5, 9, 10, 11 and 12) $\phi'_{p;triaxial;ps}$ is larger than $\phi'_{p;CPT}$, the difference between the two is approximately a factor 9/8. This difference is visualised by the grey dots, which are the $\phi'_{p;CPT}$ values multiplied by 9/8. It appears that the difference between the two is caused by the plane strain conversion factor. The CPT correlation of Mayne and Kulhawy [1990] is calibrated using triaxial test results. Therefore, the peak friction angles calculated with the CPT correlation are valid for triaxial test conditions. If the CPT correlation is multiplied by a factor 9/8 it shows a good match with the triaxial test data.
  - For soil layers 6 and 7, which have a high percentage of fines, $\phi'_{p;CPT}$ is more or less equal to $\phi'_{p;triaxial;ps}$, taking the previous remark into account it seems that for layer 6 and 7 the CPT correlation overestimates the peak friction angle for plane strain conditions.
  - For the sand layers the average peak friction angle calculated with the triaxial test results, $\phi'_{p;triaxial;ps}$, is used for the a priori FE model. For the maximum and minimum values of the peak friction angle the range determined with the CPT correlation is used.
  - For the clay layers (2 and 8) the average peak friction angle calculated with the triaxial test results, $\phi'_{p;triaxial;ps}$, is used for the a priori FE model as well as there are no results for the CPT correlation. The range of the peak friction angle is assumed to be 2°.
- Effective cohesion
  - The effective cohesion of the clay layers is based on the triaxial test results. The sand layers are assumed to have no cohesion. However, to make the Fe model more stable the cohesion of the sand layers is set to 1 kPa.
- Stiffness moduli
  - The average stiffness moduli based on the CPT correlation are slightly higher than those based on the triaxial test results. Since the triaxial test results are based on local soil samples it is decided to use the results of the triaxial tests. Therefore, the average stiffness moduli used in the a priori FE model are those determined with the triaxial test results.
- m-parameter
  - The m-parameter value of each layer is comparable for sections B4 and D1. Therefore, these are not regarded separately. The m-parameters determined with the correlation are rounded to the closest 0.05 value. For the clay layers the m-parameter is set to 1.0 according to Brinkgreve et al. [2010].

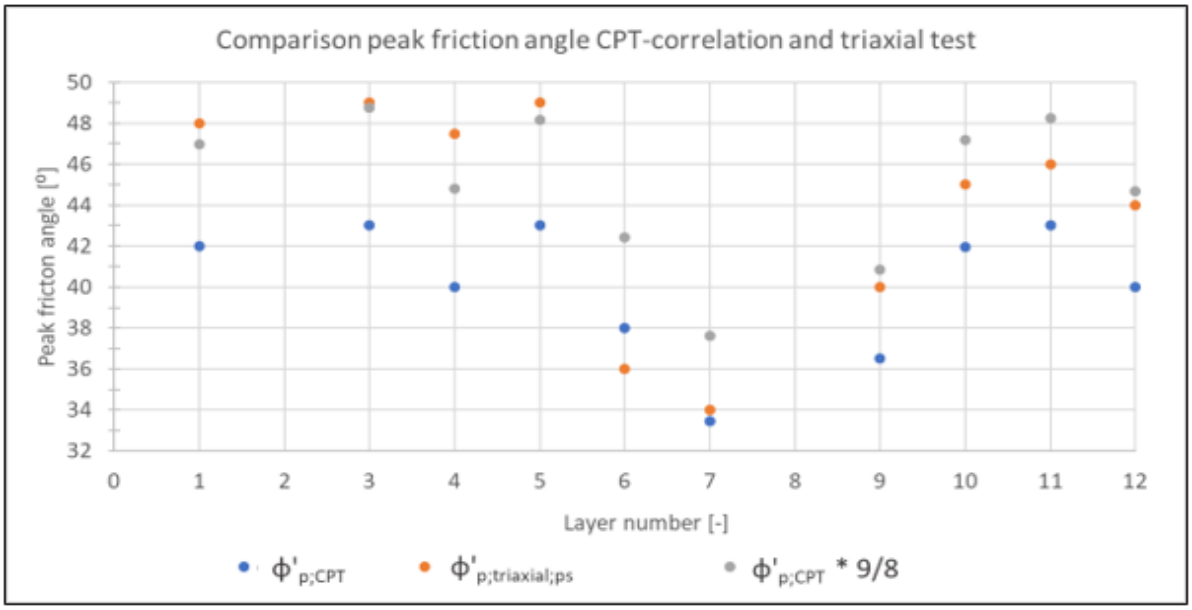

Figure 5.8: Comparison peak friction angles CPT's and triaxial test

The soil parameters that are used in the a priori FE model are shown in Table 5.4. Additional input parameters such as Poisson's ratio or the interface stiffness are presented in Table 5.5.

layer number		1		2[1]		3		4		5		6[1]		7[1]		8[1]		9		10		11		12	
Cross-section		B4	D1	B4	D1	B4	D1	B4	D1	B4	D1	B4	D1	B4	D1	B4	D1	B4	D1	B4	D1	B4	D1	B4	D1
γ_{dry} [kN/m^3]	Average	16.5		15.5		17.0		16.0		17.0		15.0		14.0		16.5		15.0		16.5		17.0		16.0	
γ_{sat} [kN/m^3]	Average	20.0		15.5		20.5		19.5		20.0		19.0		18.5		16.5		19.0		20.0		20.5		20.0	
ϕ_p' [°]	Average	48.0	48.0	32.0	32.0	49.0	48.0	47.5	48.0	49.0	48.5	36.0	36.0	34.0	34.0	32.0	32.0	40.0	-	45.0	44.5	46.0	45.5	44.0	43.5
	Min	46.0	47.0	30.0	30.0	48.0	55.5	46.0	46.5	47.0	47.5	35.0	35.0	32.5	31.5	30.0	30.0	38.0	-	43.5	43.0	45.0	44.5	42.0	41.5
	Max	50.0	49.0	34.0	34.0	50.0	50.5	49.0	49.5	51.0	49.5	37.0	37.0	35.5	36.5	34.0	34.0	42.0	-	46.5	46.0	47.0	46.5	46.0	45.5
ψ [°]	Average	6.5	6.0	-	-	8.0	6.5	5.0	6.5	7.5	7.0	3.5	3.5	0.0	0.0	-	-	2.0	-	7.0	6.0	8.0	7.0	5.0	5.0
c' [kPa]	Average	1	1	8	8	1	1	1	1	1	1	1	1	1	1	10	10	1	-	1	1	1	1	1	1
E_{oed}^{ref} [MPa]	Average	50	45	3	3	70	60	45	45	50	45	30	30	8	8	3	3	30	-	45	45	50	50	40	40
	Min	35	30	2	2	60	50	40	40	35	40	25	25	5	5	2	2	25	-	40	40	45	45	30	30
	Max	65	60	4	4	80	70	50	50	65	50	35	35	10	10	4	4	35	-	50	50	55	55	50	50
E_{50}^{ref} [Mpa]	Average	50	45	5	5	70	60	45	45	50	45	30	30	8	8	6	6	30	-	45	45	50	50	40	40
	Min	35	30	4	4	60	50	40	40	35	40	25	25	5	5	4	4	25	-	40	40	45	45	30	30
	Max	65	60	6	6	80	70	50	50	65	50	35	35	10	10	8	8	35	-	50	50	55	55	50	50
E_{ur}^{ref} [Mpa]	Average	150	135	25	25	210	180	135	135	150	135	90	90	24	24	30	30	90	-	135	135	150	150	125	125
	Min	105	90	20	20	180	150	120	120	105	120	75	75	15	15	20	20	75	-	120	120	135	135	90	90
	Max	195	180	30	30	240	210	150	150	195	150	105	105	30	30	40	40	105	-	150	150	165	165	150	150
m [-]	Average	0.50		1.00		0.45		0.50		0.50		0.55		0.65		1.00		0.60		0.50		0.45		0.50	

Table 5.4: Soil parameters a priori FE model; [1] friction angle is determined for 5% strain level since peak friction angle occurred at >5% and this does not coincide with clean sand layers

Parameter	Symbol	Unit	Value
Coefficient of eart pressure	$K_{0;NC}$	[-]	1 - sinϕ'
Poisson' ratio	v	[-]	0.2
Reference stress	p_{ref}	[kPa]	100
Failure ratio	R_f	[-]	0.9
Interface stiffness	R_{inter}	[-]	0.8

Table 5.5: Additional input parameters

In literature no information was found about the overconsolidation of the soil layers in the port of Rotterdam area. Therefore, it is unknown if the soil layers are overconsolidated. The overconsolidation ratio (OCR) does have an influence on the horizontal deformations of the combined wall. If the OCR of the soil layers is kept equal to 1 horizontal deformations of the combined wall develop early in the construction process, without any significant loads on the quay wall. These early developments of horizontal deformations do not seem to match with reality. Therefore, a small OCR of 1.5 is given to the Pleistocene sand layers (layers 9, 10, 11 and 12).

5.4. Modelling the construction phases

Based on information provided by the construction company the construction process is divided in multiple phases. In this section the relevant construction phases are explained. In the illustrations shown below the height references are given in metres to NAP and the width measurements are in millimetre.

- Phase 0: Initial phase

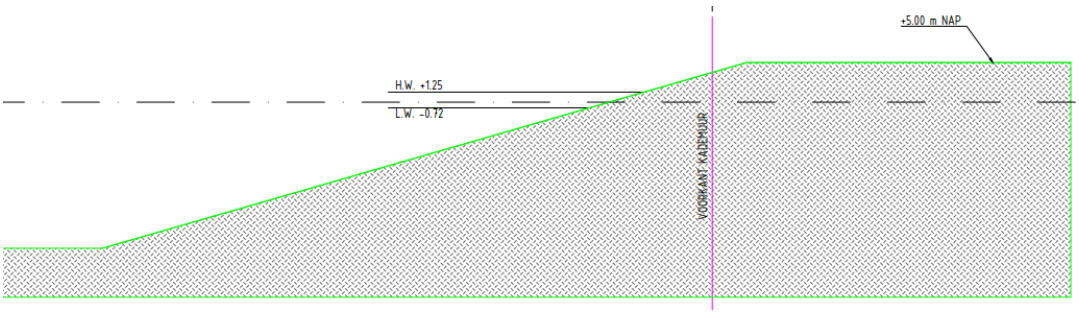

  - Initial phase with a natural slope 1:4 from NAP +5.0 m to NAP -24.5 m
- Phase 1A and 1B: excavation of soil and construction of temporary MV-platform

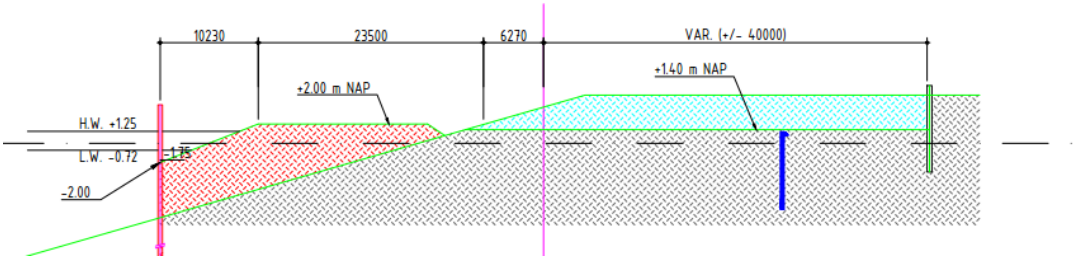

  - Phase 1A: Installation of temporary sheet pile walls (both sides of the building pit) and excavation of soil to NAP +1.4 m. The temporary sheet pile walls are modelled as slopes to reduce the complexity of the model. The applied slope angles are 1:2.
  - Phase 1B: construction of the MV-platform to NAP +2.0 m. The clay layer (layer 2) is removed and replaced by sand to improve the stability of the MV-platform.
- Phase 2: Installation and activation of drainage system in building pit
  - The drainage system is set to reduce the water table inside the building pit to NAP -3.0 m.
- Phase 3: Excavation of soil to NAP -2.10 m

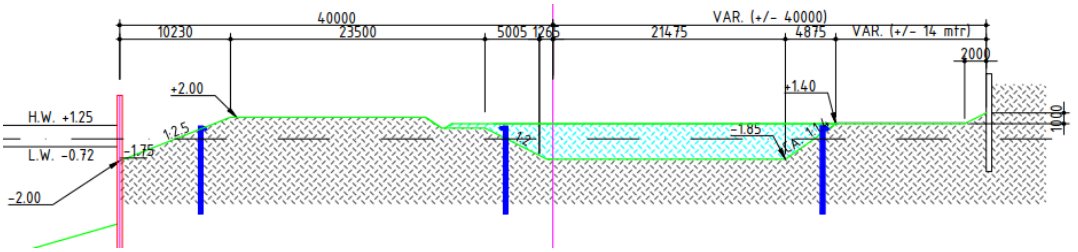

  - The height difference is accounted for by a slope with an angle of 1:2.

- Phase 4: Installation of bearing piles (only applies for section B4)

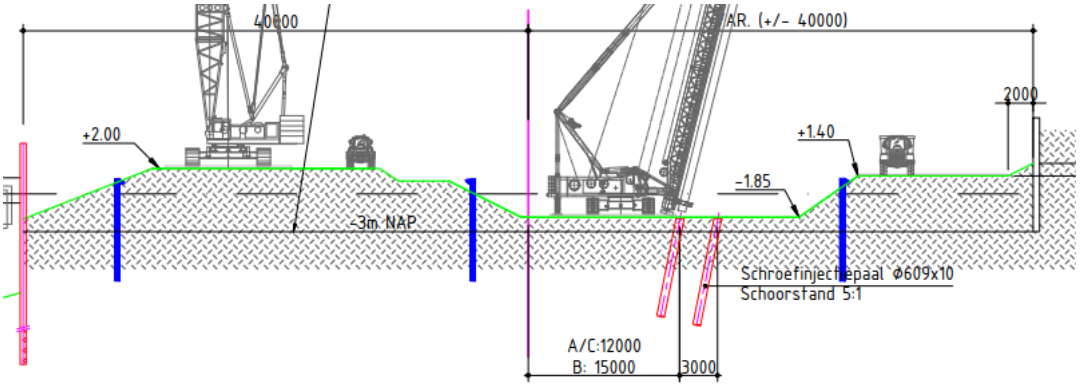

- Phase 5: Installation combined wall

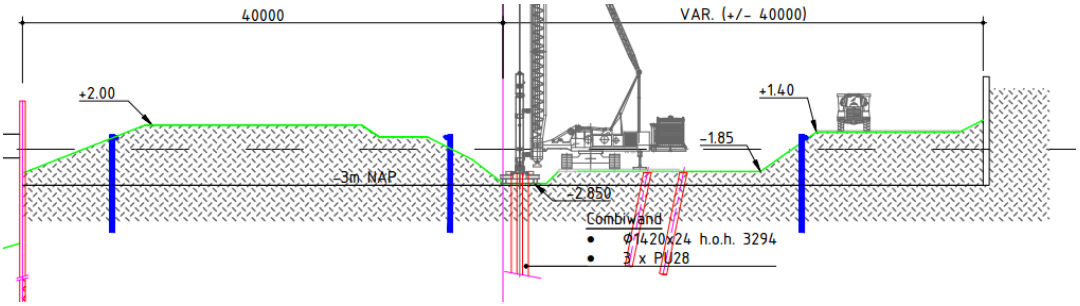

  - A narrow trench to a depth of NAP -2.85 m is dug out to be able to install the combined wall
- Phase 6: Installation of MV-piles

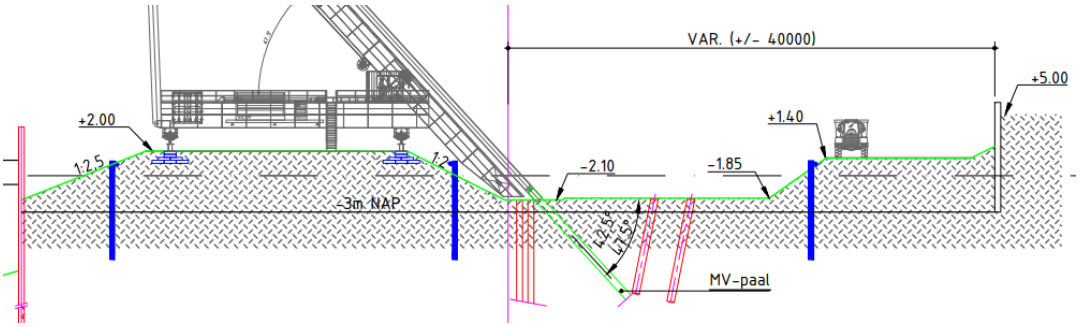

- Phase 7: Construction of the concrete relieving platform / concrete bar

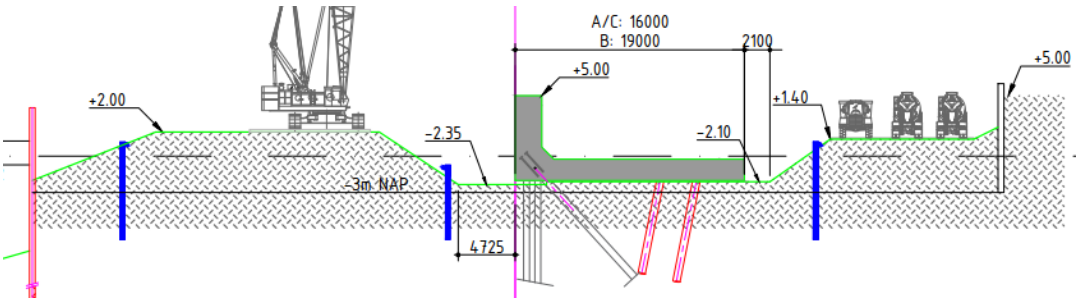

- Phase 8: Constructing sand fill behind relieving platform / concrete bar to NAP +4.5 m

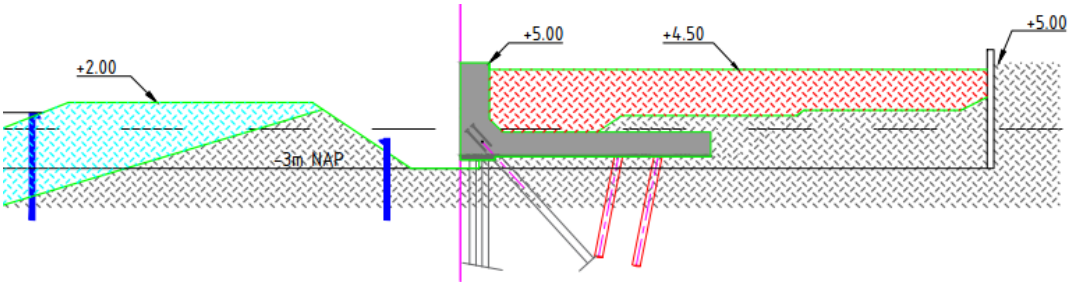

- Phase 9: Stopping of drainage system en restoring of the natural ground water table
- Phase 10: Excavating soil in front of quay wall and removing all temporary sheet pile walls.
  - At section B4 the soil is excavated to a depth of NAP -5 m, at section D1 this is done to a depth of NAP -4 m
  - After the excavation the quay wall is equipped with Bollards and fenders etc.
- Phase 11: Dredging of the soil in front of the quay wall until the required design depth
  - The dredging work is divided in sub phases based on the depth in front of the quay wall

To provide more detail about the construction process a timeline is created based on information provided by the construction company, see Table 5.6. The construction of the quay wall started at the beginning of 2018. For phase 0 to phase 6 there is no detailed time schedule available, all that is known is that these phases are executed in 2018.

phase	Section		remark
	B4	D1	
phase 0 to 6	2018	2018	reference measurement anchor and bearing piles FBG sensors at the end of phase 6
Phase 7	11-2018	03-2019	reference measurement inclinometer and XYZ-deformations at the end of phase 7
Phase 8	03-2019	05-2019	-
Phase 9	05-2019	06-2019	-
Phase 10	06-2019	06-2019	-
Phase 11	07-2019	07-2019	-

Table 5.6: Time schedule construction process

Phase 11 is divided into multiple sub-phases to more accurately model the increasing retaining height, which results in an incremental increase of the loads on the quay wall. The bottom level in front of the quay wall was measured by performing surveys 3 to 6 times a week from the start of the dredging process in July 2019. These surveys provide a detailed profile of the depth of the waterway in front of the quay wall. In Figures 5.9 and 5.10 the sub-phases and the corresponding depth of the waterway are presented.

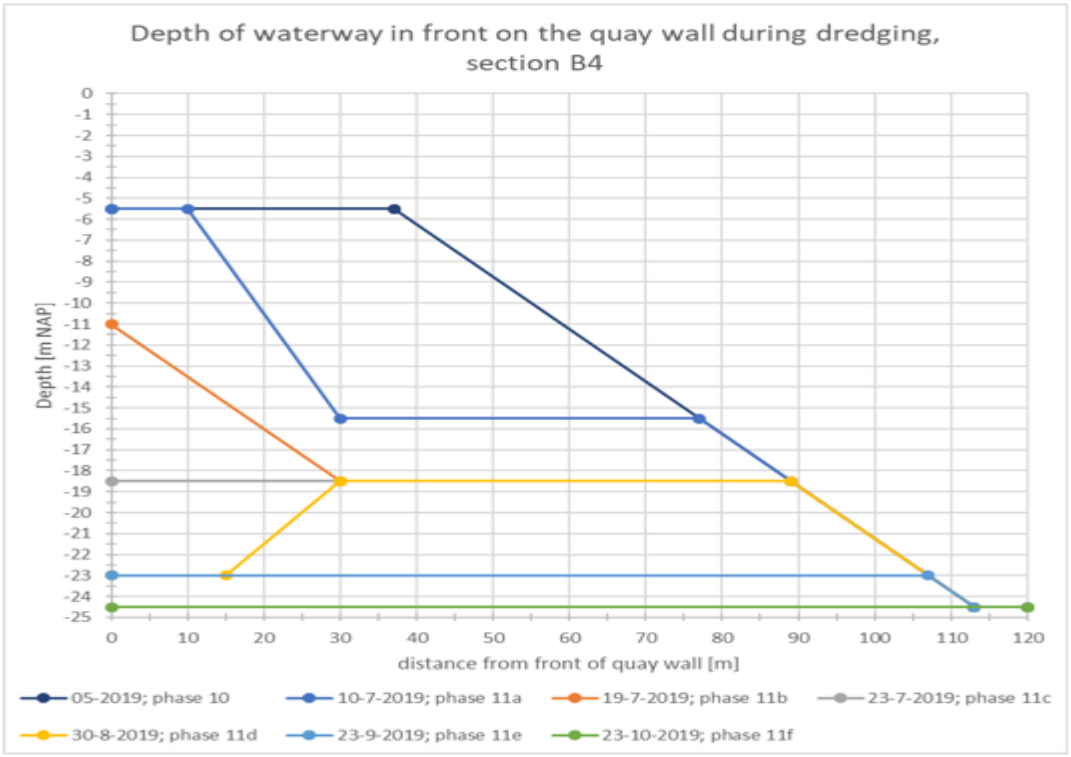

Figure 5.9: Depth waterway during dredging section B4

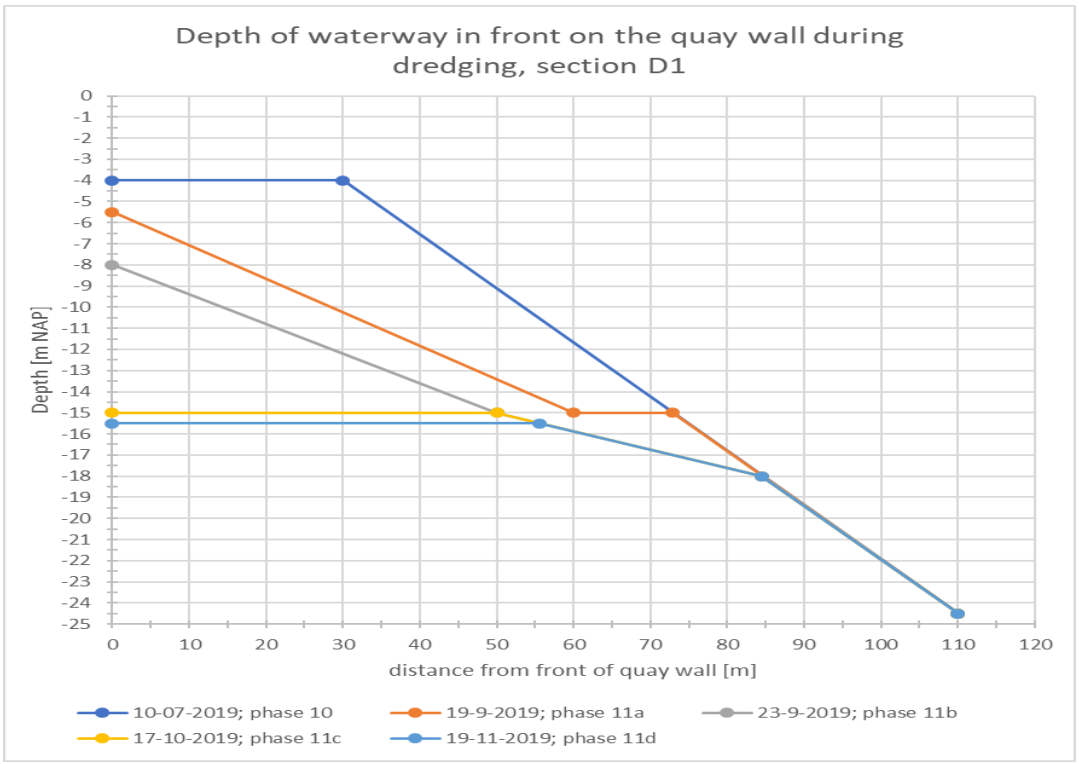

Figure 5.10: Depth waterway during dredging section D1

5.5. Model input

Element type and model dimensions
To increase the accuracy of the calculation 15-noded elements are used for the finite element mesh. The mesh consists of roughly 5000 elements. The amount of elements was increased until no significant change of the FE model results occurred. The origin of the x-axis in the FE model is located at the front of the quay wall, the y-axis is equal to NAP 0 m+. The FE model has a total width of 200 metres, stretching 120 metres to the water side and 80 metres to the land side. The height of the FE model is 55 metres, going from NAP +5 m to NAP -50 m. The bottom of the FE model has a minimal distance of 12 metres to the toe of the combined wall.

Structural elements
The applied structural elements and their properties are presented in Table 5.7. For the stiffness properties of the structural elements lower bounds, mean values and upper bounds are presented.

Element	Tubular piles combined wall	3 x PU 28 sheet piles combined wall	MV-piles (HEB600)	SI-piles	Floor relieving platform	Front wall relieving platform
Dimensions [mm]	D_{outer} : 1420	Width: 1800 Heigth: 454	Width: 300 Heigth: 600	$D_{steel\ tube}$: 609 $D_{screw\ tip}$: 850	Width: 16800 Height: 1750	Width: 2200 (B4) / 2800 (D1) Height: 7000
Thickness steel [mm]	B4: 24 D1: 19	-	Flange: 30 Web: 15.5	10 (steel tube)	-	-
Center-to-center distance [mm]	3295	3295	B4: 3845 D1: 3295	Perpendicular: 3000 Parallel: 3295	-	-
Material quality	X70 (steel)	S355GP (steel)	S420M (steel)	Steel: S355 J2H Concrete: C35/45	C35/45 (concrete)	
Youngs Modulus [kN/m^2]	$E_{max} = 210 * 10^6$ $E_{mean} = 200 * 10^6$ $E_{min} = 190 * 10^6$			steel: see left concrete: see right	$E_{uncracked} = 30 * 10^6$ $E_{mean} = 20 * 10^6$ $E_{cracked} = 10 * 10^6$	
Cross-sectional area [mm^2/m]	B4: 31955 D1: 25380	120	B4: 7025 D1:8195	steel: 5715 concrete: 82715	$175 * 10^4$	B4: $220 * 10^4$ D1: $280 * 10^4$
Moment of Inertia [mm^4/m]	B4: $7786 * 10^6$ D1: $6228 * 10^6$	$323 * 10^6$	B4: $445 * 10^6$ D1: $520 * 10^6$	steel: $256 * 10^6$ concrete: $1794 * 10^6$	$446615 * 10^6$	B4: $887333 * 10^6$ D1: $1829000 * 10^6$

Table 5.7: Structural elements applied in the quay wall

The combined wall of the quay wall is constructed of alternating tubular piles and triple PU28 sheet piles. To determine the system width of the combined wall the locks, which are welded on the tubular piles, have to be taken into account as well, the applied type of locks is C9. The total system width is equal to 3.294 m (1420 mm + 1800 mm + 2 * 37 mm). Since the combined wall is a continuous wall it can be modelled as a plate element. Over the bottom metres of the combined wall the sheet pile elements are not present anymore. Nevertheless, due to the large diameter of the tubular piles and arching effects in the soil it is still valid to consider the tubular piles as a continuous plate element in the FE model. A plate element in Plaxis has no cross-sectional area and thus has zero end bearing capacity. As a result the plate element would punch through the underlying soil layers if a vertical load is applied to it. To prevent this unrealistic punching behaviour from occurring the plate element is restricted from punching through the bottom soil layers. This is done by restricting a soil volume surrounding the bottom of the plate element from undergoing any plasticity. However, the intention of the prevent punching option is not to represent a realistic end bearing capacity, it's just a method to prevent unrealistically large vertical deformations of the plate element.

The relieving platform (section B4) and concrete bar (section D1) are modelled as plate elements as well. As the relieving platform and the concrete bar are continuous elements in the out of plane direction a Poisson's ratio is implemented to account for the out of plane stiffness.

The SI-piles and MV-piles are modelled with embedded beam elements to simulate 3 dimensional effects near the piles, such as shielding effects. For the axial and bending stiffness of the SI-piles the grout material is not taken into account. The bearing capacity F_{max} and friction capacity T_{max} of the SI-piles are estimated with equation 5.17 and 5.18. In these equations α_p and α_s are pile factors which are equal to respectively 0.63 and 0.09, q_b and q_s are the base and shaft cone resistance with are set equal to respectively 10 MPa and 15 MPa. The area of the pile tip is 0.56 m^2 and the circumference area is 2.67 m^2.

Plate		EA [kN/m]		EI [kNm²/m]		v [-]	Weight [kN/m/m]
		B4	D1	B1	D1		
Tubular piles + sheet piles combined wall	mean	$6.41 * 10^6$	$5.1 * 10^6$	$1.622 * 10^6$	$1.310 * 10^6$	0	0
	min	$6.09 * 10^6$	$4.85 * 10^6$	$1.541 * 10^6$	$1.245 * 10^6$		
	max	$6.74 * 10^6$	$5.36 * 10^6$	$1.703 * 10^6$	$1.376 * 10^6$		
Tubular piles combined wall	mean	$6.39 * 10^6$	$5.08 * 10^6$	$1.557 * 10^6$	$1.245 * 10^6$	0	0
	min	$6.07 * 10^6$	$4.82 * 10^6$	$1.479 * 10^6$	$1.183 * 10^6$		
	max	$6.71 * 10^6$	$5.33 * 10^6$	$1.635 * 10^6$	$1.301 * 10^6$		
Cast iron saddle	-	$210 * 10^9$	$210 * 10^9$	$210 * 10^9$	$210 * 10^9$	0	0
Floor relieving platform	mean	$35 * 10^6$	-	$8.932 * 10^6$	-	0.2	17.5
	cracked	$17.5 * 10^6$	-	$4.466 * 10^6$	-		
	uncracked	$52.5 * 10^6$	-	$13.398 * 10^6$	-		
Front wall relieving platform	mean	$44 * 10^6$	$56 * 10^6$	$17.747 * 10^6$	$36.580 * 10^6$	0.2	B4: 35.2 D1: 44.8
	cracked	$22 * 10^6$	$28 * 10^6$	$8.873 * 10^6$	$18.290 * 10^6$		
	uncracked	$66 * 10^6$	$84 * 10^6$	$26.620 * 10^6$	$54.870 * 10^6$		

Table 5.8: Input parameters plate elements

$$F_{max} = \alpha_p \cdot q_b \cdot A_{tip} \tag{5.17}$$

$$T_{max} = \alpha_s \cdot q_s \cdot A_{circumference} \tag{5.18}$$

There are 6 MV-piles at the HHTT-quay which have been test loaded prior to the construction of the quay wall. From the test load results the following conclusions can be made [Greft et al., 2019]:

- The test results indicate that the axial stiffness of the MV-piles is between 5 and 15 % higher than the theoretical axial stiffness of the HEB600 profile ($E_{steel} * A_{HEB600}$). The grout surrounding the steel HEB600 profile could contribute to the axial stiffness of the MV-pile, however during the load test large tensional strains where present in the MV-piles. Grout has a limited tensional capacity and cracks if tensional stresses exceed the yield stress. With increasing tensional strain levels the contribution of grout to the axial stiffness vanishes and the axial stiffness of the MV-piles should reduce to the theoretical axial stiffness of the HEB600 profile. During the load test strain losses between the MV-pile and the strain sensors could also lead to an apparent increase in the axial stiffness of the MV-pile. The difference between the axial stiffness from the load tests and the theoretical axial stiffness is limited and therefore it seems valid to apply the theoretical axial stiffness of the MV-piles in the a priori FE model.
- The average maximum shaft friction in the deep Pleistocene sand layers (layer 9 to 12) has a lower bound of 300 kPa, which is determined based on a circumference area of 2 m^2 per metre length of MV-pile. Therefore, the lower bound of the maximum shaft friction is 600 kN per metre length of pile.

The embedded beam elements that represent the MV-piles in the a priori FE model interact with the soil to generate shaft friction in order to withstand a tensional force. The MV-piles are designed under the assumption that no shaft friction is generated in the active zone (soil layers above the deep Pleistocene sand layers). This assumption is made because large soil deformations are expected to occur in the active zone when the quay wall is in failure. At the end of the construction process the quay wall should be far from failure and therefore soil deformations are expected to be limited. The limited amount of soil deformations means that the MV-piles might be capable of generating shaft friction in the active zone as well. If shaft friction is generated in the active zone less deformation of the MV-piles can be expected. In the a priori FE model the embedded beam element that represents the MV-piles has a possible shaft friction in the active zone. Whether any shaft friction is generated in the active zone depends on the relative deformations between the embedded beam element and the surrounding soil.

In Table 5.9 the input parameters for the SI-piles and the MV-piles are presented, the presented parameters are for 1 pile. The base capacity, F_{max} of the MV-pile is set to 200 kN. This capacity will probably not be exceeded as the MV-pile is mainly loaded in tension.

Embedded beam		EA [kN]	EI [kNm^2]	$A_{circumference}$ [m^2]	$L_{spacing}$ [m]	F_{max} [kN]	T_{max} [kN/m]
SI-pile	mean	9.213 * 10^6	2.870 * 10^5	2.67	3.295	3500	360
	min/cracked	6.300 * 10^6	2.195* 10^5				
	max/uncracked	12.126 * 10^6	3.545 * 10^5				
MV-Pile	mean	5.400 * 10^6	3.422 * 10^5	2.32	B4: 3.845 D1: 3.295	200	600
	min	5.132 * 10^6	3.251 * 10^5				
	max	5.672 * 10^6	3.593 * 10^5				

Table 5.9: Input parameters SI-piles

There is an ongoing discussion if the connection between the bearing piles and relieving platform behaves as a hinge or a fixed connection. For the a priori FE model the connection is assumed to be fixed.

Water levels

The water levels used in the a priori FE model are shown in Table 5.11. Layer 8 is a clay layer known as 'Laag van Wijchen' which acts as an impermeable boundary. Based on measurements of the ground water head in the layers beneath layer 8 Putteman et al. [2017] concluded that an over pressure is present, which is approximately 0.5 metre above the water level of the harbour. In Figure 5.12 two situations are distinguished. Situation A is when the dredging depth is above layer 8 and the over pressure is present. Situation B occurs when the dredging depth is beneath the bottom of layer 8 and the over pressure is no longer present since the impermeable layer is removed. The phreatic line in the layers beneath layer 8 are then equal to the harbour water level. Situation B does not occur at section D1 since the the maximum dredging depth is above layer 8.

Phase	Water level harbour	Ground water level
0 - 1	+0.25 m NAP	+0.25 m NAP
2 - 10		-3 m NAP
11 - 12		+0.25 m NAP

Figure 5.11: Applied water levels during construction for both sections

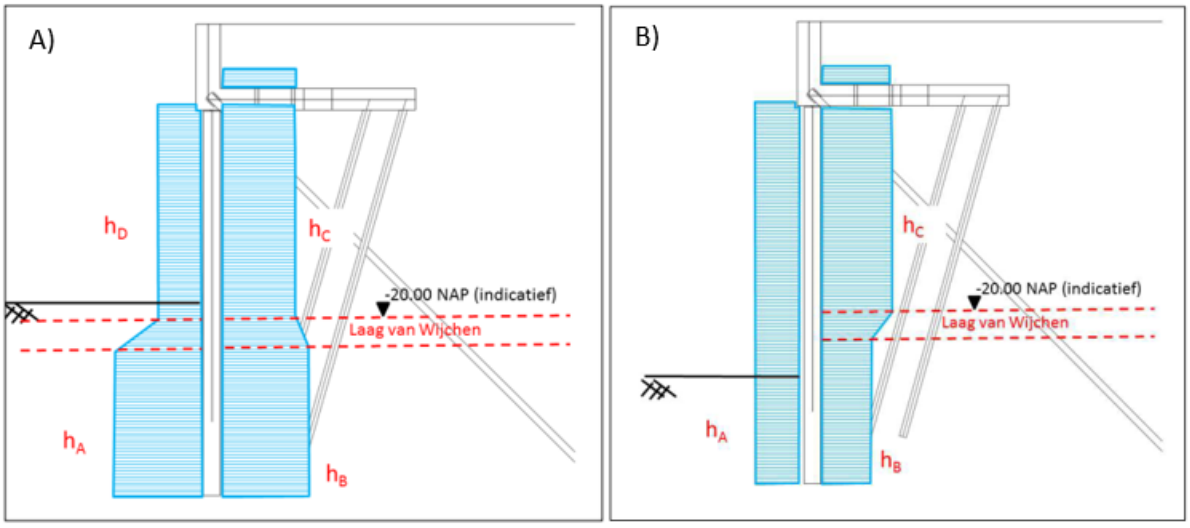

Figure 5.12: A) Ground water head for dredging depth above layer 8, B) Ground water head for dredging depth below layer 8

5.6. Validation of the a priori FE model

In this section the calculation results of the a priori FE model are compared with the measurement data. From this comparison it is possible to determine if the a priori FE model results are in line with the measurement data, and whether changes to the a priori FE model (parameters) are necessary.

Inclinometer results
In Figures 5.13 and 5.14 the horizontal deformations of the inclinometer measurements and the a priori FE model results are compared. Besides the inclinometer measurements of sections B4 and D1 other inclinometer results from zone B and D respectively are shown. This is done to allow for a more general comparison of the measurements with the a prior FE model results.

The toe deformation of the inclinometer measurements is equal to zero in the graphs. This is because inclinometer measurements are made relative to toe of the measurement. In reality a small toe deformation of the combined wall towards the waterside is thought to be realistic. The toe deformation is likely to increase as the bottom level increases, since the toe needs to deform to increase the passive resistance of the soil. Notice that the a priori FE model generates a toe deformation of approximately 5 millimetres and that this toe deformation barely increases in between the presented calculation phases. It seems likely that the toe deformation of the inclinometer is a few millimetres in reality. Since the XYZ-deformation measurements are questionable and can not be linked to the inclinometer results it is not possible to determine the toe deformation of the inclinometer measurements. Therefore, the toe deformation of the inclinometer measurements is kept equal to zero in the presented graphs.

For section D1 phase 10 the a priori FE model results deviate from the inclinometer measurements, the shape of the horizontal deformation does not correspond. It is noted that the bottom level during phase 10 is at NAP -4 m, and therefore no significant deformations of the combined wall are expected. As the deformations are small during this phase it is not very representative for the comparison.

For phase 11c of section B4 and D1 the curvature of the inclinometer measurements are less than that of the calculation results. This becomes visible in the point of the maximum horizontal deformation, for the inclinometer measurements this point is located higher than for the calculation results, which could be due to stiffer behaviour of the soil. However, it must be noted that these inclinometer measurements where taken shortly after a significant amount of soil was removed in front of the quay wall. Therefore, it is likely that the deformations where not fully developed at the time of the inclinometer measurements.

For section D1 (without a relieving platform) phase 11d the measured deformations of the quay wall are in line with the calculation results. If a toe deformation of approximately 5 millimetres is taken into account for the inclinometer measurements the measured deformations are within the maximum and minimum a priori calculation results.

For section B4 (with a relieving platform) phase 11f the measured horizontal deformations are best in line with the maximum a priori FE model results. This does not necessarily mean that the soil parameters used in the calculation of section B4 are too low. Section B4 has a more complicated FE model due to the presence of the relieving platform and the bearing piles. These elements influence the outcome of the FE model.

Overall a good comparison is found between the measured horizontal deformations and the calculated horizontal deformations. In the presented graphs the inclinometer measurements do not have a toe deformation, according to the a priori FE models a toe deformation between 5 and 10 millimetres could occur. If this toe deformation is taken into account the calculated deformations are in line with the measured deformations.

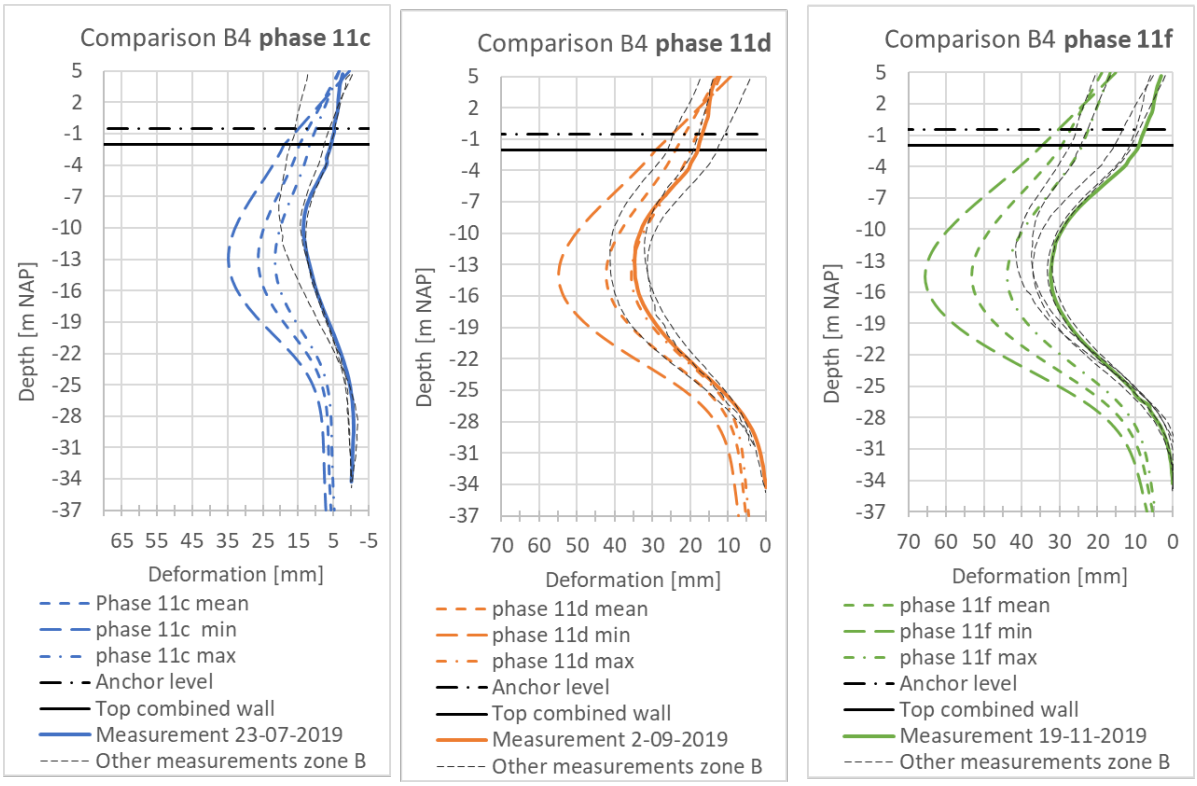

Figure 5.13: Comparison horizontal deformations section B4

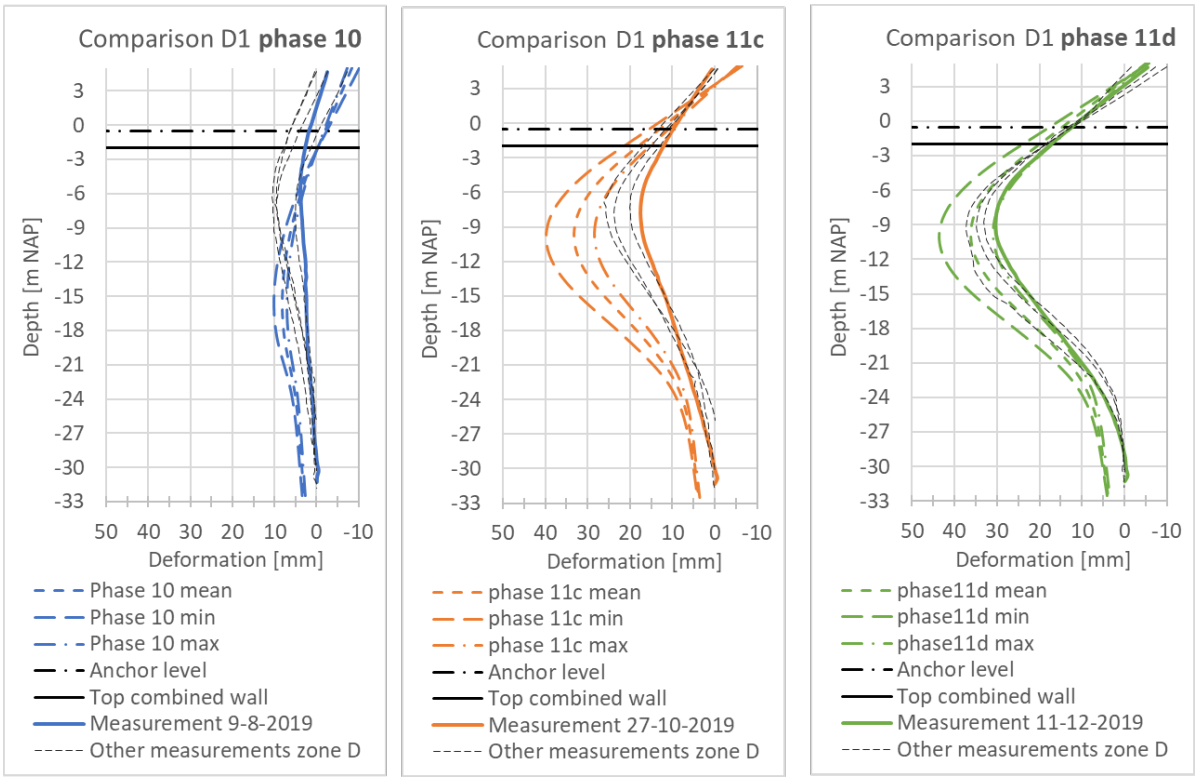

Figure 5.14: Comparison horizontal deformations section D1

Anchor forces
In Figures 5.15 and 5.16 the anchor forces of the a priori FE model results and the measurements are compared. The forces calculated with the a priori FE model are converted from forces per metre length of quay wall to forces per MV-pile. For both sections the measured anchor forces are very similar to the calculation results. The direction of the bending moment in the calculations is opposite to the measurements for section D1. However, the difference is only small because the absolute value of the bending moments is limited.

The axial stiffness of the MV-piles used in the a priori FE model is an important input parameter as this has an effect on the calculated force and the calculated horizontal deformation at the MV-pile connection. The axial stiffness used in the a priori FE model is equal to the axial stiffness of the HEB600 profile of the MV-piles. Load test have been performed on 6 MV-piles at the project location, which indicated that the axial stiffness of the MV-piles is between 5 and 15% higher than the axial stiffness of the HEB600 profile [Greft et al., 2019]. This could be due to the influence of the grout around the HEB600 profile. However when tensional strain levels increase the grout cracks and should not contribute to the axial stiffness of the MV-piles anymore. For both sections the measured horizontal deformation at MV-pile connection are similar to the calculated horizontal deformation, which indicates that the axial stiffness used in the a priori FE model is valid.

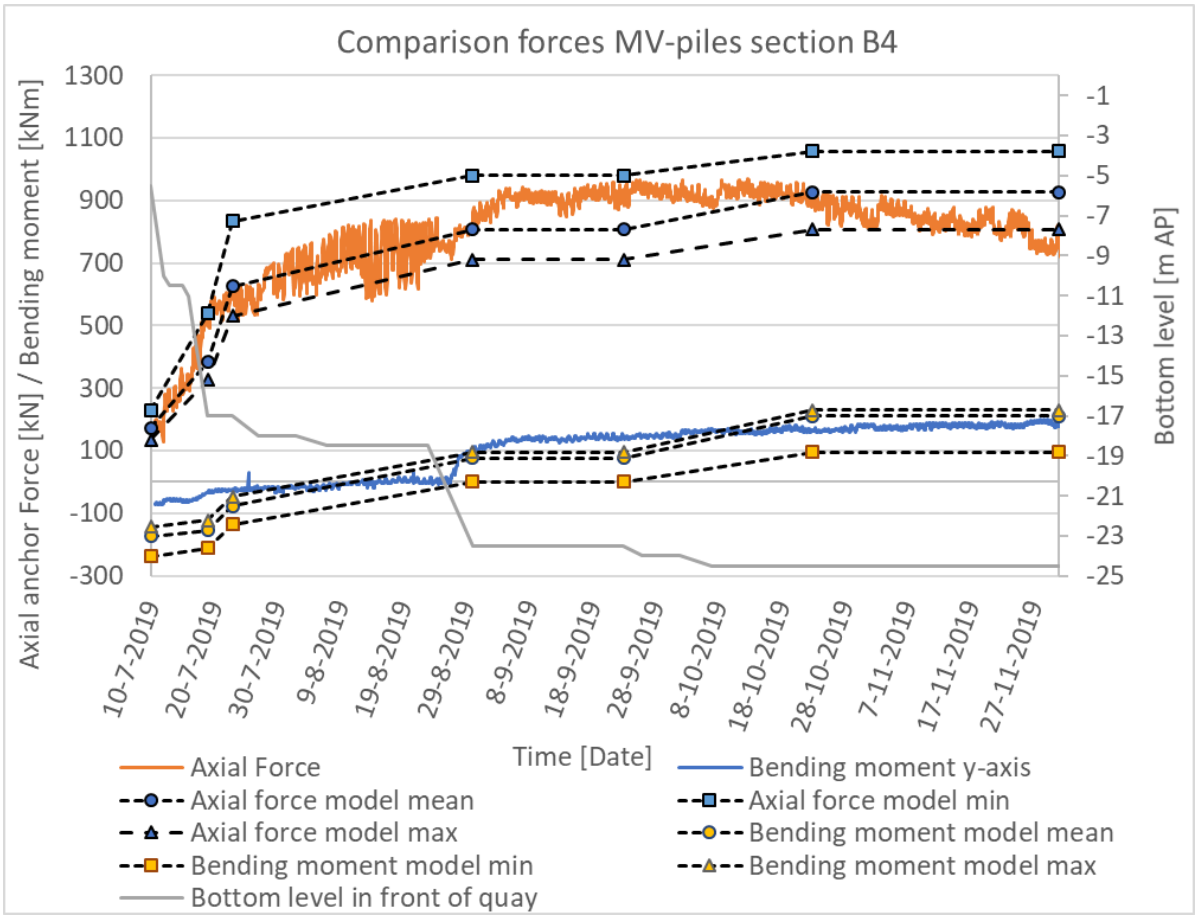

Figure 5.15: Comparison anchor forces section B4

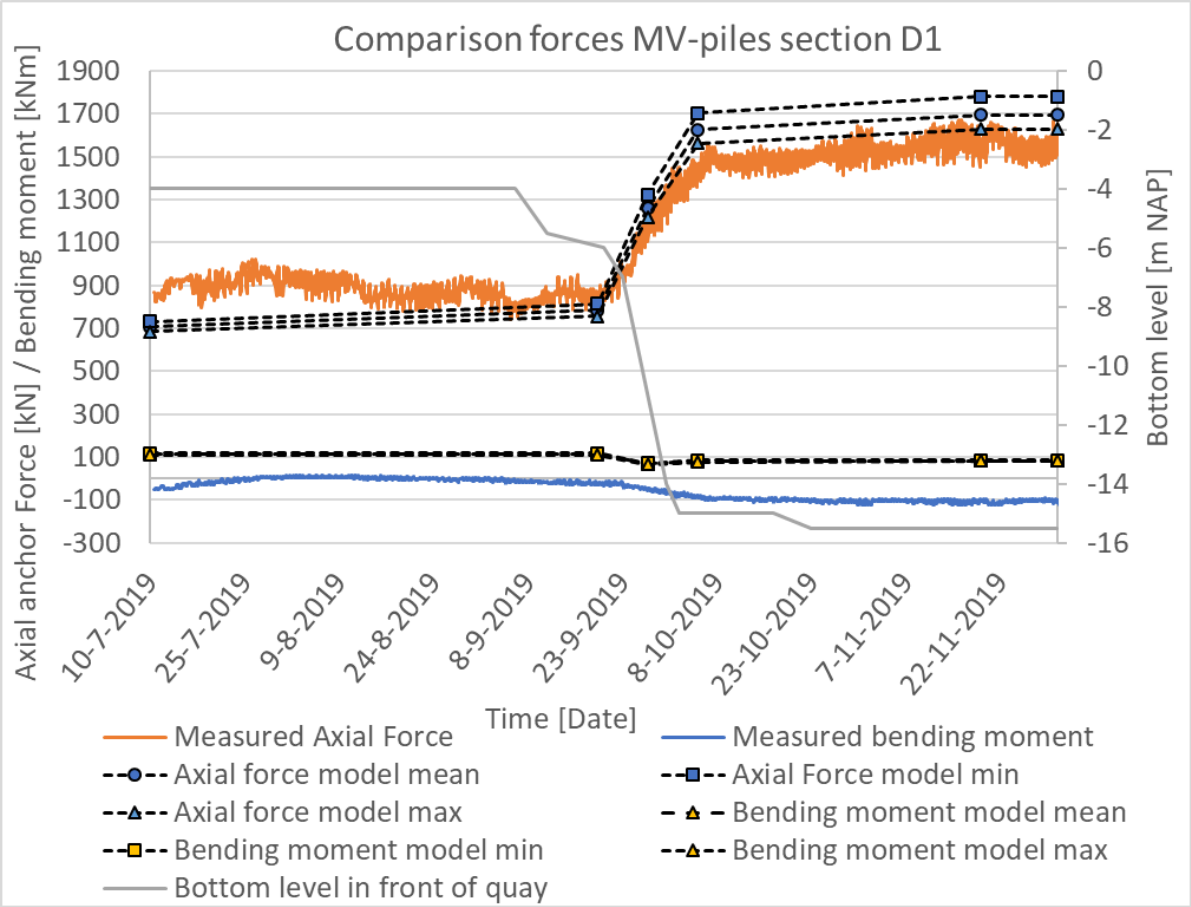

Figure 5.16: Comparison anchor forces section D1

Horizontal deformations top of concrete front wall

In Figures 5.17 and 5.18 the horizontal deformations of the concrete front wall are presented, these deformations are calculated with the mean a priori FE model. A negative deformation is orientated towards the landside and a positive one towards the waterside. A comparison with the XYZ-deformation measurements is not presented as it was already concluded in chapter 4 that the XYZ-deformation measurements do not seem usable.

In Figure 5.17 the calculated horizontal deformations of the top of the front wall for section B4 are shown. It is visible that the top of the front wall moves towards the landside due to a rotation of the front wall, the value of this deformation is approximately 10 millimetres. After the bottom level is dredged beyond a depth of NAP -11 m (phase 11c and later) the top of the front wall starts to move towards the waterside, which corresponds with the inclinometer measurements.

In Figure 5.18 the calculated horizontal deformation of the top of the front wall for section D1 are presented. These deformations are calculated with the mean a priori FE model. The horizontal deformation is initially orientated towards the landside and then undergoes a small deformation towards the waterside., which corresponds with the inclinometer measurements as well.

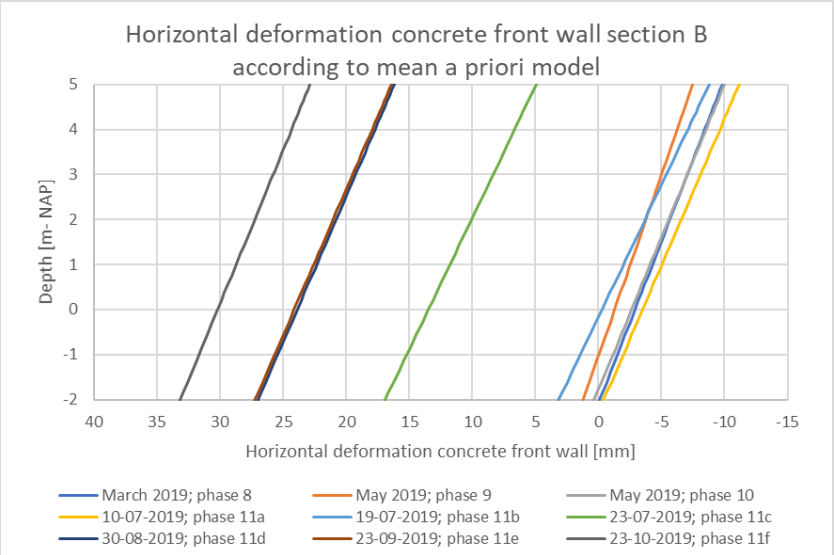

Figure 5.17: Horizontal deformation front wall section B4, mean a priori FE model

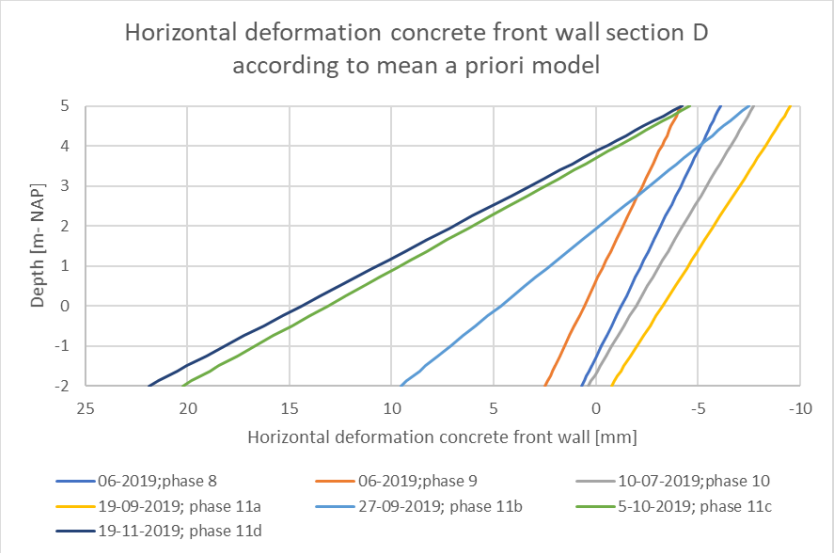

Figure 5.18: Horizontal deformation front wall section D1, mean a priori FE model

5.7. Discussion on a priori FE model

Bearing capacity combined wall
In the FE model the combined wall is modelled as a plate element, these elements have no cross-sectional area in the FE model. Therefore, plate elements do not generate any base resistance in the FE model. Without any precautions the plate elements could punch through the underlying soil layers. A method to overcome this punching behaviour is to allocate a soil volume beneath the plate element that is excluded from any plasticity. This method, known as the prevent punching option, is not intended to represent a realistic end bearing capacity of the plate element. It is merely a way to prevent the plate element from undergoing excessive vertical deformations under the presence of a vertical force. Another method to prevent a plate element from undergoing these excessive vertical deformations is by applying a fixed-end anchor beneath the plate element. This fixed-end anchor acts as a spring support. Using a fixed-end anchor might result in a more realistic development of vertical deformations in the FE model.

Constitutive model
The a priori calculations are performed with the HS constitutive model. This soil model takes into account the stress dependency of the soil stiffness that is often observed in general soil behaviour. However, the stiffness of soil is also strain dependent, in general the stiffness of soil decays with increasing strain levels. Another constitutive model which is available in Plaxis is the HSsmall model, which does take into account the strain dependency of soil stiffness. Using the HSsmall model could lead to reduced horizontal deformations of the quay wall and less heave of the soil in front the quay wall [Brinkgreve, 2019a].

MV-piles
The embedded beam element that represents the MV-piles in the FE model interacts with the soil to generate shaft friction. Whether any shaft friction is generated depends on the relative deformation between the embedded beam element and the surrounding soil. The embedded beam element is allowed to generate shaft friction both in the active zone and the deep Pleistocene sand layers. According to the a priori FE model results the deformation in the active zone is limited during the construction process and therefore it seems plausible that a shaft friction is generated in the active zone, see Figure 5.19. The generation of shaft friction in the active zone leads to less horizontal deformation at the MV-pile connection. This is because there is less axial deformation of the MV-pile since the axial load is already transferred to the soil in the active zone. The calculated horizontal deformation and measured horizontal deformation at the MV-pile connection are comparable, see Figure 5.13 and 5.14, which indicates that the decision to allow for shaft friction to develop in the active zone is valid. A note must be made about the axial stiffness of the MV-pile that is used in the a priori FE model. Only the axial stiffness of the HEB600 profile is used in the a priori FE model, it is assumed that the grout is cracked and does not contribute to the axial stiffness. If the grout is not cracked the axial stiffness of the MV-pile would be higher, this would also lead to less horizontal deformation at the MV-pile connection. If a load is applied on the quay wall deformations in the active zone will increase, which would lead to relaxation of the soil near the MV-pile and a reduction in the relative displacement between the MV-pile and the soil. Therefore, it seems likely that the generation of shaft friction in the active zone reduces as the soil deformations increase.

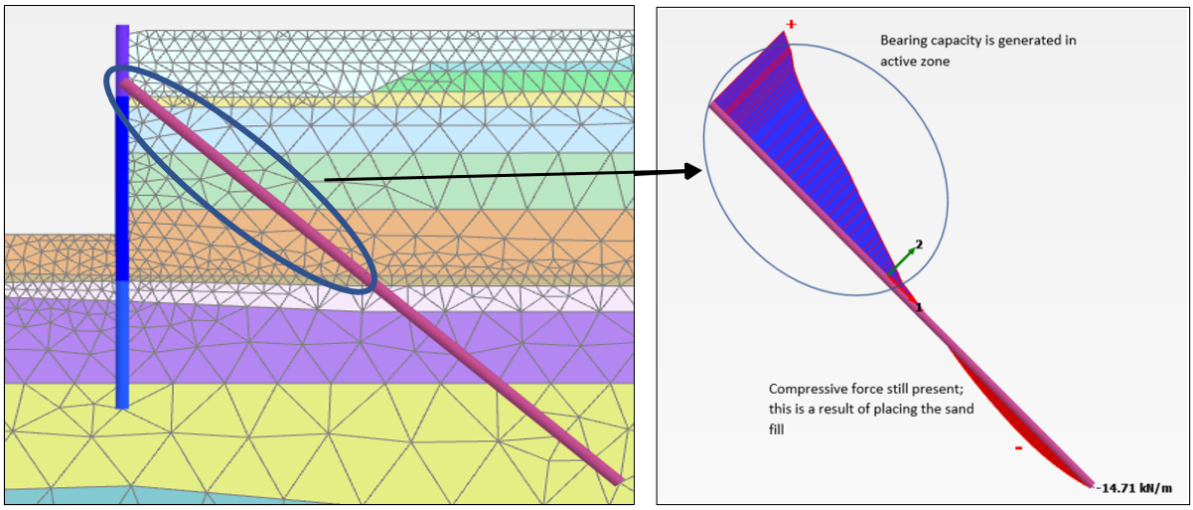

Figure 5.19: Shaft friction generated in active zone at end of construction process, section D1

SI-piles

The SI-piles underneath the relieving platform are modelled with embedded beam elements as well. These elements allow for interaction between the SI-piles and the soil. The interaction between the soil and the SI-piles determines how much horizontal soil stresses are carried by the SI-piles, and therefore how much the horizontal stresses on the combined wall are reduced. This phenomena is known as the shielding effect. The larger the shielding effect is the lower the horizontal soil stresses on the combined wall are. On the other hand a larger shielding effect increases the horizontal force that is transmitted from the SI-piles to the relieving platform. The interaction between the soil and the SI-piles that is calculated by the FE model depends on the properties of the embedded beam elements. Especially the (lateral) interface stiffness and the connection between the relieving platform and the SI-piles are important. The interface stiffness factors for the embedded beam elements are now determined by default and depend on the soil stiffness and the spacing of the SI-piles. According to the Plaxis 2D manual the default formulas for the interface stiffness factors are valid for bored piles. To check if these default interface stiffness factors are valid information about the horizontal deformation of the bearing piles is necessary. However, this information is not available. Moreover, as concluded in chapter 4 it is not possible to determine if the connection between the SI-piles and the relieving platform behaves as a hinge or a fixed connection based on the measured strains.

Softening behaviour of soil

The shear strength of soil depends on the relative density and the amount of strain that occurs. For medium dense to dense sand layers a peak strength develops due to the dilative behaviour of the soil. After this peak a reduction in the shear strength is often observed, this behaviour is known as softening. In the case study used in this thesis the soil layers predominantly consists of medium dense to dense sand layers. Therefore, the development of a peak shear strength and softening are expected to occur. Softening behaviour is also observed in the triaxial tests performed on soil samples taken from the project location. In the a priori FE model the shear strength of the sand layers is set equal to the peak strength values. The HS constitutive model is used to describe the stress-strain behaviour of the soil. This constitutive model does not take into account any softening behaviour that could occur in reality. If the peak shear strength level is exceeded in the FE model the strength might be overestimated since no softening is accounted for by the constitutive model. The FE model is checked for plastic failure points. These are stress points that are in failure which means that the maximum shear strength is reached in that specific stress point. The plastic failure points at the end of the construction process are presented in Figure 5.20 for both sections. For both sections almost no plastic points are present in the FE model, which means that the mobilised shear strength is lower than the peak shear strength. According to the FE model the peak shear strength of the soil is not exceeded at the end of the construction process.

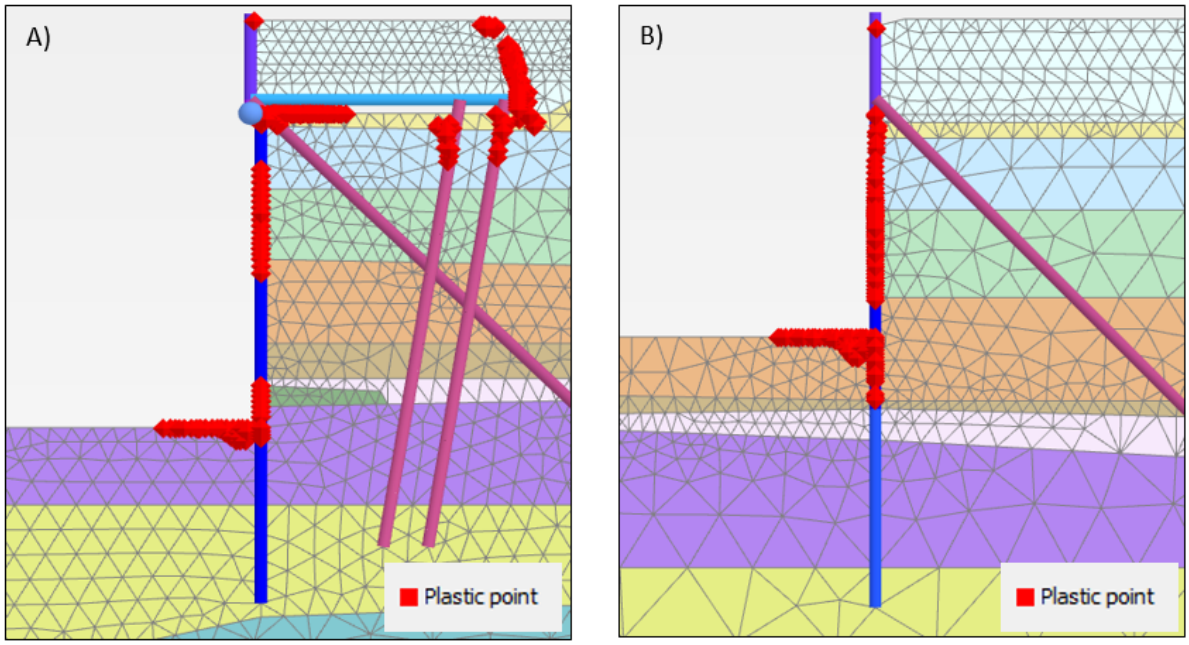

Figure 5.20: Plastic failure points in the FE model at the end of the construction process, in A) section B4 and in B) section D1

5.8. Conclusion

In this chapter the set-up of the a priori FE model used to make an estimation of the behaviour of the quay wall is explained. In the a priori FE model three parameters sets are considered to account for the uncertainty in the input parameters. These sets represent lower bound, mean and upper bound parameter values. The a priori FE model results are compared to the measurement data to validate the a priori FE model. It is concluded that the a priori FE model results are in line with the measurement data. For section D1 (without a relieving platform) the measurement data lies within the boundaries of the upper and lower bound a priori FE model results, which indicates that the used soil parameters at section D1 are valid. The soil conditions at section B4 and section D1 are comparable, since good results are obtained at section D1 it is likely that good results are obtained at section B4 as well. However, at section B4 the measurement data shows slightly less horizontal deformation than the a priori FE model results do. This is most likely caused by the presence of the relieving platform and the SI-piles. The interaction between the soil and these two structural elements increases the complexity of the FE model. Nevertheless, a reasonable estimation of the quay wall behaviour is still achieved for section B4. As a good comparison is found between the measurement data and the a priori FE model results it does not seem necessary to optimise the mean value of the soil parameters. It does seem possible to reduce the standard deviation of the soil parameters. Recent studies showed that using a sophisticated inverse analysis techniques, such as Bayesian updating, can result in a reduction of the standard deviation when a comparable result is found between the calculation results and the measurement data [Den Adel, 2018]. A reduction in the standard deviation would lead to a higher reliability of the quay wall. If a sophisticated inverse analysis technique is used it would be possible to quantify a possible reduction in the standard deviation of the soil parameters. The aim of this study is to determine if the measurement data obtained during the construction process could be used to optimise the functionality of the quay wall. It does not aim to accurately quantify how large this optimisation would be. Therefore, applying a sophisticated inverse analysis technique is not part of this thesis. For the remainder of this thesis the soil parameters as determined in this chapter will be used.

In the a priori FE model the shear strength of the soil is set equal to the peak shear strength values. According to the FE model a limited amount of plastic points are present in the FE model. These plastic points indicate the presence of stress points in which the maximum shear stress of the soil is reached. Therefore, it seems valid to calculate with peak shear strength values for the construction process.

In the previous section some of the model techniques used in the FE model are discussed. The end bearing capacity of the combined wall is currently modelled with the prevent punching option, it could also be modelled with an fixed-end anchor. The applied constitutive model used in the a priori calculations is the HS model. This model does not account for the small strain stiffness of soil. The HSsmall model could lead to less horizontal deformation of the combined wall and less heave in front of the quay. In the next chapter it is considered if these adjustments to the FE model input have a significant influence on the FE model results.

6

Influence of adjustments to the a priori model

In this chapter the influence of two adjustments to the a priori FE model are considered. First of all the method to model the end bearing capacity of the combined wall is reviewed. Secondly, the HS constitutive model is compared to the HSsmall constitutive model. The input parameters used in this chapter are the mean values as determined in the previous chapter.

6.1. Modelling the end bearing capacity of tubular piles

The tubular piles of the combined wall generate a bearing capacity to withstand normal forces. This capacity consist of a frictional resistance along the shaft of the piles and a base resistance beneath the tip of the bearing piles, see Figure 6.1 for a general impression of the bearing capacity of piles. In the a priori FE model the combined wall is modelled as a plate element, which have no cross-sectional area. Therefore, plate elements do not generate any base resistance themselves in a FE model, without any precautions the plate elements could punch through the underlying soil layers. A method to overcome this punching behaviour is to allocate a soil volume beneath the plate element that is excluded from any plasticity. The diameter of this soil volume depends on the properties of the plate element and is described by $D_{equivalent} = \sqrt{\frac{12EI}{EA}}$. This method, known as the prevent punching option, is not intended to represent a realistic end bearing capacity of the plate element. It is merely a way to prevent the plate element from undergoing excessive vertical deformations under the presence of a vertical force.

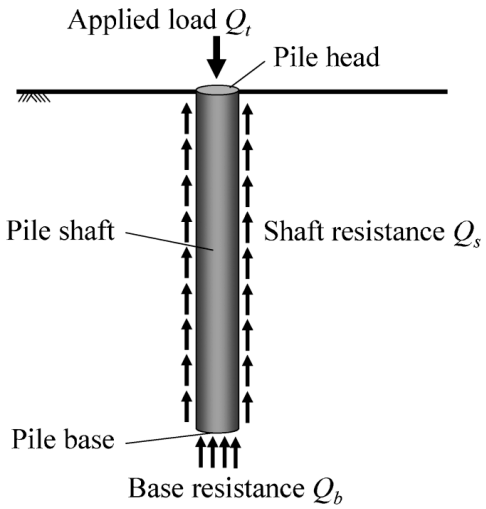

Figure 6.1: Bearing capacity of piles

Another method to prevent a plate element from undergoing these excessive vertical deformations is by applying a fixed-end anchor beneath the plate element. This fixed-end anchor acts as a spring support. The stiffness of the fixed-end anchor should be iteratively determined such that the vertical deformations are according to what would be expected. To determine the influence of the fixed-end anchor stiffness on the vertical deformations of the quay wall a series of calculations are made in which the stiffness of the fixed-end anchor varies. The axial stiffness of the fixed-end anchor is set to 1, 50.000, 100.000 and 150.000 kN. The stiffness of 1 kN is an unrealistic value and is only used to determine the maximum influence that the fixed-end anchor has on the vertical deformations of the quay wall. A stiffness in the range of 50.000 to 150.000 kN is often used for a fixed-end anchor in a FE model. The out of plane spacing of the fixed-end anchor in the FE model is set equal to the center-to-center distance of the tubular piles, which is 3.295 metres. In Figure 6.2 the vertical deformation of the bottom of the combined wall is presented for the varying stiffness of the fixed-end anchor. On the left side the results of section B4 are presented and on the right side the results of section D1. In the aforementioned Figure the results of the a priori FE model are presented as well, the a priori FE model was calculated with the prevent punching option. A negative deformation indicates a downward orientated displacement of the quay wall. In Figure 6.3 the normal forces in the combined wall are shown for the final phase of the construction process. From these figures the following remarks can be made:

- The maximum vertical deformation occurs for the a priori FE model (prevent punching option) and the FE model with a fixed-end anchor stiffness of 1 kN. In these models the normal force in the combined wall is fully carried by shaft friction and therefore more deformation of the bottom of the combined wall is necessary.
- With an increasing stiffness of the fixed-end anchor the vertical deformation reduces since more base resistance develops in these models.
- At phase 8 the sand fill is in place which results in a downward displacement of the quay wall. After phase 8 the bottom level in front of the quay wall increases in depth which results in heave of the soil in front of the quay. The heave increases until a depth of ± NAP -10 m. After a depth of ± NAP -10 m the vertical anchor force and negative skin friction along the combined wall become governing over the heave which results in the quay wall moving downwards again.

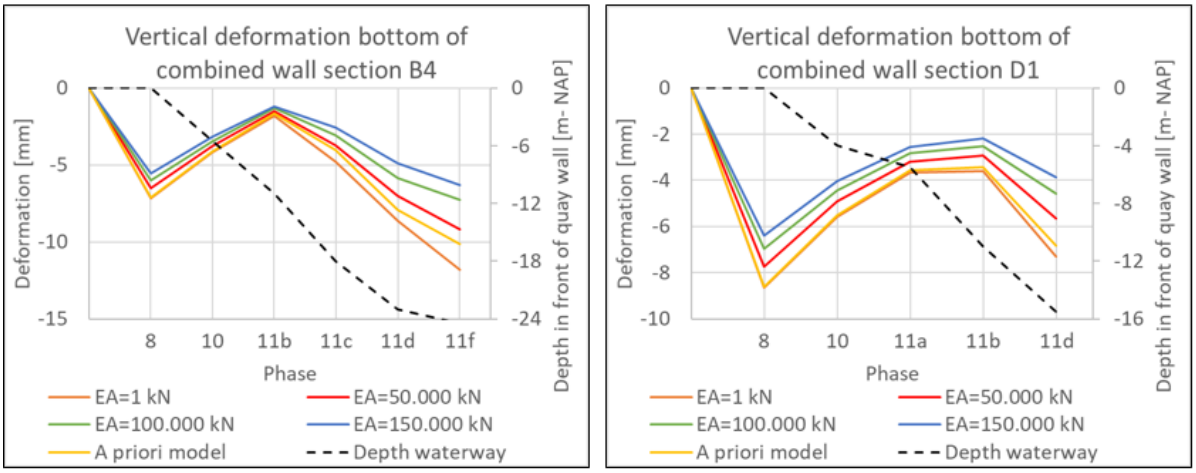

Figure 6.2: Vertical deformation top of combined wall based on different stiffness fixed-end anchor

Due to the large diameter of the tubular piles it is likely that some base resistance develops in reality. The a priori FE model (prevent punching option) does not generate any base resistance. Whereas, the models with a fixed-end anchor underneath the combined wall do generate a base resistance. Therefore, it seems that the FE model with a fixed-end anchor underneath the combined wall is able to better predict the vertical deformation of the quay wall. The stiffness of the fixed-end anchor should be determined such that the vertical deformations are according to what would be expected.

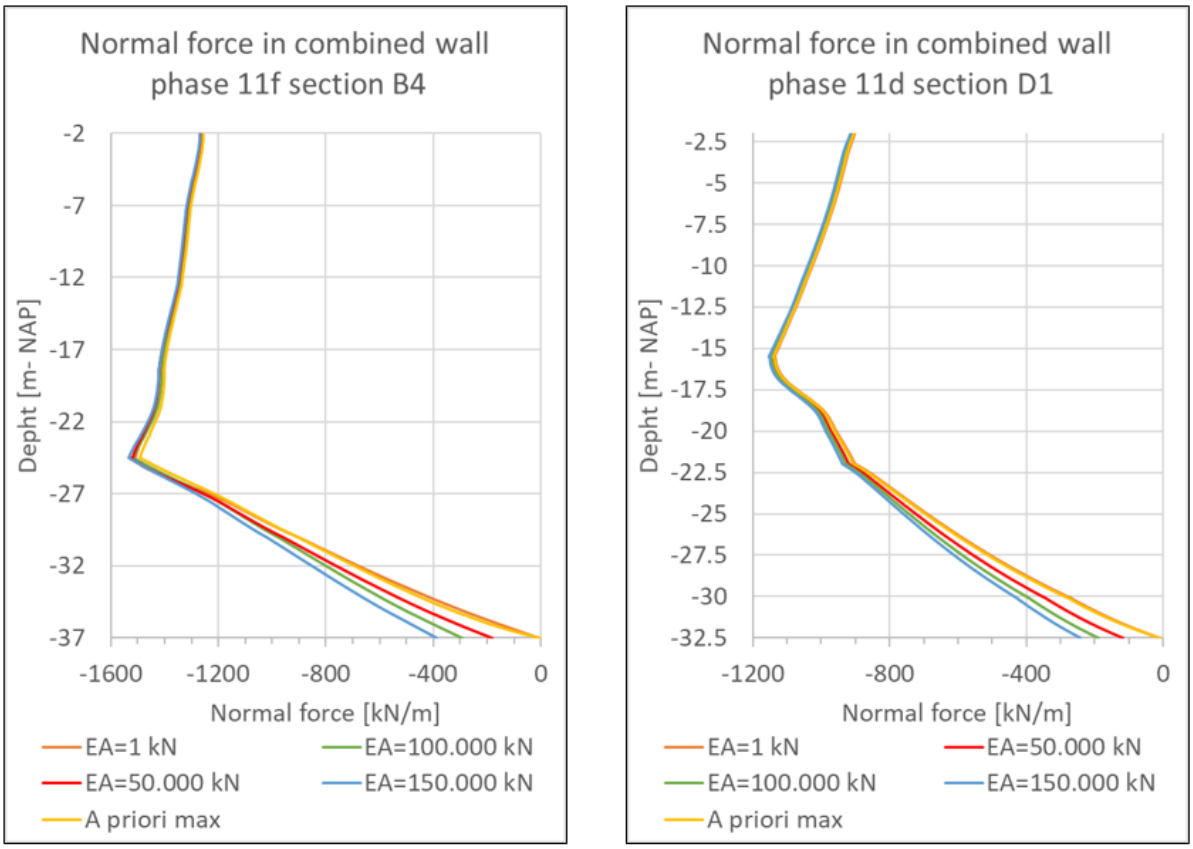

Figure 6.3: Normal force in combined wall based on different stiffness fixed-end anchor

The vertical deformations of the top of the quay wall are measured multiple times during the construction process, these are the XYZ-measurements as mentioned in chapter 4. In Figures 6.4 and 6.5 the measured and calculated vertical deformation of the top of the combined wall are presented. According to the measurements the top of the quay wall rises more than is calculated. This does not mean that the fixed-end anchor stiffness should be higher than currently considered. The measured vertical deformations of the quay wall also depend on the amount of heave that occurs. It is not possible to determine the fixed-end anchor stiffness based on the available deformation measurements. For the considered fixed-end anchor stiffness values the maximum difference between the calculated vertical deformation of the bottom of the combined wall is less than 3 millimetres, see Figure 6.2. Since this difference is quite small it seems valid to use either three of the considered fixed-end anchor stiffness values, for further calculations the middle value of 100000 kN is used.

It can be seen that the quay wall rises at section B4 until the end of the construction process, whereas at section D1 the quay wall moves downwards after the bottom level reaches a depth of approximately NAP -10 m. This could be due to the presence of the relieving platform at section B4, which causes the vertical effective stress to be lower. Therefore, more heave can occur beneath the combined wall which could result in the upward deformation of the quay wall. An attempt is made to model this behaviour by implementing a plate element perpendicular to the combined wall at the toe. However, this did not lead to the rise of the quay wall as observed by the measurements.

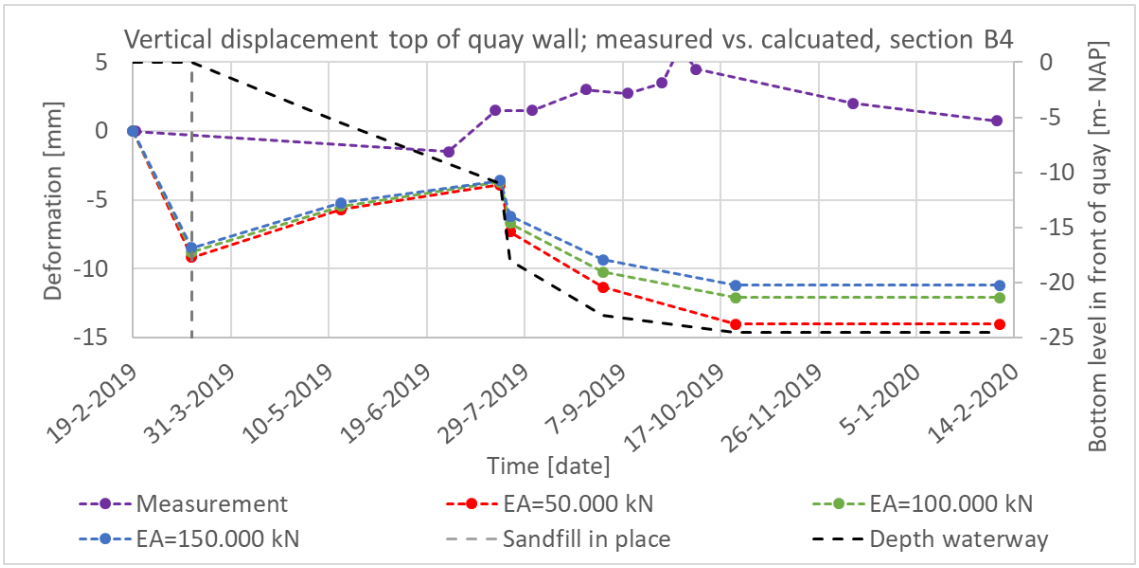

Figure 6.4: Comparison measured and calculated vertical displacement top of quay wall, section B4

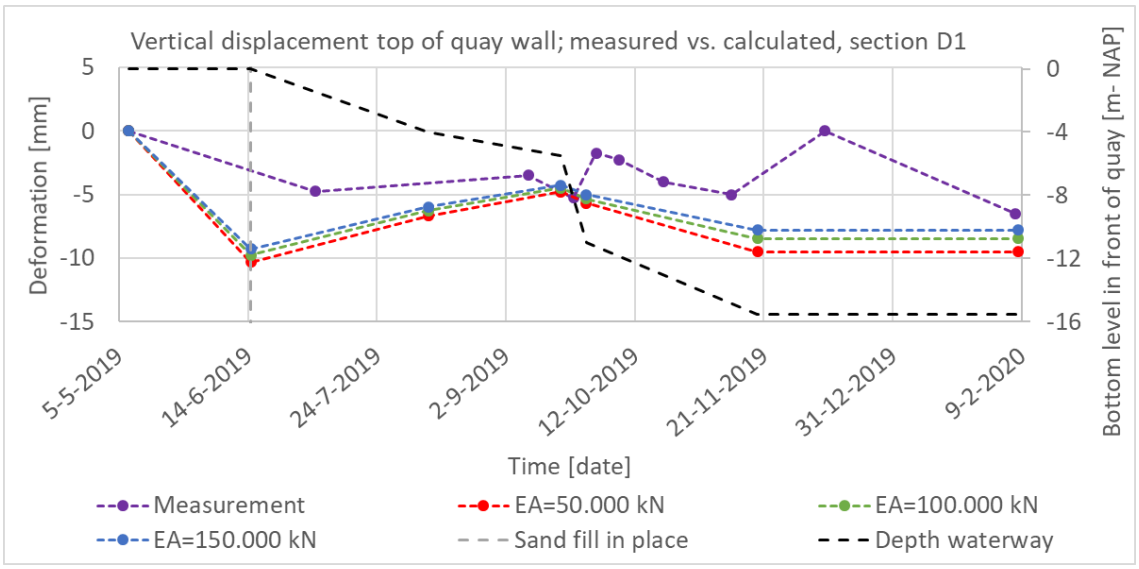

Figure 6.5: Comparison measured and calculated vertical displacement top of quay wall, section D1

6.2. Hardening Soil small strain model

The HS constitutive model takes account of the stress dependency of soil stiffness. It does not account for the strain dependency of soil stiffness. The HSsmall constitutive model does take into account the strain dependency of soil stiffness. The strain dependency of soil stiffness could lead to less horizontal deformation of the retaining wall and a reduction of heave [Brinkgreve, 2019a].

The HSsmall model has 2 additional parameters compared to the HS-model, which are the reference small strain shear modulus, G_0^{ref}, and the threshold shear strain level, $\gamma_{0.7}$. The threshold shear strain level is the strain level at which the secant shear modulus has reduced to a value of approximately 70% of the small strain shear modulus. The reference small strain shear modulus is determined with equation 6.1, in which E_0^{ref} is the initial reference soil stiffness and ν_{ur} is Poisson's ratio in unloading/reloading conditions. The initial reference stiffness of the soil is determined with equation 6.2 in which E_{50}^{ref} is the reference secant stiffness Obrzud and Truty [2018].

$$G_0^{ref} = \frac{E_0^{ref}}{2 \cdot (1 + \nu_{ur})} \tag{6.1}$$

$$E_0^{ref} = E_{50}^{ref} \cdot 5 \tag{6.2}$$

For sand the threshold shear strain level typically varies between $1 * 10^{-4}$ and $2 * 10^{-4}$. The first mentioned value is for dense sand layers and the latter for loose sand layers [Brinkgreve et al., 2010]. Based on the analyses of the CPT results in chapter 5.2 the relative density of the sand layers is between 50 and 80%, see Figure 5.5. This indicates that the sand layers are medium dense to dense sand layers. Therefore, a threshold shear strain level of $1.3 * 10^{-4}$ is seen as a good estimation for the sand layers.

For clay layers the reference small strain shear modulus is assumed to be equal to the reference unloading/reloading stiffness (G_0^{ref} = E_{ur}^{ref}). The threshold shear strain level of the clay layers is set equal to $4 * 10^{-4}$. In Table 6.1 the additional soil parameters for the HSsmall model are presented.

Parameter	Section	Layer											
		1	2	3	4	5	6	7	8	9	10	11	12
G_0^{ref} [MPa]	B4	105	30	145	95	105	65	35	30	65	95	105	85
	D1	95	30	125	95	95	65	35	30	-	94	105	85
$\gamma_{0.7}$ [-]	-	1.3E-04	4.0E-04	1.3E-04	1.3E-04	1.3E-04	1.3E-04	1.3E-04	4.0E-04	1.3E-04	1.3E-04	1.3E-04	1.3E-04

Table 6.1: Soil parameters HSsmall model

For section B4 and D1 calculations are made with the HSsmall constitutive model. In Figure 6.6 a comparison is made between the horizontal deformations of the quay wall for the HSsmall model and the HS model, the presented results are limited to a few calculation phases. As was expected the small strain stiffness that is implemented in the HSsmall model leads to less horizontal deformations of the quay wall. However, the difference in horizontal deformation is limited to 1 à 3 millimetres and seems negligible.

The small strain stiffness in the HSsmall model could reduce the heave that occurs in front of the quay wall. In Figure 6.7 the heave at 10 metres in front of the quay wall is plotted over the height of the soil layers at the end of the construction process. Again the difference between the HSsmall model and the HS model is limited to 1 à 2 millimetres and seems negligible.

Based on a comparison of results between the HSsmall model and the HS model it appears that the difference between both models is small. This applies both to the horizontal deformation of the quay wall and the occurrence of heave. A reason for the little influence of the HSsmall model might be that the stiffness moduli of the HS model are already quite high. Therefore, the effect of small strain stiffness is limited. Since the HSsmall model requires more calculation time than the HS model it is most effective to continue calculations with the HS model.

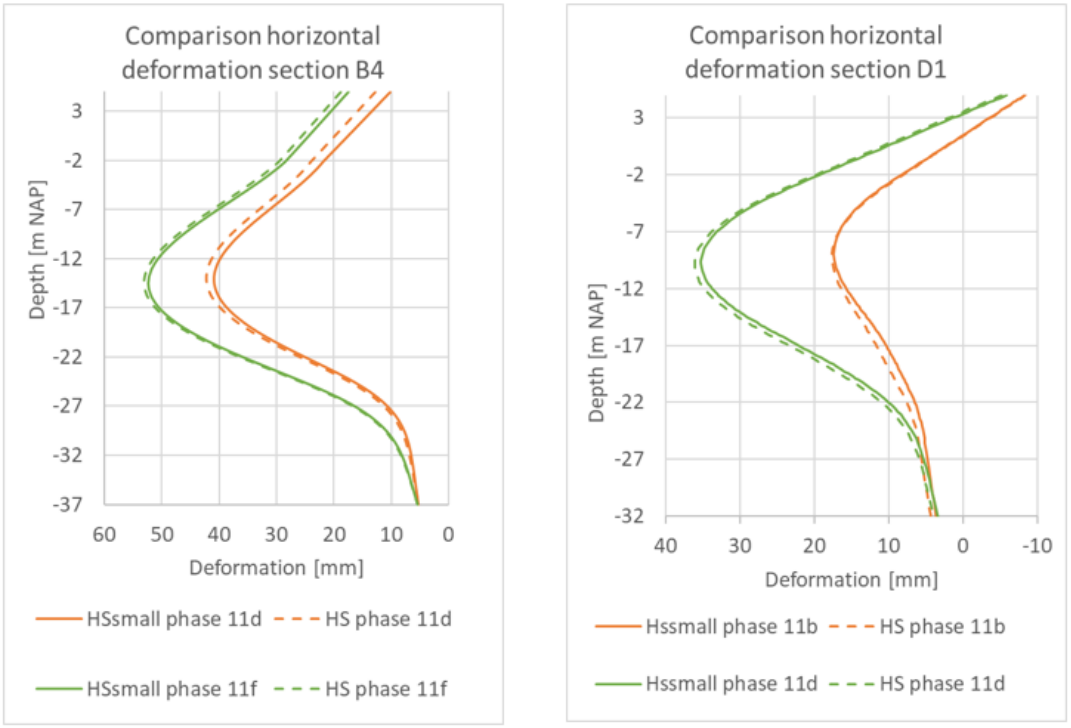

Figure 6.6: Horizontal deformations quay wall HSsmall model versus HS model

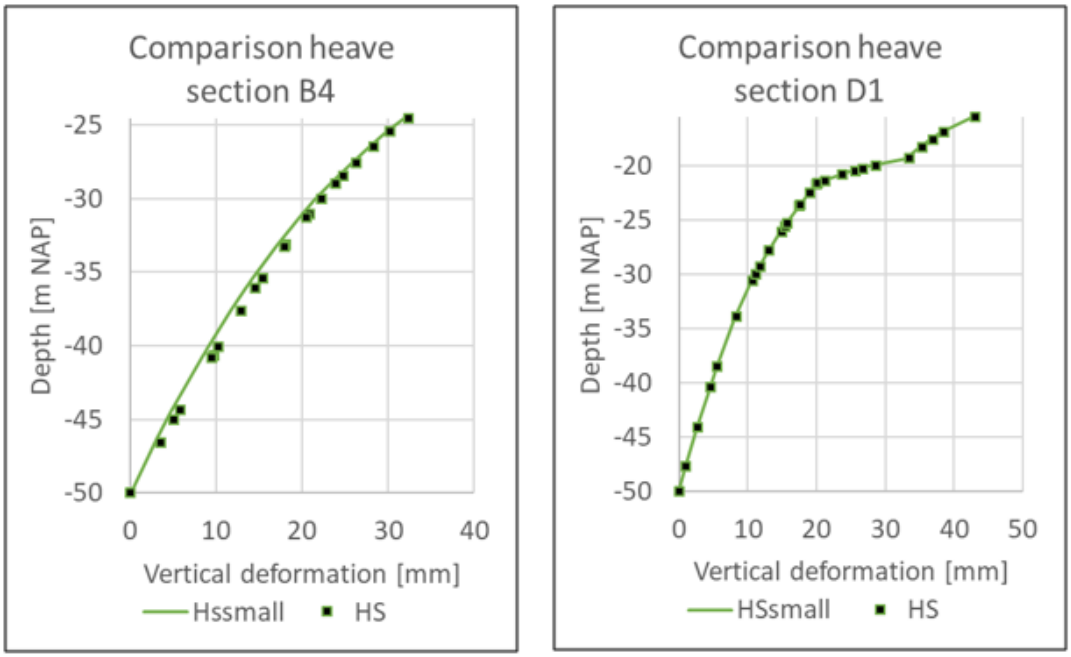

Figure 6.7: Heave at 10 metres in front of the quay wall during the final construction phase

6.3. Conclusion

The tubular piles of the combined wall have a large diameter which makes it likely that an end-bearing capacity is generated when the pile are loaded with a vertical force. The a priori FE model (with the prevent punching option) does not generate any base resistance. Whereas, the FE model with a fixed-end anchor does generate a end-bearing capacity. Therefore, the FE model with the fixed-end anchor is better capable of predicting the vertical deformation of the quay wall. An attempt was made to determine the stiffness of the fixed-end anchor based on vertical measurements of the top of the quay wall. However, the vertical deformation of the top of the quay wall depends on other factors as well, such as the shaft resistance of the combined wall, axial stiffness of the combined wall and amount of heave that occurs. Therefore, the stiffness of the fixed-end anchor could not be determined with a high accuracy. For the considered fixed-end anchor stiffness values the maximum difference between the calculated vertical deformation of the bottom of the combined wall is less than 3 millimetres, see Figure 6.2. Since this difference is quite small it seems valid to use either three of the considered fixed-end anchor stiffness values, for further calculations the middle value of 100000 kN is used.

Based on a comparison of results between the HSsmall model and the HS model it appears that the difference between both models is small, this applies both to the horizontal deformation of the quay wall and the occurrence of heave. Since the HSsmall model requires more calculation time than the HS model it is most effective to continue calculations with the HS model.

7

Relevance of the construction process compared to the limit states

The validated FE model is extended to predict the behaviour of the quay wall during the Serviceability Limit State (SLS) and Ultimate Limit State (ULS). With this model it is possible to determine the relevance of the construction process compared to the limit states. If the construction process proves to be significant compared to the limit states the potential of the measurement data obtained during the construction process increases. In this chapter a comparison is made between the magnitude of the deformations and forces that occur during the construction process and those during the limit states. Furthermore, the influence of the strength and stiffness of the soil layers is determined by performing a sensitivity analysis. Finally, it is possible to quantify how much the functionality of the quay wall can be optimised. This chapter allows to answer the third, fourth and fifth research sub-questions.

7.1. Model input for semi-probabilistic design approach

The validated FE model is extended to predict the behaviour of the quay wall during the Serviceability Limit State (SLS) and Ultimate Limit State (ULS). A semi-probabilistic design approach is used in this study. In a semi-probabilistic design approach uncertainty in loads and material parameters is dealt with by applying so-called partial factors to them. This means that the loads are multiplied with the partial factors and the material parameters are divided by the partial factors. The Eurocode presents three different design approaches. Each design approaches uses different partial factors on the loads, soil parameters and resistances. In accordance with NEN 9997-1, the Dutch standard for the design of geotechnical structures, **design approach 3** is used. In design approach 3 partial factors are applied to the loads and the soil parameters.

In subsections 7.1.1 to 7.1.4 the additional model input for the SLS and ULS calculation phases are presented. A summary of the additional model input is presented below.

- Construction phase
  - The construction phases are calculated with characteristic values of the soil strength parameters and the mean values of the stiffness parameters.
  - The geometrical parameters for the construction phases are equal to those of the a priori models. So no increase in the water level difference and bottom depth in front of the quay.
  - In the construction phases no surface loads are present and no partial factors are applied on any of the soil parameters.
- SLS phase
  - SLS calculation phases are performed with characteristic values of soil strength parameters

and mean values for the stiffness parameters.
  - The loads applied in the SLS calculation phases are characteristic values.
  - SLS calculations are performed with the additional bottom depth in front of the quay wall and the presence of a water level difference
- ULS phase
  - ULS calculations are performed with design values of the soil strength parameters and loads
  - The soil stiffness in the ULS calculations is a characteristic value (cautious estimate), in accordance with CUR166 and CUR211 the characteristic value is determined by dividing the mean with a factor 1.5
  - ULS calculations are performed with the additional bottom depth in front of the quay wall and the presence of a water level difference
  - ULS phases are calculated according to scheme B; the ULS calculation phases are performed for each SLS calculation separately, which means that only the last calculation phase uses design values of soil parameters and partial factors on loads

7.1.1. Soil parameters

In SLS and ULS calculations the uncertainty in the soil parameters should be taken into consideration. This means that performing the calculations with mean values of the parameters might be too optimistic. Therefore, a more cautious estimate of the soil parameters is required for some soil parameters. In this subsection the soil parameters used for the SLS and ULS calculation phases are discussed.

Characteristic values
The **mean** value of the soil parameters used in this chapter are equal to the soil parameter values of the **mean** a priori model, as presented in Table 5.4. The standard deviations used to determine the lower and upper bound values of the 95% confidence interval are those determined in chapter 5 based on the CPT results, see Table 5.2. No coefficient of variation is determined for the cohesion of the soil layers. Therefore, the coefficient of variation as mentioned in table 2b of NEN 9997-1 is used, which is 20%.

For the SLS calculations the soil strength parameters should be chosen such that they are cautious estimates of the values that effect the governing limit state, the cautious estimate is also known as the **characteristic value** of a soil parameter. The limit states considered in this chapter all involve the mobilisation of large volumes of soil. Therefore, the characteristic value of the soil strength parameter should be a cautious estimate of the mean value of the soil parameter. According the NEN 9997-1 the cautious estimate of the mean value of a soil parameter is calculated based on a interval that contains the actual mean value with 95% confidence. For the soil strength parameters a low value is governing for the occurrence of a limit state, which means that the cautious estimate of the mean is the lower value of the 95% interval. The lower bound value of the 95% interval is determined with equation 5.1.

For the stiffness parameters the mean value is used in the SLS calculations to estimate the deformations of the quay wall as best as possible. For the volumetric unit weight, the power parameter (m) and dilatancy angle (ψ) the characteristic values are assumed to be equal to the mean value as well. In table 7.1 the soil parameters used in the SLS calculation phase are presented.

Design values
Partial factors should be applied to the strength parameters of the soil to account for uncertainty in these parameters. This means that the characteristic value of the strength parameters is reduced by dividing them with a partial factor, see equation 7.1 in which γ is the partial factor. Different partial factors exist for the cohesion and the friction angle. The partial factors depend on the amount of uncertainty in the parameter and the influence of the parameter on the considered limit state. Furthermore, the partial factors depend on the reliability class of the quay wall and the design life. The quay wall is designed for a period of 100 years and has reliability class RC2 [Putteman et al., 2017]. The partial factors presented in the CUR211 are based on a design life of 50 years, since the design life of the quay wall is 100 years the partial factors should be increased. The increase in the partial factors is equal to 1.016 for the friction angle and 1.032 for the cohesion, see CUR166 chapter 2.4.7 for the applied formula.

layer	Cross-section	γ_{dry} [kN/m^3]	γ_{sat} [kN/m^3]	ϕ_p' [^{0}]	ψ [^{0}]	c' [kPa]	E_{oed}^{ref} [MPa]	E_{50}^{ref} [MPa]	E_{ur}^{ref} [MPa]	m [-]
1	B4	16.5	20.0	46.0	6.5	1	50	50	150	0.50
	D1			47.0	6.0	1	45	45	135	
2	B4	15.5	15.5	30.0	-	5	3	5	25	1.00
	D1			30.0	-	5	3	5	25	
3	B4	17.0	20.5	48.0	8.0	1	70	70	210	0.45
	D1			45.5	6.5	1	60	60	180	
4	B4	16.0	19.5	46.0	5.0	1	45	45	135	0.50
	D1			46.5	6.5	1	45	45	135	
5	B4	17.0	20.0	47.0	7.5	1	50	50	150	0.50
	D1			47.5	7.0	1	45	45	135	
6	B4	15.0	19.0	35.0	3.5	1	30	30	90	0.55
	D1			35.0	3.5	1	30	30	90	
7	B4	14.0	18.5	32.5	0.0	1	8	8	25	0.65
	D1			31.5	0.0	1	8	8	25	
8	B4	16.5	16.5	30.0	-	7	3	6	30	1.00
	D1			30.0	-	7	3	6	30	
9	B4	15.0	19.0	38.0	2.0	1	30	30	90	0.60
	D1			-	-	-	-	-	-	
10	B4	16.5	20.0	43.5	7.0	1	45	45	135	0.50
	D1			43.0	6.0	1	45	45	135	
11	B4	17.0	20.5	45.0	8.0	1	50	50	150	0.45
	D1			44.5	7.0	1	50	50	150	
12	B4	16.0	20.0	42.0	5.0	1	40	40	125	0.50
	D1			41.5	5.0	1	40	40	125	

Table 7.1: Soil parameters used for SLS calculation phases

The partial factors used for the ULS calculations are presented in Table 7.3.

$$X_{design} = \frac{X_{characteristic}}{\gamma} \tag{7.1}$$

In the ULS calculation phase a cautious estimate of the stiffness parameters should be used to account for the uncertainty in the stiffness of the soil. For the stiffness of the soil it is unknown beforehand whether a high or low value of the stiffness moduli is governing for the forces in the structural components. In general low stiffness moduli result in the highest value of the bending moment in the retaining wall. Whereas, high stiffness moduli lead to the highest anchor forces [De Gijt and Broeken, 2013]. To see what influence the high and low stiffness moduli have on the anchor forces additional calculations are made. According to these calculations the difference between the anchor forces was limited. This is most likely because the stiffness moduli are only change for the ULS calculation phase. It was decided to perform the ULS calculations with low values of the stiffness moduli only. No partial factors exist to convert the mean values of the soil stiffness moduli to design values. It is standard practice to divide the mean stiffness moduli by a factor 1.5 in order to obtain the design values of the stiffness moduli [De Gijt and Broeken, 2013]. In chapter 5 the lower bound value of the mean stiffness moduli was determined based on the CPT results. For the different soil layers the lower bound of the 95% confidence interval of the mean was a factor 1.1 to 1.4 lower than the mean value, the average factor is approximately 1.25. Nevertheless, it is decided to determine the design value of the stiffness moduli by dividing the mean value with a factor 1.5, which is in line with common practise.

7.1.2. Loads on the quay wall and load combinations

According to the design report of the quay wall [Putteman et al., 2017] the following representative loads can be present on the quay wall:

- SL: Uniform surface load of 40 kPa, present from the front of the quay wall to 46 metres behind it.
- TL: Tank Load of 168 kPa, present from 46 metres of the quay wall.
- BF: Bolder force, this force is per metre length of quay wall. The bolder force acts in the horizontal plane and is located 500 millimetres above the top of the quay wall. Therefore, a moment is created by the bolder force as well.
  - section B4: 265 kN/m + 132.5 kNm/m (265 kN/m * 0.5 m)
  - section D1: 165 kN/m + 82.5 kNm/m (165 kN/m * 0.5 m)

From the presented representative loads multiple load combinations can be made. In Figure 7.1 the general equations for making load combinations are shown. In these equation $G_{k;j}$ is a permanent load due to the soil weight, which is always present. Each load combination has 1 primary load $Q_{k,1}$ and 1 or 2 secondary loads $Q_{k,i}$. The ψ-factors that are used for the load combinations are based on those presented in CUR211. Only the governing load combinations based on the design report are used in this thesis. The load combinations (LC) used are numbered and each LC is calculated in SLS and ULS. It is noted that no partial factors on the loads are applied in SLS calculation phases. In Table 7.2 the factors applied to the representative loads are visualised for each LC (these factors are including the partial factors). The partial factors applied on the loads are presented in Table 7.3.

- **LC1**: main load= SL ; side load= TL
- **LC2**: main load= BF ; side load = SL

SLS $$\sum_{j\geq 1} G_{k,j} + Q_{k,1} + \sum_{i>1} \psi_{0,i} Q_{k,i}$$

ULS $$\sum_{j\geq 1} \gamma_{G,j} . G_{k,j} + \gamma_{Q,1} . Q_{k,1} + \sum_{i>1} \gamma_{Q,i} . \psi_{0,i} Q_{k,i}$$

Figure 7.1: Equations for making load combinations in SLS and ULS

Load Combination	Load type		
	SL	TL	BF
1-SLS	1	0.7	0
2-SLS	0.7	0	1
1-ULS	1.1	0.77	0
2-ULS	0.77	0	1.3

Table 7.2: Overview of factors applied on representative loads for each load combination

Soil parameters		Loads		
$\gamma_{\phi'}$ [1]	γ_c	γ_{SL}	γ_{TL}	γ_{BF}
1.27	1.5	1.1	1.1	1.3

Table 7.3: Partial factors soil parameter and loads, based on RC2 and design life of 100 years according to CUR211; [1] Partial factor is applied to $\tan\phi'$

7.1.3. Geometrical input parameters

The geometrical input parameters for the SLS and ULS calculation phases are based on the design report of the quay wall [Putteman et al., 2017].

Bottom depth
For the a priori FE models the bottom depth in front of the quay wall is based on the surveys performed during the construction process. During the lifetime of the quay wall the bottom depth in the front of the quay wall might increase. This could happen if too much soil is dredged during maintenance work or due to bowthruster-induced flow of ships. The bowthruster-induced flow could result in scour holes in the bottom since no bottom protection is applied at the HHTT-quay. To account for this uncertainty the bottom depth is increased in the SLS **and** ULS calculation phases. For section B4 the bottom depth becomes NAP -25.5 m near the combined wall (it was NAP -24.5 m) and at a distance of 12.5 metres from the combined wall the bottom depth increases to NAP -26.6 m under a slope of 1:4. At section D1 the bottom depth becomes NAP -16.1 m (it was NAP -15.5 m) and at a distance of 5.5 metres from the combined wall the bottom depth increases to NAP -17.7 m under a slope of 1:4.

Water levels
During the construction process no water level differences where measured. This is because the drainage system was already operational during the construction process. During the lifetime of the quay wall a water level difference might occur. Therefore, a water level difference of 0.5 metres is introduced for the SLS **and** ULS calculation phases. The ground water level is NAP -0.35 m and the harbour water level is NAP -0.85 m.

Failure of the drainage system could lead to a substantial increase in the water level difference. In the design report load combinations including this substantial water level difference where checked. The substantial water level difference did not lead to a governing situation for the considered limit states and is therefore not considered in this study.

7.1.4. Calculation scheme

It is noted that all the load combinations start from the final construction process, which means that the different load combinations are calculated separately and do not influence each other. The question is how to perform the SLS and ULS calculations with respect to each other. In general there are two possible calculation schemes, scheme A and scheme B see Figure 7.2.

In the case of scheme A calculations are performed by using design values of soil parameters and partial factors on loads in each calculation phase, meaning that the ULS calculation phases are performed subsequently. In the case of calculation scheme B the ULS calculation phases are performed for each SLS calculation separately, which means that only the last calculation phase uses design values of soil parameters and partial factors on loads.

If SLS calculation results are also desired two different calculation paths are required in the case of scheme A, these are shown in the aforementioned figure. Therefore, calculation scheme A requires more calculation time than calculation scheme B.

In the case of scheme B reduced stiffness moduli of the soil are only applied to calculate displacements that occur because of the higher ULS loads and the redistribution of stresses due to reduced strength parameters. Whereas, for scheme A the reduced stiffness is also used during the construction phase and the representative load. This means that deformations and forces are generally higher in the case of calculation scheme A.

The decision is made to apply calculation scheme B since this scheme uses characteristic values of strength parameters and mean values of the stiffness moduli during the construction process. From the analysis performed in chapter 5 it was concluded that the a priori FE model is in line with the measurement data. Therefore, it seems unrealistic to calculate phases prior to the ULS calculation phase with design values of the strength and stiffness parameters.

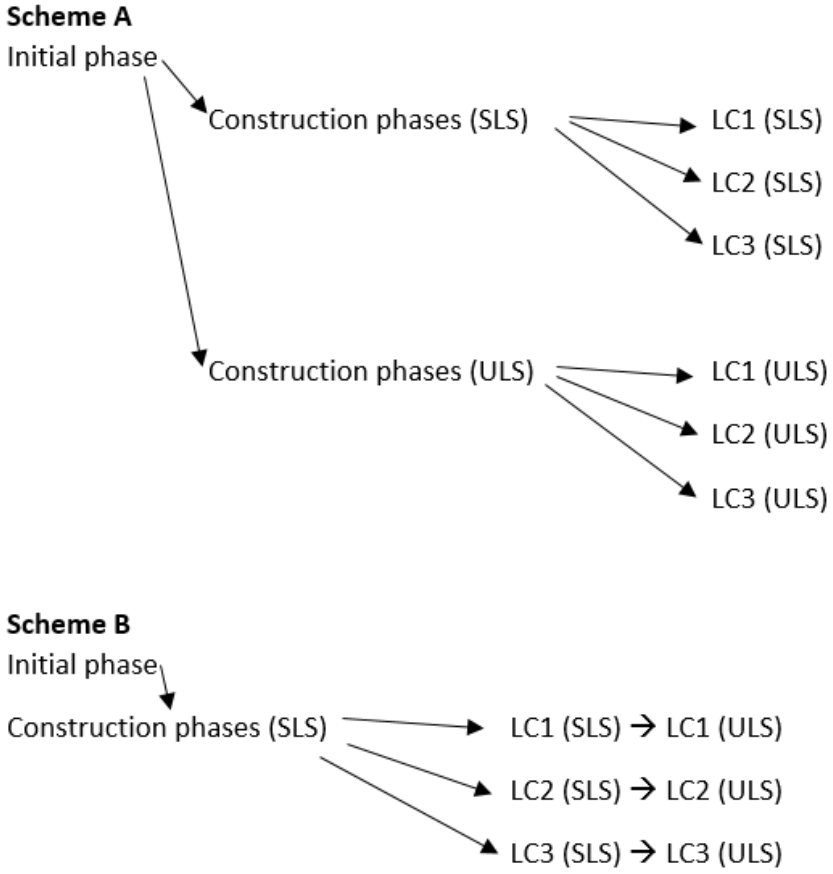

Figure 7.2: Calculation scheme A versus B

7.2. Softening behaviour

In section 5.7 the a priori FE model was checked for plastic points at the end of the construction process to estimate if softening behaviour of the soil could be expected. The amount of plastic points was limited and no softening behaviour is expected. Therefore, it is valid to calculate with the peak shear strength for the construction process.

In the SLS and ULS phases the loads on the quay wall are higher compared to the construction process. Therefore, the strains will increase and it might be that the peak shear strength is reached in a large soil volume at the end of the SLS or ULS phase. To determine if the peak shear strength is reached the FE model is checked for plastic points in the SLS and ULS phases. In Figures 7.3 and 7.4 the plastic points are presented in the SLS and ULS phases respectively.

In both the SLS and ULS phases plastic points occur in the active zone at the interface between the combined wall and the soil. At the interface the normal stresses reduce due to the horizontal deformation of the combined wall. Whereas, the shear stresses increase as a result of the shaft friction. The plastic points at the interface have a local effect and should not be considered to determine if softening behaviour occurs in the active zone. In the active and passive soil wedges the amount of plastic points is still limited during the **SLS** phase. In the **ULS** phase more plastic points are visible compared to the **SLS** phase. However, the volume of soil that shows plastic points is not large and a continuous shear band that is in failure is not visible either. Nevertheless, it could be that softening is starting to occur in the **ULS** phase. To determine what the influence of softening is on the behaviour of the quay wall **additional** calculations are made in which the shear strength value is reduced.

To account for softening it is common practise to use the shear strength value that occurs at a 5% strain level during triaxial tests. At these strain levels softening has not fully occurred yet, meaning that the friction angle is still higher than the constant volume friction angle. The sand layers that showed signs of softening behaviour during the triaxial tests are layers 3 to 5 and 9 to 12, all these layers have a high relative density. According to the triaxial test results the difference between the peak friction angle and the friction angle at 5% axial strain is 1 à 2 degrees for the aforementioned layers. To determine the maximum influence of softening the peak friction angles of layers 3 to 5 and 9 to 12 are reduced with **with 2 degrees** compared to the values presented in Table 7.1.

During the triaxial tests of layers 6 to 8 the peak shear strength occurred beyond an axial strain level of 5%. Therefore, the shear strength of these layers was already determined based on a 5% axial strain level. As a result it is not necessary to reduce the friction angle of layers 6 to 8.

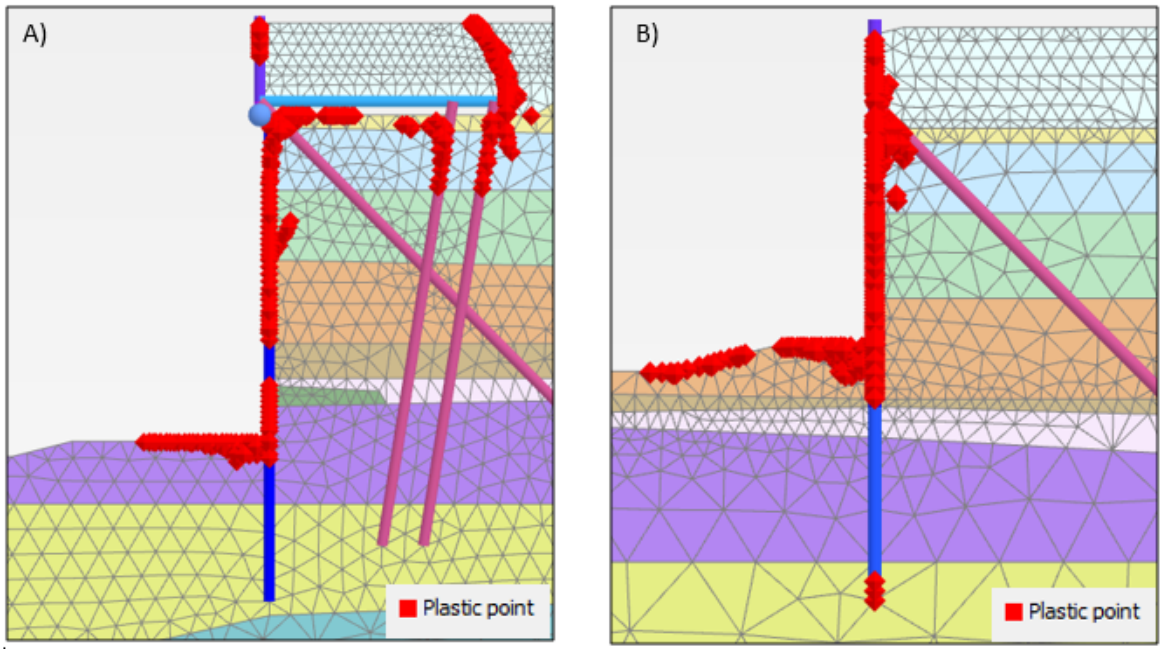

Figure 7.3: Plastic stress points in the FE model for SLS phase, A) section B4 and B) section D1

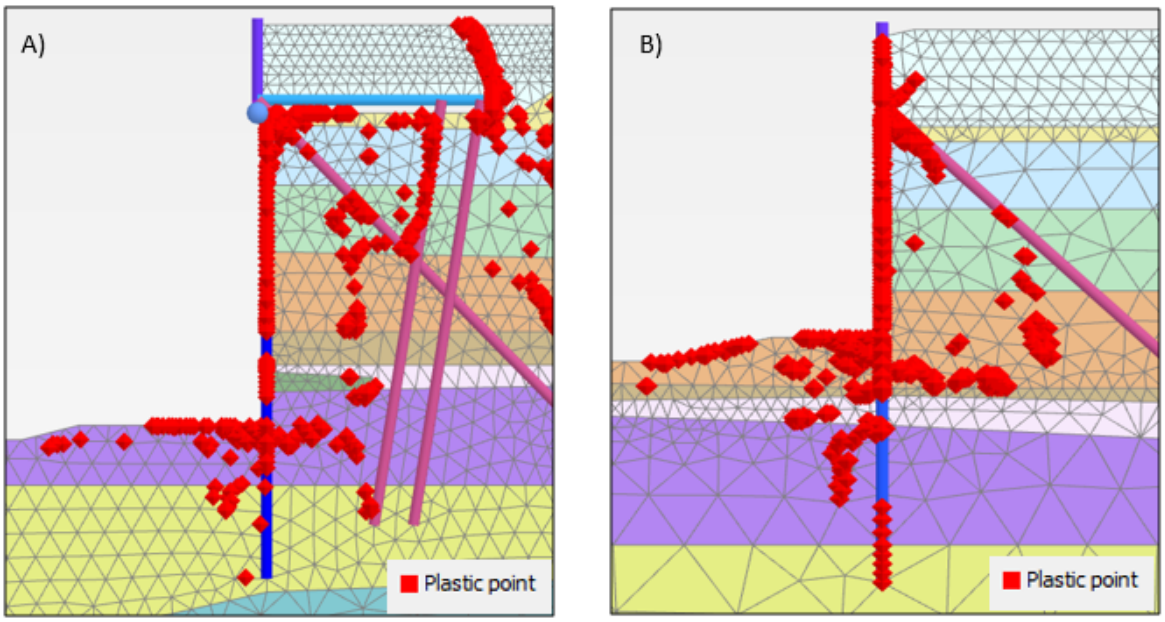

Figure 7.4: Plastic stress points in the FE model for ULS phase, A) section B4 and B) section D1

7.3. The significance of the deformations and forces of the construction process

To better understand if measurement data obtained during the construction process could be used to optimise the functionality of a quay wall we must get an indication of how significant the forces and deformations are at the end of the construction process compared to the SLS and ULS. If the construction process is responsible for a significant part of the forces and deformations that occur in the SLS and ULS the potential of the measurement data is larger.

The important deformations and forces of the quay wall are considered to be the maximum horizontal deformation of the combined wall, the maximum bending moment in the combined wall and the maximum anchor force. The FE model results of these deformations and forces are presented in Figures 7.5 to 7.7 for the final construction, SLS and ULS phases. In the aforementioned figures two lines are presented for each section, these lines represent the FE model results **with and without** softening behaviour. It can be seen that the difference in calculation results between the situation with and without softening is limited to approximately 5%. This is an indication that the majority of the soil volume is far from yielding. If the soil would be close to yielding it is expected that reducing the friction angle of the soil would result in a larger increase of forces and deformations due to the occurrence of large amounts of plasticity.

The deformations and forces that occur during the construction process are compared to those that occur during the SLS and ULS phases. The ratio between the deformations and forces at the end of the construction process and those at the SLS and ULS are presented in Table 7.4 as a percentage. There is no significant difference between the situation with and without softening behaviour. Therefore, the percentages presented in the aforementioned table are valid for both situations.

Section	Ratio	Horizontal deformation	Bending moment	Anchor force
B4	FC / SLS	65%	80%	35%
	FC / ULS	45%	65%	25%
D1	FC / SLS	50%	65%	55%
	FC / ULS	35%	50%	45%

Table 7.4: Ratio between construction process and SLS or ULS phase

The horizontal deformation and bending moment in the combined wall that develop during the construction process are quite significant compared to SLS and ULS. The ratio of the horizontal deformation and bending moment are higher for section B4 than for section D1, even tough the applied surface load is equal for both sections. The reason for this is the presence of the relieving platform at section B4, which transfers most of the surface load to deeper layers and thus relieves the active zone. Therefore, the surface load at section B4 results in a lower increase in horizontal deformation and bending moments than it does at section D1.

The ratio of the anchor force is higher for section D1 because the anchor force is influenced by the sand fill. During the construction process a sand fill is placed, which causes the soil to settle and increases the anchor force. At section B4 this effect does not take place due to the presence of the relieving platform. Therefore, the ratio at section D1 is higher than it is at section B4.

Overall the construction process accounts for a large part of the total deformations and forces of the quay wall that occur during the SLS and ULS. Therefore, it seems that the measurement data which is obtained during the construction process has the potential to provide insight into the behaviour of the quay wall during the limit states.

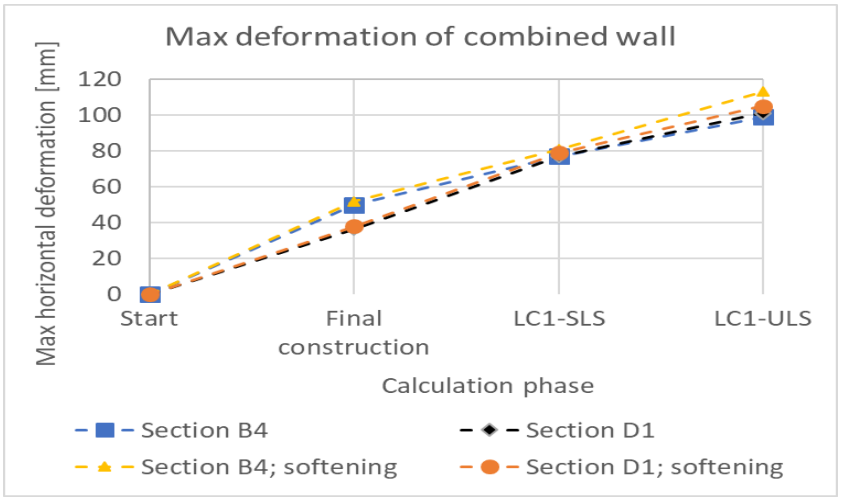

Figure 7.5: Development of maximum horizontal deformation of the combined wall

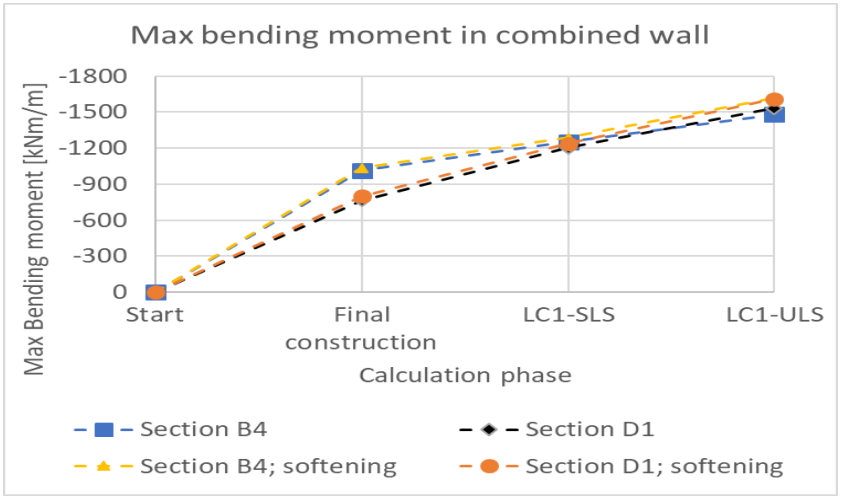

Figure 7.6: Development of maximum bending moment in the combined wall

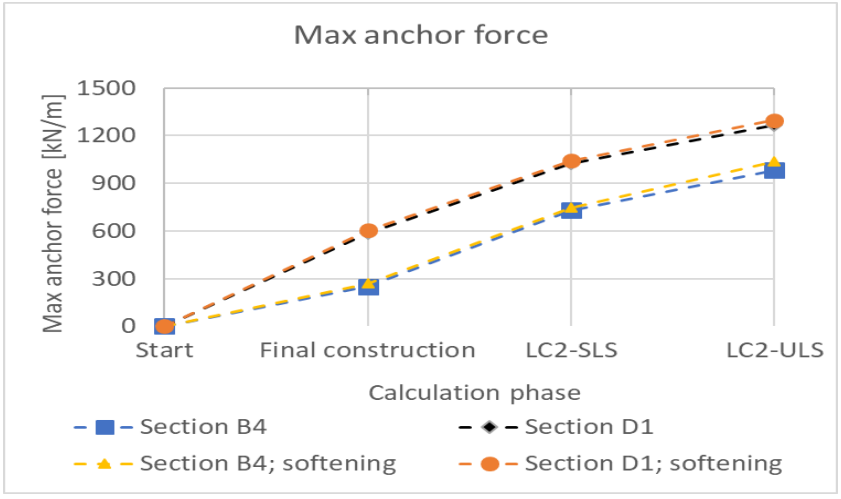

Figure 7.7: Development of maximum anchor force

7.4. Sensitivity analysis

7.4.1. Considered phases, criteria used and selection of soil parameters

The phases considered in the sensitivity analysis are the final construction phase (FC), SLS phase and ULS phase. For the final construction phase and the SLS phase the results of the sensitivity analysis turned out to be comparable for the situation with and without softening. Therefore, only the situation without softening is presented for these phases. For the ULS phase a difference in sensitivity is visible for the situation **with and without** softening, as a results both situations are presented for the ULS phase.

The sensitivity of the soil layers is based on 2 criteria, which are the maximum horizontal deformation and the maximum bending moment of the combined wall. These criteria are used because their significance at the end of construction process is large compared to the limit states, see the previous section. Both the maximum bending moment and the maximum horizontal deformation occur during load combination 1. As a results the sensitivity analysis is performed by using this load combination only.

The soil parameters considered in the sensitivity analysis are the friction angle (strength) and stiffness moduli. These two parameters are considered to be the dominant soil parameters. Cohesion is not considered because the soil profile predominantly consists of cohesionless soil layers. To assure a fair comparison between the two parameters they are both varied **± 1 times the standard deviation**. For the stiffness moduli the coefficient of variation is **10%**, this value is prescribed by NEN 9997-1. In the calculations performed for the sensitivity analysis the ratio between the stiffness moduli (E_{50}^{ref}, E_{oed}^{ref} and E_{ur}^{ref}) is kept constant. From the analysis of the CPT's in chapter 5 a coefficient of variation between 1 à 4% was found for the friction angle. This value is lower than the 10% prescribed by the NEN 9997-1. It is decided to the set the coefficient of variation of the friction angle equal to **5%**.

7.4.2. Explanation sensitivity score

The sensitivity of the soil parameters is based on the sensitivity score [Brinkgreve, 2019b]. The sensitivity score is a method which can be used to determine how much influence a parameter has on the model outcome. In this section an explanation is given on how the sensitivity score is determined. The sensitivity score is determined separately for each criteria. The method is presented step by step. As an example the sensitivity score of section D1 during the final construction phase with the criteria maximum bending moment is shown.

1. For each parameter considered in the sensitivity analysis the maximum and minimum parameter values are determined
   - The parameters are varied ± 1 times the standard deviation.
2. Perform calculations with the maximum and minimum value of each parameter.
   - In each calculation 1 parameter is set equal to the maximum **or** minimum value and all other parameters are set to the base value. When n parameters are used in the sensitivity analysis a total of 2*n calculation are performed.
3. The criteria are retrieved from the calculation results and the global score of each parameter is determined. The friction angle and stiffness of each layer are denoted as ϕ_i and E_i respectively with i equal to the layer number.
   - The global score of a parameter x_i is calculated as:

$$x_{i;globalscore} = | f(x_{i;max}) - f(x_{i;min}) | \tag{7.2}$$

in which $f(x_{i;max})$ is the result obtained when the maximum parameter value is used and $f(x_{i;min})$ the result when the minimum parameter value is used. In the next table the global score is presented for section D1 during the final construction phase with the criteria maximum bending moment.

Parameter	Bending moment [kNm/m]		
	$f(x_{i;max})$	$f(x_{i;min})$	Global score
φ_5	-710	-764	54
φ_6	-710	-768	58
φ_7	-739	-739	0
φ_8	-738	-740	2
φ_{10}	-737	-739	2
φ_{11}	-738	-738	0
E_5	-737	-751	14
E_6	-734	-754	20
E_7	-739	-739	0
E_8	-737	-745	8
E_{10}	-739	-740	1
E_{11}	-737	-740	3

4. Determine the sensitivity score of each parameter
   - From the global score of each parameter it is possible to determine the sensitivity score with:

$$x_{i;sensitivity} = 100 \cdot \frac{x_{i;globalscore}}{\sum_{i=1}^{n} x_{i;globalscore}} \tag{7.3}$$

in which n is the number of parameters used in the sensitivity analysis. In the next table the sensitivity score is presented for section D1 during the final construction phase with the criteria maximum bending moment. Next to the table a figure is shown to illustrate how the results of the sensitivity analysis are presented in the next subsection.

Parameter	Global score	Sum global score	Sensitivity score
φ_5	54	162	32%
φ_6	58		35%
φ_7	0		1%
φ_8	2		1%
φ_{10}	2		2%
φ_{11}	0		1%
E_5	14		8%
E_6	20		12%
E_7	0		0%
E_8	8		5%
E_{10}	1		1%
E_{11}	3		2%

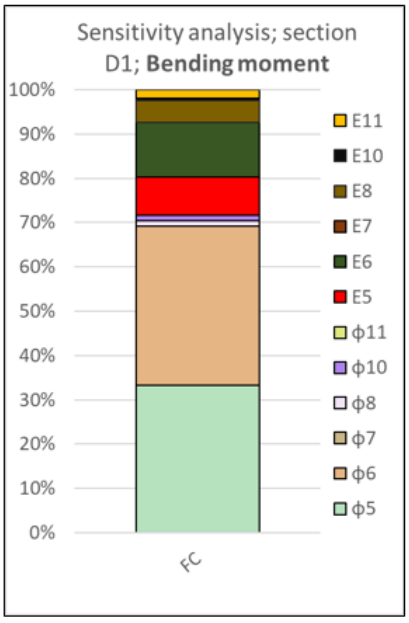

7.4.3. Results sensitivity analysis

The sensitivity analysis is performed for sections B4 and D1 separately, which are the sections with a relieving platform and without a relieving platform respectively.

Section B4
The soil layers that are included in the sensitivity analysis are layers 5 to 11 with the exception of layer 9, this is because layer 9 is a very thin soil layer. Layers 1 to 4 are located in the upper part of the soil profile and are expected to have a limited influence on the behaviour of the quay wall. Before the results of the sensitivity analysis are presented a resume is given on the soil profile present at section B4, see Figure 7.11. Layers 5 to 8 are located in the active zone, whereas layers 10 and 11 are located in the passive zone.

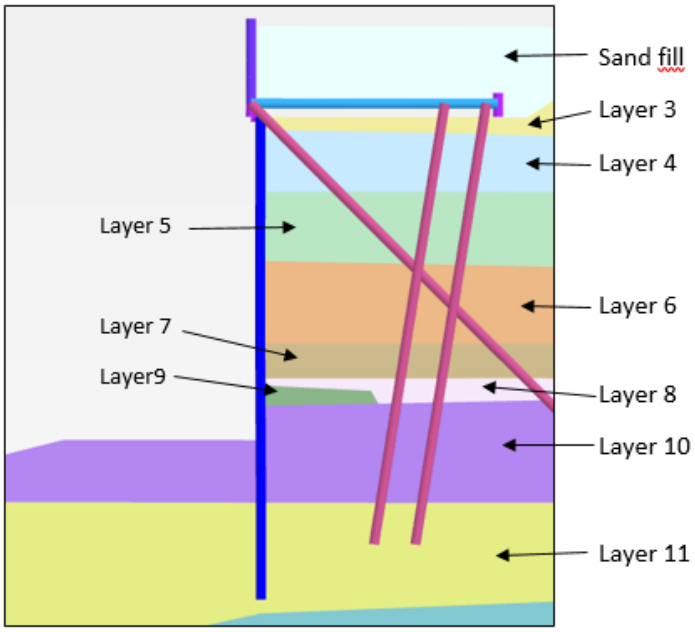

Figure 7.8: Soil profile at section B4

In Figure 7.10 the results of the sensitivity analysis are presented for section B4. On the left side of the figure the criteria on which the sensitivity score is based is the horizontal deformation and on the right side the bending moment. First the results of the sensitivity analysis are discussed for every phase individually and then the conclusions are given.

Final construction phase
For both criteria it can be seen that the overall influence of the friction angle is slightly larger than the stiffness moduli, the contribution of the friction angle is approximately 60% and that of the stiffness moduli approximately 40%. In Figure 7.9 the hardening points in the FE model during the final construction phase are presented. These hardening points indicate that the shear strength of the soil is being mobilised. It can be seen that the hardening points are present in all considered layers, as a result the strength of all these layers has an influence.

The layers in the active zone have the biggest influence on the horizontal deformation and bending moment during the final construction phase. This is because the parameters of these layers influence the magnitude of the active horizontal load on the quay wall. Layers 10 and 11 are responsible for the passive resistance on the quay wall, the passive resistance is only partially mobilised and therefore the parameters of layer 10 and 11 are less influential during the final construction phase.

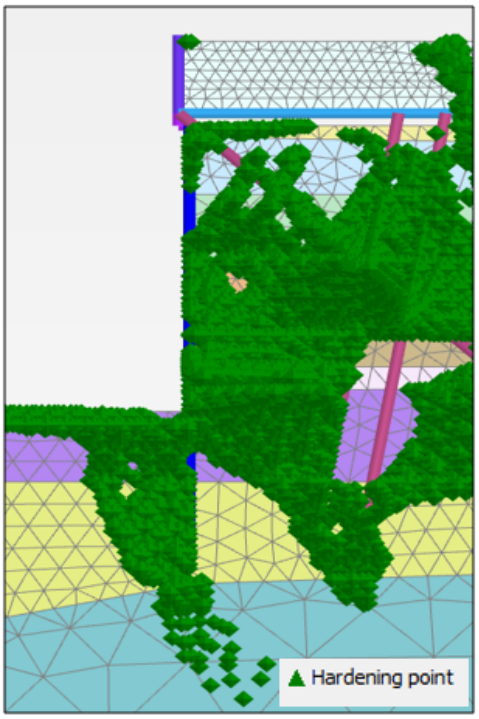

Figure 7.9: Hardening points during Final construction phase at section B4

SLS phase
In general the sensitivity in the SLS phase is comparable to the final construction phase. There is an increase in the sensitivity of the friction angle of layer 10. Due to the loads on the quay wall the horizontal deformations increase, which leads to a higher mobilisation of the shear strength in layer 10. Near the bottom level, where layer 10 is located, the horizontal deformations are larger than at the location of layer 11. Consequently, the friction angle of layer 10 has more influence than the friction angle of layer 11.

The influence of active layers is still present in the SLS phase. Especially for the bending moment the friction angle and the stiffness of layer 6 and 7 have an influence, which is because layer 6 and 7 are located at the height of the maximum bending moment.

ULS phase
In the ULS phase partial factors are applied to the loads and soil parameters. This means that the strength of the soil is lower compared to the final construction and SLS phase. This leads to more plasticity in the model and therefore the friction angle becomes increasingly influential. Overall the strength of the soil layers accounts for 75% of the sensitivity. Moreover, a further increase in the influence of the strength of layer 10 can be observed. This indicates that the sensitivity shifts from the soil layers in the active zone towards the layers in the passive zone as the deformations increase. The friction angle of layers 6, 7, and 10 are governing for the behaviour of the quay wall in the ULS phase.

ULS with softening
Due to softening behaviour the strength of the sand layers decreases, which leads to more deformation of the quay wall. Therefore, the sensitivity shift further towards the passive zone. This can be seen by the increased influence of the friction angle of layers 10 and 11.

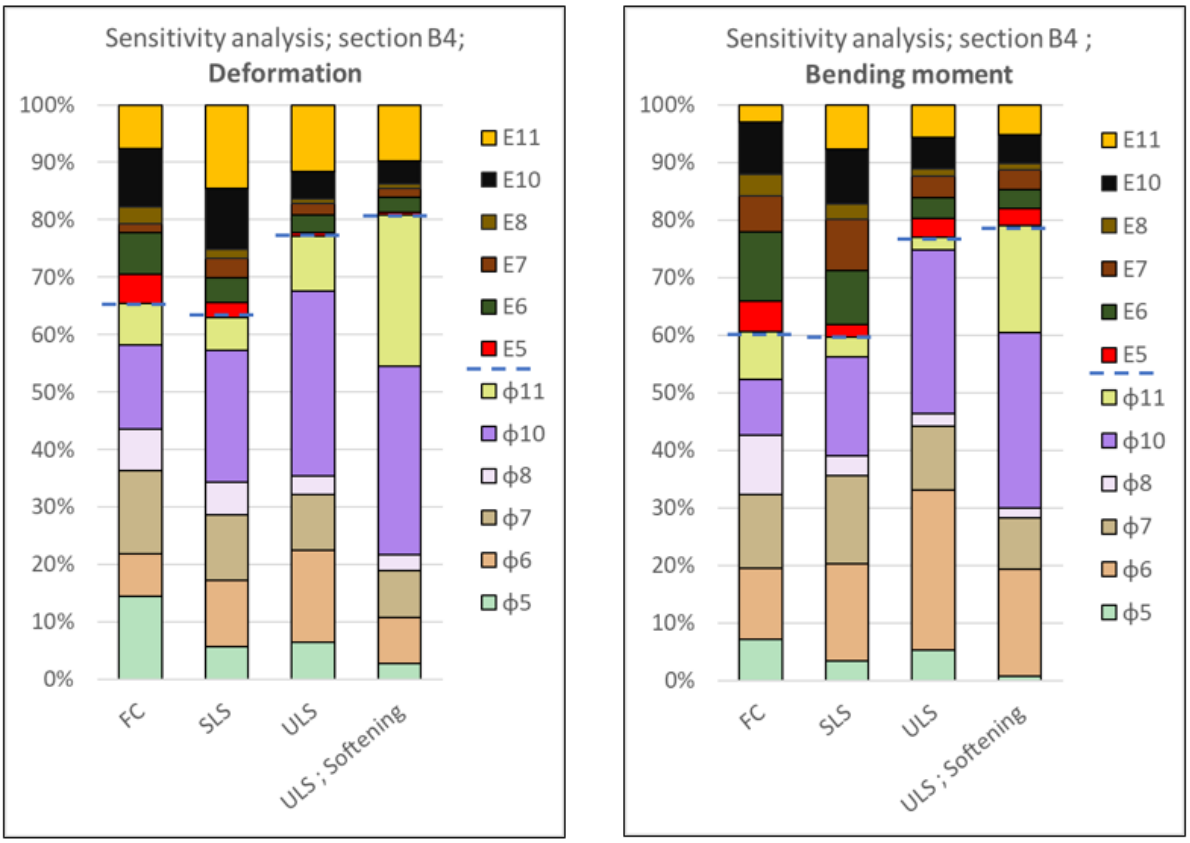

Figure 7.10: Results sensitivity analysis section B4; criteria are maximum deformation and bending moment in the combined wall

The **conclusions** of the sensitivity analysis of section B4 are:

- The overall influence of the friction angle on the behaviour of the quay wall during the final construction phase is slightly larger than the stiffness moduli. The contribution of the friction angle is approximately 60% and that of the stiffness moduli approximately 40%.
- The friction angle of the layers in the active zone have the biggest influence on the horizontal deformation and bending moment during the construction process. This is because the friction angle of these layers influence the magnitude of the active horizontal load on the quay wall.
- With increasing deformations the influence of the friction angle in the passive zone increases.
- In the ULS phase the behaviour of the quay wall is predominantly influenced by the strength of the soil
- In the ULS phase the governing soil parameters are the friction angle of layers 6, 7 and 10. If softening behaviour is considered the influence of the friction angle of layer 11 becomes important too.
- If softening behaviour is considered the influence of friction angle of the layers in the passive zone increase

Section D1
The soil layers that are included in the sensitivity analysis are layers 5 to 11 with the exception of layer 9 because this layer is not present at section D1. Layers 1 to 4 are located in the upper part of the soil profile and are expected to have a limited influence on the behaviour of the quay wall. Before the results of the sensitivity analysis are presented a resume is given on the soil profile present at section D1, see Figure 7.11. Layer 5 is located in the active zone, layers 7 to 11 in the passive zone and layer 6 in both zones. At section D1 soil layer 7 is very thin, the thickness of this layer is approximately 0.75 metres.

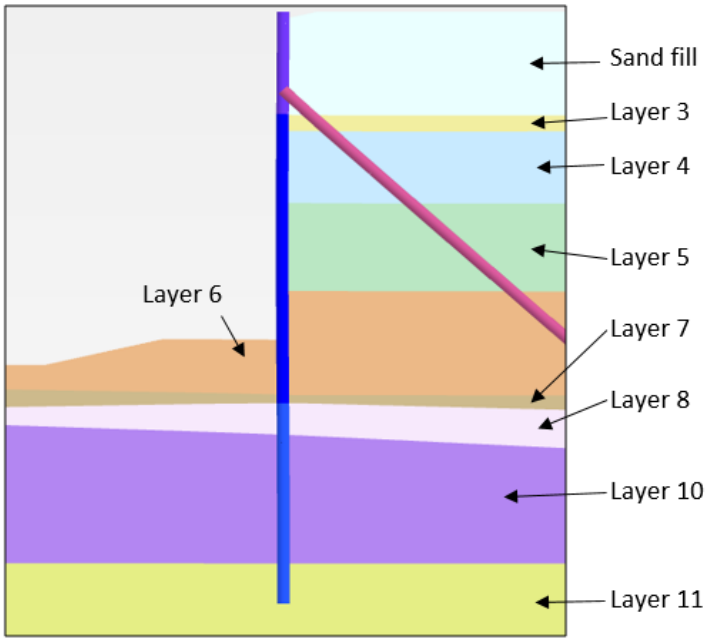

Figure 7.11: Soil profile at section B4

In Figure 7.14 the results of the sensitivity analysis for section D1 are presented. On the left side of the figure the criteria on which the sensitivity score is based is the horizontal deformation and on the right side the bending moment. First the results of the sensitivity analysis are discussed for every phase individually and then the conclusions are given.

Final construction phase
For both criteria the overall influence of the friction angle is larger than the stiffness moduli, the contribution of the friction angle is 70% of the total. The behaviour of the quay wall is dominated by the friction angle of layers 5 and 6. Especially layer 6 has a large influence because this layer is located both in the active zone and the passive zone.

To get more insight into where the horizontal deformations develop in the FE model it is useful to plot the horizontal phase displacement of the final construction phase, see the left side of Figure 7.12. The horizontal phase displacement show how much horizontal displacement develops in the considered calculation phase. In the aforementioned figure it is visible that most horizontal deformation develops in layers 5 and 6 in the active zone.

In the passive zone the majority of the horizontal deformation occurs in layers 6, 7 and 8. Layer 7 is a very thin layer and layer 8 is a soft layer as a results these layers have very little influence. Layers 10 and 11 show less development of horizontal deformation. This indicates that the passive resistance of these layers is only mobilised for a small part, as a result the friction angle is not influential yet. In Figure 7.13 the hardening points in the FE model during the final construction phase are presented. Most hardening points in the passive zone are located in layers 6, 7 and 8. The amount of hardening points in layers 10 and 11 are lower, which confirms that the mobilised passive resistance is lower in these layers.

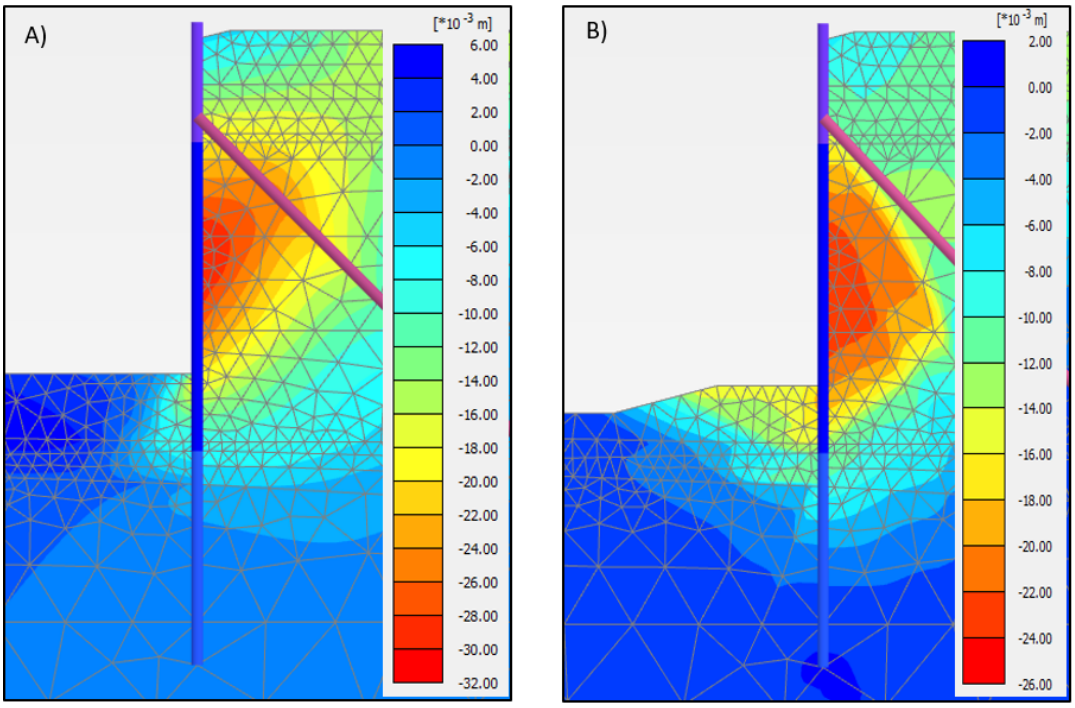

Figure 7.12: Horizontal phase displacement section D1, A) Final construction phase, B) ULS phase

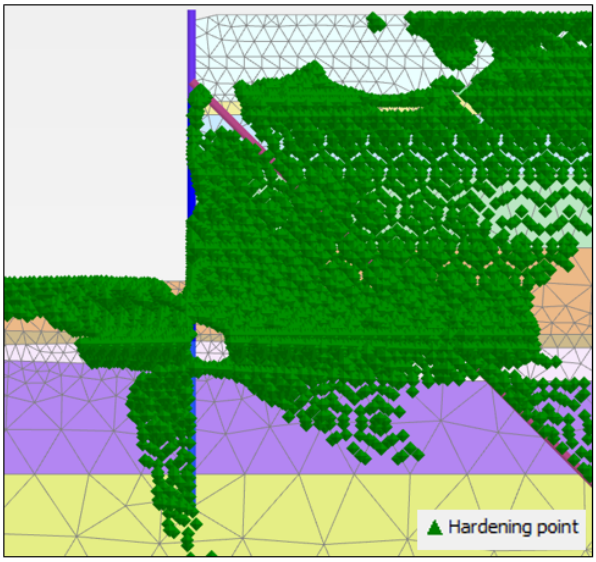

Figure 7.13: Hardening points during Final construction phase at section D1

SLS phase

In the SLS phase the sensitivity scores are comparable to the final construction phase. The friction angle of layer 5 and 6 remain dominant for the behaviour of the quay wall. There is a small increase in the influence of the friction angle of layer 10, but this is not significant.

ULS phase

In the ULS phase more plasticity occurs in the model due to the lower friction angles. Overall the influence of the friction angle of the soil layers accounts for 80% of the sensitivity. In the ULS phase the friction angle of layers 5 and 6 is dominant for the behaviour of the quay wall as well. Even tough the significance of the friction angle of layer 10 increases it does not become bigger than the influence of layers 5 and 6. On the right side of Figure 7.12 the horizontal phase displacement of the ULS phase is shown. It can be seen that the horizontal phase displacement in layer 10 did increase compared to the final construction phase. This explains the increase off the influence of the friction angle of this layers. If the horizontal deformations in these layers would increase the passive resistance is further mobilised and the strength of these layers would become more important.

ULS with softening

Softening behaviour appears to have little effect on the sensitivity score, the strength of layers 5 and 6 remain dominant.

The **conclusions** of the sensitivity analysis of section D1 are:

- For both criteria the overall influence of the friction angle is larger than the stiffness moduli during the final construction phase, the contribution of the friction angle is 70% of the total.
- The friction angle of layer 5 and 6 have dominant influence on the behaviour of the quay wall. This dominant influence remains in all phases.
- There is an increase in the influence of the friction angle of the deep Pleistocene layers (layer 10 and 11) towards the ULS phase, however the total influence of these layers stays limited.
- Softening behaviour appears to have little effect on the sensitivity.

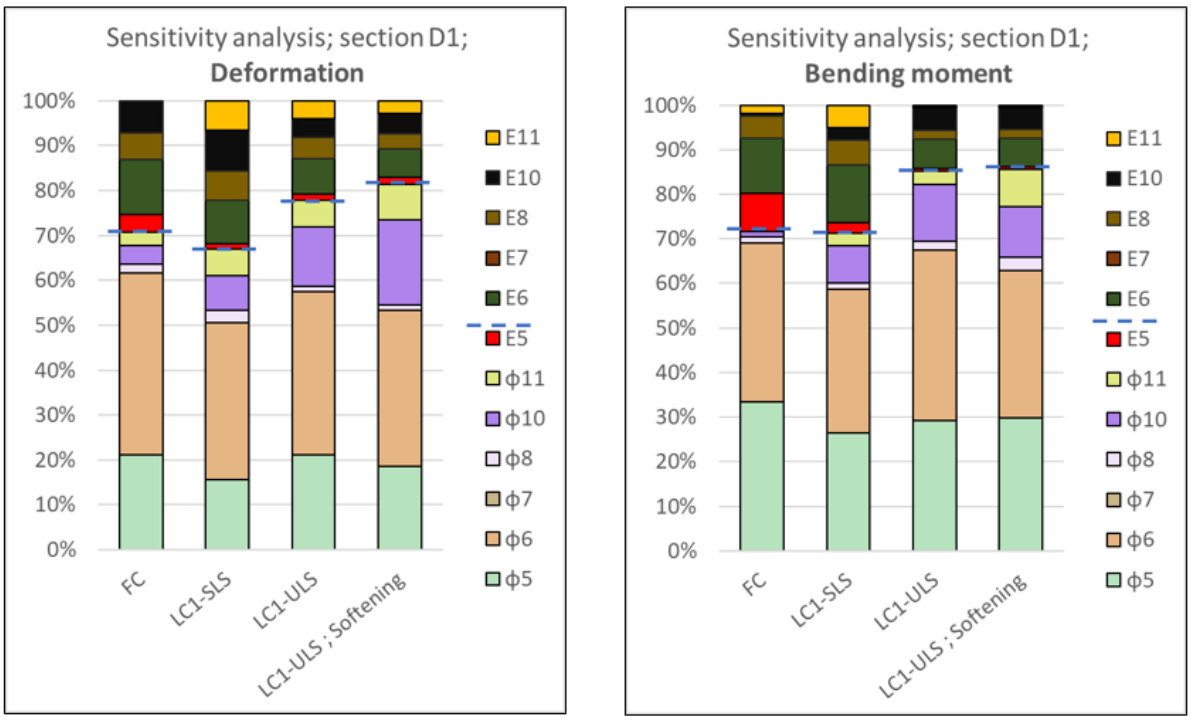

Figure 7.14: Results sensitivity analysis section D1; criteria are maximum deformation and bending moment in the combined wall

7.4.4. Strength versus stiffness evaluation

The Hardening Soil model is an advanced constitutive model that accounts for non-linear soil behaviour under primary deviatoric loading with a hyperbolic stress-strain relationship. This hyperbolic relationship depends both on the soil stiffness and on the soil strength. Therefore, it is difficult to fully separate the influence of the strength and stiffness parameters on the soil behaviour. Based on the sensitivity analysis performed in the previous subsection it was concluded that the overall influence of the friction angle on the behaviour of the quay wall is larger than that of the stiffness moduli. In this subsection the behaviour of soil under primary deviatoric loading is looked at in more detail to support the aforementioned conclusion.

In the Plaxis software package a SoilTest facility is available in which soil tests can be simulated. With the SoilTest facility it is possible to gain more insight into how the strength and stiffness parameters influence the deformation behaviour of the soil. This insight can help to support the conclusions found with the sensitivity analysis. The yield strength and stiffness of soil depend on the effective stress conditions. To be able to link the SoilTest results to the FE model it is important to use stress conditions that are present in the FE model.

Set-up of the laboratory test simulation
The set-up of the laboratory test simulation is explained based on 4 aspects. These are the type of soil test, the considered stress points in the FE model, effective stress conditions and the parameter variation.

In the SoilTest facility drained triaxial tests are simulated to determine how the strength and stiffness parameters influence the behaviour of the soil under deviatoric loading conditions. See Figure 7.15 for an impression of the input parameters for a drained triaxial test in the SoilTest facility. A drained triaxial test can consist of a compression or an extension test. In a compression test the major principle effective stress is increased until failure occurs, in an extension test the minor principle effective stress is reduced until failure occurs. For stress points in the passive zone compression tests are performed and for stress points in the active zone extension tests are performed. It is noted that during a triaxial test there are no intermediate principle effective stresses ($\sigma_2' = \sigma_3'$). Whereas, in the FE model there are intermediate principle effective stresses ($\sigma_2' \neq \sigma_3'$). This means that the stress conditions during a triaxial test are a simplification compared to those that act in the FE model.

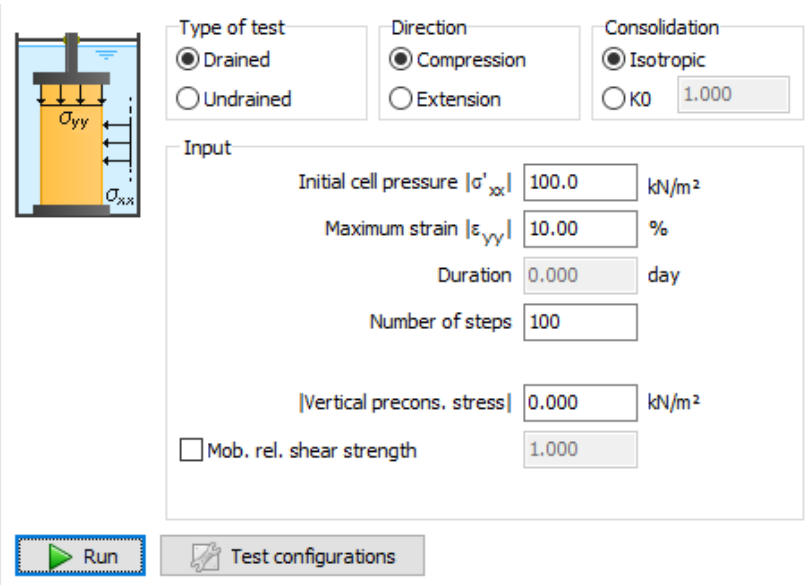

Figure 7.15: Input for triaxial test in SoilTest facility

In the FE model there are many stress points. The idea is not to examine all stress points in the FE model but rather to examine a few stress points that are relevant for the behaviour of the quay wall.

Therefore, it is decided to examine 1 stress point in the active zone and 1 stress point in the passive zone for both sections. The stress points are located at approximately 2 metres from the combined wall. This is because the soil close to the wall has the largest influence on the behaviour of the quay wall. The stress points are selected in layers that proved to be significant for the behaviour of the quay wall based on the sensitivity analysis.

The behaviour of soil depends on the effective stresses that acts on it. To take the effective stresses that act in the FE model into account the principle effective stresses are retrieved from the FE model. The principle effective stresses are shown for different phases. In Figures 7.16 and 7.17 the location of the stress points and the principle effective stresses are presented for section B4 and D1 respectively. The stresses have a negative sign which means that they are compressive stresses.

	Principal Effective stress [kPa]			
phase	σ'_1	σ'_2	σ'_3	$\lvert\sigma'_1 - \sigma'_3\rvert$
8	-160	-112	-90	70
FC	-80	-55	-23	57
SLS	-70	-53	-19	51
ULS	-68	-53	-25	43

	Principal Effective stress [kPa]			
Phase	σ'_1	σ'_2	σ'_3	$\lvert\sigma'_1 - \sigma'_3\rvert$
8	-298	-126	-121	177
FC	-283	-112	-68	215
SLS	-340	-125	-75	265
ULS	-263	-109	-72	191

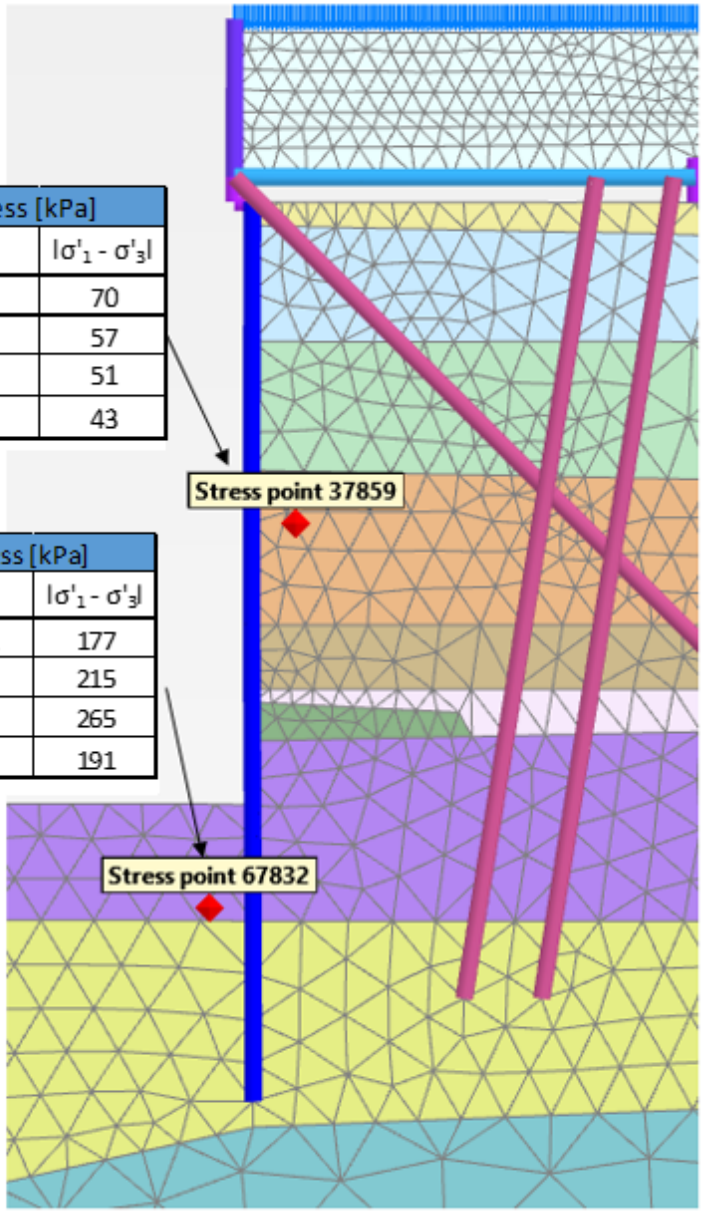

Figure 7.16: Location stress points and effective principle stresses section B4

The friction angle and stiffness parameters are varied in the same way as it was done for the sensitivity analysis. This means that both the strength and stiffness are varied ± 1 times the standard deviation. For the friction angle this is equal to ±5% and for the stiffness parameters this is ±10%.

phase	Principal Effective stress [kPa]			
	σ'_1	σ'_2	σ'_3	$\lvert\sigma'_1 - \sigma'_3\rvert$
8	-148	-51	-51	70
FC	-125	-46	-38	87
SLS	-122	-42	-34	88
ULS	-102	-44	-40	62

Phase	Principal Effective stress [kPa]			
	σ'_1	σ'_2	σ'_3	$\lvert\sigma'_1 - \sigma'_3\rvert$
8	-210	-126	-100	70
FC	-120	-63	-34	86
SLS	-90	-55	-24	66
ULS	-61	-48	-21	40

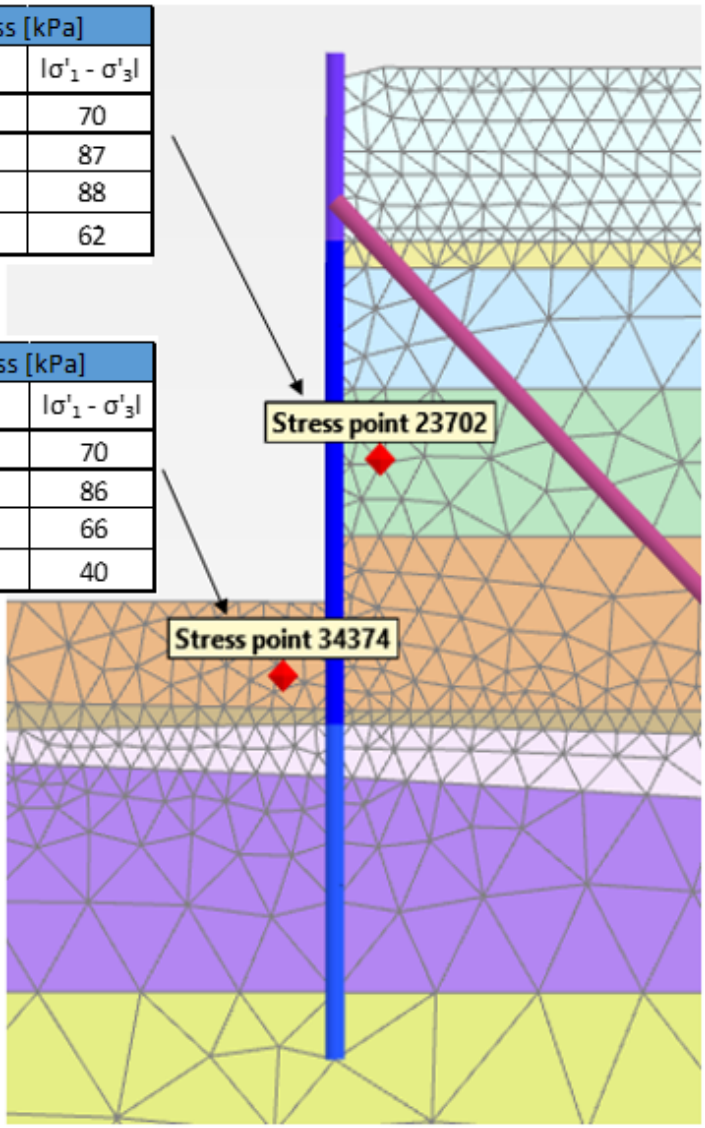

Figure 7.17: Location stress points and effective principle stresses section D1

Results of the triaxial test simulations

For each stress point a triaxial test simulation is performed with stress conditions that occur during the Final Construction phase and the SLS phase. The ULS phase is not presented since results where very similar compared to the SLS phase. In this way it is possible to determine the influence of the strength and stiffness parameters for the different phases. For each phase the influence of the strength and stiffness parameters is determined as follows:

- Perform a triaxial test simulation with the base soil parameters.
- Perform triaxial test simulations in which the soil parameters are varied.
- Plot all the triaxial test results in graph. The axis of the graph show the axial strain ϵ_1 and the deviatoric stress $|\sigma_1$-$\sigma_3|$.
- Plot a line on the graph which indicates the deviatoric stress that acts in the FE model.
- From the plot it is then possible to determine if strength or stiffness parameters have more influence on the deformation behaviour of the soil.

In **Appendix E** all the performed triaxial test simulations and results are presented in detail. As an example the triaxial test simulation for stress point 67832 in section B4 is examined here, see Figures 7.18 and 7.19. This stress point is located in the passive zone. The results are shown for stress conditions that act during the Final Construction phase and the SLS phase.

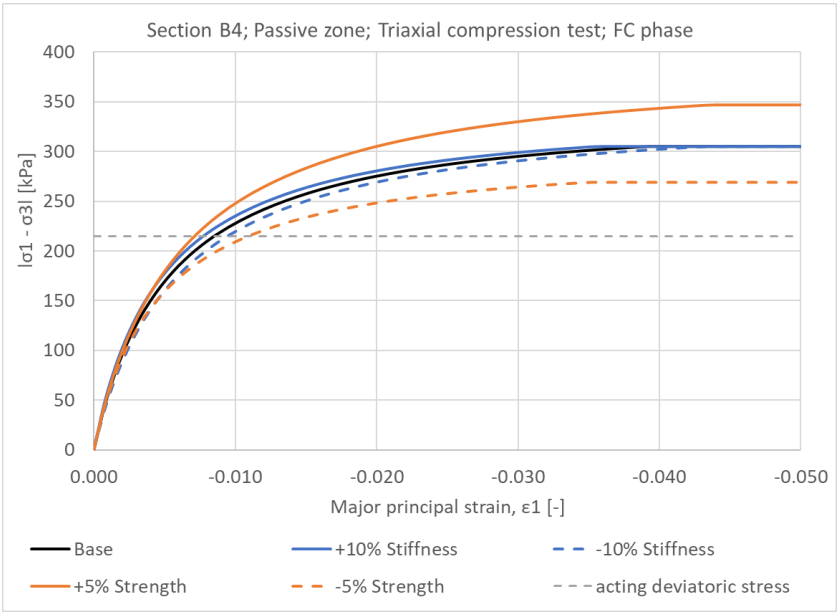

Figure 7.18: Results triaxial compression tests section B4 for the passive zone during Final construction phase

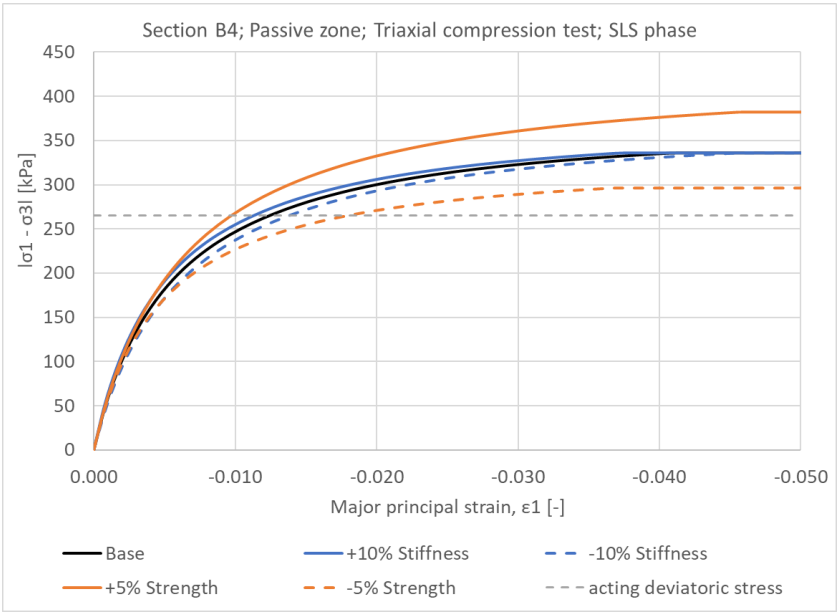

Figure 7.19: Results triaxial compression tests section B4 for the passive zone during SLS phase

In general it applies that the closer the deviatoric stress is to the maximum deviatoric stress the more influence the strength has on the behaviour of the soil. This is because the amount of plasticity increases towards the maximum deviatoric stress and the strength has more influence on the plasticity than the stiffness. This can be seen in Figures 7.18 and 7.19. The orange lines represent a change in the friction angle of the soil, with increasing strain levels the difference between the black and orange lines increases.

For all the performed triaxial test simulations the conclusion was similar. For the considered stress conditions the friction angle has more influence on the behaviour of the soil than the stiffness parameters have. This is already the case for the stress conditions that act during the Final Construction phase. This conclusion supports the results of the sensitivity analysis.

7.5. Quantifying the optimisation of the quay wall functionality

In this section it is determined how much the functionality of the quay wall could be optimised. As mentioned before the functionality of a quay wall refers to the retaining or bearing functionality. Therefore, an optimisation of the functionality consists of an increase in the retaining height or the surface load. The retaining height is increased by lowering the bottom level in front of the quay wall. The maximum increase of the bottom depth is limited to 2 metres since there is a minimal required depth between the bottom level and the underside of the sheet pile wall elements. A realistic value for the increase of the surface load is assumed to be 50%. In additional calculations either the retaining height or the surface load are increased. There are no additional calculations in which both are increased simultaneously. In the additional calculations the effect of softening on the soil strength is taken into account. As discussed in section 7.2 the soil volume that approaches failure increases in the ULS. Therefore, it seems likely that if the retaining height or surface loads are increased a bigger soil volume will approach failure and the peak strength could be exceeded.

Two failure mechanisms are assessed in this section. These are yielding of the combined wall and yielding of the MV-piles. It is decided to use these two failure mechanisms since the measurement data provides insight into these two failure mechanisms.

The yielding of the combined wall and the MV-piles are assessed by performing an unity check in which the stress levels in the elements are compared with the yield stress, see equation 7.4 in which σ_s is the stress level in the element and f_y the yield stress. The stress levels in the elements are determined with the FE model results. The acting stresses in the combined wall are determined with equation 7.5 in which M_{combi} is the bending moment in the combined wall, W_{combi} is the section modulus, N_{combi} is the normal force in the combined wall and A_combi is the cross-sectional area of the combined wall. The acting stresses in the MV-piles are determined by equation 7.6 in which F_{MV} is the axial force in the MV-pile and A_{MV} the cross-sectional area of the MV-pile. In Table 7.5 the properties of the combined wall and the MV-piles are presented. It is noted that the properties of the combined wall are only based on the tubular piles. Furthermore, the properties are determined by taking into account corrosion, which is 1.2 millimetres over a period of 100 years (design life of the quay wall). In the aforementioned table the yield stress f_y of the elements are shown as well. The tubular piles are made of steel quality X70 and the MV-piles have a steel quality of S420. The yield stress should be reduced with a factor 1.016 because the design life is 100 years. Furthermore, the yield stress of the MV-piles should be reduced with an additional factor of 1.25.

$$\frac{\sigma_s}{f_y} \leq 1 \tag{7.4}$$

$$\sigma_{combi} = \frac{M_{combi}}{W_{combi}} + \frac{N_{combi}}{A_{combi}} \tag{7.5}$$

$$\sigma_{combi} = \frac{F_{MV}}{A_{MV}} \tag{7.6}$$

Properties per element	
W_{combi} [cm^3]	Section B4: 32650 , Section D1: 25360
A_{combi} [mm^2]	Section B4: 94900 , Section D1: 73150
A_{MV} [mm^2]	22650
$f_{y;combi}$ [N/mm^2]	470
$f_{y;MV}$ [N/mm^2]	330

Table 7.5: Properties of combined wall and MV-piles per element

In Table 7.6 the FE model results are presented for 3 different situations. These are the situation for which the quay wall is designed (no optimisation), the situation were the bottom depth is increased with 2 metres and the situation in which the surface load is increased with 50% (from 40 kPa to 60 kPa). The presented values represent ULS values and are for 1 element, so not per metre length of quay wall. This is done because the values can now directly be used to determine the stress levels in the elements. Furthermore, the table shows the stress levels that act in the elements and the results of the unity check.

Section	Forces			Stresses		Unity check	
	Combined wall		MV-pile	Combined wall	MV-pile	Combined wall	MV-pile
	M_{combi}	N_{combi}	F_{MV}	σ_{combi}	σ_{MV}		
	kNm	kN	kN	[N/mm^2]	[N/mm^2]		
Optimisation: none							
B4	5275	7150	3980	237	176	0.50	0.53
D1	5370	5965	4180	293	185	0.62	0.56
Optimisation: retaining heigth +2 metres							
B4	7400	7680	4790	308	211	0.65	0.64
D1	6870	6655	4710	362	208	0.77	0.63
Optimisation: Surface load +50%							
B4	5670	7900	4160	257	184	0.55	0.56
D1	6095	6640	4630	331	204	0.70	0.62

Table 7.6: Results FE model ULS phase, values are per element

Based on the unity checks that are performed it seems that the combined wall and the MV-piles have sufficient capacity to optimise the functionality of the quay wall. The retaining height can be increased up to 2 metres and the surface load can be increased with 50%, from 40 kPa to 60 kPa. It should be noted that this is only based on the assessment of the yielding of the combined wall and the MV-piles. Other failure mechanisms, such as the bearing capacity of the bearing piles, should be assessed as well.

7.6. Conclusion

Magnitude of the forces and deformations
From the analysis performed in this chapter is it concluded that a significant part of the deformations and forces that occur during the SLS and ULS are developed during the construction process. In table 7.4 the ratio between the forces and deformations of the construction process and the limit states is quantified.

The significance of the horizontal deformations and the bending moment that occur during the construction process is larger for the section with the relieving platform (section B4). This is because the relieving platform takes up a large part of the surface loads the occur during the limit states. Consequently, the retaining wall experiences less influence of the surface loads compared to the situation where no relieving platform is present.

On the other hand the significance of the anchor force the occurs during the construction process is larger for the section without a relieving platform (section D1). The reason for this is the increased anchor force that is generated by settlement of the soil due to the weight of the sand fill. In the case where there is relieving platform present the sand fill does not cause much settlement of the soil since the relieving platform takes up the weight of the sand fill.

Sensitivity analysis
The goal of the sensitivity analysis is to determine what soil parameters influence the behaviour during the construction process and during the limit states. The friction angle and stiffness moduli are seen as the most important soil parameters and are therefore considered in the sensitivity analysis.

From the sensitivity analysis it can be concluded that the friction angle has more influence on the behaviour of the quay wall than the stiffness moduli. Furthermore, it can be seen that the influence of the friction angle increases from the construction process to the ULS. During the construction process the overall influence of the friction angle is 60% for the section with a relieving platform and 70% for the section without a relieving platform. Towards the ULS the influence of the friction angle increases to approximately 80% for both sections.

To support the conclusions of the sensitivity analysis a series of drained triaxial tests were simulated in the SoilTest facility of Plaxis. With the SoilTest facility it was possible to gain more insight into how the strength and stiffness parameters influence the deformation behaviour of the soil. The drained triaxial tests were simulated with effective stress conditions that act in the FE model. The results of these simulations support the conclusion that the friction has more influence on the behaviour of the quay wall than the stiffness parameters.

To better predict the behaviour of the quay wall insight must be gained into the friction angle of the soil. This study focuses on using measurement data which is obtained during the construction process. To be able to use this measurement data the behaviour of the quay wall during the construction process should be influenced by the friction angle of soil layers that also have an influence behaviour of the quay wall during the limit states.

For both sections the behaviour of the quay wall is dominated by the same soil layers during the construction process as it is during the SLS. For the ULS it is more complicated. The layers in the active zone and in the top part of the passive zone have an influence during both the construction process and during the ULS. However, the deeper layers in the passive zone have no significant influence during the construction process but they do have a influence during the ULS. Therefore, it will be difficult to gain insight into the friction angle of deeper soil layers in the passive zone based on the measurement data that is obtained during the construction process. Nevertheless, the measurement data obtained during the construction process is still valuable as it does provide insight into the friction angle of the layers in the active zone as well as layers in the top part of the passive zone.

Quantifying the optimisation of the quay wall functionality
Based on the unity checks that are performed it seems that the combined wall and the MV-piles have sufficient capacity to optimise the functionality of the quay wall. The bottom depth can be increased up to 2 metres and the surface load can be increased with 50%, from 40 kPa to 60 kPa. It should be noted that this is only based on the assessment of the yielding of the combined wall and the MV-piles. Other failure mechanisms, such as the bearing capacity of the bearing piles, should be assessed as well.

8

Conclusions and recommendations

8.1. Conclusions

The conclusions are presented in this section. First the sub-questions are answered based on the outcomes of the case study, then the main research question is answered.

8.1.1. Sub-questions

1. **What is needed to optimise the functionality of a quay wall?**

Relevant aspects for optimising the functionality of a quay wall are:

- Insight into the parameter uncertainties that play an important role in the reliability of quay walls
- Measurement data of sufficient quality that provides insight into the behaviour of the quay wall
- A load on the quay wall which results in significant deformations and forces of the quay wall
- Insight into the mechanics of a quay wall and the way it is modelled in the calculation model as well as insight into the possibilities and limitations of the calculation model
- A method for updating the relevant (soil) parameters and/or reliability based on the measurement data, which in turn allows to optimise the functionality.

2. **Does the currently collected measurement data provide sufficient information about the behaviour of a quay wall, if not, what data is missing?**

Yes the currently collected measurement data did provide sufficient information about the behaviour of the quay wall. A more detailed answer to this sub-question is divided into three parts. First of all it is described what information the currently collected measurement data provides. Secondly, remarks are made about the missing or incomplete information and finally, the frequency of the (reference) measurements are discussed.

Information currently collected measurement data
From the measurement data that was collected in the elaborated case the inclinometer measurements and anchor strains provided useful information about the behaviour of the quay wall. The inclinometer measurements and the anchor strains quantify the relative horizontal deformations of the retaining wall and the anchor forces. Moreover, the curvature of the retaining wall can be deduced from the inclinometer measurements, the curvature can in return be used to determine the bending moments. The relative horizontal deformations, bending moments and anchor forces are predominantly related to the retaining and bearing function of the quay wall. Therefore, these measurements provide information about the retaining capacity of the quay wall.

Water levels and the bottom depth in front of the quay wall are measured as well. These measurements did not provide information about the behaviour of the quay wall. However, these measurements did provide information on the boundary conditions at the quay wall, which where necessary during the analyses performed in this study.

Missing information
It was not possible to link the inclinometer measurements to the absolute deformation measurements of the top of the quay wall (XYZ-deformations). Therefore, the measured horizontal deformations remain relative to the toe of the inclinometer measurement. This means that the horizontal toe deformation of the retaining wall remains unknown. The toe deformation of the retaining wall could provide more information on the retaining capacity of the quay wall since it is an indicator of how much horizontal deformation occurs in the passive zone.

For the quay wall with a relieving platform the retaining capacity is also influenced by the lateral interaction between the bearing piles and the soil, the so-called shielding effect. Measurements of the horizontal deformations of the bearing piles could provide more insight into how much interaction takes place. Another aspect that influences the shielding effect is the connection between the bearing piles and the relieving platform. Strains in this connection have been measured, but the measured strains are not compelling enough to determine if the connection acts as a hinge or as a fixed connection.

The anchor strains are currently measured in one cross-section of the MV-piles, which is located near the top of the MV-piles. There is no information available about the force distribution in the MV-piles. If the force distribution in the anchor is known it would be possible to determine if a significant amount of shaft friction is generated in the active zone. If this is the case less axial deformation of the MV-pile occurs and the anchor capacity would be higher.

The bearing piles beneath the relieving platform and the retaining wall are also designed to withstand vertical forces. However, no detailed information is available about the vertical behaviour of the retaining wall or the bearing piles. Measurements of the axial strains in the retaining wall and the bearing piles could provide information about the vertical bearing capacity that is generated.

Measurement frequency
The inclinometer measurement were performed several times during the construction process. When the retaining height in front of the quay wall was limited (approximately < 10 metres) the measured relative horizontal deformations were small < 5 millimetres. The usability of these measurements is limited since the possible error in the measurements has a similar magnitude.

The inclinometer measurements and the XYZ-deformation measurements were occasionally taken several days apart from each other. During the construction process the retaining height could increase with several meters in a few days. To be able to link the inclinometer measurements to the XYZ-deformation measurements it is advised to fit the timing of the two measurements as much as possible.

The reference measurement of the XYZ-deformation measurements is measured once before the start of the construction process. Consequently, it is not possible to determine if any deformation of the reference point itself occurred. Deformations of the reference point itself can cause significant disturbances in the XYZ-deformation measurement results.

The reference measurement of the FBG-sensors are also only measured once. These sensors might not have been stabilised and could show signs of drift. If multiple reference measurements would be performed it is possible to exclude that any drift occurs in the sensors and a more stable reference measurement is obtained.

3. **Which soil parameters have a dominant influence on the behaviour of the quay wall, and do these soil parameters have a reducible uncertainty?**

In chapter 7 a sensitivity analysis is performed to determine which soil parameter has the biggest influence on the behaviour of the quay wall. The soil parameters considered in the sensitivity analysis are the friction angle (strength) and stiffness moduli, these two parameters are considered to be the dominant soil parameters. Cohesion is not considered because the soil profile predominantly consists of cohesionless soil layers.

From the results of the sensitivity analysis it can be concluded that the friction angle has more influence on the behaviour of the quay wall than the stiffness moduli. In the case study two sections are analysed, one with a relieving platform (section B4) and one without a relieving platform (section D1). During the construction process the overall influence of the friction angle is 60% for the section with a relieving platform and 70% for the section without a relieving platform. For both sections the influence of the friction angle increases towards 80% in the ULS phase.

To support the conclusions of the sensitivity analysis a series of drained triaxial tests were simulated in the SoilTest facility of Plaxis. With the SoilTest facility it was possible to gain more insight into how the strength and stiffness parameters influence the deformation behaviour of the soil. The drained triaxial tests were simulated with effective stress conditions that act in the FE model. The results of these simulations support the conclusion that the friction has more influence on the behaviour of the quay wall than the stiffness parameters.

The friction angle of soil is an epistemic uncertainty, which means that the true value of the parameter exists but is unknown due to a lack of knowledge. Furthermore, the uncertainties in the friction angle are time-independent, which means that a reduction in the uncertainty can be made early in the service life of the quay wall. During the construction process the influence of the friction angle on the horizontal deformation and bending moments of the combined wall is 60 - 70 %. Therefore, the measurement data obtained during the construction process provides insight into the value of the friction angle of the soil.

4. **Is the behaviour of the quay wall dominated by the same soil layers during the construction process as it is during the limit states?**

In the sensitivity analysis performed in chapter 7 the individual influence of the strength and stiffness of each soil layer is determined. In the previous sub-question is was concluded that the friction angle is the most dominant soil parameter. Therefore, the influence of soil layers is determined by the influence of the friction angle only.

For both sections the behaviour of the quay wall is dominated by the same soil layers during the construction process as it is during the SLS. For the ULS it is more complicated. The layers in the active zone and in the top part of the passive zone have an influence during both the construction process and during the ULS. However, the deeper layers in the passive zone have no significant influence during the construction process but they do have a influence during the ULS. Therefore, it will be difficult to gain insight into the friction angle of deeper soil layers in the passive zone based on the measurement data that is obtained during the construction process. Nevertheless, the measurement data obtained during the construction process is still valuable as it does provide insight into the friction angle of the layers in the active zone as well as layers in the top part of the passive zone.

5. **To what extent is the validated FE model capable of predicting the behaviour of the quay wall?**

As described in the second sub-question the friction angle has a large influence on the behaviour of the quay wall. Therefore, to predict the behaviour of the quay wall as best as possible it seems important to have a realistic estimation of the friction angle in the FE model. In this thesis the friction angle of the sand layers is determined based on the peak value of the shear strength. For the prediction of the behaviour of the quay wall during the construction process the peak value of the shear strength resulted in a good match between FE model results and the measurement data. The use of the peak value of the shear strength seems valid for the construction process since the deformations of the soil are limited.

The validated FE model is then extended to predict the behaviour of the quay wall during the SLS and ULS. Reviewing the plastic points in the extended FE model indicated that in the ULS the peak shear strength of the soil is exceeded locally. The hardening soil model is used in this thesis to describe the stress-strain relationship of the soil. This model does not include softening behaviour and can therefore overestimate the soil strength if the peak value is reached. This means that if the volume of soil that reaches the peak shear strength increases the validated FE model underestimates the deformations and forces of the quay wall.

With additional calculations an estimation is made on how large the effect of softening behaviour is on the forces and deformations of the quay wall. To account for the softening behaviour the friction angle of the sand layers was reduced with 2 degrees, this value was based on triaxial test results. For the situation with softening behaviour the horizontal deformations and forces in the quay wall are approximately 5% higher compared to when the peak shear strength value is used. It appears that the influence of softening behaviour is not that big. However, for this case the majority of the soil volume has a lot of capacity left and therefore is not close to yielding. If the soil was close to yielding the influence of softening behaviour would have been larger.

Another aspect which is not included in the FE model is the installation effects of the structural elements. The installation effects of the combined wall, MV-piles and the SI-piles causes local stress changes in the soil. These stress changes are not incorporated in the FE model.

8.1.2. Main research question

The objective of this thesis is to determine if measurement obtained during the construction process has the potential to optimise the functionality of a smart quay wall. The main research question that is based on this objective is presented and after that an answer to this question is given.

How to use the measurement data of smart quay walls obtained during the construction process to optimise their functionality?

The case study elaborated in this thesis shows that measurement data obtained during the construction process of a smart quay wall has the potential to validate FE models and reduce the uncertainty in the friction angle of the soil, which is a dominant parameter for the behaviour of the quay wall. The reduction in the uncertainty of the friction angle can lead to FE models that are better capable of predicting the behaviour of the quay wall. With these FE models it is possible to determine if an increase in the retaining height or the surface load is allowed. Therefore, it seems that the measurement data obtained during the construction process of the HHTT-quay has good potential to optimise the functionality of the quay wall. Arguments that support this conclusion are:

- A good match between the FE model results and the measurement data is found when realistic estimates of the friction angle are used. These realistic estimates are determined by taking into account the peak behaviour of the soil strength and the influence of plane strain conditions on the soil strength (9/8-factor). These realistic estimates of the friction angle are significantly higher than the characteristic values used in the design.
- The construction process introduces a significant part of the horizontal deformations and forces that occur during the SLS and ULS:
  - The horizontal deformations are 50 - 65 % of the value found in SLS
  - The bending moments are 50 - 65% of the value found in ULS
  - The anchor forces are 25 - 45 % of the value found in ULS.
- The friction angle accounts for 80% of the horizontal deformations and bending moments in the combined wall during the ULS. Therefore, the friction angle has a dominant role in the behaviour of the quay wall in the ULS.
- Moreover, uncertainties in the friction angle are epistemic uncertainties, therefore these uncertainties can be reduced when additional information becomes available. The uncertainties in the friction angle are also time-independent, this means that a reduction in the uncertainty can be

made early in the service life of the quay wall. During the construction process the influence of the friction angle on the horizontal deformation and bending moments of the combined wall is 60 - 70 %. Therefore, the measurement data obtained during the construction process provides information about the value of the friction angle of the soil.
- With the validated FE model, using the realistic estimates of the friction angle, the bending moment in the combined wall and anchor force are determined for the ULS. The bending moment in ULS is approximately 50 - 60% of the allowable value and the anchor force in ULS is approximately 55% of the allowable value. This indicates that the structural elements have capacity left and there is a large potential for increasing the retaining height or the surface load, and therefore optimising the functionality of the quay wall.
- Based on the assessment of the yielding of the combined wall and the MV-piles the functionality of the quay wall could be increased. The water depth in front of the quay wall could be increased up to 2 metres and the surface load could be increased with 50% from 40 kPa to 60 kPa.

The case study used in this thesis shows that measurement data obtained during the construction process already provides important information that can be used to optimise the functionality of the quay wall. This indicates that for smart quay walls the construction process can act as a load test and this could reduce the necessity to perform a load test during the service life. There are several advantages of using the construction process as a load test compared to performing a load test during the service life of a quay wall, such as:

- For a new quay wall the construction process is always performed, therefore there are no additional risks and costs involved (besides the costs of the sensors).
- During the construction process the water levels and the bottom depth are regularly measured and a surface load is often absent. This means that the external loads on the quay are well known.
- The measurement data starts from an 'unloaded' situation, meaning that insight is gained in the development of deformations and forces.
- Insight into the behaviour of the quay wall is gained directly after the construction process, meaning that knowledge of an additional strength of the soil is available as soon as possible.

In this study it was the plan to manually update the soil parameters if a (significant) difference between the measurement data and the a priori FE model results was found. A manual update would only results in a update of the mean value of the soil parameters, a manual update does not allow for a reduction in the standard deviation of the soil parameter. Since a good comparison was found between a priori model results and the measurement data it did not seem necessary to update the mean values of the soil parameters. Even tough it was not necessary to update the mean value of the soil parameters it does seem possible to optimise the functionality of the quay wall based on the measurement data since the friction angle values used in this study are significantly higher than those used in the design. It should be noted that the sensitivity analysis showed that the measurement data obtained during the construction process did not provide a lot of insight into the friction angle of the deeper layers in the passive zone. Therefore, the friction angle of the deep passive layers should be treated with care.

8.2. Recommendations

In this section recommendations are presented. These recommendations are divided into three parts. First of all general recommendations are shown, after which recommendations related to optimising the functionality of a quay wall based on measurement data are presented. Finally, several recommendations are given to improve the measurement methods and data.

8.2.1. General recommendations

- If a quay wall is designed with a FE model it is recommended to increase the friction angle which is determined under triaxial test stress conditions with a factor 9/8 to account for plane strain stress conditions that occur at a quay wall. This factor is based on theoretical background [Teunissen, 2016, Wroth, 1984] and is also included in NEN9997-1. Furthermore, the measurement data obtained during the construction process of the HHTT-quay supports the validity of this factor.

- If a CPT-correlation is used to determine the friction angle of the soil it is important to consider how this CPT-correlation is validated. A lot of CPT-correlations are validated with triaxial test results, these correlations than provide a friction angle which is valid for triaxial test stress conditions only. In this thesis a CPT-correlation of Mayne and Kulhawy [1990] was used, which was validated with triaxial test results. Therefore, CPT-correlation results were increased with a factor 9/8 to account for plane strain stress conditions.

8.2.2. Recommendations related to optimising the functionality based on measurement data

- In this thesis it is demonstrated that the measurement data obtained during the construction process of the HHTT-quay has the potential to optimise the functionality of the quay wall. To better quantify the optimisation of the functionality of the quay wall a more rigorous approach should be used. With a probabilistic analysis that is coupled to a sophisticated parameter updating technique, such as Bayesian updating, it is possible to better include the uncertainties of the (soil) parameters in the updating process. This should allow to quantify the possible optimisation of the functionality in a more detailed way.
- The potential of the measurement data obtained during the construction process should be determined for more smart quay walls. If the potential of the data proves to be larger for more smart quay walls it is recommended to make an inverse analysis based on monitoring data obtained during the construction process a standard plan of approach for new quay walls.

8.2.3. Recommendations measurement methods and data

In chapter 4 it is concluded that not all measurement methods result in useful measurement data. Several recommendations regarding the measurement methods and the frequency of these methods are presented.

- It is recommended to review the measurement data directly when it comes available during the construction process. In this way if any mistakes or shortcomings in the measurement data are identified it is still possible to take action, this could improve the quality of the measurement data.
- The location which is used as a reference point for absolute deformations measurements (XYZ-deformation measurements) should be remeasured multiple times during the construction process. In this way it is possible to determine if the reference point itself is showing signs of deformations.
- Ideally the absolute deformation measurements (XYZ-deformations measurements) are linked to the inclinometer measurements. To make this as easy as possible the timing of the two measurements should be fitted as much as possible.
- The reference measurement of the FBG-sensors used in the case are also only measured once. These sensors might not have been stabilised and could show signs of drift. If multiple reference measurements would be performed it is possible to exclude that any drift occurs in the sensors and a more stable reference measurement is obtained.
- It seems necessary to test the FBG-sensors on the MV-piles since very diverse measurement data is obtained. To make the FBG-sensors robust there is a lot of material between the sensor and the MV-pile, e.g. steel plate, epoxy glue and welds. The effect of these materials on the strain transfer between the FBG sensor and the MV-pile is unknown. By testing the installed FBG-sensors the accuracy of the measurement method can be validated. A possible testing method could be a load test.

References

Brinkgreve, R.B.J. (2019a). *PLAXIS Material Models Manual*. PLAXIS BV Netherlands.

Brinkgreve, R.B.J. (2019b). *PLAXIS Scientific Manual*. PLAXIS BV Netherlands.

Brinkgreve, R.B.J., Engin, E., and Engin, H.K. (2010). Validation of empirical formulas to derive model parameters for sands. In *Numerical Methods in Geotechnical Engineering (NUMGE 2010)*, Benz, T., and Nordal, S., CRC Press, 2010, pp. 137-142.

Büller, J.M. (2019). *Reliability updating of sheet pile walls; An analysis on the parameter updating process*. MSc Thesis. Delft University of Technology.

Calle, E., Vrouwenvelder, J., Hannink, G., and Bruijn, E. (2008). Representatieve waarden voor grondparameters in de Geotechniek. *Vakblad Geotechniek*, 2008-2, pp. 24-29.

CUR (2003). *Bepaling geotechnische parameters*. CUR-rapport 2003-7, CUR, Gouda.

Gijt, J.G. de, and Broeken, M.L. (2013). *Quay Walls, Second Edition*. CRC press, 2013.

Adel, N. den (2018). *Load testing of a quay wall: An application of Bayesian Updating*. Msc Thesis. Delft University of Technology.

Dijkstra, A. (2016). *Geotechnisch onderzoek, Project Hartel Tank Terminal te Rotterdam*. Technical Report, Wiertsema & Partners Raadgevend Ingenieurs.

Dijkstra, A. (2017). *Geotechnisch laboratoriumonderzoek, Project Hartel Tank Terminal te Rotterdam*. Technical Report, Wiertsema & Partners Raadgevend Ingenieurs.

Fedorov, A.K., Lazarev, V., Pniov, A.B., and Karasik, V.E. (2015). Structural monitoring system with Fiber Bragg Grating sensors: Implemantation and software solution. *Journal of Physics: Conference Series*, Volume 594, pp. 12-18.

Greft, H.C. van der, Dijk, S. van, and Heezik, M. (2019). *Interpretatie rapport / eindrapportage proefbelastingen MV-palen*. Technical report, MariTeam.

Head, K.H., and Epps, R.J. (2014). *Manual of Soil laboratory Testing; Volume III: Effective Stress Tests 3rd Edition*. Whittles Publishing, 2014, pp. 59-77.

Hughes, A.F., Iles, D.C., and Malik, A.S. (2011). *Design of steel beams in torsion*. Steel Construction Institute, Publication P385, 2011, pp. 1-28.

Jamiolkowski, M., Lo Presit, D., and Manassero, M. (2003). Evaluation of relative density and shear strength of sands from CPT and DMT. In *Soil Behaviour and Soft Ground Construction*, Germaine, J.T., Sheahan, T.C., and Whitman, R.V., 2003, pp. 201-238.

Jonkman, S.N., Steenbergen, R.D.J.M., Morales-Nápoles, O., Vrouwenvelder, A.C.W.M., and Vrijling, J.K. (2017). *Probabilistic Design: Risk and reliability analysis in Civil Engineering*. Delft University of Technology

Kim, J., Kim, C., Choi, S., and Lee, B.Y. (2017). Enhanced Strain Measurements Range of an FBG Sensor Embedded in Seven-Wire Steel Strands. *Sensors, 2017, 17*

Korff, M. (2018). *Deep Excavations; Design, Execution and monitoring of Deep excavations with Retaining Walls.* Delft University of Technology, pp 44-112

Mayne, P.W. (2001). Stress-Strain-Strength-Flow parameters from enhanced in-situ tests. *Proceedings. International Conference on In-Situ Measurements of Soil Properties & Case Histories*, May 2001, pp. 27-48.

Mayne, P.W., and Kulhawy, F.H. (1990). *Manual on estimating soil properties for foundation design*. Technical Report, Cornell University, New York.

Obrzud, R.F., and Truty, A. (2018). *The Hardening soil model – a practical guidebook*. Technical Report, Zace Services Ltd.

Putteman, J., Gootjes, G., and Tuunter, T.C. (2017). *Uitgangspunten diepzeekade*. Technical Report, MariTeam.

Qiu, G., Grabe, J. (2012). Active earth pressure shielding in quay wall construction: numerical modelling. *Acta Geotechica*, volume 7, pp. 343-355.

Roubos, A.A. (2019). *Enhancing Reliability-Based Assessments of Quay Walls*. PhD Thesis, Technical University of Delft

SBRCUR (2017). *Richtlijn Geotechnisch laboratoriumonderzoek*. CROW, Ede.

Schanz, T., Vermeer, P.A., and Bonnier, P.G. (1999). The Hardening Soil model: Formulation and verification. In *Beyond 2000 in Computational Geotechnics – 10 years of Plaxis*. Balkema, Rotterdam, pp. 281-296.

Srigopol, J.D. (2018). *Comprehending the behaviour of Muller-Verpress piles under tensional loading*. MSc Thesis. Delft University of Technology.

Stark, T.D. (2008). Slope inclinometers for landslides. *Landslides*, 5, pp. 339-350.

Teunissen, H. (2016). Wrijving in sterkteberekeningen. *Vakblad Geotechniek*, 2016-3, pp. 8-13.

Gelder, P. van (2000). *Statistical methods for the risk-based design of civil structures*. PhD Thesis, Technical University of Delft

Weijst, W.M.L. (2010). *Grondonderzoek van Uden Stevedoring Maasvlakte Rotterdam*. Technical Report, Fugro

Wroth, C.P. (1984). The interpretation of in-situ soil tests. *Géotechnique*, 34(4), pp. 449-489.

Appendices

A

Presentation of the measurement data

In Appendix A the available measurement data is presented. This measurement data is collected during the construction process of the HHTT-quay.

A.1. Measurements MV-piles

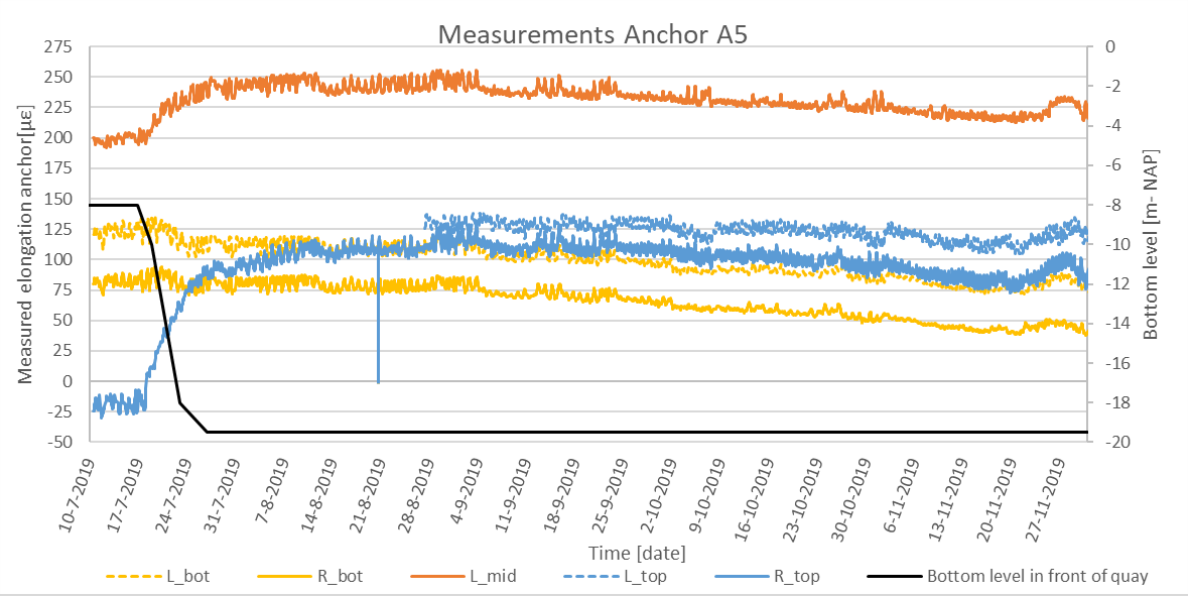

Figure A.1: Measured elongation of MV-anchor A5

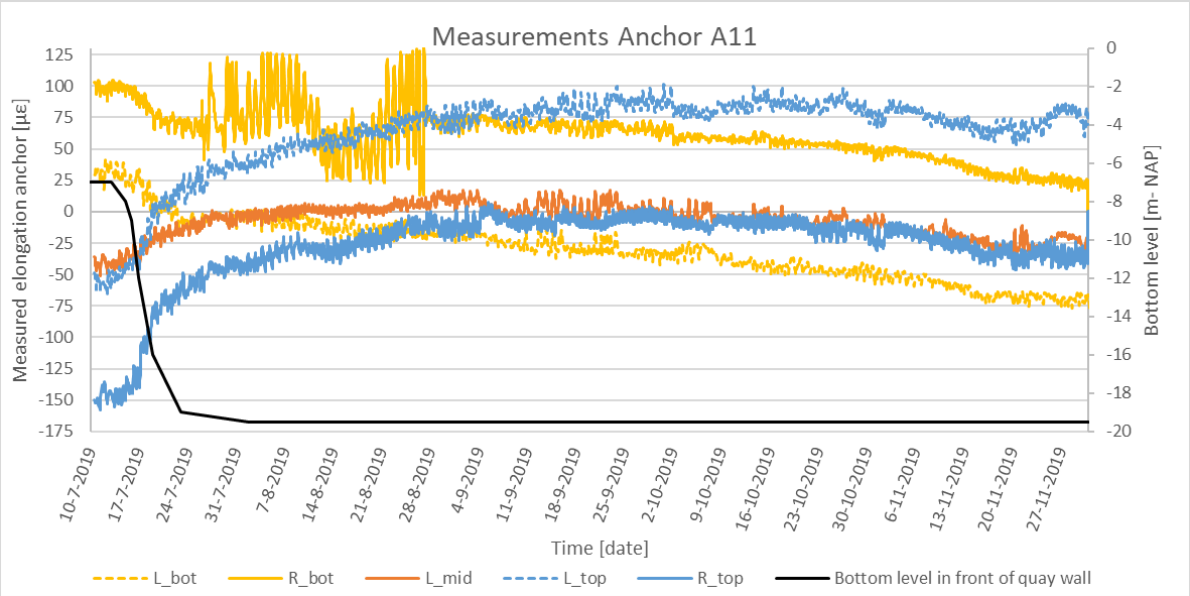

Figure A.2: Measured elongation of MV-anchor A11

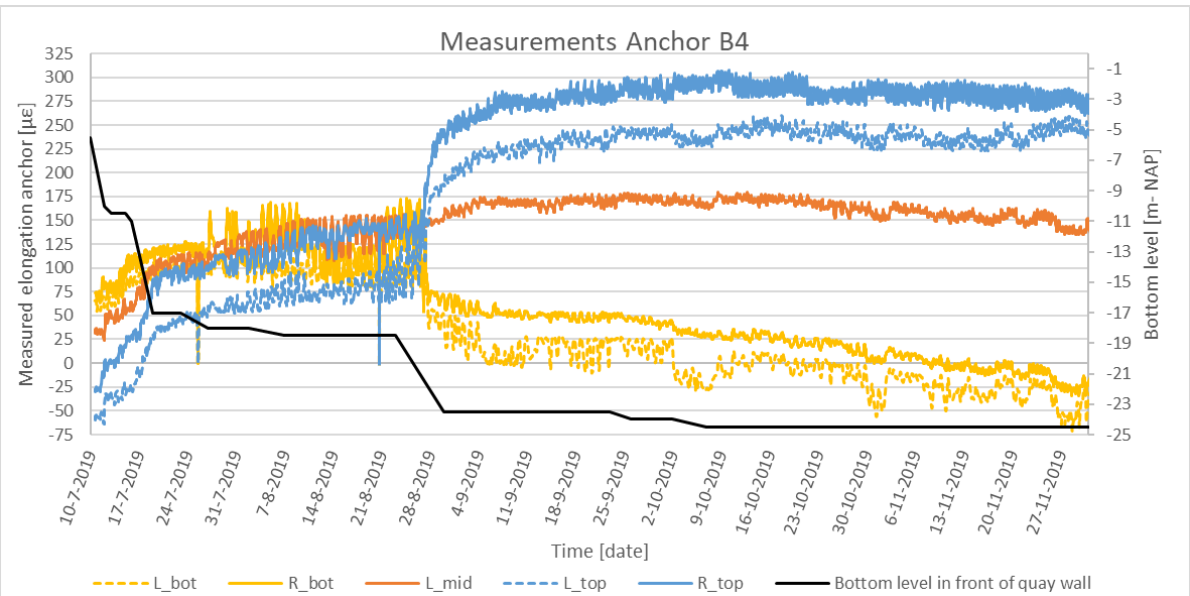

Figure A.3: Measured elongation of MV-anchor B4

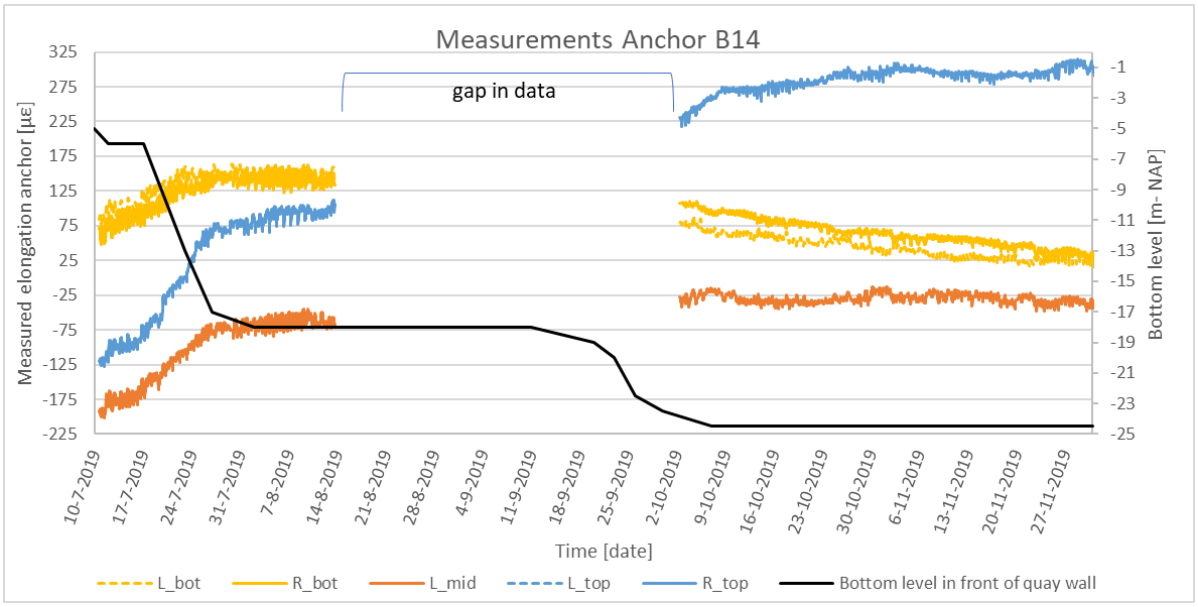

Figure A.4: Measured elongation of MV-anchor B14

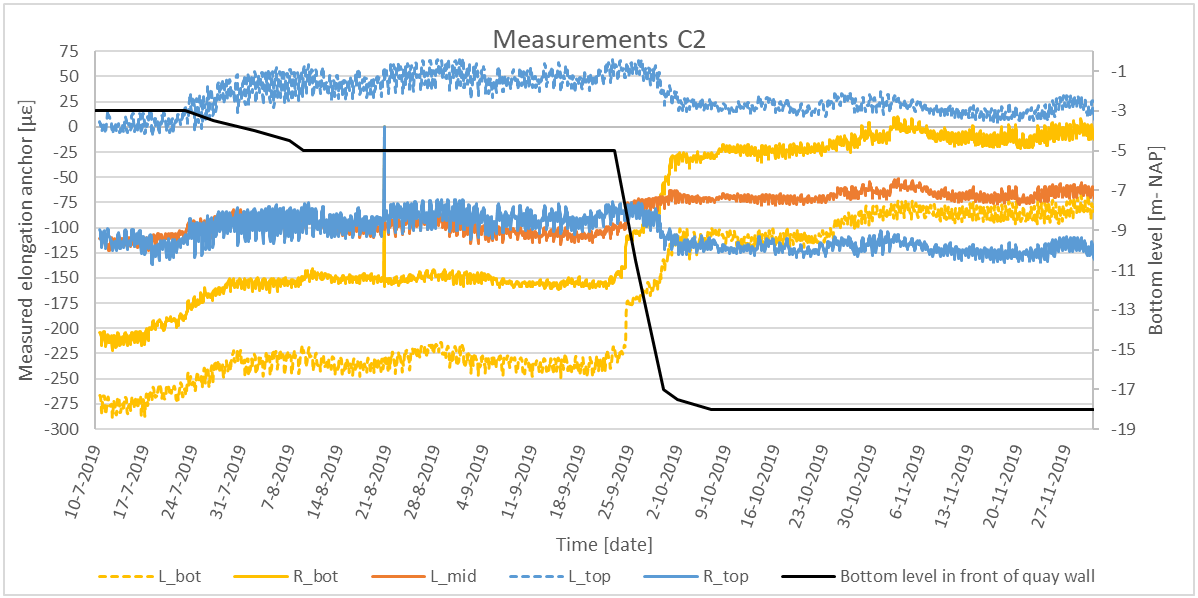

Figure A.5: Measured elongation of MV-anchor C2

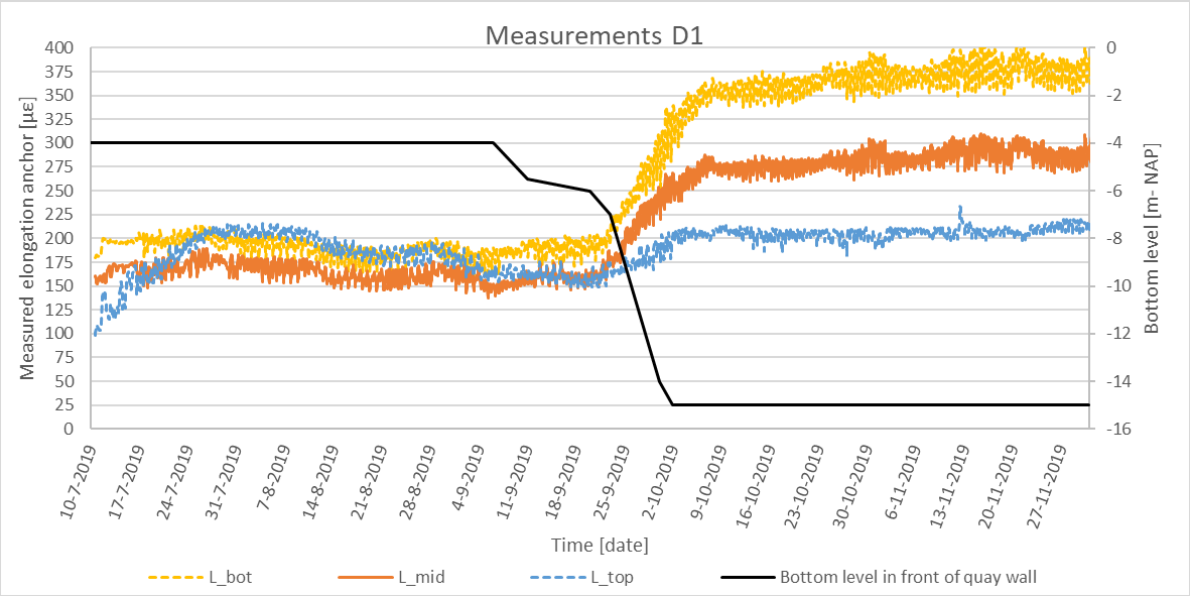

Figure A.6: Measured elongation of MV-anchor D1

A.2. Strains in connection bearing piles and relieving platform

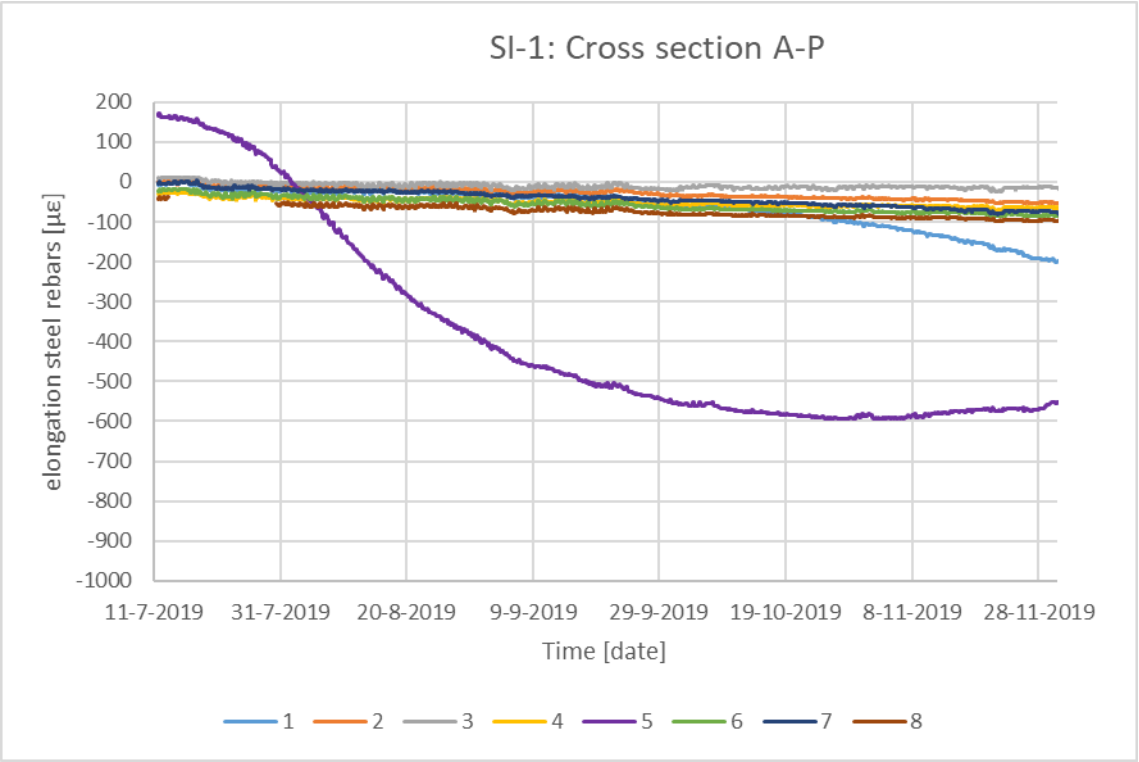
SI-1: Cross section A-P
elongation steel rebars [με]
200
100
0
-100
-200
-300
-400
-500
-600
-700
-800
-900
-1000
11-7-2019
31-7-2019
20-8-2019
9-9-2019
29-9-2019
19-10-2019
8-11-2019
28-11-2019
Time [date]
1
2
3
4
5
6
7
8

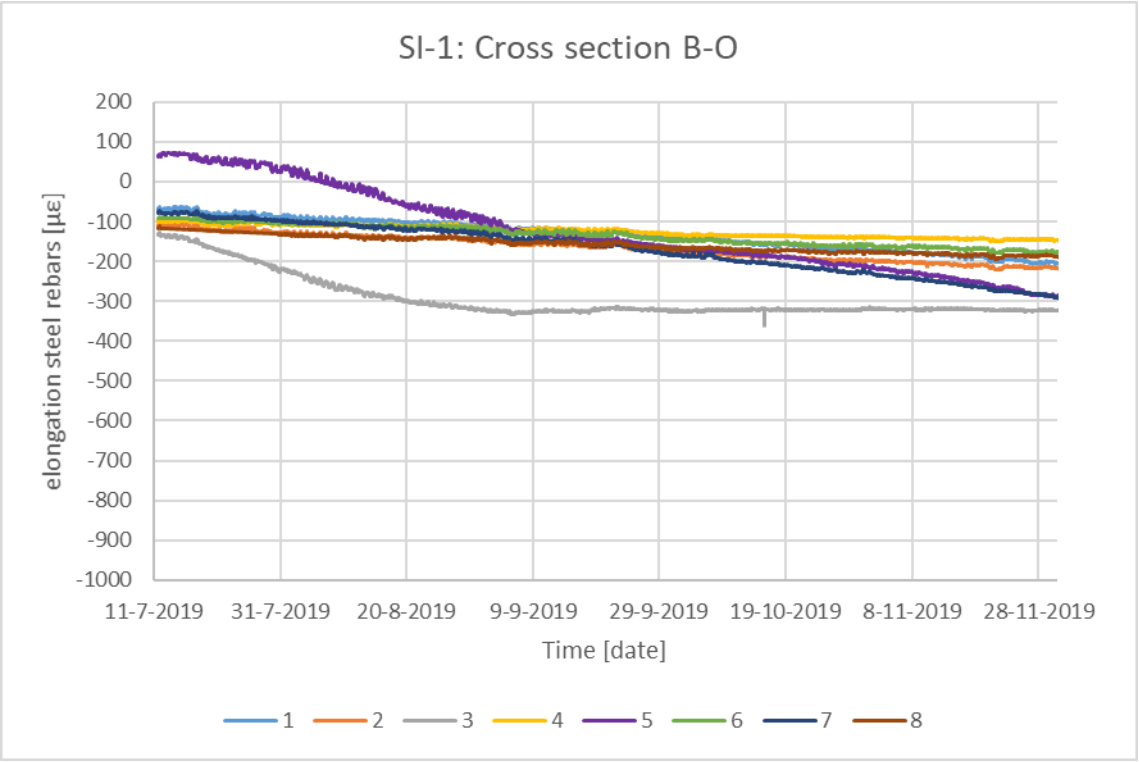
SI-1: Cross section B-O
elongation steel rebars [με]
200
100
0
-100
-200
-300
-400
-500
-600
-700
-800
-900
-1000
11-7-2019
31-7-2019
20-8-2019
9-9-2019
29-9-2019
19-10-2019
8-11-2019
28-11-2019
Time [date]
1
2
3
4
5
6
7
8

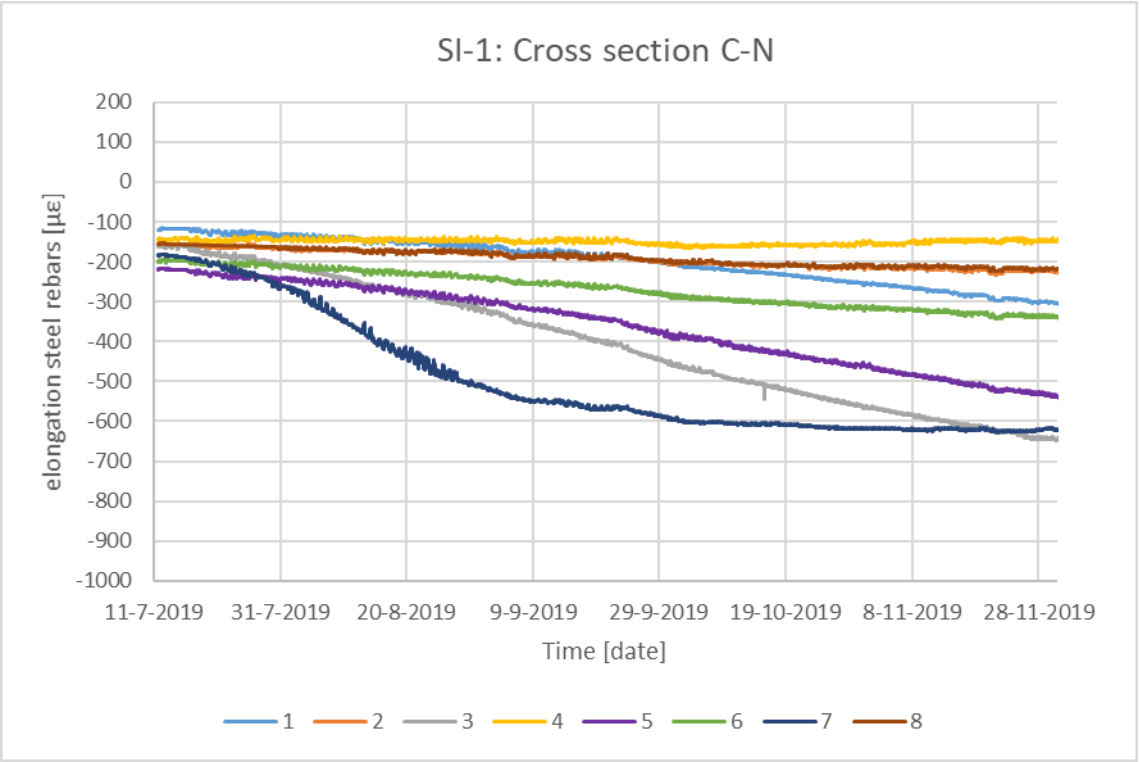
SI-1: Cross section C-N
200
100
0
-100
-200
-300
-400
-500
-600
-700
-800
-900
-1000
elongation steel rebars [με]
11-7-2019
31-7-2019
20-8-2019
9-9-2019
29-9-2019
19-10-2019
8-11-2019
28-11-2019
Time [date]
1
2
3
4
5
6
7
8

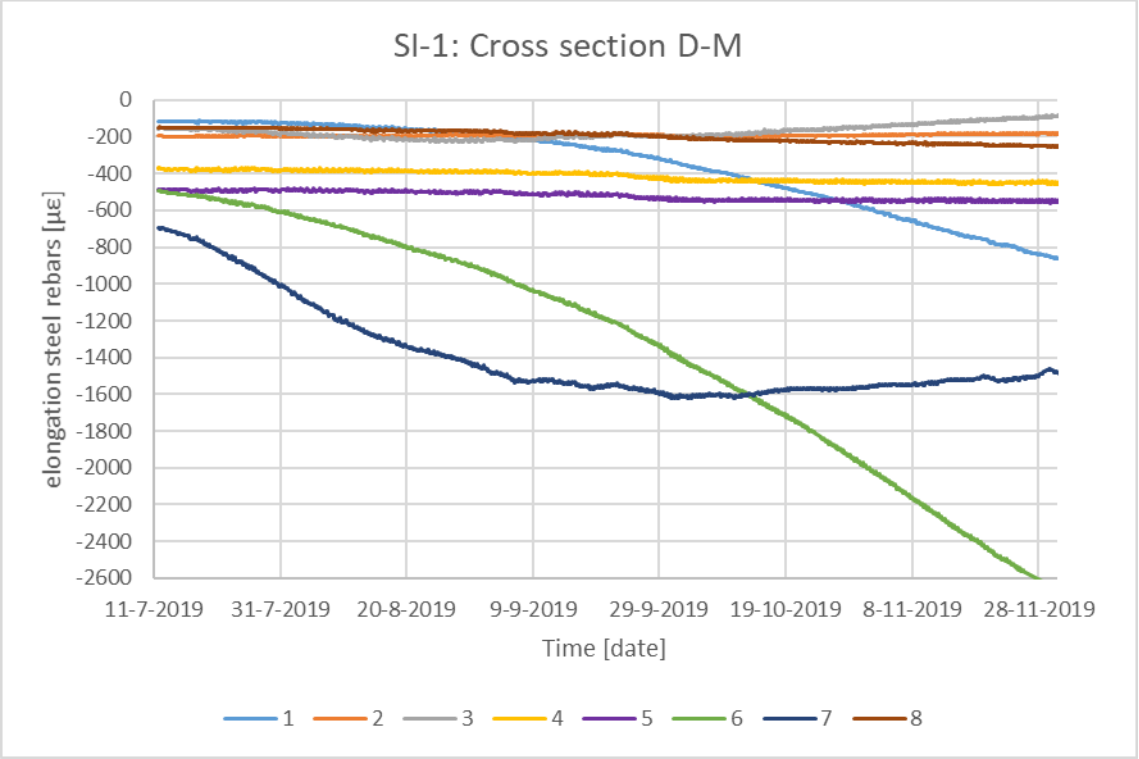
SI-1: Cross section D-M
0
-200
-400
-600
-800
-1000
-1200
-1400
-1600
-1800
-2000
-2200
-2400
-2600
elongation steel rebars [με]
11-7-2019
31-7-2019
20-8-2019
9-9-2019
29-9-2019
19-10-2019
8-11-2019
28-11-2019
Time [date]
1
2
3
4
5
6
7
8

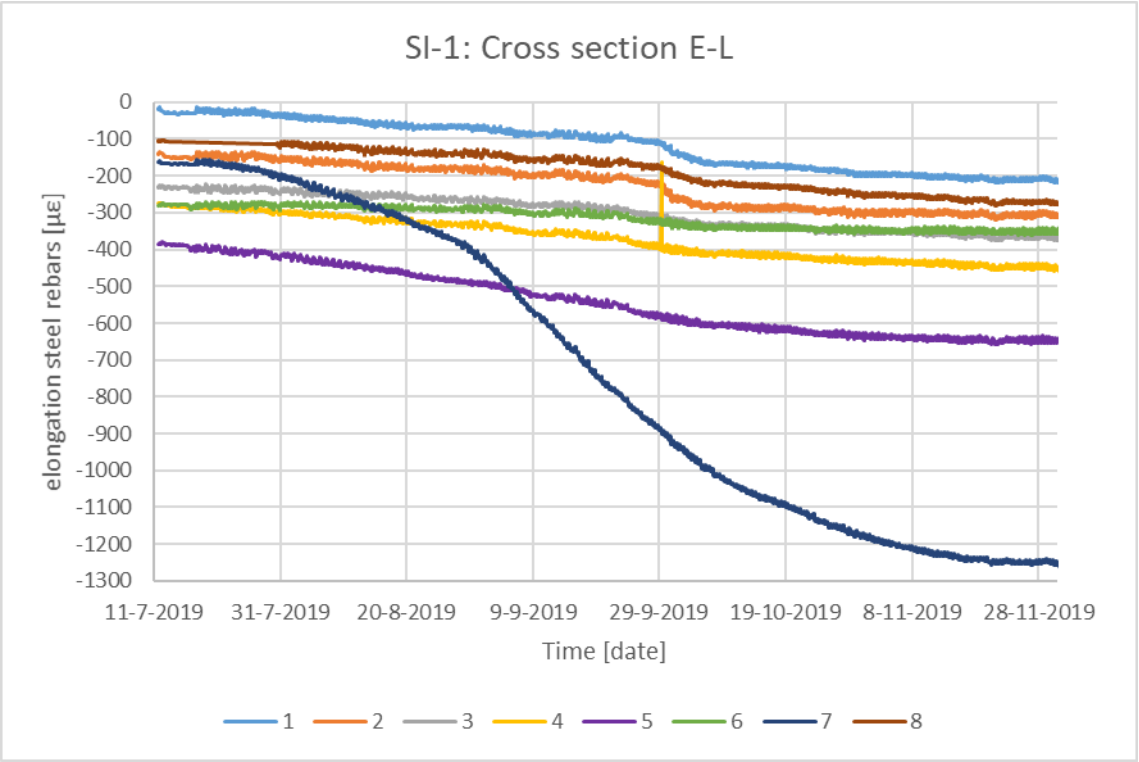
SI-1: Cross section E-L
0
-100
-200
-300
-400
-500
-600
-700
-800
-900
-1000
-1100
-1200
-1300
elongation steel rebars [με]
11-7-2019
31-7-2019
20-8-2019
9-9-2019
29-9-2019
19-10-2019
8-11-2019
28-11-2019
Time [date]
1
2
3
4
5
6
7
8

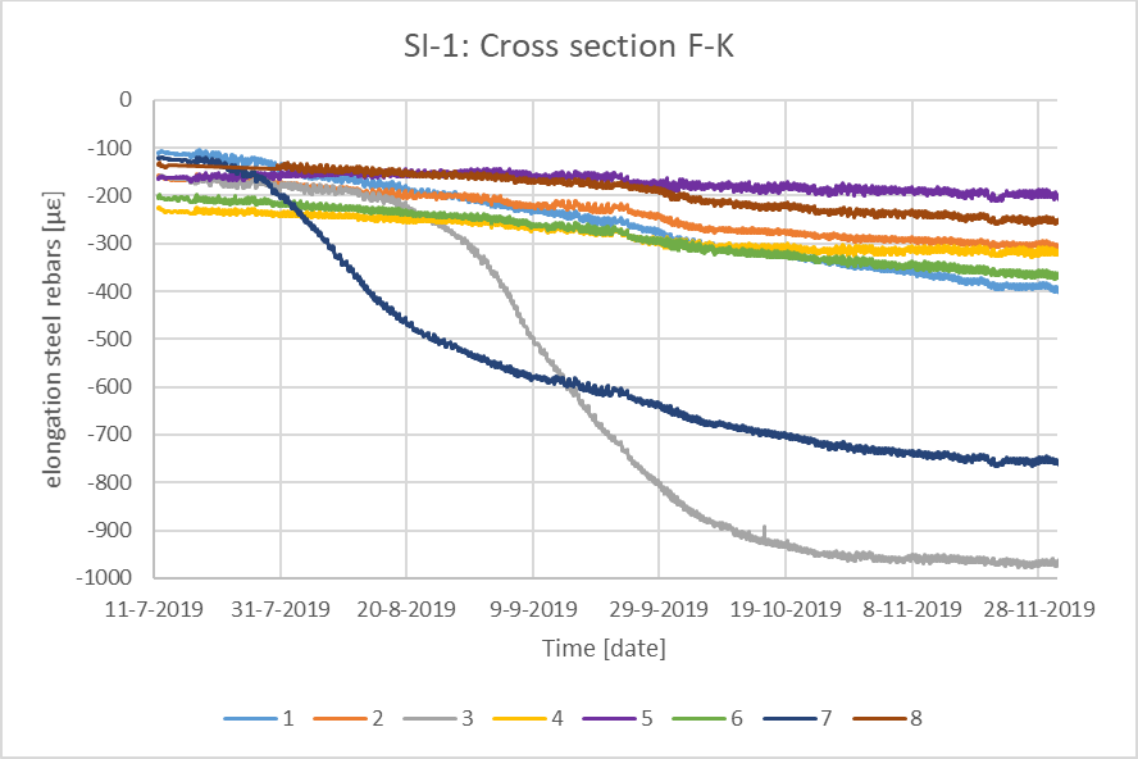
SI-1: Cross section F-K
0
-100
-200
-300
-400
-500
-600
-700
-800
-900
-1000
elongation steel rebars [με]
11-7-2019
31-7-2019
20-8-2019
9-9-2019
29-9-2019
19-10-2019
8-11-2019
28-11-2019
Time [date]
1
2
3
4
5
6
7
8

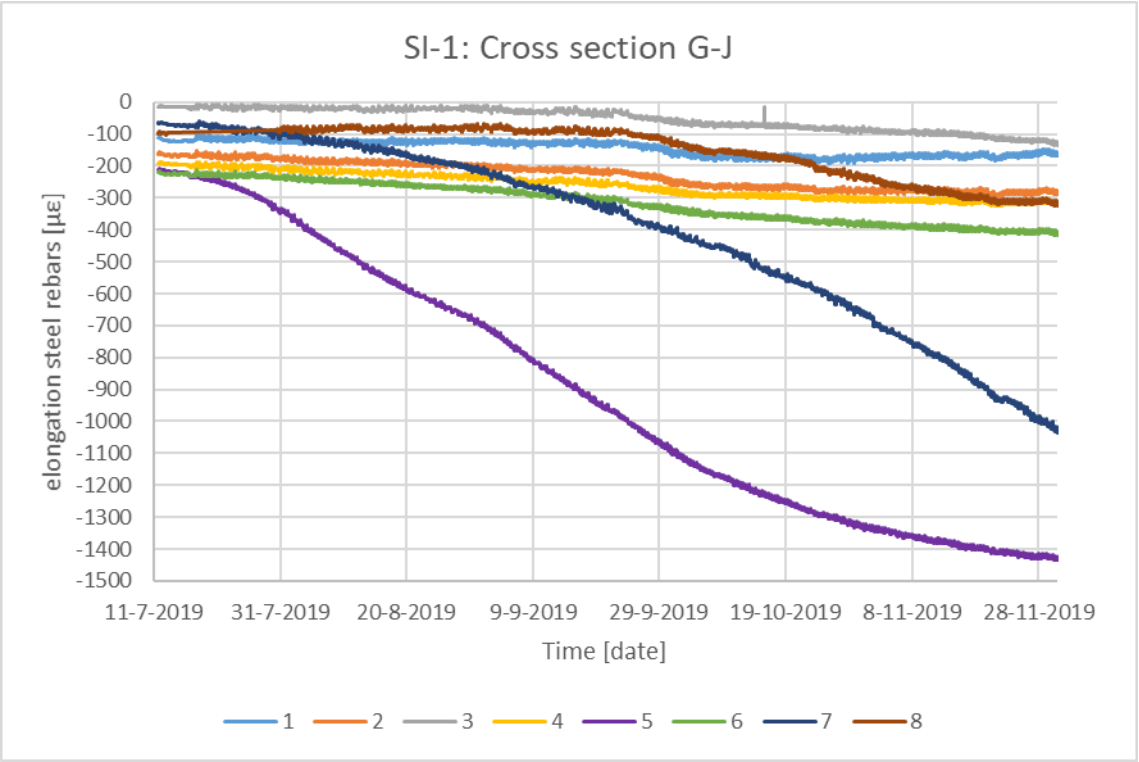
SI-1: Cross section G-J
0
-100
-200
-300
-400
-500
-600
-700
-800
-900
-1000
-1100
-1200
-1300
-1400
-1500
elongation steel rebars [με]
11-7-2019
31-7-2019
20-8-2019
9-9-2019
29-9-2019
19-10-2019
8-11-2019
28-11-2019
Time [date]
1
2
3
4
5
6
7
8

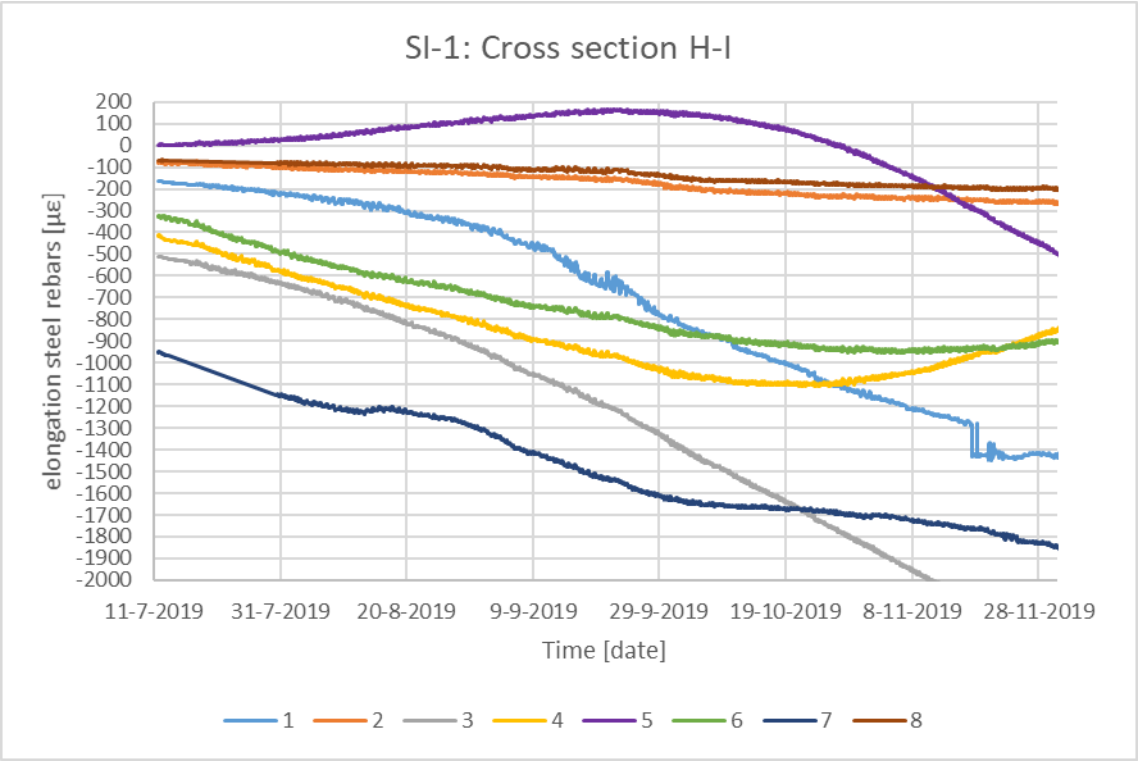
SI-1: Cross section H-I
200
100
0
-100
-200
-300
-400
-500
-600
-700
-800
-900
-1000
-1100
-1200
-1300
-1400
-1500
-1600
-1700
-1800
-1900
-2000
elongation steel rebars [με]
11-7-2019
31-7-2019
20-8-2019
9-9-2019
29-9-2019
19-10-2019
8-11-2019
28-11-2019
Time [date]
1
2
3
4
5
6
7
8

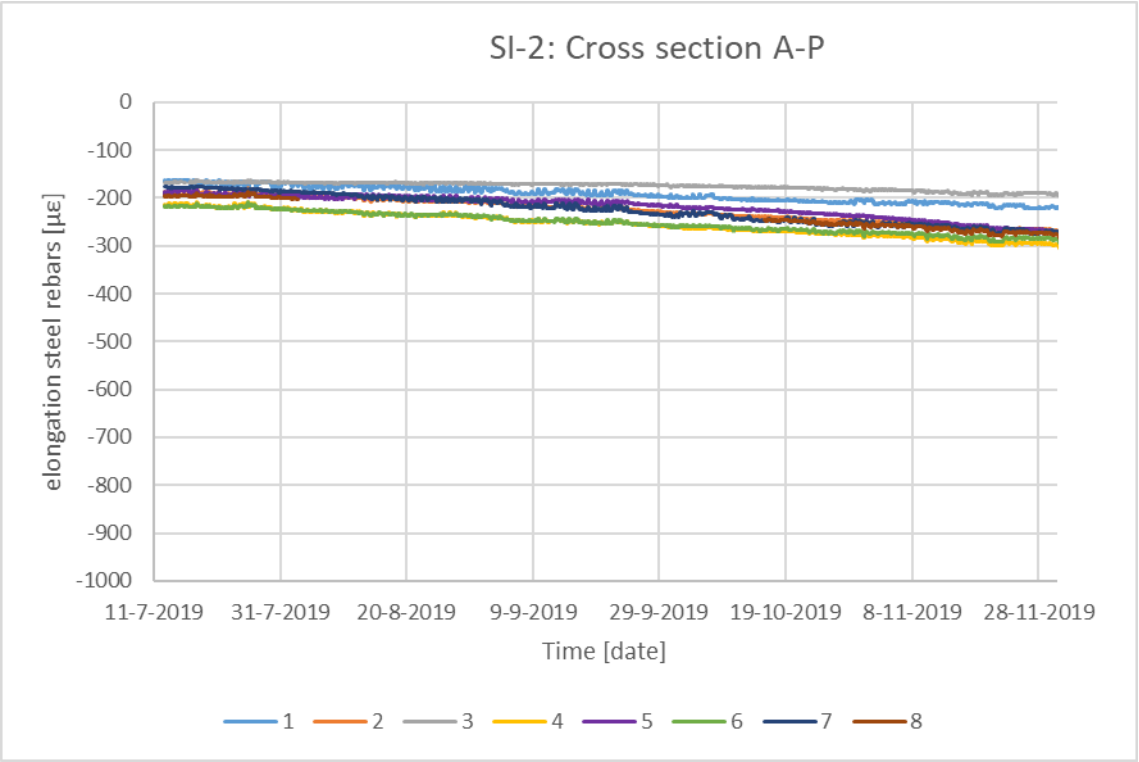
SI-2: Cross section A-P
0
-100
-200
-300
-400
-500
-600
-700
-800
-900
-1000
elongation steel rebars [με]
11-7-2019
31-7-2019
20-8-2019
9-9-2019
29-9-2019
19-10-2019
8-11-2019
28-11-2019
Time [date]
1
2
3
4
5
6
7
8

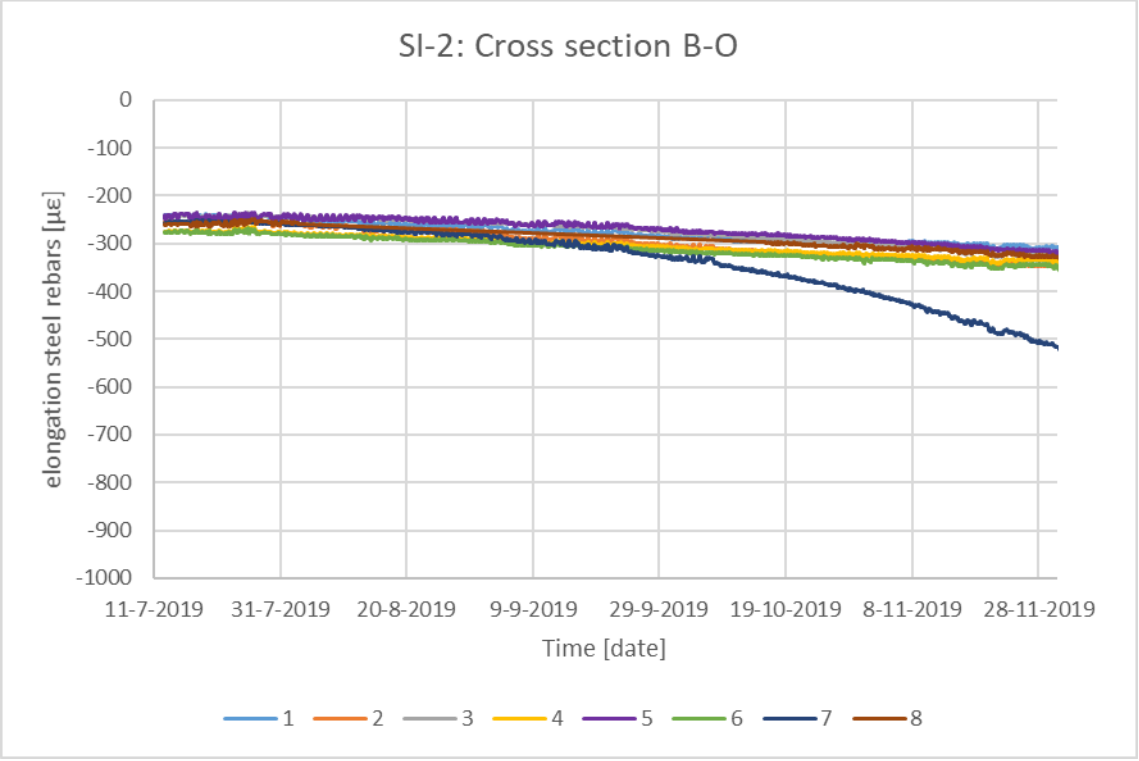
SI-2: Cross section B-O
0
-100
-200
-300
-400
-500
-600
-700
-800
-900
-1000
elongation steel rebars [με]
11-7-2019
31-7-2019
20-8-2019
9-9-2019
29-9-2019
19-10-2019
8-11-2019
28-11-2019
Time [date]
1
2
3
4
5
6
7
8

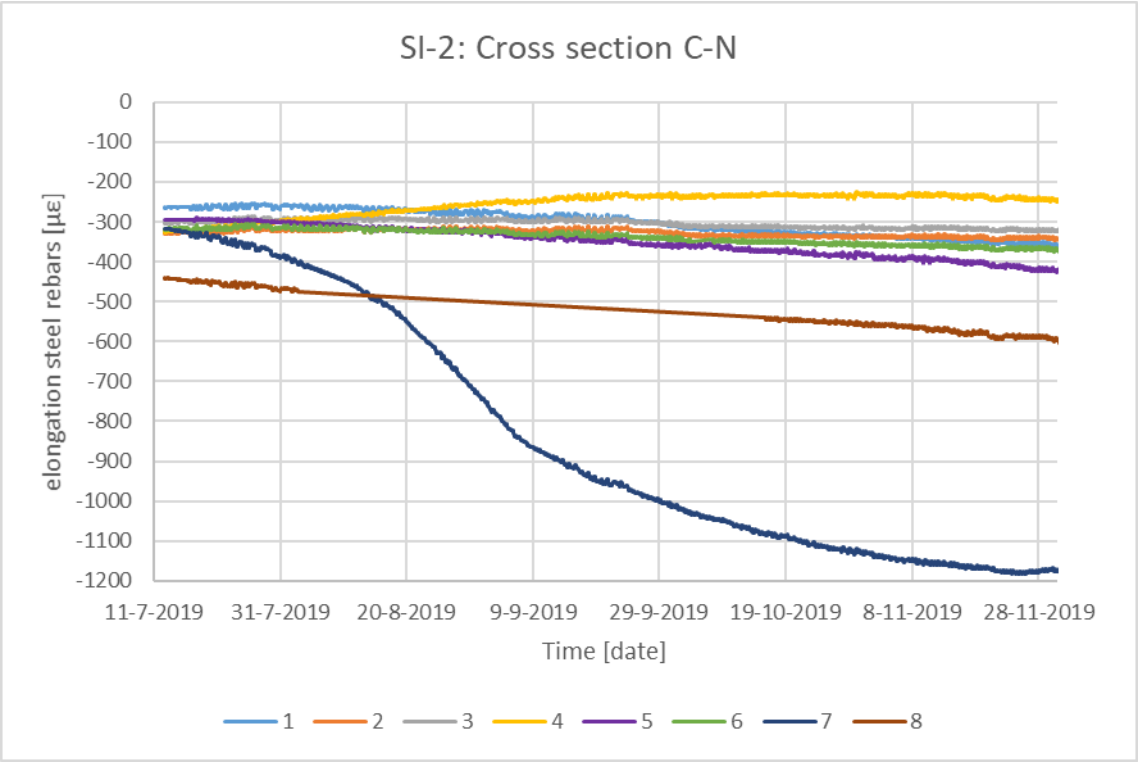
SI-2: Cross section C-N
0
-100
-200
-300
-400
-500
-600
-700
-800
-900
-1000
-1100
-1200
elongation steel rebars [με]
11-7-2019
31-7-2019
20-8-2019
9-9-2019
29-9-2019
19-10-2019
8-11-2019
28-11-2019
Time [date]
1
2
3
4
5
6
7
8

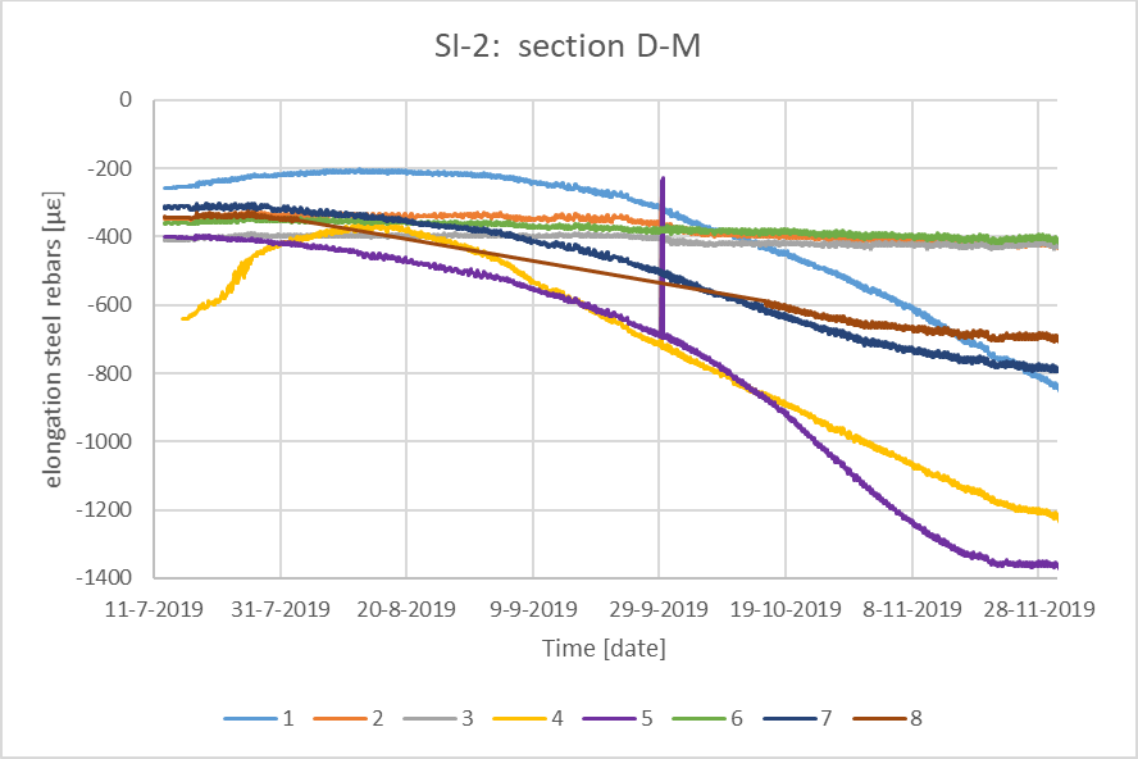
SI-2: section D-M
0
-200
-400
-600
-800
-1000
-1200
-1400
elongation steel rebars [με]
11-7-2019
31-7-2019
20-8-2019
9-9-2019
29-9-2019
19-10-2019
8-11-2019
28-11-2019
Time [date]
1
2
3
4
5
6
7
8

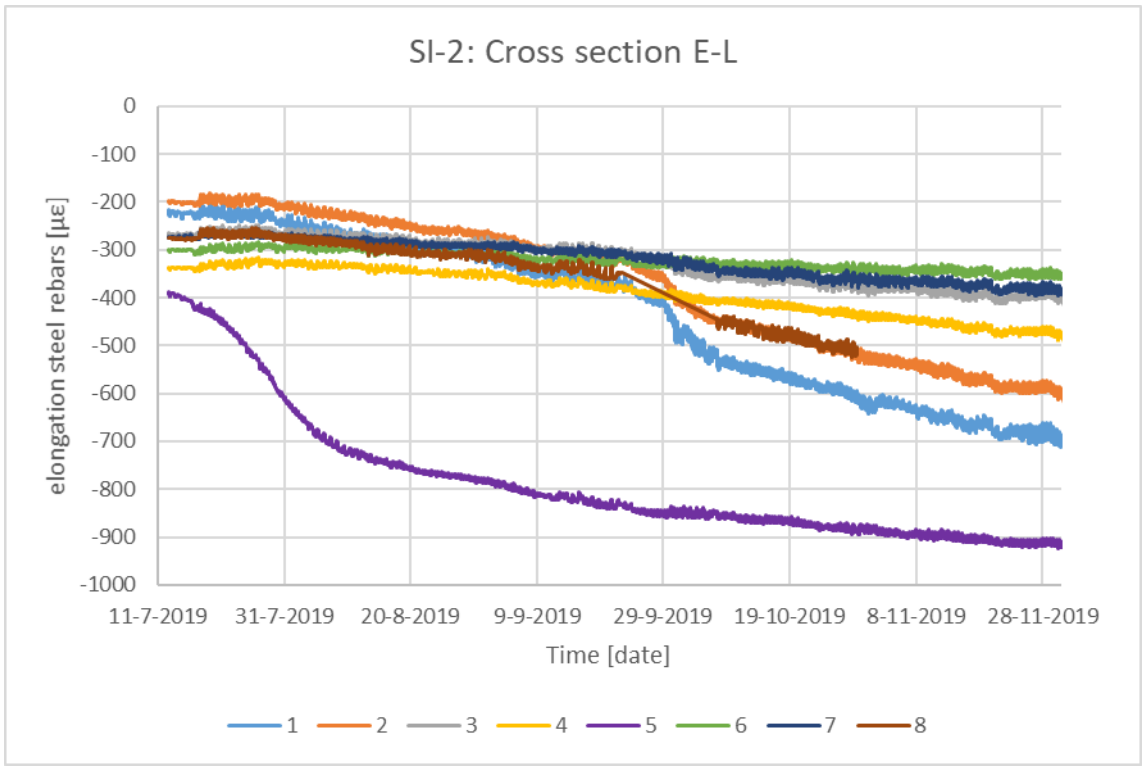
SI-2: Cross section E-L
0
-100
-200
-300
-400
-500
-600
-700
-800
-900
-1000
elongation steel rebars [με]
11-7-2019
31-7-2019
20-8-2019
9-9-2019
29-9-2019
19-10-2019
8-11-2019
28-11-2019
Time [date]
1
2
3
4
5
6
7
8

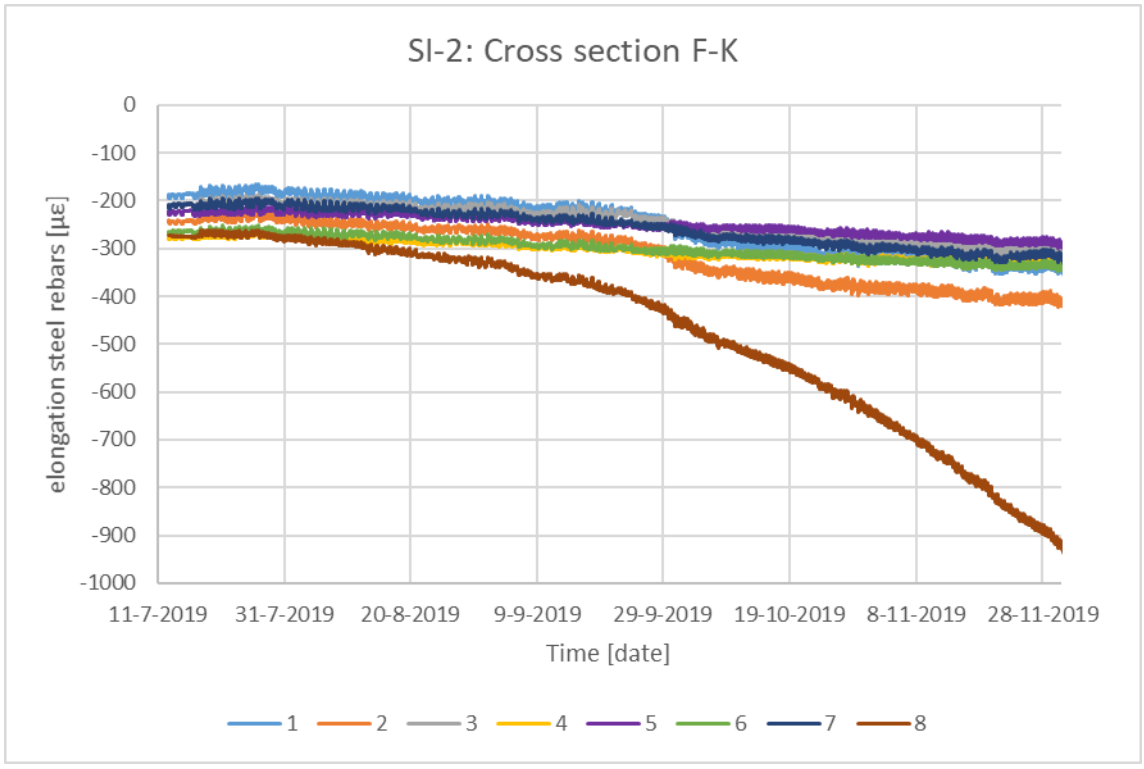
SI-2: Cross section F-K
0
-100
-200
-300
-400
-500
-600
-700
-800
-900
-1000
elongation steel rebars [με]
11-7-2019
31-7-2019
20-8-2019
9-9-2019
29-9-2019
19-10-2019
8-11-2019
28-11-2019
Time [date]
1
2
3
4
5
6
7
8

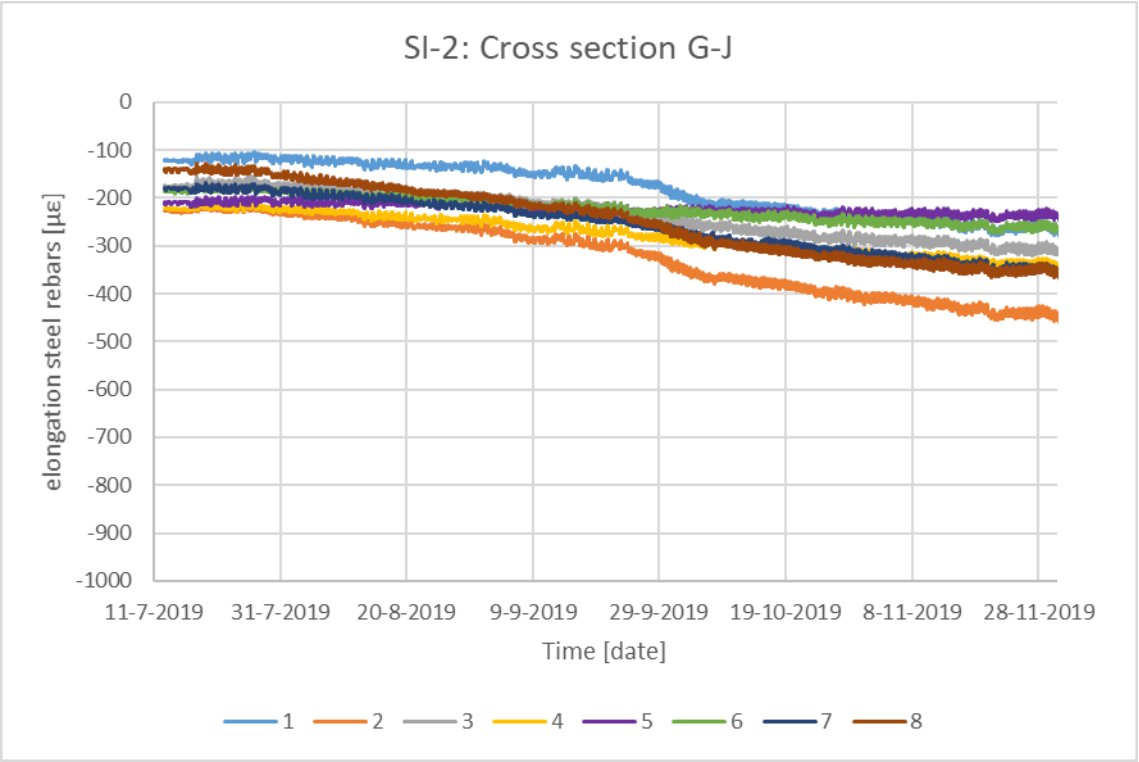
SI-2: Cross section G-J
0
-100
-200
-300
-400
-500
-600
-700
-800
-900
-1000
elongation steel rebars [με]
11-7-2019
31-7-2019
20-8-2019
9-9-2019
29-9-2019
19-10-2019
8-11-2019
28-11-2019
Time [date]
1
2
3
4
5
6
7
8

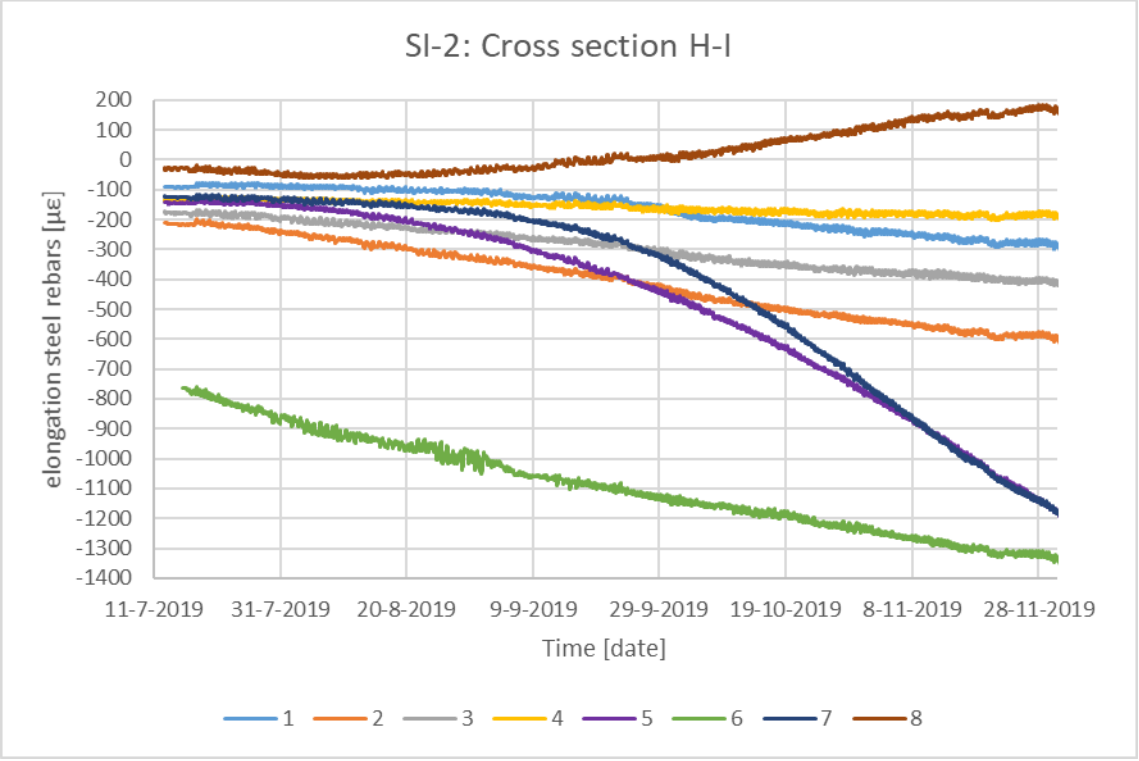
SI-2: Cross section H-I
200
100
0
-100
-200
-300
-400
-500
-600
-700
-800
-900
-1000
-1100
-1200
-1300
-1400
elongation steel rebars [με]
11-7-2019
31-7-2019
20-8-2019
9-9-2019
29-9-2019
19-10-2019
8-11-2019
28-11-2019
Time [date]
1
2
3
4
5
6
7
8

A.3. XYZ-measurements

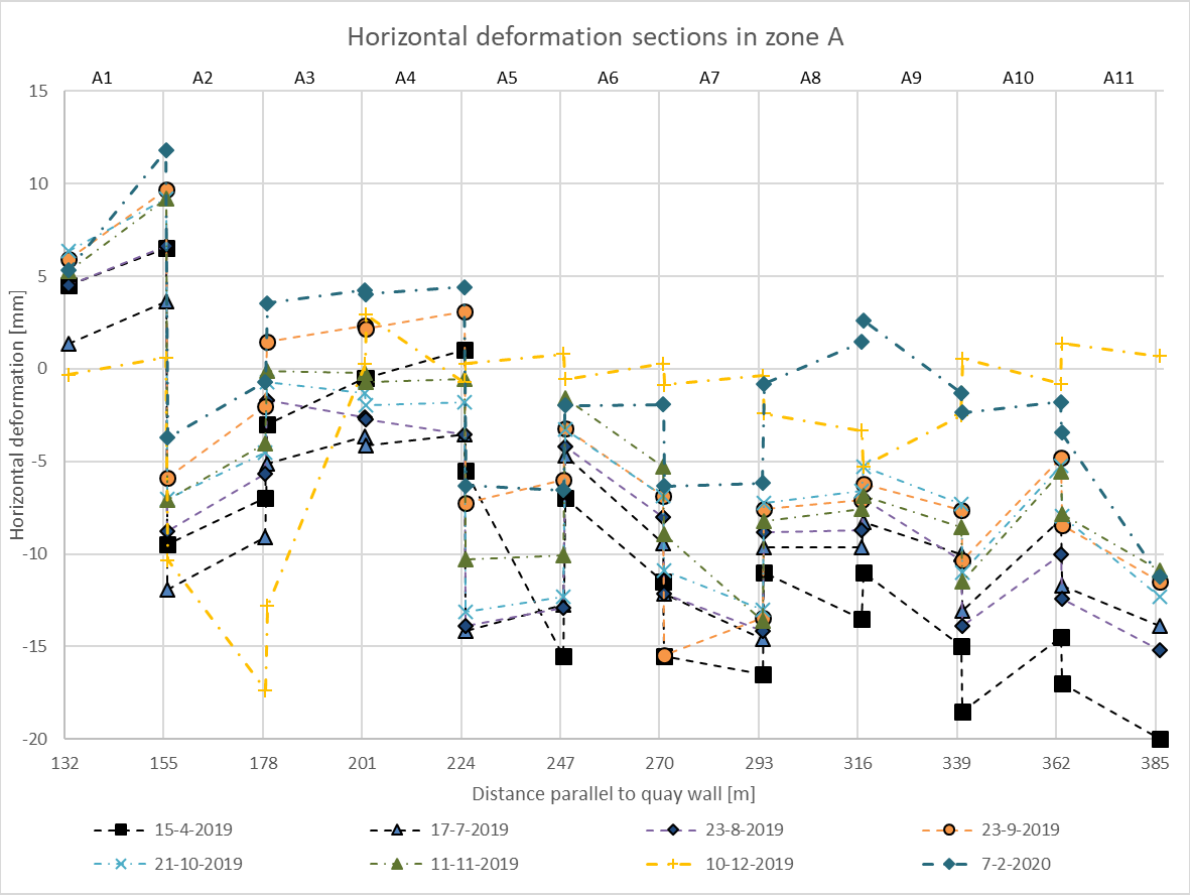

Figure A.7: Horizontal deformation zone A

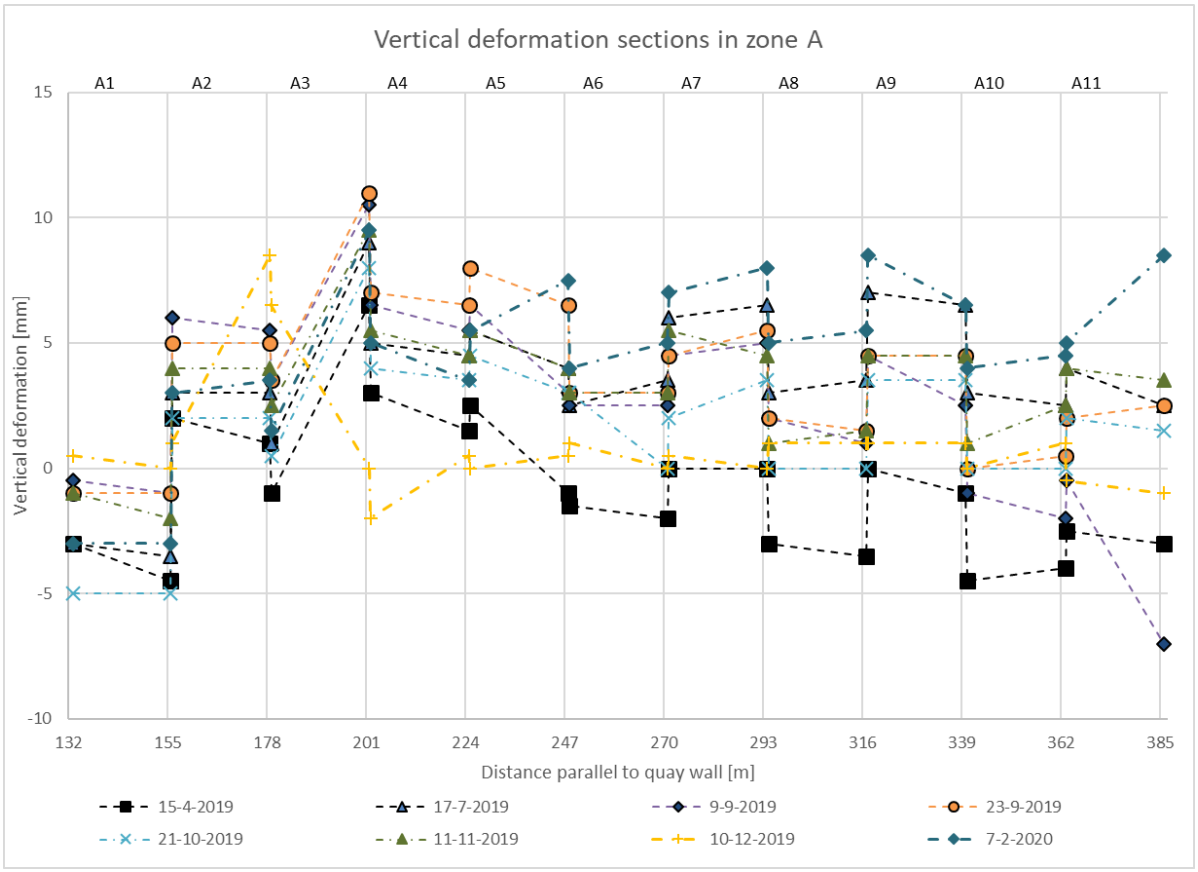

Figure A.8: Vertical deformation zone A

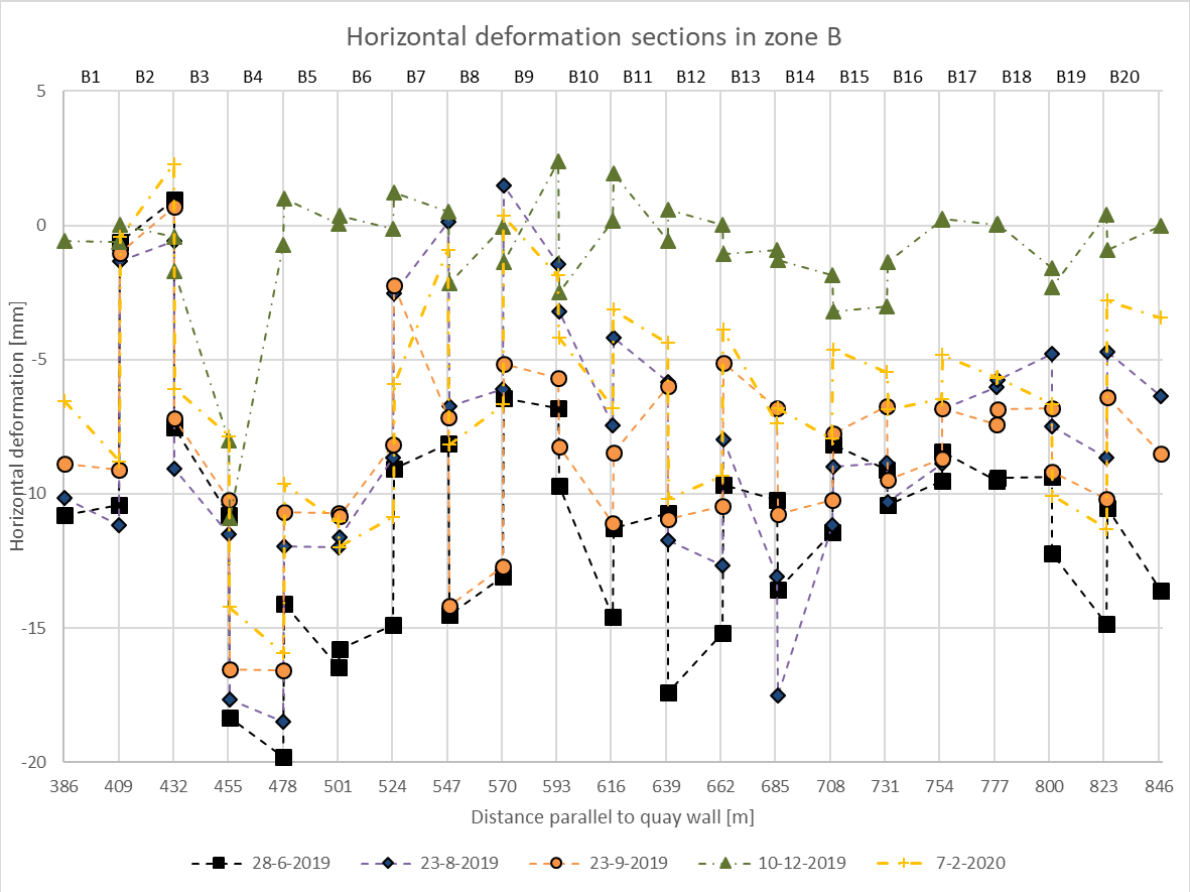

Figure A.9: Horizontal deformation zone B

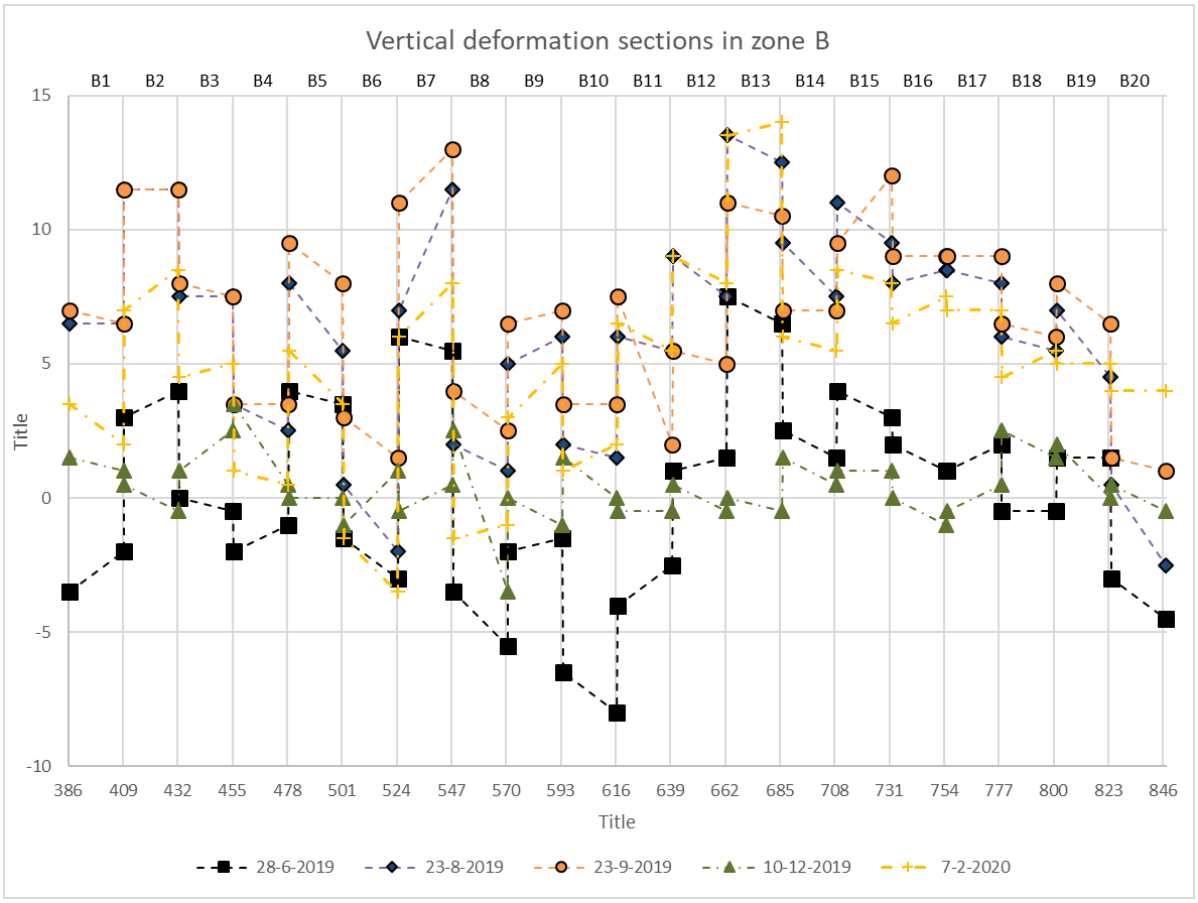

Figure A.10: Vertical deformation zone B

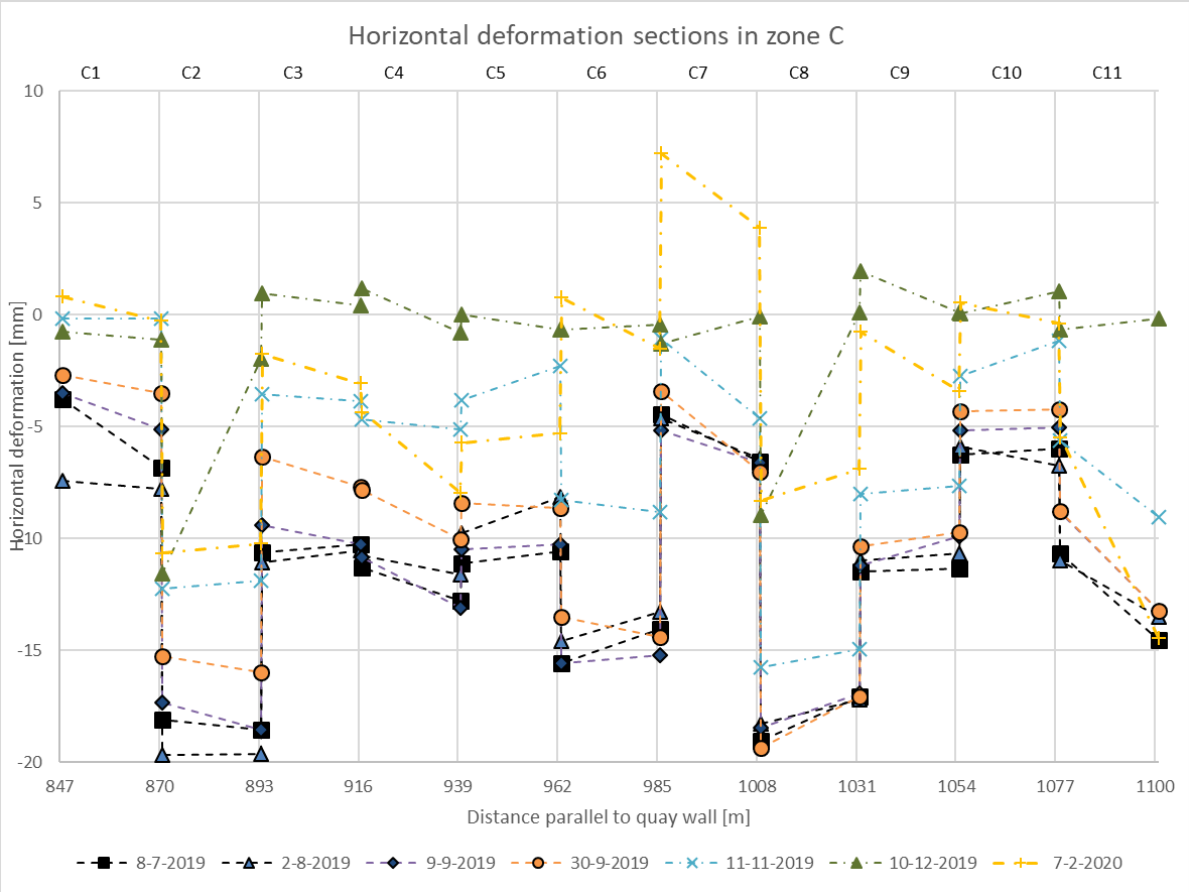

Figure A.11: Horizontal deformation zone C

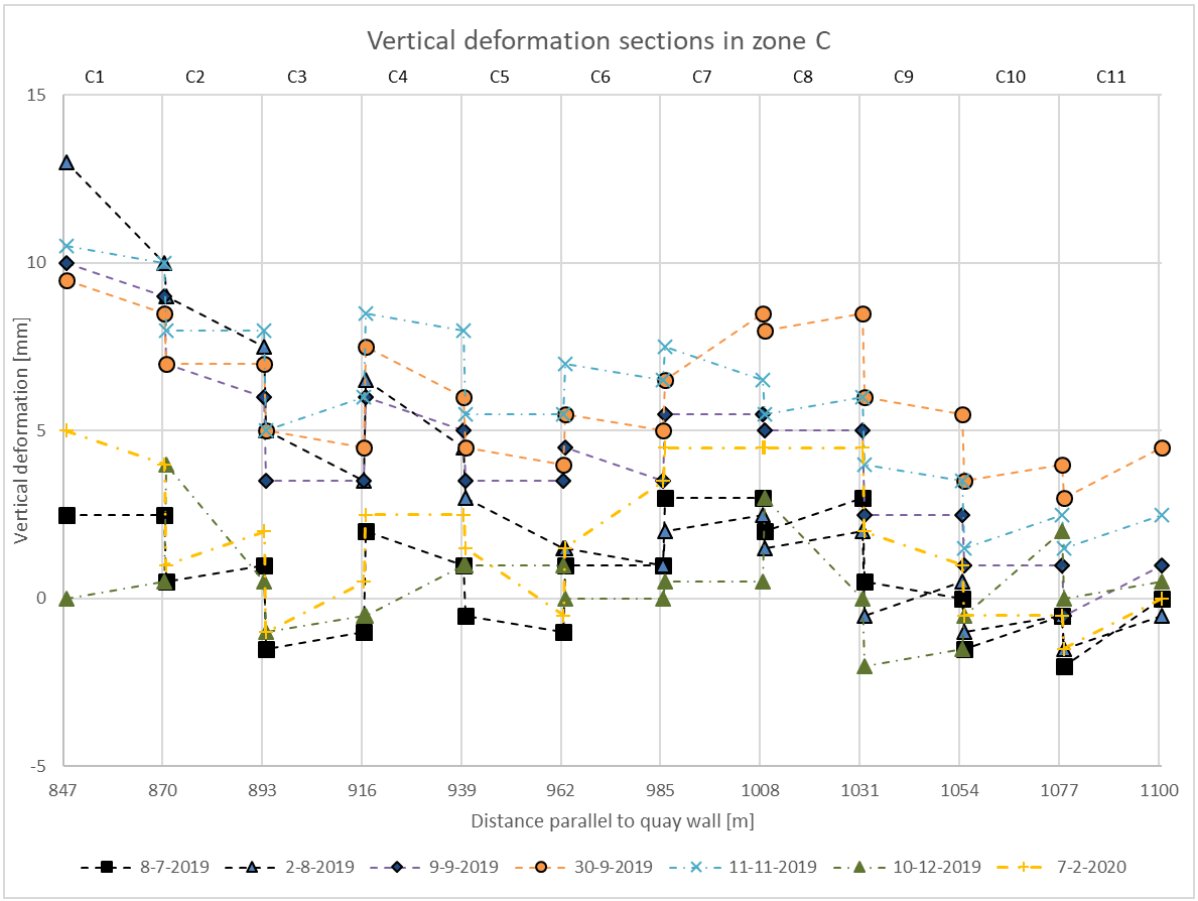

Figure A.12: Vertical deformation zone C

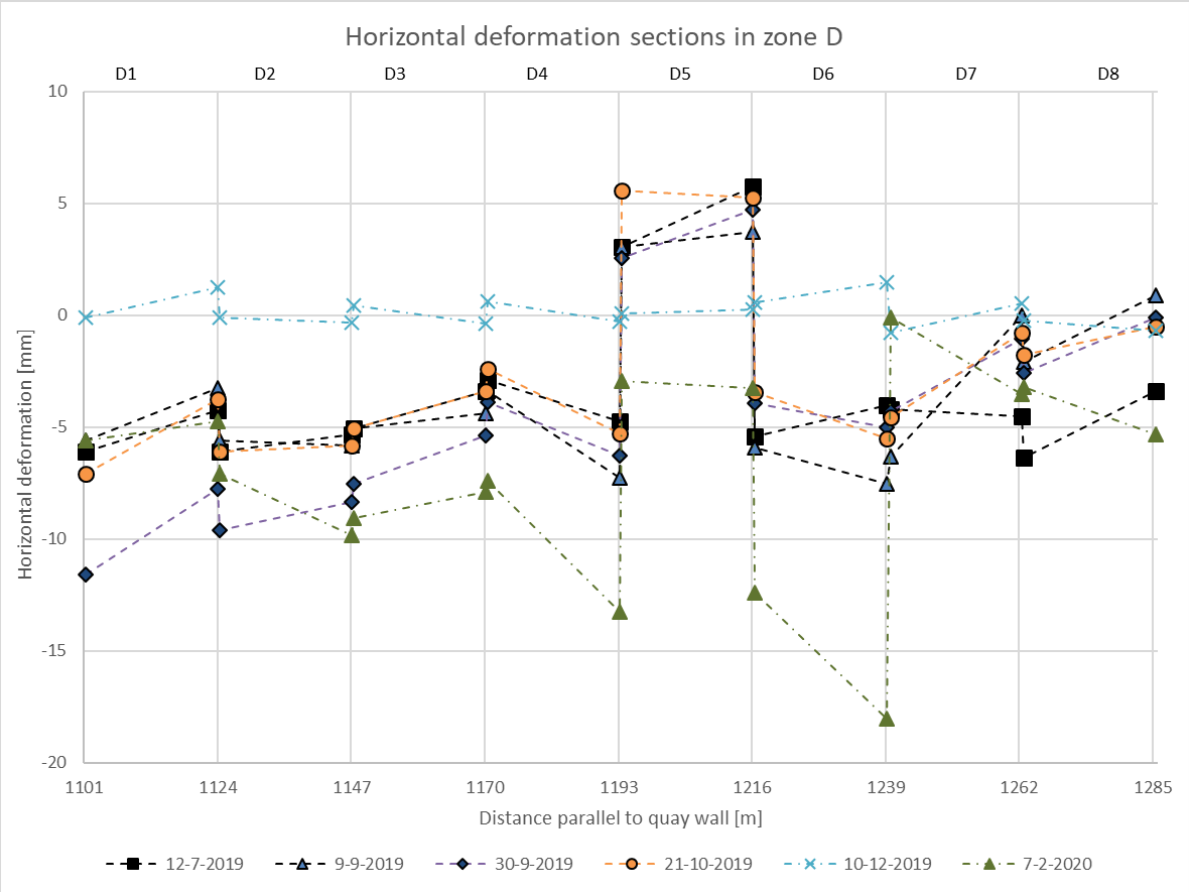

Figure A.13: Horizontal deformation zone D

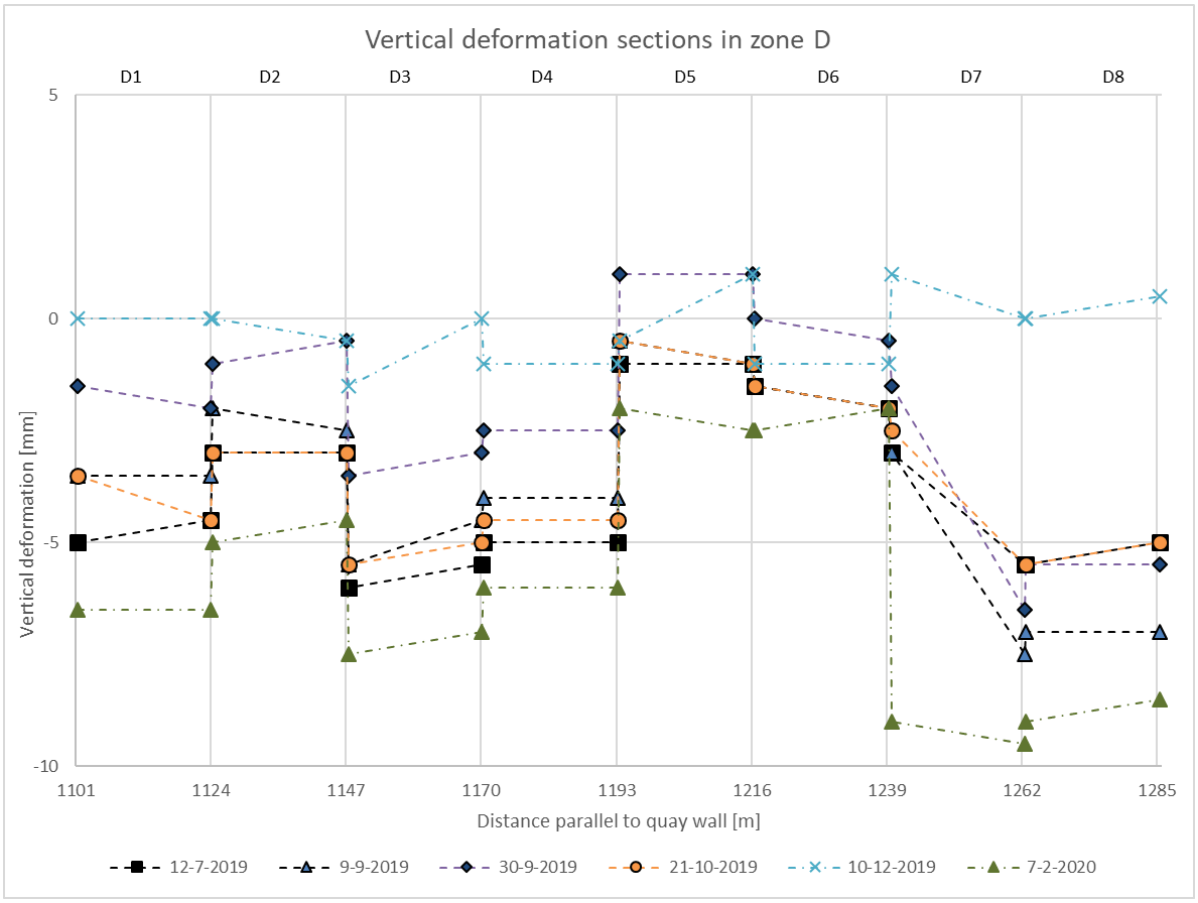

Figure A.14: Vertical deformation zone D

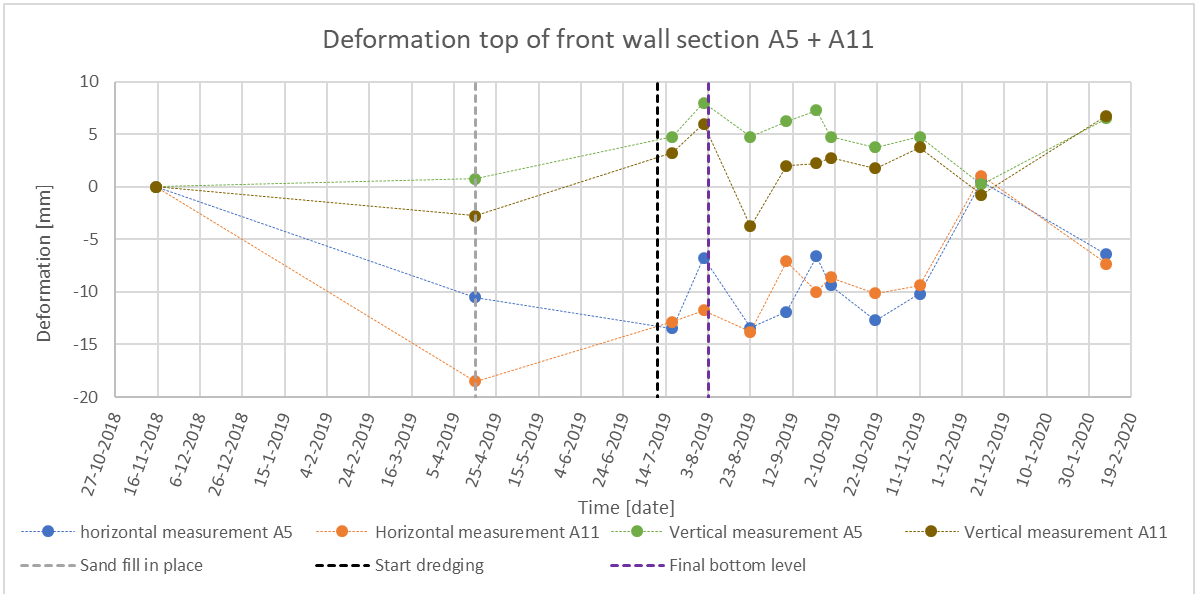

Figure A.15: Deformation measurements section A5 + A11

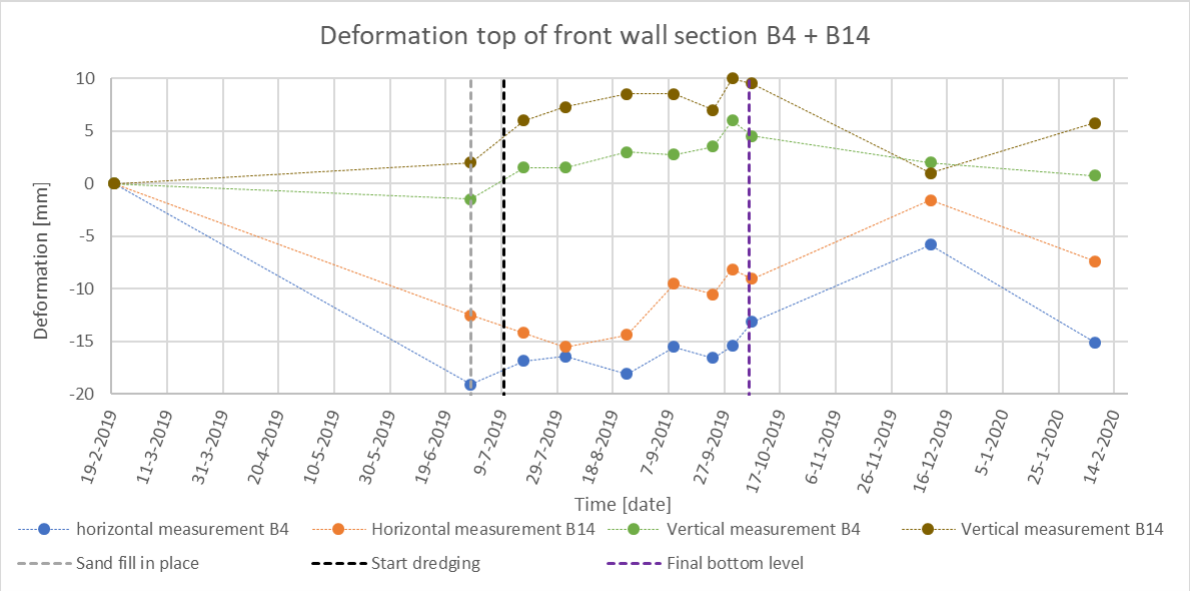

Figure A.16: Deformation measurements section B4 + B14

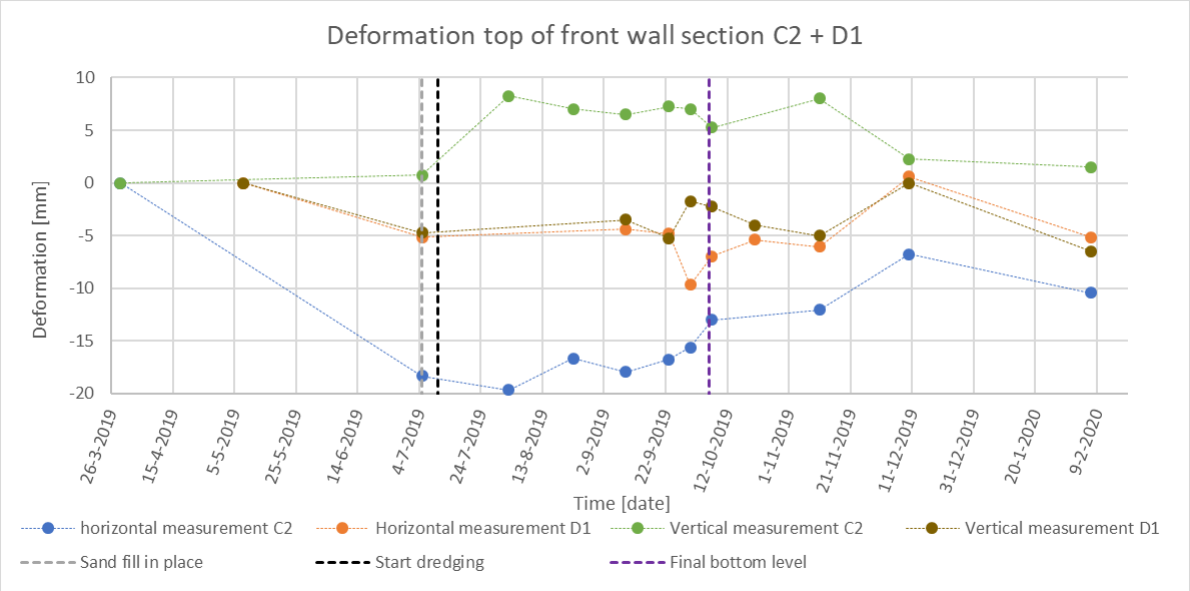

Figure A.17: Deformation measurements section C2 + D1

A.4. Inclinometer

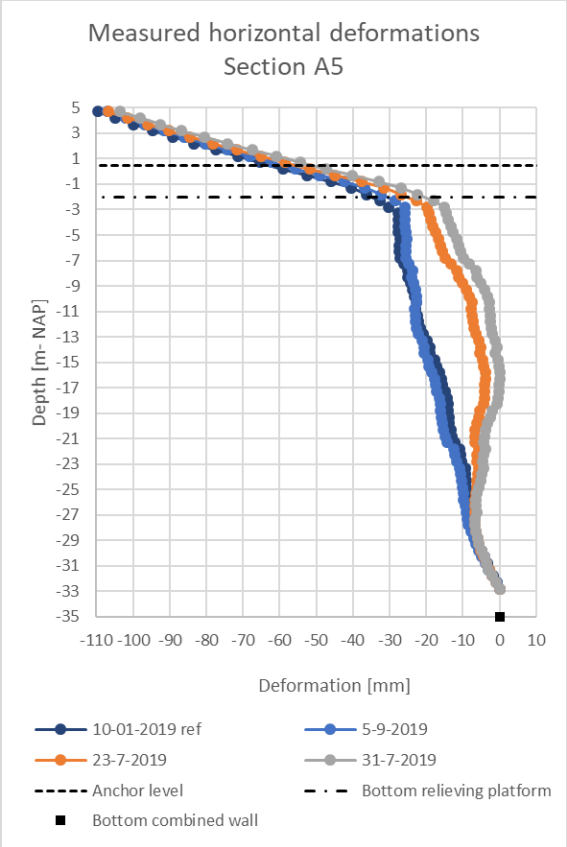
Measured horizontal deformations
Section A5
Depth [m- NAP]
Deformation [mm]
10-01-2019 ref
5-9-2019
23-7-2019
31-7-2019
Anchor level
Bottom relieving platform
Bottom combined wall

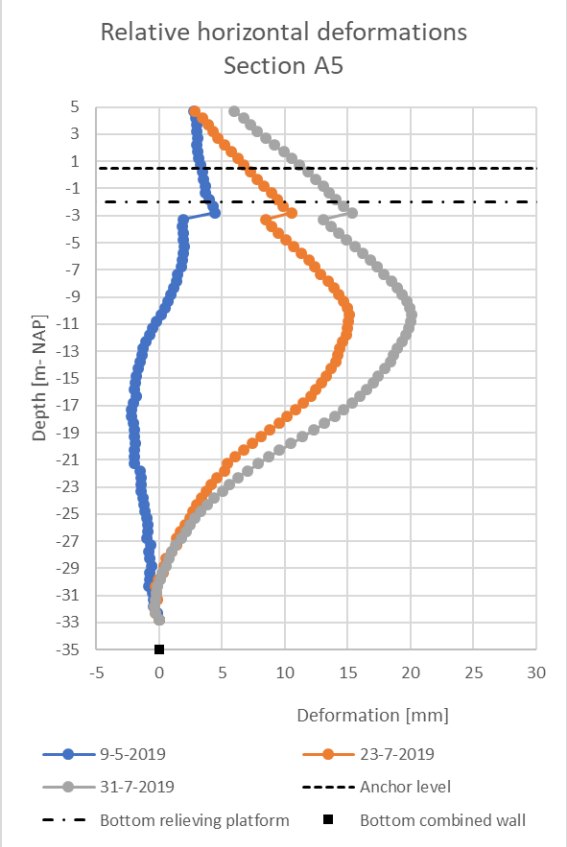
Relative horizontal deformations
Section A5
Depth [m- NAP]
Deformation [mm]
9-5-2019
23-7-2019
31-7-2019
Anchor level
Bottom relieving platform
Bottom combined wall

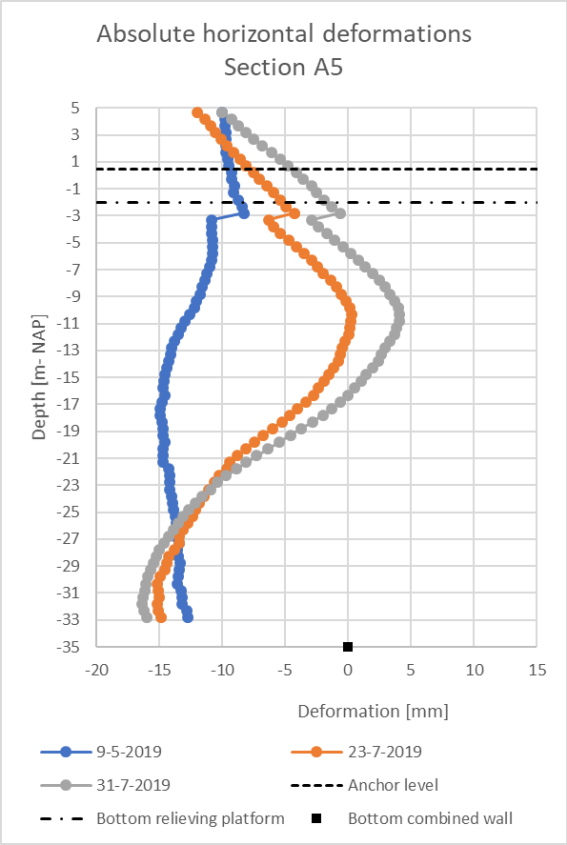
Absolute horizontal deformations
Section A5
Depth [m- NAP]
Deformation [mm]
9-5-2019
23-7-2019
31-7-2019
Anchor level
Bottom relieving platform
Bottom combined wall

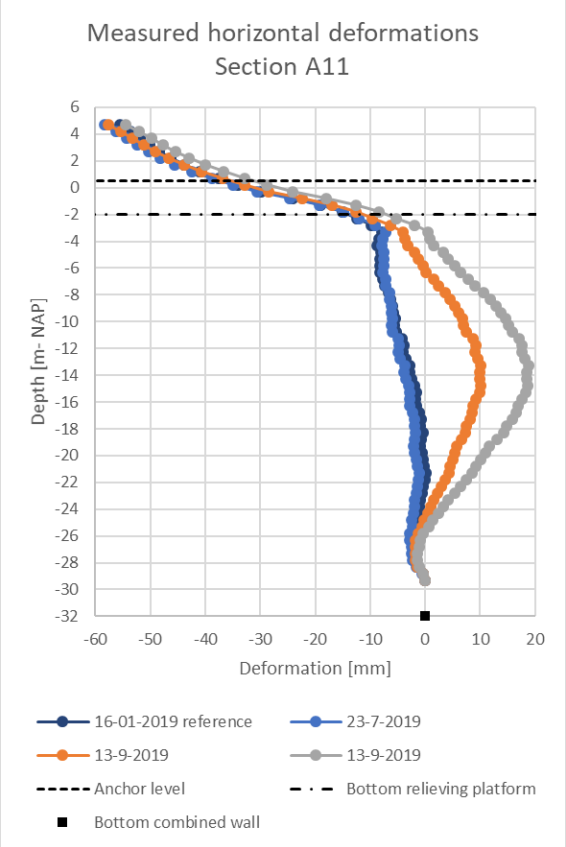
Measured horizontal deformations
Section A11
Depth [m- NAP]
Deformation [mm]
16-01-2019 reference
23-7-2019
13-9-2019
13-9-2019
Anchor level
Bottom relieving platform
Bottom combined wall

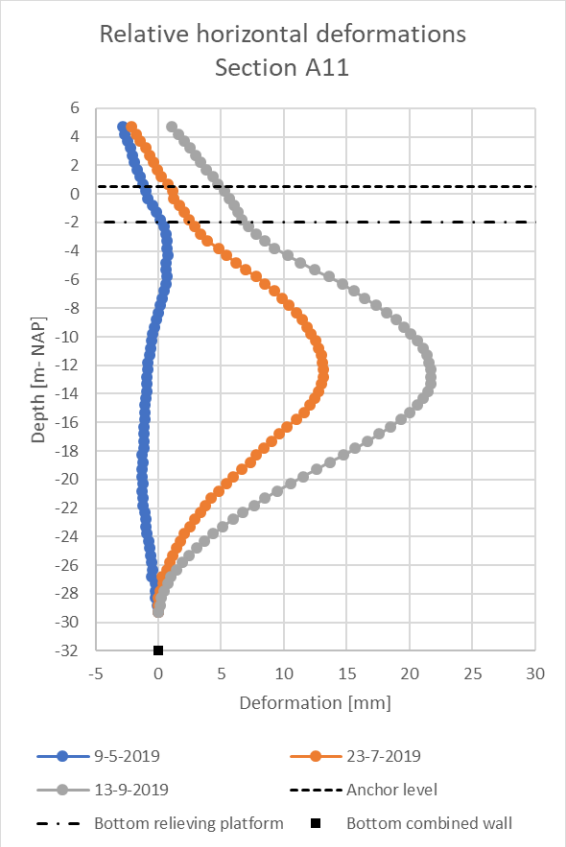
Relative horizontal deformations
Section A11
Depth [m- NAP]
Deformation [mm]
9-5-2019
23-7-2019
13-9-2019
Anchor level
Bottom relieving platform
Bottom combined wall

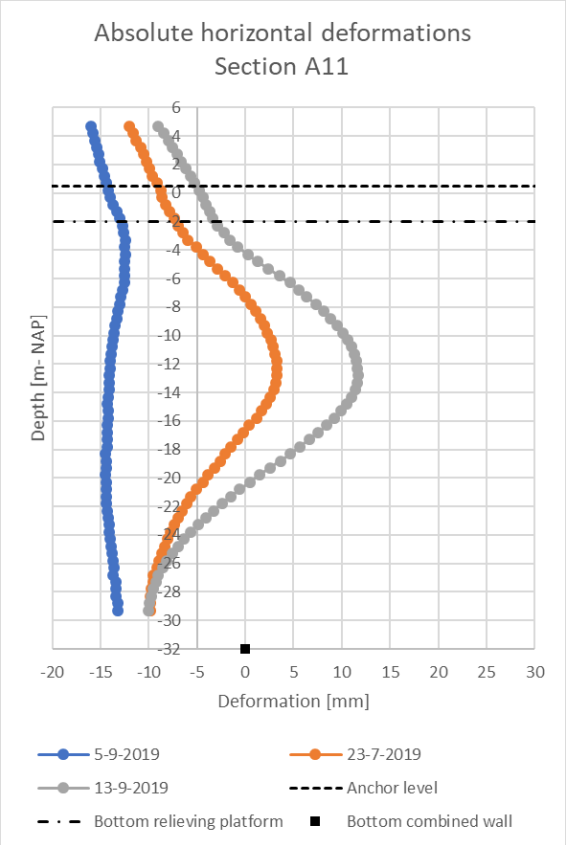
Absolute horizontal deformations
Section A11
Depth [m- NAP]
Deformation [mm]
5-9-2019
23-7-2019
13-9-2019
Anchor level
Bottom relieving platform
Bottom combined wall

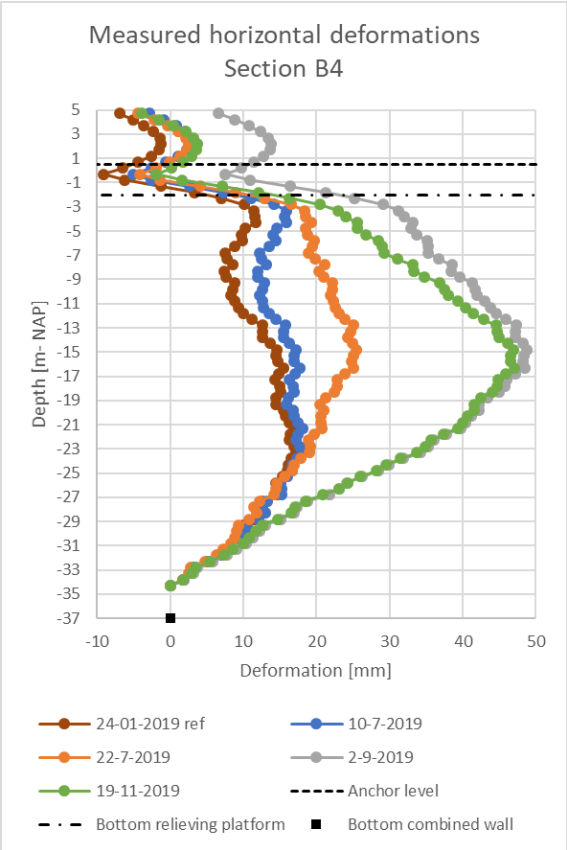
Measured horizontal deformations
Section B4
Depth [m- NAP]
Deformation [mm]
24-01-2019 ref
10-7-2019
22-7-2019
2-9-2019
19-11-2019
Anchor level
Bottom relieving platform
Bottom combined wall

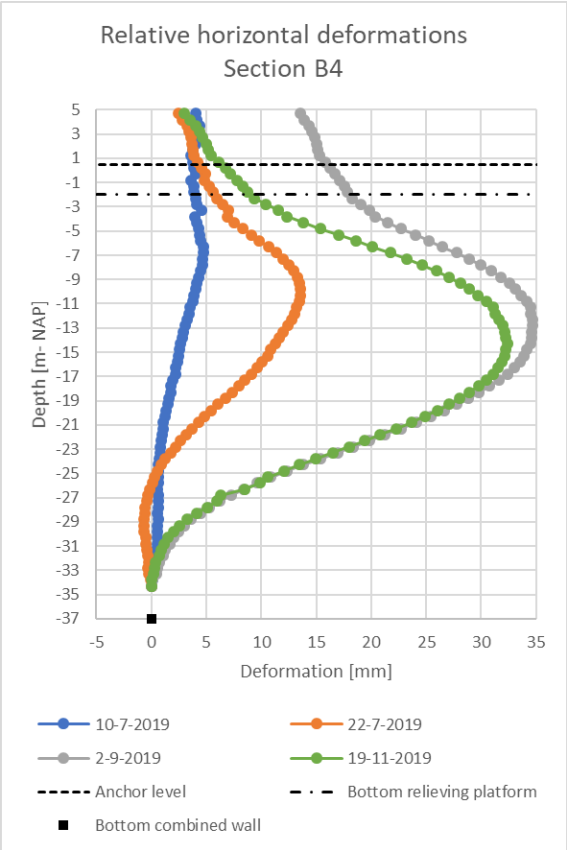
Relative horizontal deformations
Section B4
Depth [m- NAP]
Deformation [mm]
10-7-2019
22-7-2019
2-9-2019
19-11-2019
Anchor level
Bottom relieving platform
Bottom combined wall

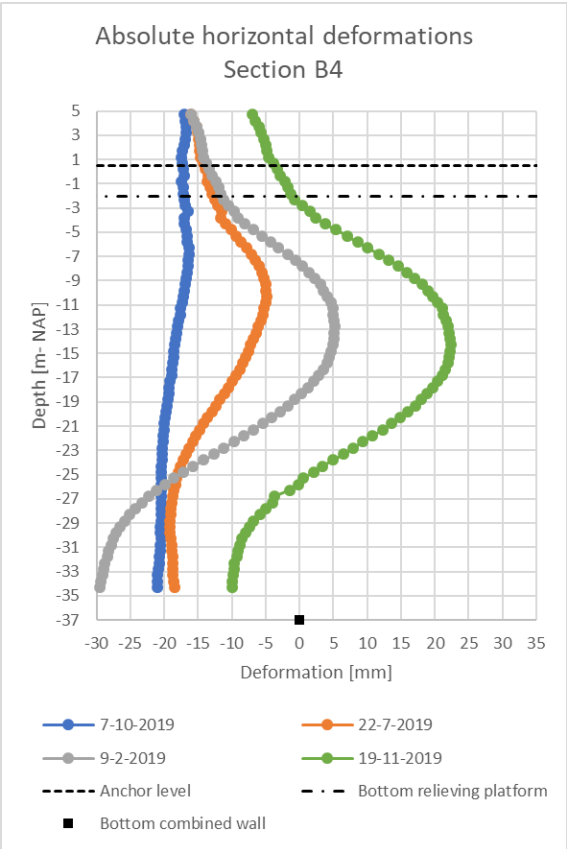
Absolute horizontal deformations
Section B4
Depth [m- NAP]
Deformation [mm]
7-10-2019
22-7-2019
9-2-2019
19-11-2019
Anchor level
Bottom relieving platform
Bottom combined wall

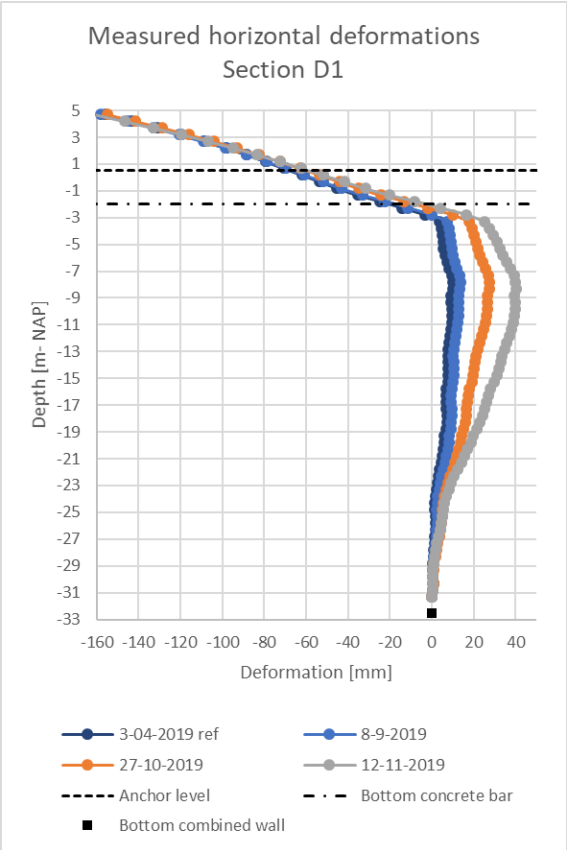
Measured horizontal deformations
Section D1
Depth [m- NAP]
Deformation [mm]
3-04-2019 ref
8-9-2019
27-10-2019
12-11-2019
Anchor level
Bottom concrete bar
Bottom combined wall

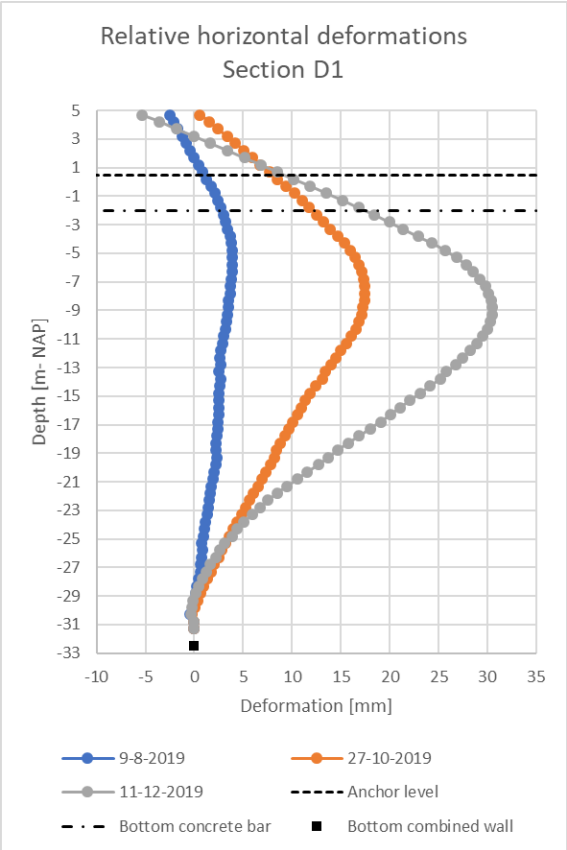
Relative horizontal deformations
Section D1
Depth [m- NAP]
Deformation [mm]
9-8-2019
27-10-2019
11-12-2019
Anchor level
Bottom concrete bar
Bottom combined wall

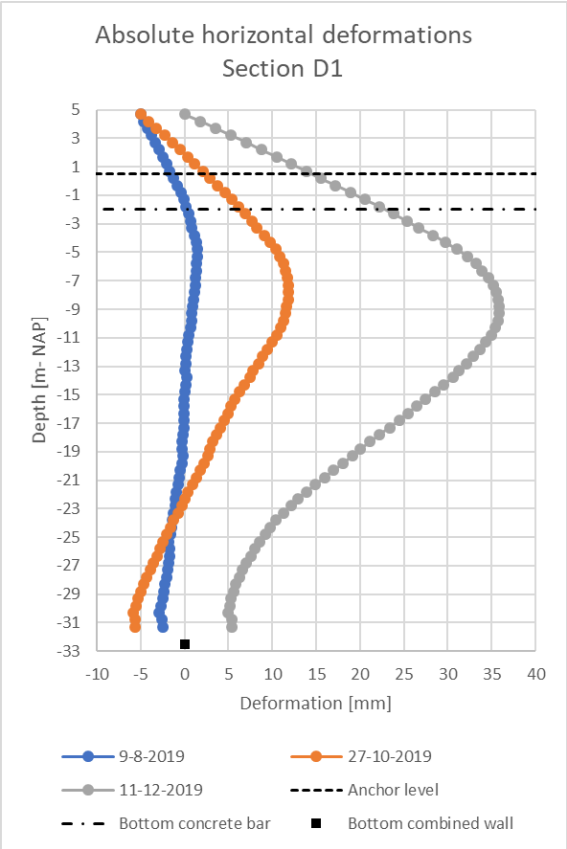
Absolute horizontal deformations
Section D1
Depth [m- NAP]
Deformation [mm]
9-8-2019
27-10-2019
11-12-2019
Anchor level
Bottom concrete bar
Bottom combined wall

A.5. Inclinometer

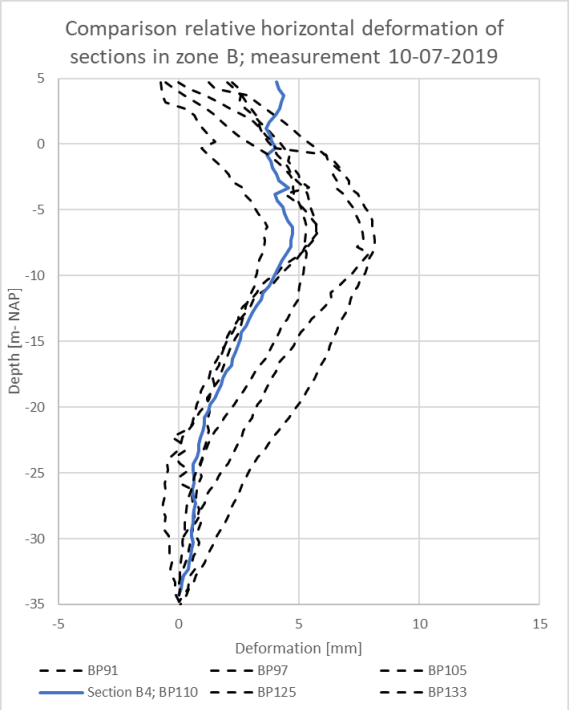
Comparison relative horizontal deformation of sections in zone B; measurement 10-07-2019
Depth [m- NAP]
Deformation [mm]
BP91
BP97
BP105
Section B4; BP110
BP125
BP133

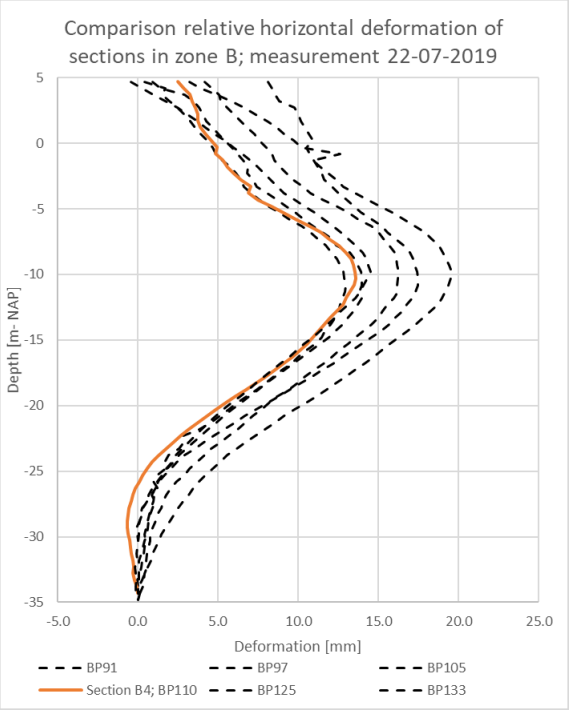
Comparison relative horizontal deformation of sections in zone B; measurement 22-07-2019
Depth [m- NAP]
Deformation [mm]
BP91
BP97
BP105
Section B4; BP110
BP125
BP133

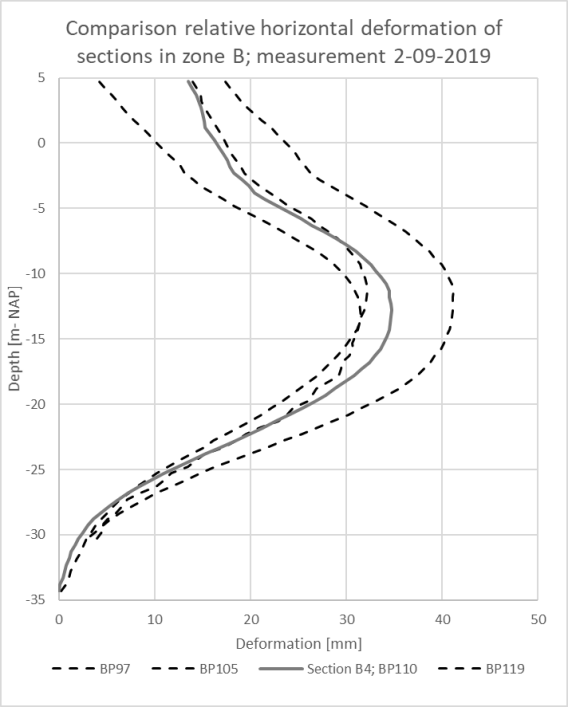
Comparison relative horizontal deformation of sections in zone B; measurement 2-09-2019
Depth [m- NAP]
Deformation [mm]
BP97
BP105
Section B4; BP110
BP119

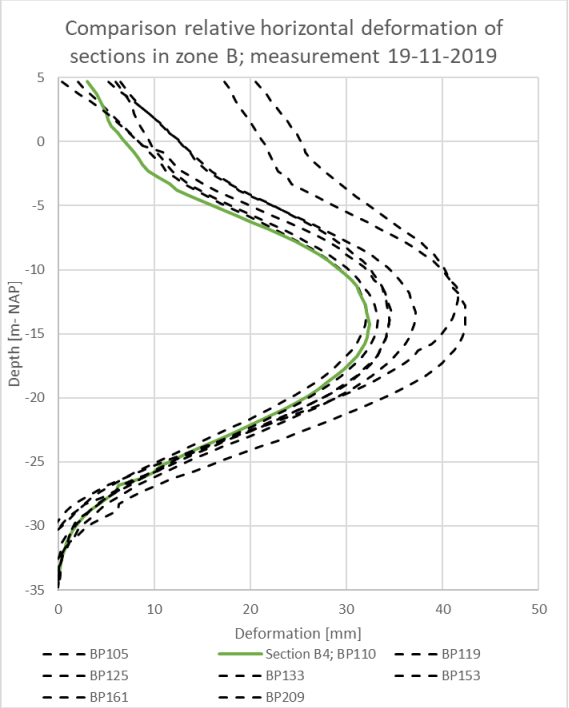
Comparison relative horizontal deformation of sections in zone B; measurement 19-11-2019
Depth [m- NAP]
Deformation [mm]
BP105
Section B4; BP110
BP119
BP125
BP133
BP153
BP161
BP209

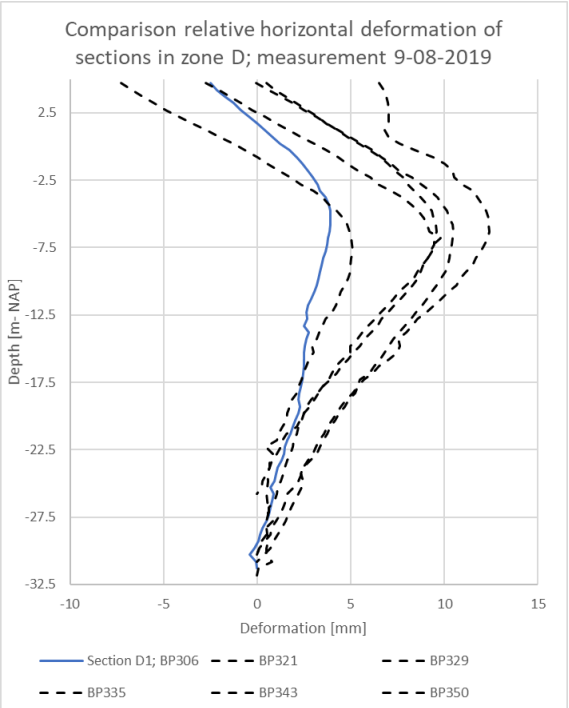
Comparison relative horizontal deformation of sections in zone D; measurement 9-08-2019
Depth [m- NAP]
2.5
-2.5
-7.5
-12.5
-17.5
-22.5
-27.5
-32.5
-10
-5
0
5
10
15
Deformation [mm]
Section D1; BP306
BP321
BP329
BP335
BP343
BP350

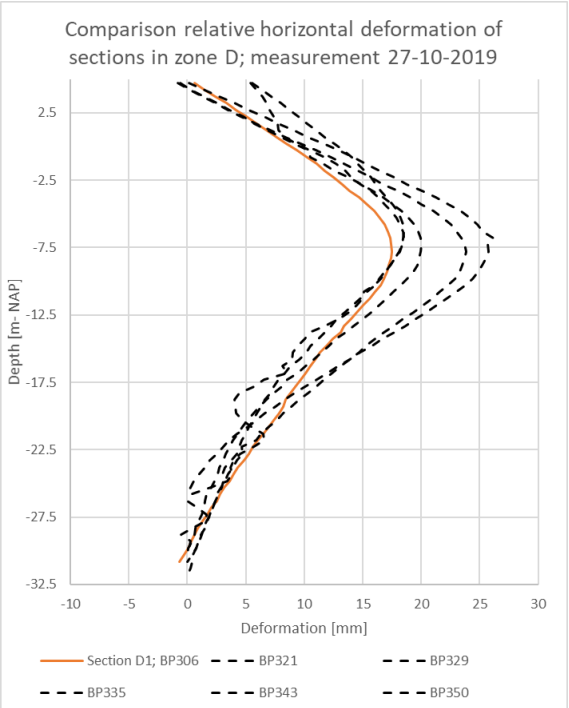
Comparison relative horizontal deformation of sections in zone D; measurement 27-10-2019
Depth [m- NAP]
2.5
-2.5
-7.5
-12.5
-17.5
-22.5
-27.5
-32.5
-10
-5
0
5
10
15
20
25
30
Deformation [mm]
Section D1; BP306
BP321
BP329
BP335
BP343
BP350

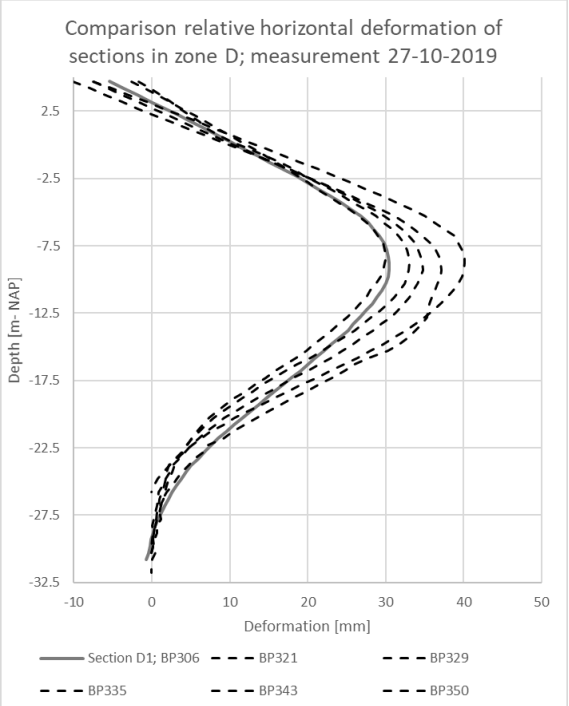
Comparison relative horizontal deformation of sections in zone D; measurement 27-10-2019
Depth [m- NAP]
2.5
-2.5
-7.5
-12.5
-17.5
-22.5
-27.5
-32.5
-10
0
10
20
30
40
50
Deformation [mm]
Section D1; BP306
BP321
BP329
BP335
BP343
BP350

B

Drawings of sections B4 and D1

Drawings of the cross section of section B4 (with a relieving platform) and section D1 (without a relieving platform are presented.

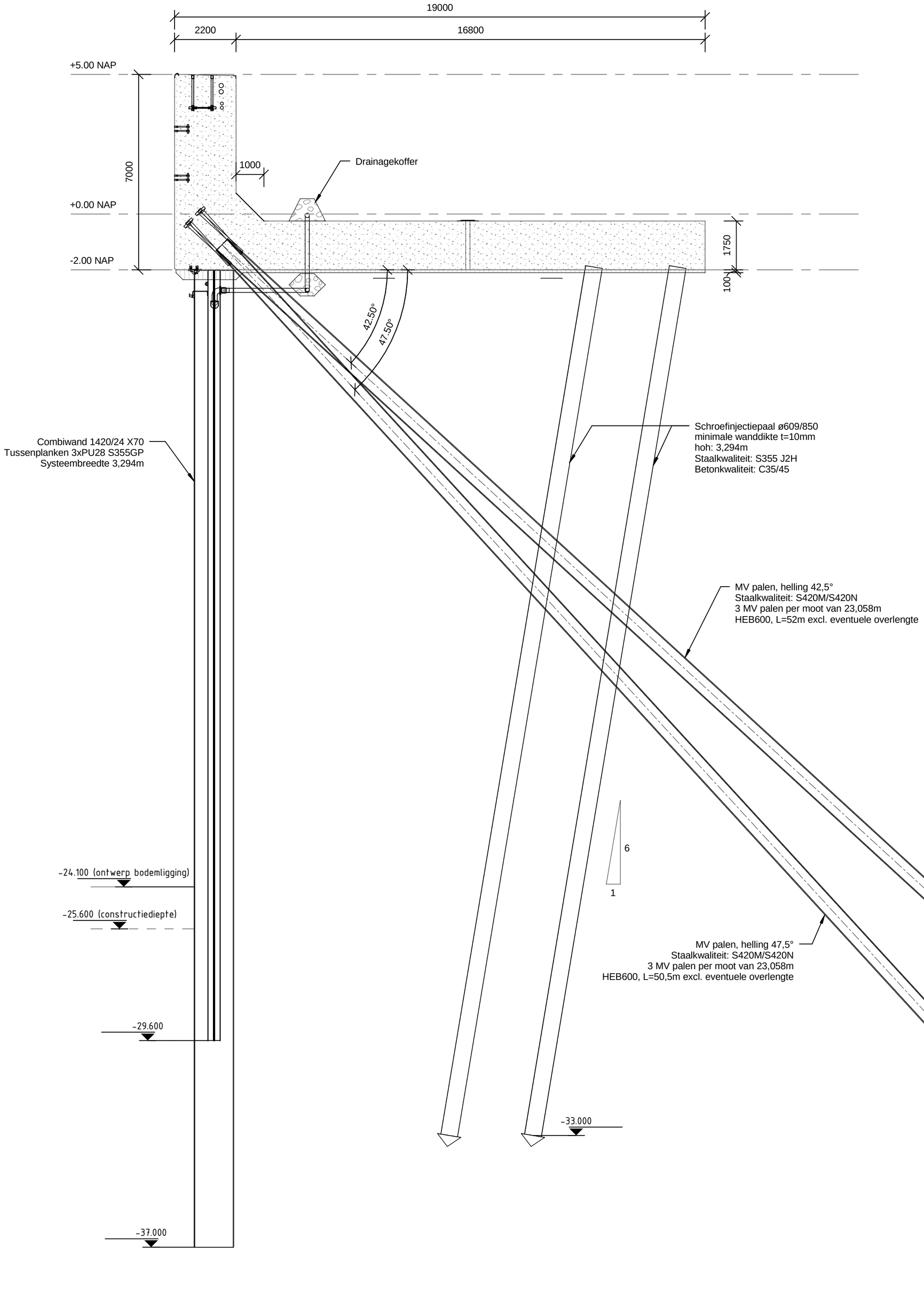
19000
2200
16800
+5.00 NAP
7000
1000
Drainagekoffer
+0.00 NAP
-2.00 NAP
1750
100
42.50°
47.50°
Combiwand 1420/24 X70
Tussenplanken 3xPU28 S355GP
Systeembreedte 3,294m
Schroefinjectiepaal ø609/850
minimale wanddikte t=10mm
hoh: 3,294m
Staalkwaliteit: S355 J2H
Betonkwaliteit: C35/45
MV palen, helling 42,5°
Staalkwaliteit: S420M/S420N
3 MV palen per moot van 23,058m
HEB600, L=52m excl. eventuele overlengte
6
1
MV palen, helling 47,5°
Staalkwaliteit: S420M/S420N
3 MV palen per moot van 23,058m
HEB600, L=50,5m excl. eventuele overlengte
-24.100 (ontwerp bodemligging)
-25.600 (constructiediepte)
-29.600
-33.000
-37.000

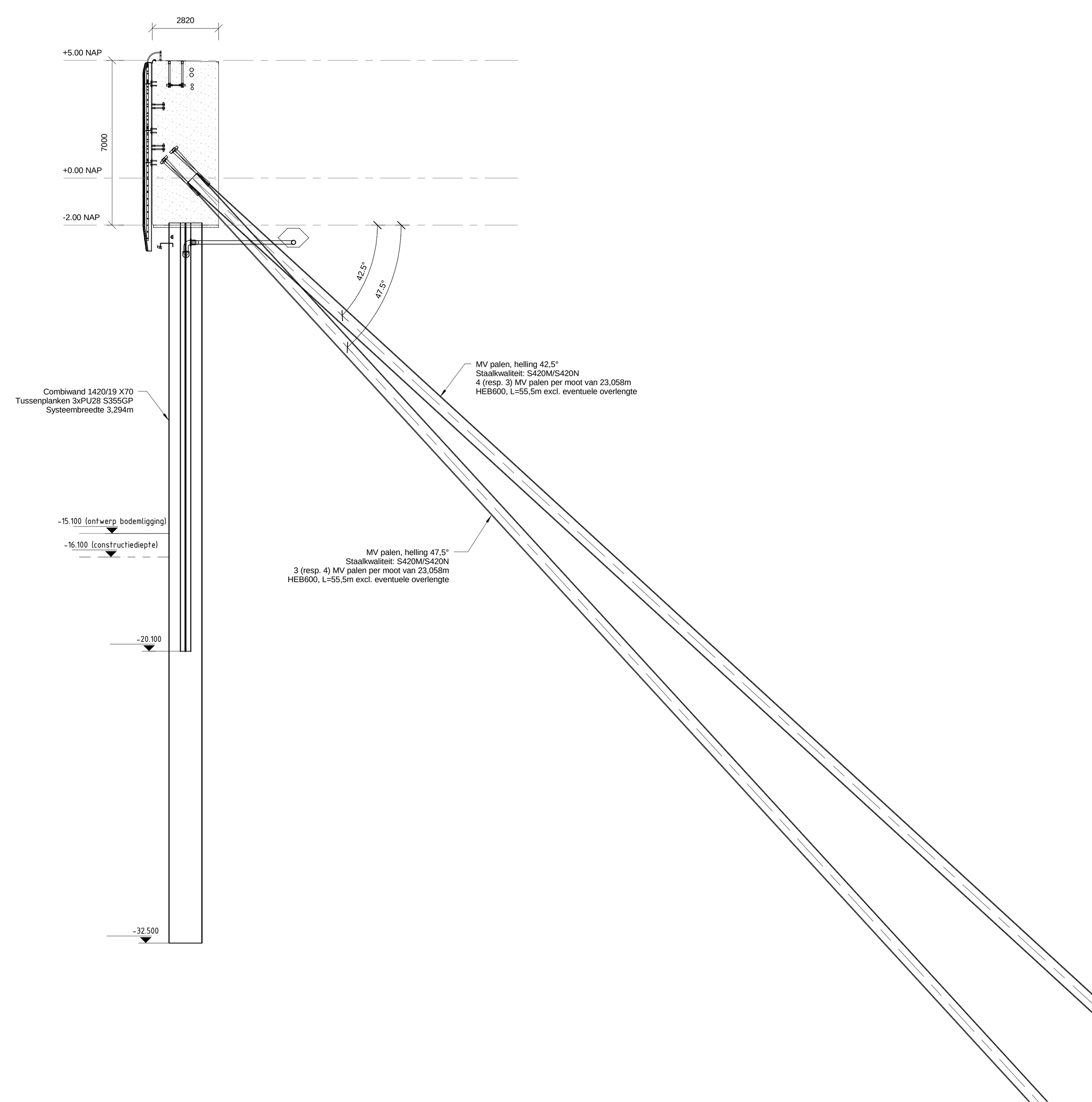
2820
+5.00 NAP
7000
+0.00 NAP
-2.00 NAP
42,5°
47,5°
MV palen, helling 42,5°
Staalkwaliteit: S420M/S420N
4 (resp. 3) MV palen per moot van 23,058m
HEB600, L=55,5m excl. eventuele overlengte
Combiwand 1420/19 X70
Tussenplanken 3xPU28 S355GP
Systeembreedte 3,294m
-15.100 (ontwerp bodemligging)
-16.100 (constructiediepte)
MV palen, helling 47,5°
Staalkwaliteit: S420M/S420N
3 (resp. 4) MV palen per moot van 23,058m
HEB600, L=55,5m excl. eventuele overlengte
-20.100
-32.500

C

Determining the soil parameters

C.1. Soil parameters from CPT correlations

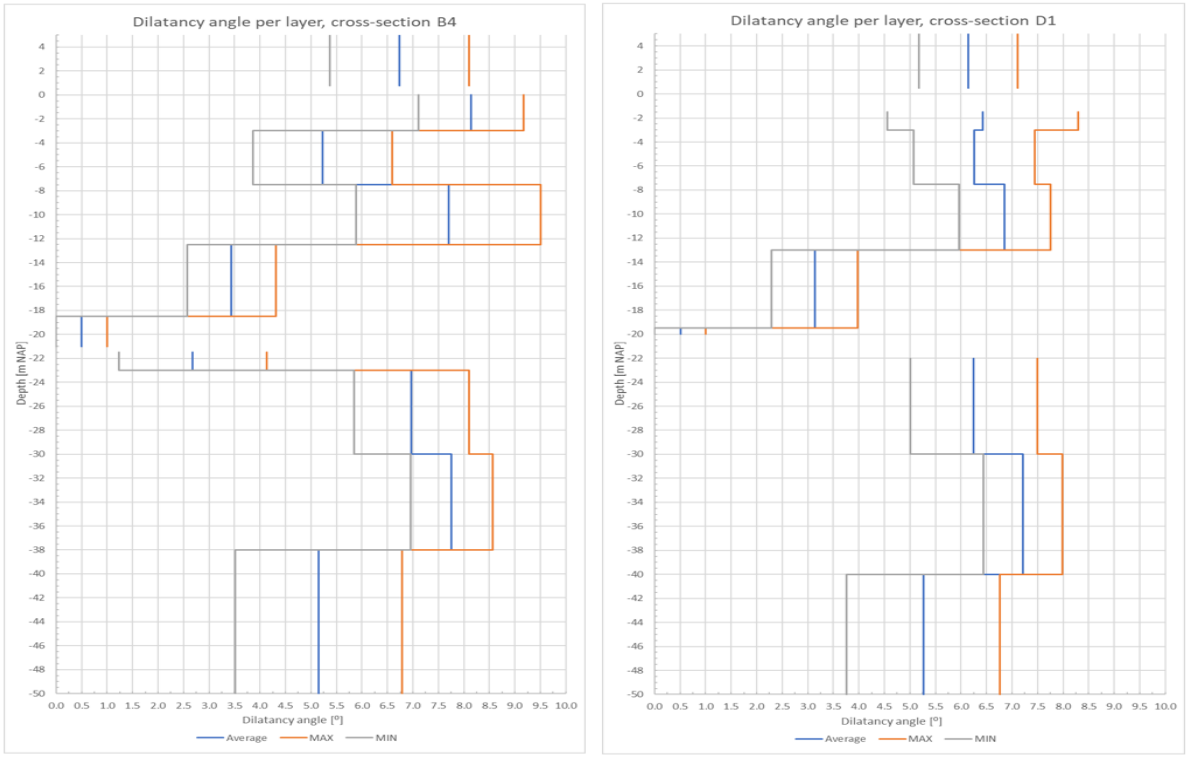

Figure C.1: Dilatancy angle vs. depth for both cross-sections

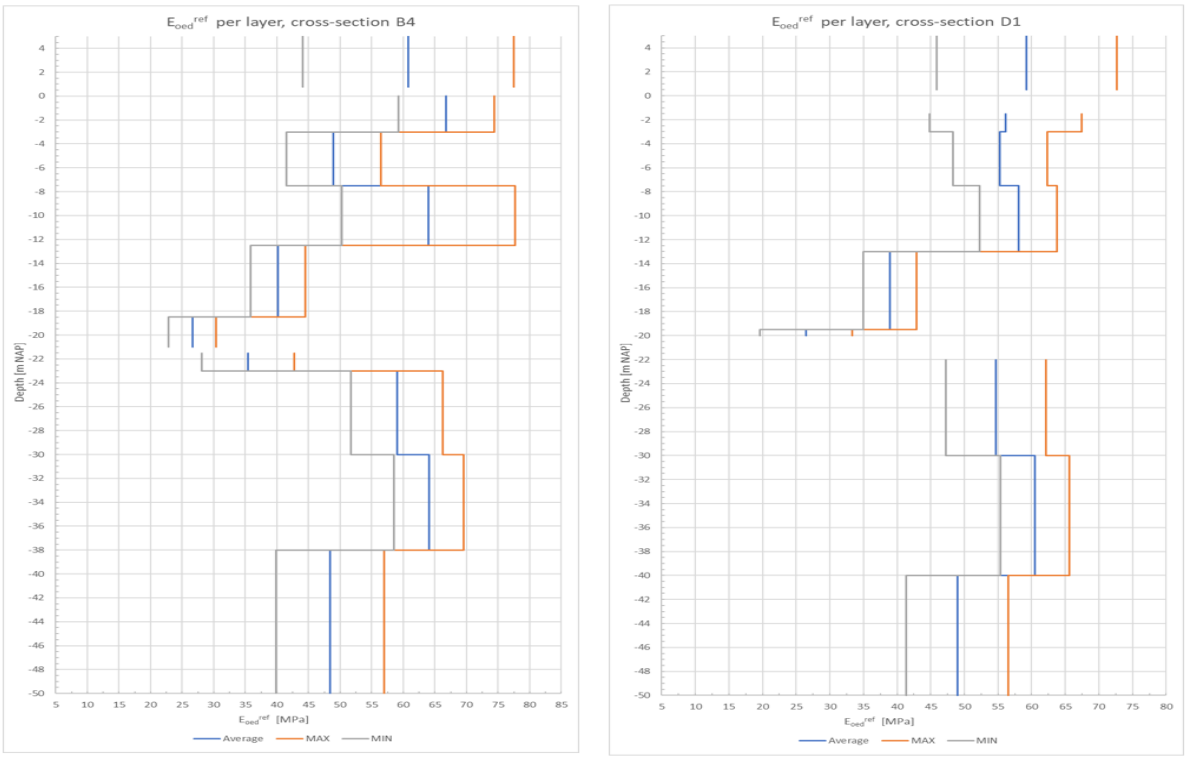

Figure C.2: E_{oed}^{ref} vs. depth for both cross-sections

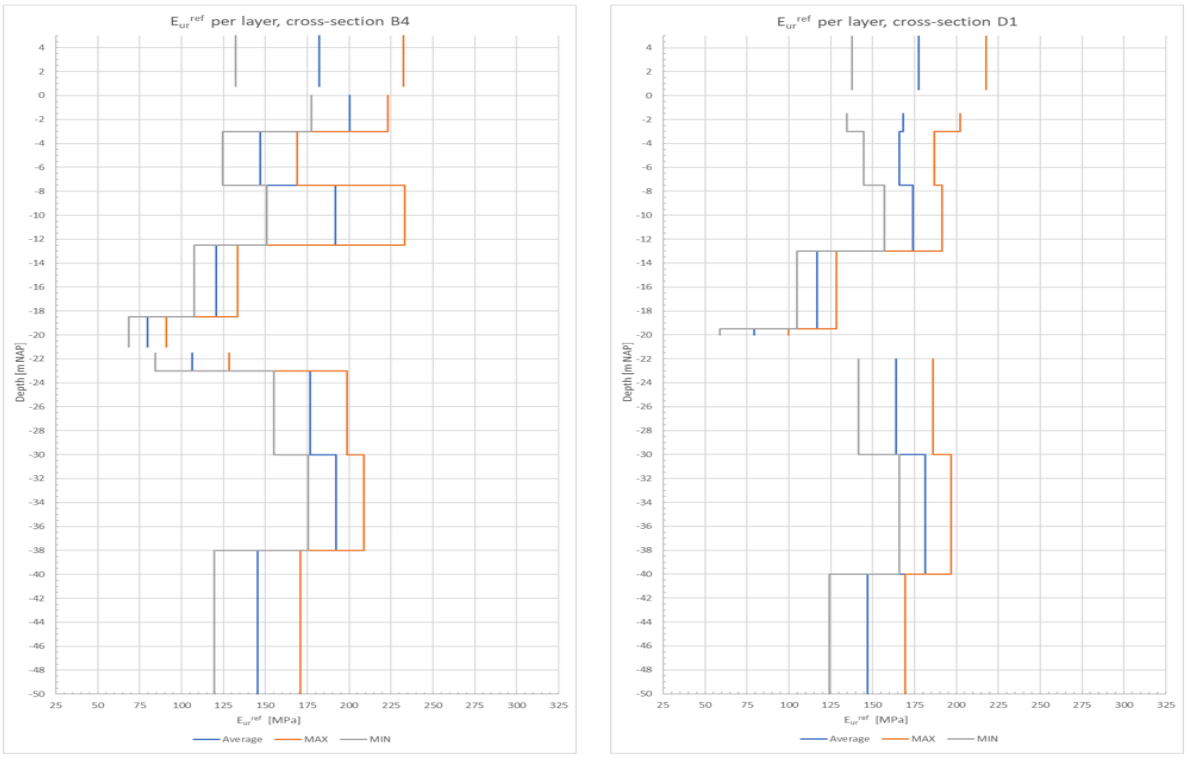

Figure C.3: E_{ur}^{ref} vs. depth for both cross-sections

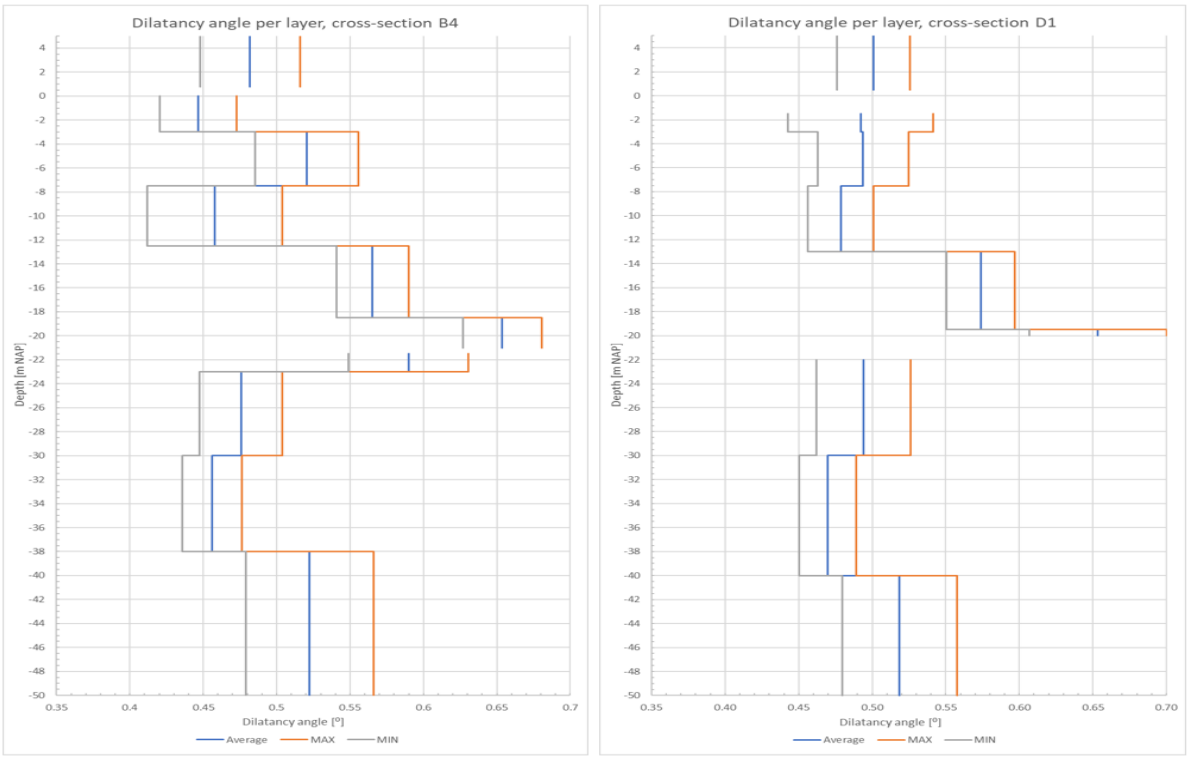

Figure C.4: m-parameter vs. depth for both cross-sections

C.2. Soil parameters based on triaxial test results

Triaxial test results of sand samples

Borehole	Sample	test	Depth	Type	soil type	$t_{\varepsilon1;2\%}$	$s'_{\varepsilon1;2\%}$	$t_{\varepsilon1;5\%}$	$s'_{\varepsilon5;2\%}$	$t_{\varepsilon1;peak}$	$s'_{\varepsilon1;peak}$	$\varepsilon_{1;50}$	E_{50}	σ'_3 start	σ'_3 failure	$\varepsilon_{1;peak}$	ρ_d	e_0	RD	E_{50}^{ref}	$\phi'_{2\%}$	$\phi'_{5\%}$	ϕ'_{peak}
			[m NAP]	[CD/CU]		[kPa]	[kPa]	[kPa]	[kPa]	[kPa]	[kPa]	[%]	[Mpa]	[kPa]	[kPa]	[%]	[ton/m3]	[-]	[%}	[Mpa]	[º]	[º]	[º]
Layer 1																							
B2_2	4	a	0.90	CD	sand	80	122	63	107	81	123	0.41	20	41	43	2.50	1.57	0.66	54	31	46.0	40.7	46.0
		b				164	247	190	273	192	274	0.84	23	82	83	4.30	1.54	0.69	47	25	47.0	49.7	49.8
		c				254	375	229	351	272	394	0.58	47	121	122	3.20	1.58	0.65	57	42	47.9	45.9	49.2
B2_2	5	b	0.40	CD	sand, low in clay	182	270	204	293	207	296	0.73	28	84	89	4.00	1.59	0.64	59	31	47.8	49.7	50.0
		c				233	357	242	366	252	376	0.38	49	124	124	3.60	1.61	0.61	63	44	45.9	46.5	47.4
Layer 3																							
B2_1	5	a	-0.20	CD	sand	81	128	86	136	87	136	0.48	18	47	49	4.20	1.53	0.70	45	26	43.8	44.3	44.8
		c				214	350	224	361	242	378	0.79	31	137	137	3.60	1.53	0.70	45	26	42.3	43.2	44.7
B2_3	7	a	-0.50	CD	sand	77	125	84	133	85	134	0.47	18	48	48	4.00	1.53	0.70	45	26	42.7	44.4	44.6
		b				171	265	154	248	177	271	0.43	40	94	94	3.00	1.57	0.66	54	42	45.2	43.1	45.9
		c				248	386	241	379	260	397	0.41	64	137	138	3.20	1.60	0.63	61	55	45.0	44.4	45.9
B3_2	10	a	-2.00	CD	sand	110	162	122	174	123	175	0.50	25	52	52	4.20	1.55	0.68	49	34	48.2	50.0	50.3
		b				232	333	237	339	246	347	0.42	58	101	101	3.40	1.56	0.67	52	58	49.6	50.0	50.7
		c				292	445	233	386	304	457	0.66	48	152	153	3.1	1.57	0.66	54	39	46.2	41.8	46.9
Layer 4																							
B2_1	12	a	-4.70	CD	sand low in silt	113	183	140	211	140	211	0.90	16	70	72	5.00	1.52	0.71	42	19	42.7	46.6	46.6
		b				274	416	233	375	288	430	0.95	56	142	142	3.20	1.58	0.65	57	47	46.3	43.2	47.3
		c				396	607	359	571	420	632	0.57	74	211	212	3.20	1.57	0.66	54	51	45.8	43.9	46.9
B2_2	16	a	-6.80	CD	sand	165	244	133	213	172	252	0.49	36	78	80	2.90	1.57	0.66	54	40	47.9	43.3	48.5
		b				325	479	245	400	339	493	0.54	63	154	154	3.00	1.53	0.70	45	51	48.1	42.6	48.9
		c				327	552	410	635	415	639	0.85	49	225	225	4.20	1.57	0.66	54	33	40.9	45.3	45.5
B2_5	17	a	-6.70	CD	sand	167	248	128	209	182	263	0.63	29	81	81	3.10	1.56	0.67	52	32	47.7	42.5	49.3
		b				328	492	354	518	359	522	0.48	75	163	164	4.10	1.57	0.66	54	59	47.1	48.5	48.8
		c				464	707	502	745	514	757	0.58	89	243	243	4.00	1.59	0.64	59	57	46.2	47.6	48.1
B3_1	10	1	-6.85	CD	fine sand	120	202	-	-	121	203	0.48	25	80	82	2.20	1.54	0.69	47	28	40.9		41.2
		2				315	476	-	-	344	504	0.78	44	159	160	3.70	1.67	0.56	76	35	46.7		48.4
B3_2	19	a	-7.31	CD	sand	191	277	167	253	196	282	0.58	34	85	86	2.80	1.60	0.63	61	36	48.9	46.4	49.4
		b				295	460	331	496	331	496	0.57	58	165	165	4.60	1.61	0.61	63	46	44.9	47.1	47.1
		c				445	690	479	724	486	731	0.61	80	242	245	3.90	1.61	0.61	63	51	45.2	46.7	46.9
Layer 5																							
B2_1	22	a	-10.90	CD	sand	226	328	234	338	242	346	0.47	52	102	104	3.60	1.61	0.61	63	52	48.9	49.3	50.0
		b				374	577	359	563	428	632	0.77	55	204	204	3.70	1.62	0.60	66	39	45.4	44.6	47.9
		c				556	857	420	721	581	881	0.57	101	301	301	2.90	1.60	0.63	61	58	45.5	40.1	46.4
B2_4	18	b	-10.10	CD	sand	210	391	310	491	327	508	1.32	25	181	182	7.10	1.53	0.70	45	18	36.5	44.0	45.0
		c				445	717	531	804	532	804	0.75	71	272	273	5.20	1.55	0.68	49	43	43.1	46.6	46.6
B3_1	11	1	-8.25	CD	fine sand	194	287	173	268	203	297	0.93	22	86	95	4.00	1.66	0.57	74	24	47.8	45.2	48.4
		2				341	511	-	-	343	514	0.71	48	170	170	3.30	1.61	0.61	63	37	47.0		47.2
B3_3	10	a	-8.10	CD	sand	202	308	217	322	218	324	0.40	54	105	105	4.00	1.62	0.60	66	53	46.3	47.6	47.7
		b				334	545	407	618	410	622	0.81	51	211	212	6.00	1.57	0.66	54	35	42.6	46.3	46.4
		c				611	925	657	971	665	981	0.51	129	315	316	4.00	1.60	0.63	61	73	46.5	47.9	48.0
Layer 6																							
B2_1	30	a	-18.20	CD	sand	163	258	181	276	188	283	0.82	23	95	95	3.80	1.56	0.67	52	23	44.1	46.0	46.8
		b				409	677	519	788	523	791	0.95	55	269	269	4.50	1.52	0.71	42	34	41.8	46.4	46.5
		c				789	1294	841	1346	889	1394	0.74	121	505	505	3.60	1.57	0.66	54	54	42.3	43.5	44.6
B2_2	34	a	-16.80	CD	sand low in clay	89	216	160	288	198	325	2.32	9	127	128	9.50	1.42	0.83	15	8	27.3	38.1	42.1
		b				139	386	272	521	367	623	2.89	13	252	256	9.60	1.42	0.83	15	8	23.7	35.3	40.6
		c				385	761	613	992	644	1024	1.54	42	378	380	6.80	1.52	0.71	42	22	34.2	42.9	43.8
B2_4	34	a	-17.80	CD	sand low in clay	165	298	149	281	167	299	0.31	54	132	132	2.50	1.50	0.73	37	47	38.0	36.0	38.2
		b				397	659	492	755	495	758	0.93	53	262	263	4.50	1.55	0.68	49	33	41.6	45.8	45.9
		c				524	916	681	1073	685	1078	0.96	71	392	392	5.80	1.61	0.61	63	36	39.2	44.3	44.4
B3_3	17	a	-16.53	CD	sand low in clay	147	296	196	346	251	402	1.31	19	150	150	12.0	1.38	0.88	4	16	33.3	38.8	43.6
		b				167	466	300	599	514	815	4.00	13	302	301	15.0	1.39	0.87	7	7	23.6	33.8	44.0
B3_3	37	a	-18.15	CD	sand	299	507	308	517	313	522	0.33	94	210	209	3.00	1.67	0.56	76	65	40.6	41.2	41.4
		b				739	1159	785	1206	797	1218	0.49	163	421	422	4.00	1.71	0.52	84	79	44.6	45.7	45.9
		c				862	1492	942	1573	943	1575	3.18	58	632	632	4.50	1.68	0.55	78	23	39.7	41.4	41.4
Layer 7																							
B2_2	40	a	-19.90	CD	sand with clay	129	266	179	316	205	342	1.35	15	138	137	11.80	1.4	0.87	24	13	32.6	38.7	41.5
		b				169	451	270	551	387	669	2.58	15	282	282	14.90	1.4	0.87	24	9	24.8	33.0	39.8
		c				214	634	369	790	538	959	2.94	18	421	421	12.90	1.4	0.86	26	9	22.2	31.4	38.4
B2_3	39	a	-20.15	CD	sand with clay	104	241	151	287	204	341	1.93	11	138	137	13.60	1.4	0.90	19	9	28.9	35.8	41.4
		b				137	416	232	510	331	712	3.58	11	281	382	17.60	1.4	0.87	24	6	21.6	30.4	31.1
		c				206	621	372	787	530	945	2.91	18	417	416	12.90	1.4	0.87	24	9	21.8	31.8	38.3
B2_4	40	a	-20.20	CD	sand with clay	115	257	156	298	176	319	1.08	16	142	142	9.70	1.4	0.91	16	14	29.8	35.5	37.8
		b				158	439	273	554	362	643	2.48	15	281	281	11.50	1.4	0.86	26	9	23.7	33.2	38.5
		c				122	546	218	641	503	927	6.19	8	424	424	24.20	1.3	0.98	3	4	14.5	22.3	37.0
B3_1	27	1	-20.55	CD	sand with clay	137	277	185	326	134	278	1.35	15	147	145	13.20	1.3	0.95	8	12	33.3	38.8	32.3
		2				139	401	253	520	205	484	2.66	13	291	280	14.10	1.4	0.91	16	8	22.9	32.8	28.1
		3				225	620	372	782	288	713	2.78	18	434	425	13.40	1.4	0.90	19	9	23.9	32.0	26.8
Layer 9																							
B2_2	46	a	-22.80	CD	sand	251	405	281	435	282	436	0.56	50	153	154	4.60	1.6	0.61	63	40	43.1	45.3	45.4
		b				424	737	502	816	503	817	0.68	74	313	313	5.70	1.6	0.59	70	42	39.5	42.8	42.8
		c				514	983	670	1139	671	1140	0.96	70	469	469	5.30	1.7	0.55	78	32	35.5	40.5	40.6
Layer 10																							
B2_1	41	a	-24.90	CD	sand	331	502	349	520	367	538	0.69	54	171	171	3.50	1.69	0.54	80	41	46.4	47.4	48.4
		b				545	885	589	930	607	948	0.54	112	341	341	3.70	1.71	0.52	84	61	42.7	44.2	44.8
		c				862	1372	861	1370	883	1393	0.29	310	509	510	2.90	1.73	0.50	88	137	43.8	43.8	44.3
B2_3	46	a	-23.70	CD	sand low in clay	293	457	323	487	327	490	0.67	49	163	163	4.00	1.57	0.66	54	38	45.0	46.8	47.0
		c				805	1287	800	1282	862	1343	0.64	135	481	482	3.40	1.62	0.60	66	61	43.6	43.4	44.9
B3_1	34	1	-24.00	CD	sand	185	345	209	368	209	368	0.51	41	159	160	4.9	1.4	0.86	10	32	36.5	38.9	38.8
		2				302	631	394	723	411	741	1.07	38	330	330	8.5	1.46	0.78	26	21	32.1	37.1	37.9
B3_1	40	1	-33.50	CD	sand	300	520	349	569	348	569	0.6	58	216	220	4.9	1.45	0.79	24	39	39.7	42.6	42.5
		2				578	1025	614	1047	630	1062	0.89	71	432	433	0.9	1.45	0.79	24	34	38.6	40.4	40.9
		3				559	1121	680	1244	683	1247	0.85	80	559	564	6.1	1.45	0.79	24	34	33.6	37.3	37.4

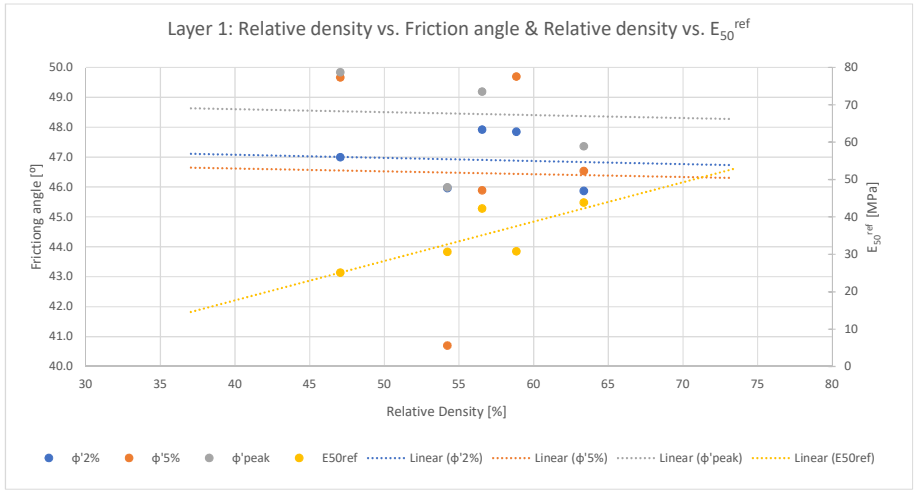
Layer 1: Relative density vs. Friction angle & Relative density vs. E50ref
Friction angle [°]
E50ref [MPa]
Relative Density [%]
ϕ'2%
ϕ'5%
ϕ'peak
E50ref
Linear (ϕ'2%)
Linear (ϕ'5%)
Linear (ϕ'peak)
Linear (E50ref)

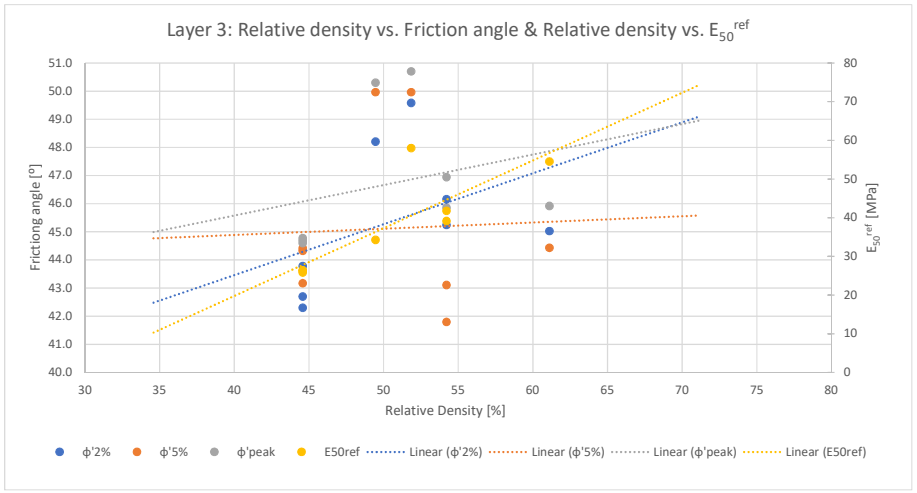
Layer 3: Relative density vs. Friction angle & Relative density vs. E50ref
Friction angle [°]
E50ref [MPa]
Relative Density [%]
ϕ'2%
ϕ'5%
ϕ'peak
E50ref
Linear (ϕ'2%)
Linear (ϕ'5%)
Linear (ϕ'peak)
Linear (E50ref)

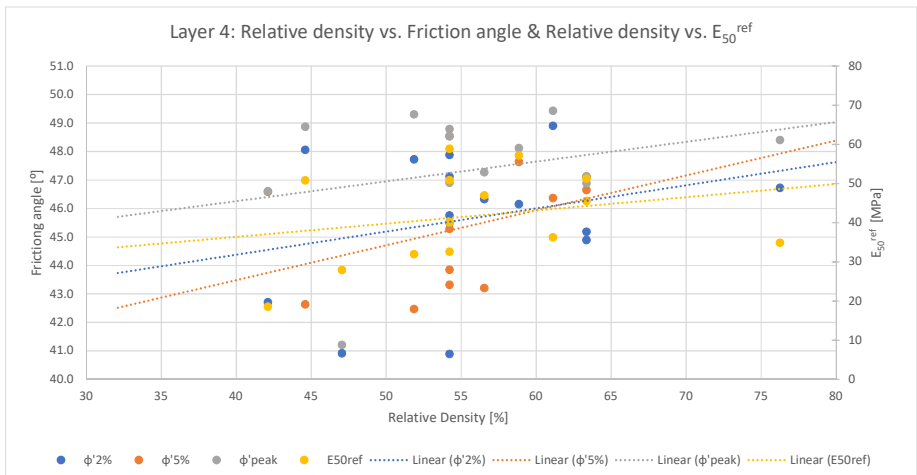
Layer 4: Relative density vs. Friction angle & Relative density vs. E50ref
Friction angle [°]
E50ref [MPa]
Relative Density [%]
ϕ'2%
ϕ'5%
ϕ'peak
E50ref
Linear (ϕ'2%)
Linear (ϕ'5%)
Linear (ϕ'peak)
Linear (E50ref)

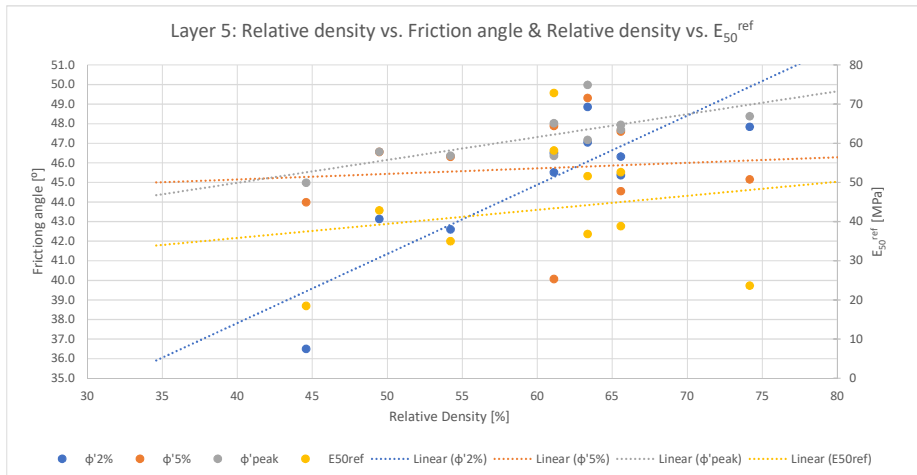
Layer 5: Relative density vs. Friction angle & Relative density vs. E50ref
Friction angle [°]
E50ref [MPa]
Relative Density [%]
ϕ'2%
ϕ'5%
ϕ'peak
E50ref
Linear (ϕ'2%)
Linear (ϕ'5%)
Linear (ϕ'peak)
Linear (E50ref)

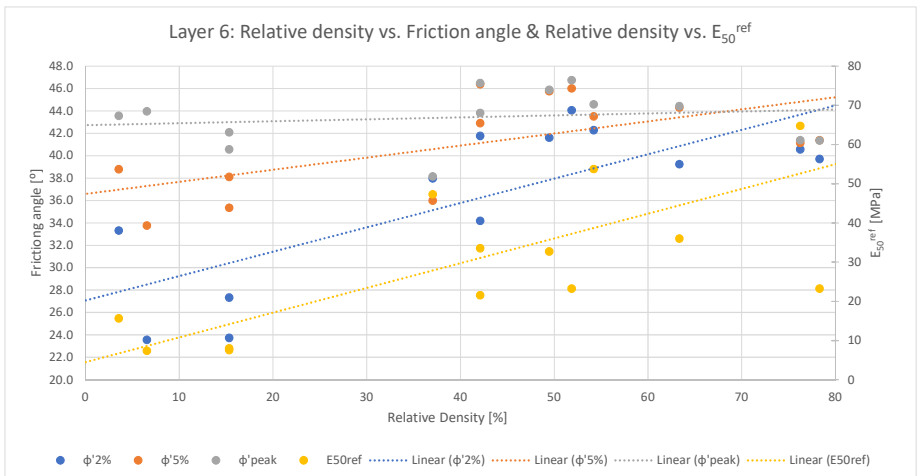
Layer 6: Relative density vs. Friction angle & Relative density vs. E50ref
Friction angle [°]
E50ref [MPa]
Relative Density [%]
ϕ'2%
ϕ'5%
ϕ'peak
E50ref
Linear (ϕ'2%)
Linear (ϕ'5%)
Linear (ϕ'peak)
Linear (E50ref)

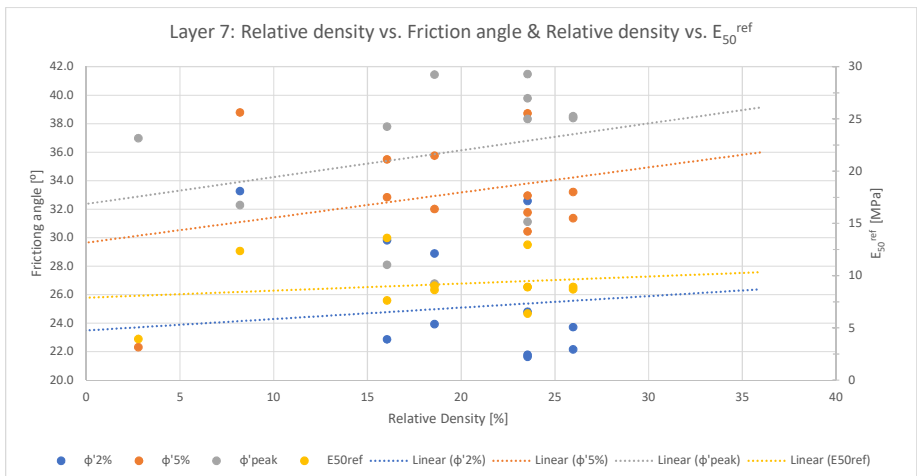
Layer 7: Relative density vs. Friction angle & Relative density vs. E50ref
Friction angle [°]
E50ref [MPa]
Relative Density [%]
ϕ'2%
ϕ'5%
ϕ'peak
E50ref
Linear (ϕ'2%)
Linear (ϕ'5%)
Linear (ϕ'peak)
Linear (E50ref)

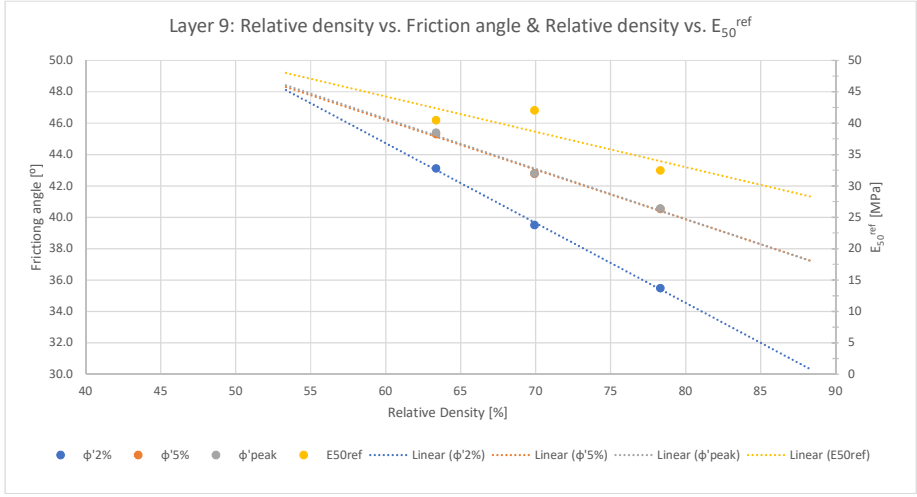
Layer 9: Relative density vs. Friction angle & Relative density vs. E50ref
Friction angle [°]
E50ref [MPa]
Relative Density [%]
ϕ'2%
ϕ'5%
ϕ'peak
E50ref
Linear (ϕ'2%)
Linear (ϕ'5%)
Linear (ϕ'peak)
Linear (E50ref)

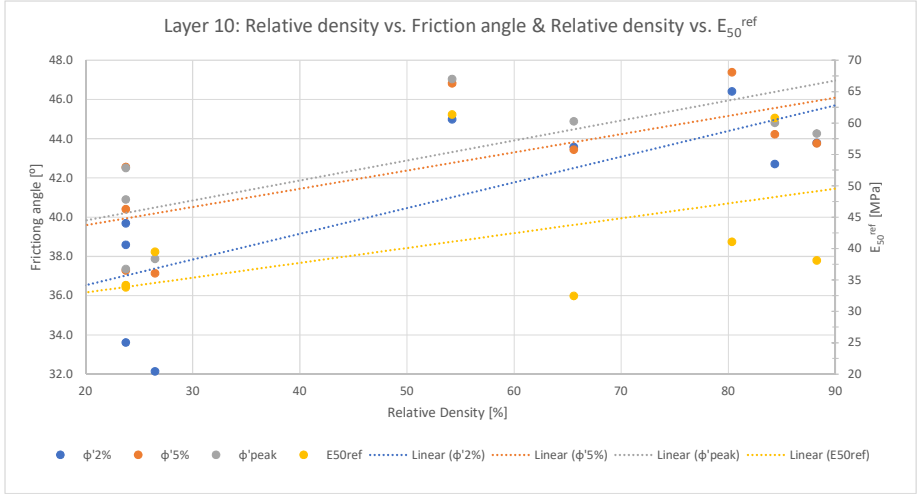
Layer 10: Relative density vs. Friction angle & Relative density vs. E50ref
Friction angle [°]
E50ref [MPa]
Relative Density [%]
ϕ'2%
ϕ'5%
ϕ'peak
E50ref
Linear (ϕ'2%)
Linear (ϕ'5%)
Linear (ϕ'peak)
Linear (E50ref)

Triaxial test results of clay samples																						
Borehole	Sample	test	Depth	Type	soil type	$t_{\varepsilon 1;2\%}$	$s'_{\varepsilon 1;2\%}$	$t_{\varepsilon 1;5\%}$	$s'_{\varepsilon 5;2\%}$	$t_{\varepsilon 1;peak}$	$s'_{\varepsilon 1;peak}$	$\varepsilon_{1;50}$	E_{50}	σ'_3 start	σ'_3 failure	$\varepsilon_{1;peak}$	ρ_d	e_0	E_{50}^{ref}	c'	$\phi'_{2\%}$	$\phi'_{5\%}$	ϕ'_{peak}
			[m NAP]	[CD/CU]		[kPa]	[kPa]	[kPa]	[kPa]	[kPa]	[kPa]	[%]	[Mpa]	[kPa]	[kPa]	[%]	[ton/m3]	[-]	[Mpa]	[kPa]	[º]	[º]	[º]
Layer 2																						
B2_1	5	b	-0.05	CU	clay	34	81	41	78	48	82	0.64	8	89	34	15.10	0.90	1.89	6	$c'_{2\%}$			
B2_4	5	a	0.5	CU	clay	22	40	27	40	26	39	0.82	3	45	13	8.60	0.86	2.02	5	6			
		b				32	63	39	64	41	67	0.52	8	80	26	7.90	1.06	1.45	7	$c'_{5\%}$	24.2	32.0	34.3
		c				39	98	46	87	48	80	0.55	9	121	33	8.80	0.84	2.10	5	8			
B2_5	7	a	0	CU	clay	19	43	30	50	38	58	1.78	2	44	21	10.70	0.93	1.80	3	c'_{peak}			
		b	0	CU		38	90	47	88	51	90	0.61	8	89	39	8.50	1.07	1.43	6	8			
		c	0	CU		51	115	63	112	64	112	0.63	10	134	48	6.90	1.06	1.45	5				
Layer 6																						
B2_5	23	a	-13.8	CU	sand with clay	55	101	62	93	57	97	0.33	17	116	40	3.50	1.18	1.20	11	$c'_{2\%}$			
		b				101	201	121	207	166	291	0.93	18	229	125	16.10	1.28	1.03	5	10			
		c				148	284	144	260	148	282	0.26	58	347	134	2.10	1.32	0.97	12	$c'_{5\%}$			
B2_5	28	a	-16.9	CU	sand with clay	69	126	83	131	89	152	0.41	22	131	62	11.40	1.32	0.97	12	14			
		b				110	200	116	201	138	234	0.37	37	260	96	10.60	1.36	0.91	10	c'_{peak}	33.6	36.2	37.0
		c				172	336	216	378	318	577	1.38	23	391	260	17.30	1.45	0.79	4	10.0			
B2_5	30	a	-17.9	CU	sand with clay	93	154	108	182	118	191	0.61	19	130	73	7.30	1.38	0.88	10				
		b				142	256	153	266	246	430	0.91	27	270	184	23.30	1.38	0.88	7				
		c				170	321	175	308	189	320	0.31	61	402	131	8.70	1.40	0.86	11				
Layer 8																						
B2_1	35	a	-20.9	CU	clay	111	235	145	279	168	314	1.07	16	151	146	11.00	1.61	0.61	7	$c'_{2\%}$			
		b				147	291	186	329	243	439	1.00	24	300	196	22.20	1.63	0.60	6	11			
		c				218	447	271	490	300	547	0.67	44	449	247	10.00	1.65	0.58	7	$c'_{5\%}$			
B2_2	43	a	-21.3	CU	clay, low in peat	78	137	92	154	93	153	0.60	15	104	60	4.60	1.04	1.50	10	11			
		c				108	317	143	313	156	314	0.94	17	317	158	10.70	1.35	0.93	4	c'_{peak}			
B2_3	44	b	-22.2	CU	clay, low in peat	136	304	155	283	156	280	0.56	28	309	124	5.30	1.13	1.30	6	6			
		c				133	439	171	397	183	367	0.82	22	465	184	8.80	1.04	1.50	3				
B2_4	44	a	-21.8	CU	clay	91	228	130	270	163	309	1.65	10	150	146	13.30	1.36	0.91	5		24.2	32.0	35.9
		b				131	299	161	297	165	297	0.66	25	302	131	6.80	1.46	0.78	6				
		c				170	385	187	348	188	342	0.41	45	448	154	6.50	1.41	0.84	7				
B2_5	39	a	-22.4	CU	clay	72	176	98	185	106	189	1.05	10	156	82	7.80	1.19	1.18	5				
		b				127	338	161	346	181	337	0.80	23	324	156	11.10	1.28	1.03	5				
		c				167	395	186	352	189	340	0.43	44	463	151	7.00	1.32	0.97	7				
B3_3	29	b	-21.69	CU	clay	112	335	142	290	148	275	0.58	25	249	127	15.10	1.30	1.00	7				
		c				135	461	156	388	172	305	0.80	21	372	134	15.10	1.28	1.03	4				

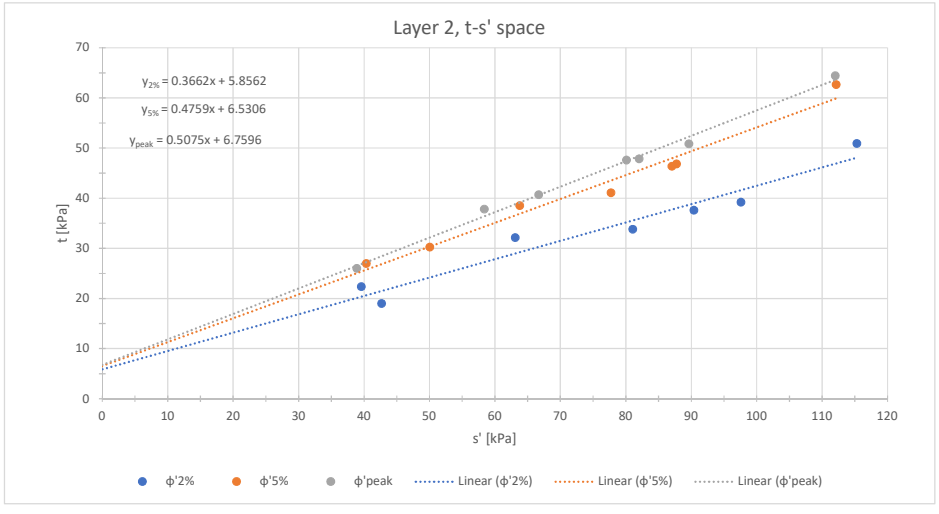

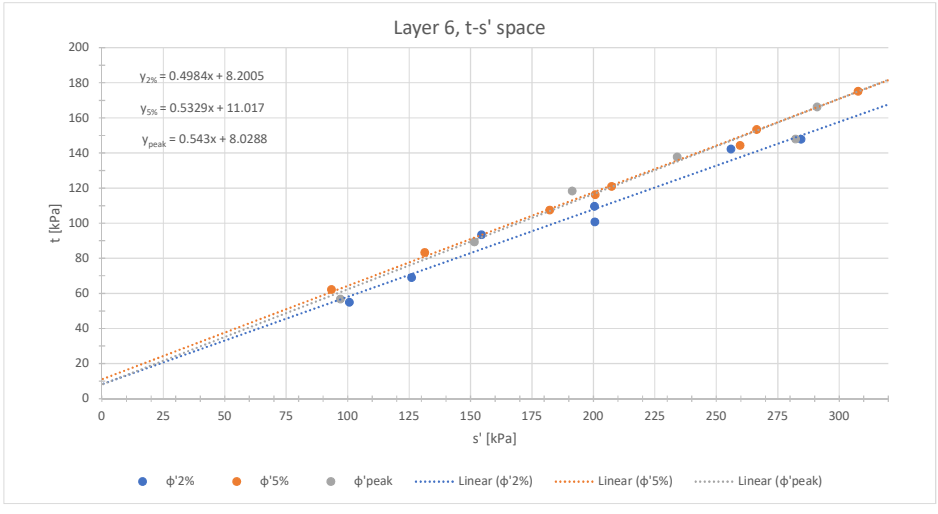

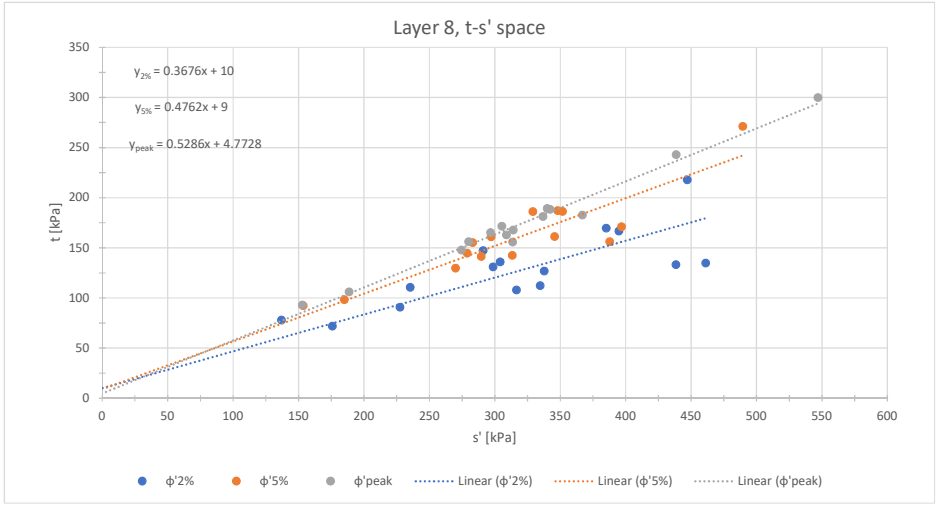

C.3. Overview soil parameters from CPT’s and Laboratory tests

All determined parameters based on CPT and triaxial results																												
layer number			1		2		3		4		5		6		7		8		9		10		11		12		Remark
Cross-section			B4	D1	B4	D1	B4	D1	B4	D1	B4	D1	B4	D1	B4	D1	B4	D1	B4	D1	B4	D1	B4	D1	B4	D1	
parameter	type of determination	Type of value																									
γ_{dry} [kN/m^3]	volumetric weigth laboratory test	Average	16.5		15.5		17.0		16.0		17.0		15.0		14.0		16.5		15.0		16.5		17.0		16.0		The volumetric weigth laboratory tests seem to give a good estimation of the volumetric weigth parameters. The volumetric weigth per layer is equal for both cross-sections
		Max	16.0		15.0		16.5		15.5		16.0		14.5		13.5		16.0		14.5		16.0		16.5		15.0		
		Min	17.0		16.0		17.5		16.5		17.5		15.5		14.5		17.0		15.5		17.0		17.5		16.5		
γ_{sat} [kN/m^3]	volumetric weigth laboratory test	Average	20.0		15.5		20.5		19.5		20.0		19.0		18.5		16.5		19.0		20.0		20.5		20.0		
		Max	19.5		15.0		20.0		19.0		19.5		18.5		18.0		16.0		18.5		19.5		20.0		19.0		
		Min	20.5		16.0		21.0		20.0		20.5		19.5		19.0		17.0		19.5		20.5		21.0		21.0		
ϕ_p' [°]	CPT correlation (Mayne and Kulhawy, 1990)	Average	42.0	41.0	-	-	43.0	41.0	40.0	41.0	43.0	42.0	38.0	37.0	33.5	33.5	-	-	36.5	-	42.0	41.0	43.0	42.0	40.0	40.0	Average peak friction angle based on triaxial test results are higher than CPT correlation for clean sand layers. This is due to 9/8 factor applied to triaxial test results. For layers with large amount of fines CPT correlation overestimates the friction angle, e.g. layers 6 and 7.
		Max	44.0	42.0	-	-	44.0	43.5	41.5	42.5	45.0	43.0	39.0	38.0	35.0	36.0	-	-	38.0	-	43.0	42.5	44.0	43.0	42.0	42.0	
		Min	40.0	40.0	-	-	42.0	48.5	38.0	39.5	41.0	41.0	37.0	36.0	32.0	31.0	-	-	34.0	-	41.0	39.5	42.0	41.0	48.0	38.0	
	Triaxial test (converted to plane strain conditions)	Average	48.0	48.0	32.0	32.0	49.0	48.0	47.5	48.0	49.0	48.5	36.0	36.0	34.0	34.0	32.0	32.0	40.0	-	45.0	44.5	46.0	45.5	44.0	43.5	
ψ [°]	CPT correlation (Brinkgreve et al, 2012)	Average	6.7	6.1	-	-	8.1	6.4	5.2	6.3	7.7	6.9	3.4	3.1	0.5	0.5	-	-	2.7	-	7.0	6.2	7.8	7.2	5.2	5.3	For layers with large amount of fines the dilatancy angle is set to zero. These are layers: 2, 7 and 8
		Max	8.1	7.1	-	-	9.2	8.3	6.6	7.4	9.5	7.8	4.3	4.0	1.0	1.0	-	-	4.1	-	8.1	7.5	8.6	8.0	6.8	6.8	
		Min	5.4	5.2	-	-	7.1	4.6	3.9	5.1	5.9	6.0	2.6	2.3	0.0	0.0	-	-	1.2	-	5.8	5.0	6.9	6.4	3.5	3.8	
c' [kPa]	Triaxial test	Average	-	-	8	8	-	-	-	-	-	-	-	-	-	-	10	10	-	-	-	-	-	-	-	-	Effective cohesion for sand layers is zero
E_{oed}^{ref} [MPa]	CPT correlation (Mayne and Kulhawy, 1990)	Average	60	60	-	-	70	55	50	55	65	60	40	40	30	25	-	-	35	-	60	55	65	60	50	50	The CPT correlation overestimates the stiffness slightly for clean sand layers. For layers with more fines the CPT correlation overstimates the stiffness by a lot. The stiffness parameters from Triaxial test results are governing. Therefore, the avarage stiffness of the CPT correlations is updated based on the avarage stiffness of the triaxial test results. The range of max and min stiffness values is preserved.
		Max	75	75	-	-	75	65	55	60	80	65	45	45	35	30	-	-	45	-	65	60	70	65	60	60	
		Min	45	45	-	-	65	45	45	50	50	55	35	35	25	20	-	-	25	-	55	45	60	55	40	40	
	Triaxial test	Average	50	45	3	3	70	60	45	45	50	45	30	30	8	8	3	3	30	-	45	45	50	50	40	40	
E_{50}^{ref} [Mpa]	CPT correlation (Mayne and Kulhawy, 1990)	Average	60	60	-	-	70	55	50	55	65	60	40	40	30	25	-	-	35	-	60	55	65	60	50	50	
		Max	75	75	-	-	75	65	55	60	80	65	45	45	35	30	-	-	45	-	65	60	70	65	60	60	
		Min	45	45	-	-	65	45	45	50	50	55	35	35	25	20	-	-	25	-	55	45	60	55	40	40	
	Triaxial test	Average	50	45	5	5	70	60	45	45	50	45	30	30	8	8	6	6	30	-	45	45	50	50	40	40	
E_{ur}^{ref} [Mpa]	CPT correlation (Mayne and Kulhawy, 1990)	Average	180	180	-	-	210	165	150	165	195	180	120	120	90	75	-	-	105	-	180	165	195	180	150	150	
		Max	225	225	-	-	225	195	165	180	240	195	135	135	105	90	-	-	135	-	195	180	210	195	180	180	
		Min	135	135	-	-	195	135	135	150	150	165	105	105	75	60	-	-	75	-	165	135	180	165	120	120	
	Triaxial test	Average	150	135	25	25	210	180	135	135	150	135	90	90	25	25	30	30	90		135	135	150	150	125	125	
m [-]	CPT correlation (Brinkgreve et al, 2012)	Average	0.48	0.50	-	-	0.45	0.49	0.52	0.49	0.46	0.48	0.57	0.57	0.65	0.65	-	-	0.59	-	0.48	0.49	0.46	0.47	0.52	0.52	The m-parameter is comparable for both cross-sections and, therefore, not regarded separately. The m-parameter is rounded to the nearst 0.05 value. For the clay layers m=1.0
		Max	0.52	0.53	-	-	0.47	0.54	0.56	0.52	0.50	0.50	0.59	0.60	0.68	0.70	-	-	0.63	-	0.50	0.53	0.48	0.49	0.57	0.56	
		Min	0.45	0.48	-	-	0.42	0.44	0.49	0.46	0.41	0.46	0.54	0.55	0.63	0.61	-	-	0.55	-	0.45	0.46	0.44	0.45	0.48	0.48	

D

3D model of MV-pile; force introduction

In Plaxis-3D a 3D-model is made of the HEB600 profile of the MV-piles. In this model several force configurations are applied to test whether the forces are evenly distributed over the profile at the cross section containing the FBG sensors. In Figure D.1 the 3D dimensional model of the HEB600 profile is visualised and the dimensions of the cross section are shown. The HEB600 profile is modelled as 3 rectangles attached to each other and the length of the HEB600 beam is 10 metres. At the origin the beam is fully fixated, at the other end the beam is free to deform and rotate. The forces are applied as line loads at the free end over a length of 700 millimetres, this mimics the force introduction by the anchor rods. The behaviour of the steel beam is modelled with the linear elastic model of which the properties are presented in table D.1.

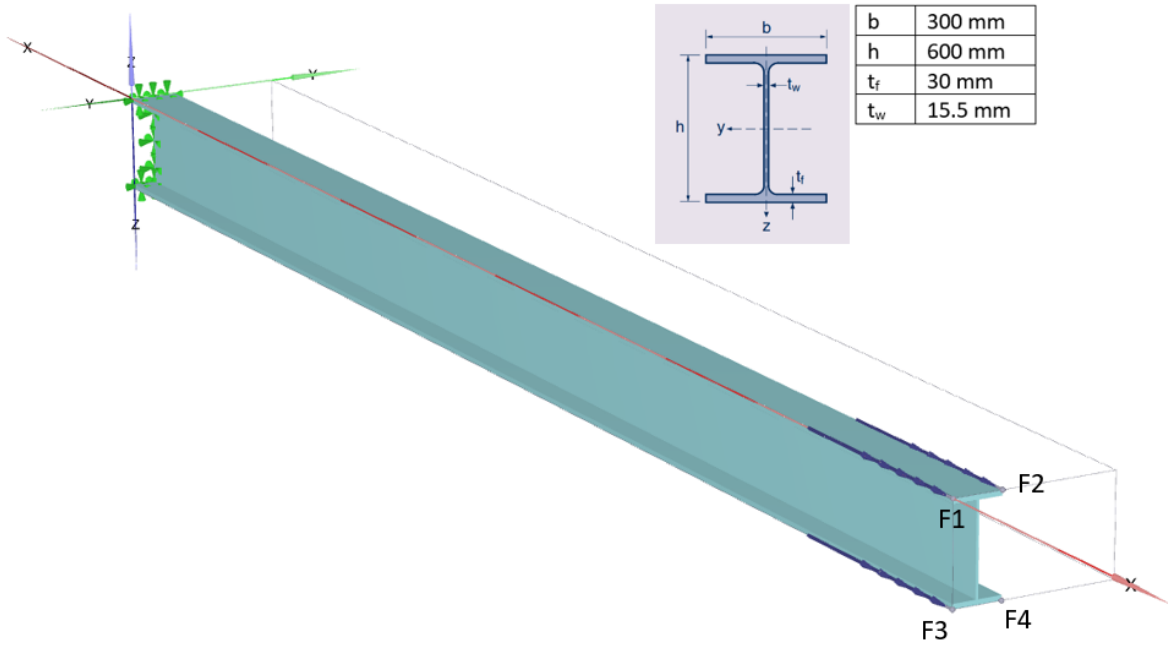

b	300 mm
h	600 mm
t_f	30 mm
t_w	15.5 mm

Figure D.1: Impression 3D-model HEB600 profile

Linear elastic model; steel			
Young's modulus	E	$210 * 10^6$	[kN/m^2]
Poisson's ratio	v	0.15	[-]
Shear modulus	G	$91.30 * 10^6$	[kN/m^2]
Oedometer stiffness	Eoed	$221.7 * 10^6$	[kN/m^2]

Table D.1: Input parameters linear elastic model steel

The 3D model is calculated with 3 different force configurations, which are presented in table D.2. The distribution of the normal strains (ϵ_{xx}) over the length of the beam are presented in Figures D.2 to D.4. Based on these calculations the forces are equally distributed over the height of the cross section at a distance of 1.2 à 1.3 metres.

Force configuration	F1	F2	F3	F4
	kN/m			
A; Axial force (symmetric)	1000	1000	1000	1000
B; Axial force + bending moment (symmetric)	750	750	1250	1250
C; Axial force + bending moment (non-symmetric)	2000	2000	0	0

Table D.2: Force configuration is the model

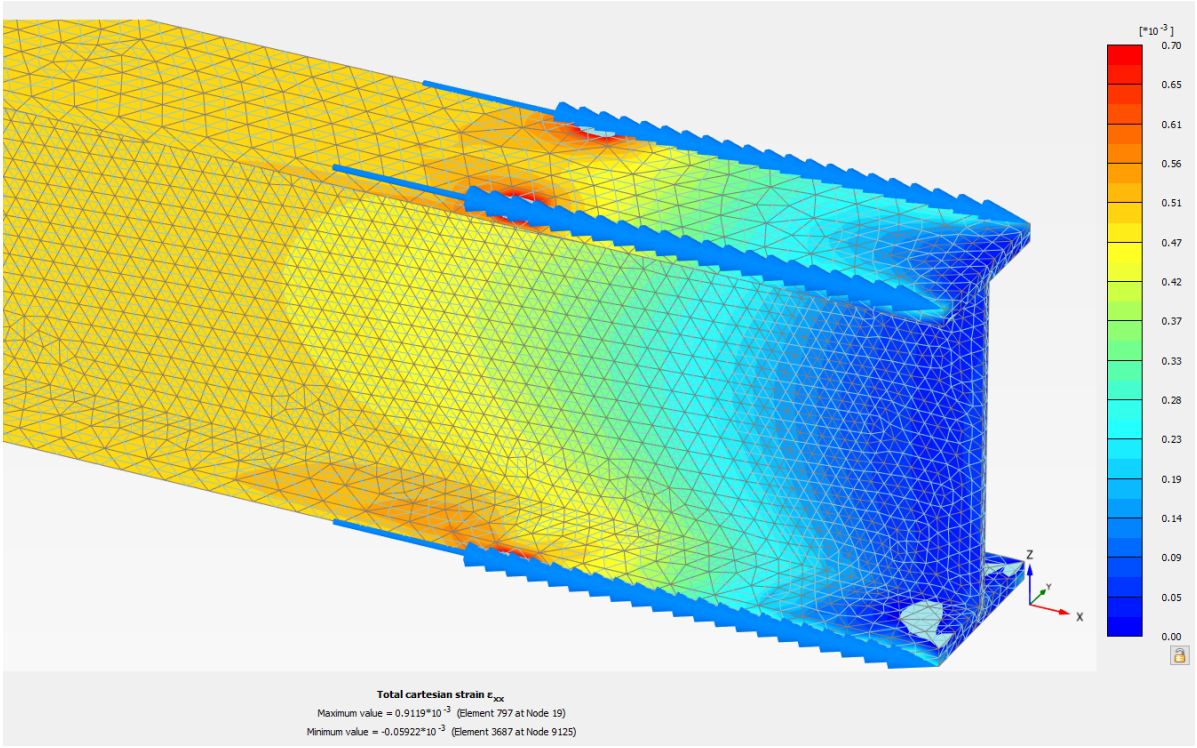

Figure D.2: Strains over the length of the HEB600 beam, force configuration A

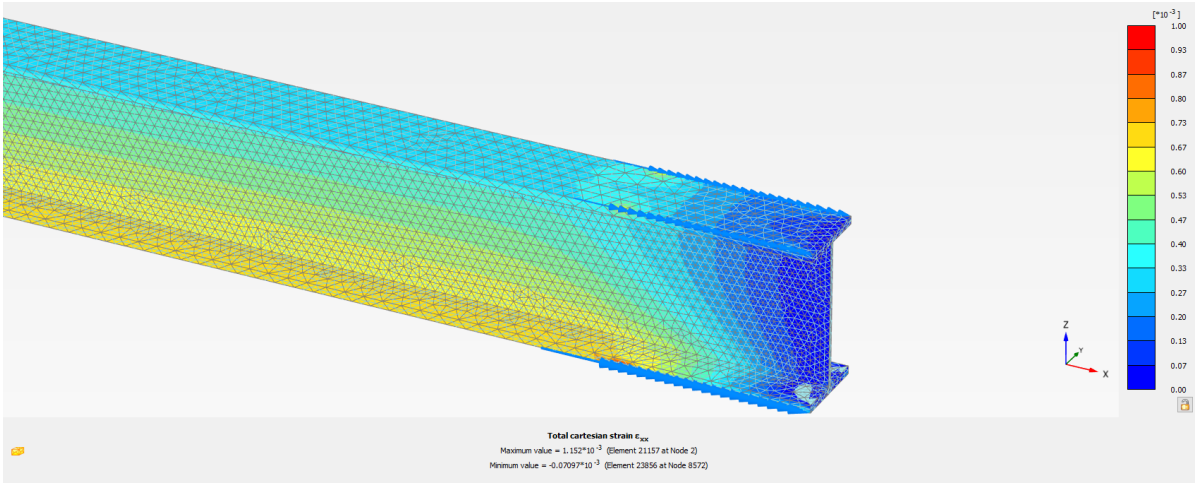

Figure D.3: Strains over the length of the HEB600 beam, force configuration B

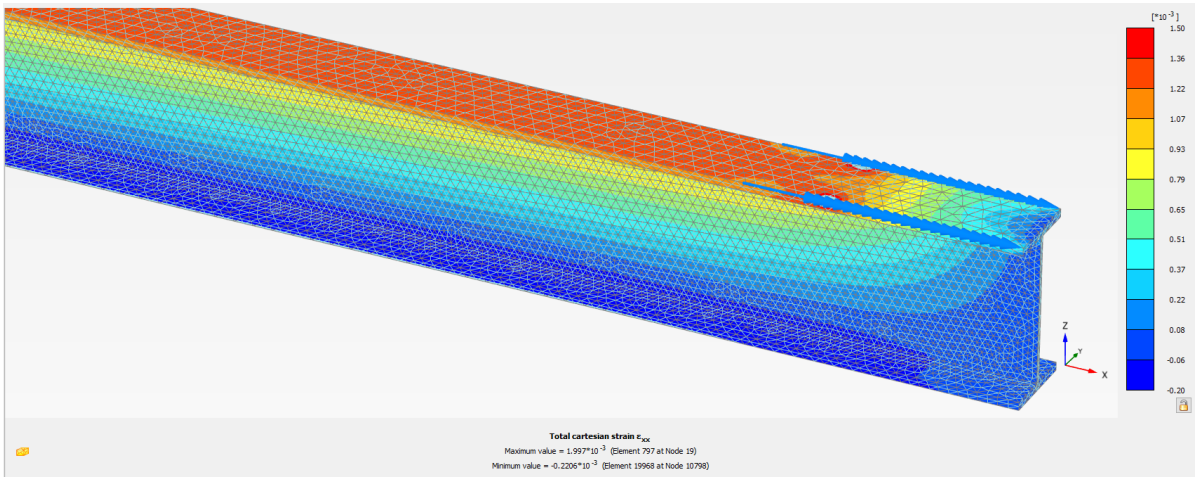

Figure D.4: Strains over the length of the HEB600 beam, force configuration C

E

Results laboratory test simulations

In this appendix the input and the results of the laboratory test simulations performed in the Plaxis SoilTest facility are presented.

E.1. Results laboratory tests section B4

The results of the laboratory tests of section B4 are presented. First the stress point on the active side is examined and then the stress point on the passive side. The base model parameters for layers 6 (active zone) and 10 (passive zone) are presented in Figure E.1.

Property	Value	Unit
Material set		
Identification	6	
Material model	Hardening soil	
Stiffness		
E_{50}^{ref}	30.00E3	kN/m²
E_{oed}^{ref}	30.00E3	kN/m²
E_{ur}^{ref}	90.00E3	kN/m²
power (m)	0.5500	
ν'_{ur}	0.2000	
K_0^{nc}	0.4500	
p_{ref}	100.0	kN/m²
Strength		
c'_{ref}	1.000	kN/m²
φ' (phi)	35.00	°
ψ (psi)	3.500	°
R_f	0.9000	
Tension cut-off	☑	
Tensile strength	0.000	kN/m²

Property	Value	Unit
Material set		
Identification	10	
Material model	Hardening soil	
Stiffness		
E_{50}^{ref}	45.00E3	kN/m²
E_{oed}^{ref}	45.00E3	kN/m²
E_{ur}^{ref}	135.0E3	kN/m²
power (m)	0.5000	
ν'_{ur}	0.2000	
K_0^{nc}	0.3500	
p_{ref}	100.0	kN/m²
Strength		
c'_{ref}	1.000	kN/m²
φ' (phi)	43.50	°
ψ (psi)	7.000	°
R_f	0.9000	
Tension cut-off	☑	
Tensile strength	0.000	kN/m²

Figure E.1: Base parameters layers 6 and 10 section B4

Stress point passive side
To simulate the increase of the major principle effective stress a compression triaxial test is performed. The input for the triaxial compression test is shown in Table E.1. The initial cell pressure is set equal to the minor principle stress that acts in the FE model.

Input	Test Final Construction phase	Test SLS phase
Type of test	Drained	
Direction	Compression	
Consolidation	Isotropic	
Initial cell pressure $\lvert\sigma'_{xx}\rvert$ [kPa]	68	75

Table E.1: Input triaxial compression tests

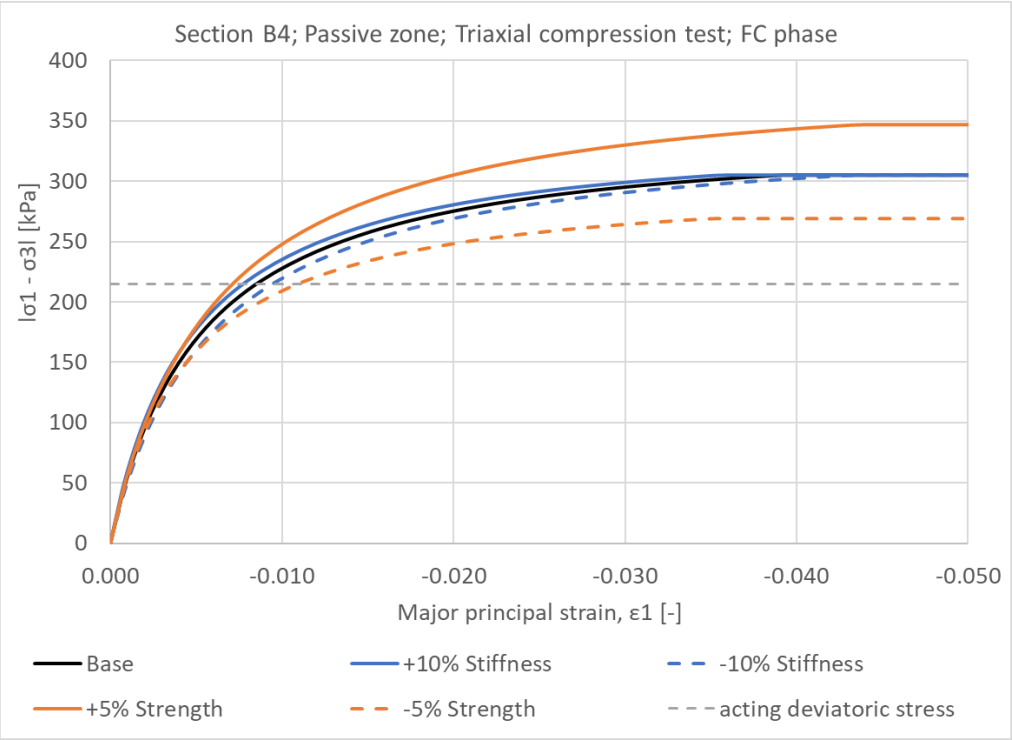

Figure E.2: Results triaxial compression tests section B4 for the passive zone during Final construction phase

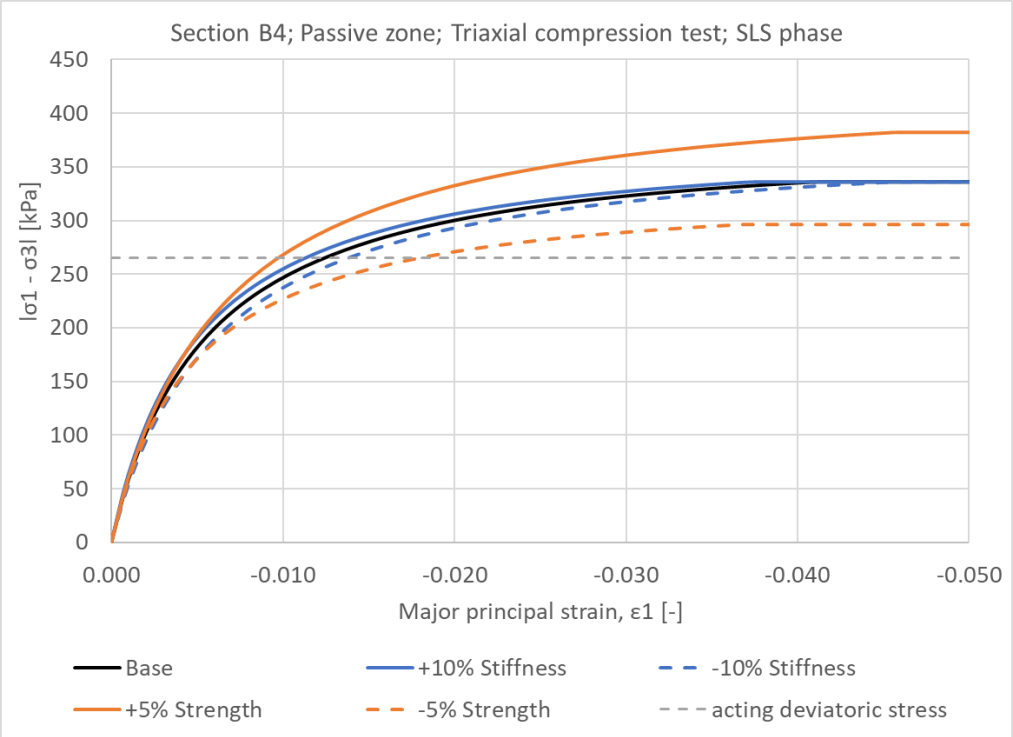

Figure E.3: Results triaxial compression tests section B4 for the passive zone during SLS phase

Stress point active side

To simulate the decrease of the minor principle effective stress a extension triaxial test is performed. The input for the triaxial extension test is shown in Table E.2. The initial cell pressure is set equal to the major principle stress that acts in the FE model.

Input	Test Final Construction phase	Test SLS phase
Type of test	Drained	
Direction	Extension	
Consolidation	Isotropic	
Initial cell pressure $\lvert\sigma'_{xx}\rvert$ [kPa]	80	70

Table E.2: Input triaxial extension tests

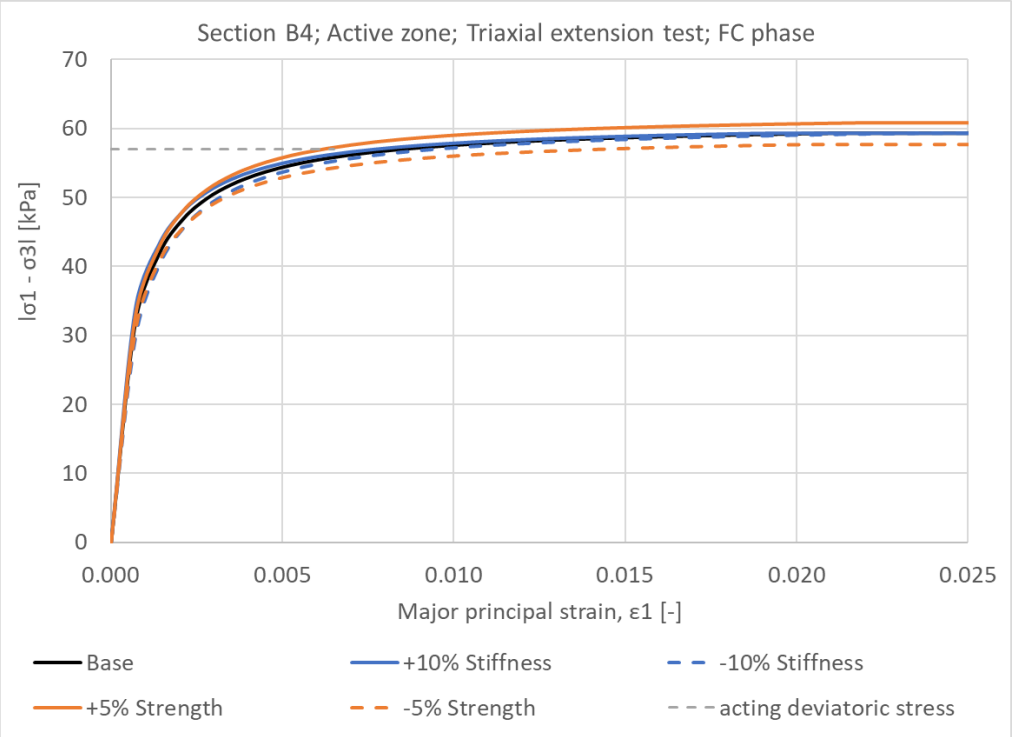

Figure E.4: Results triaxial extension tests section B4 for the active zone during Final construction phase

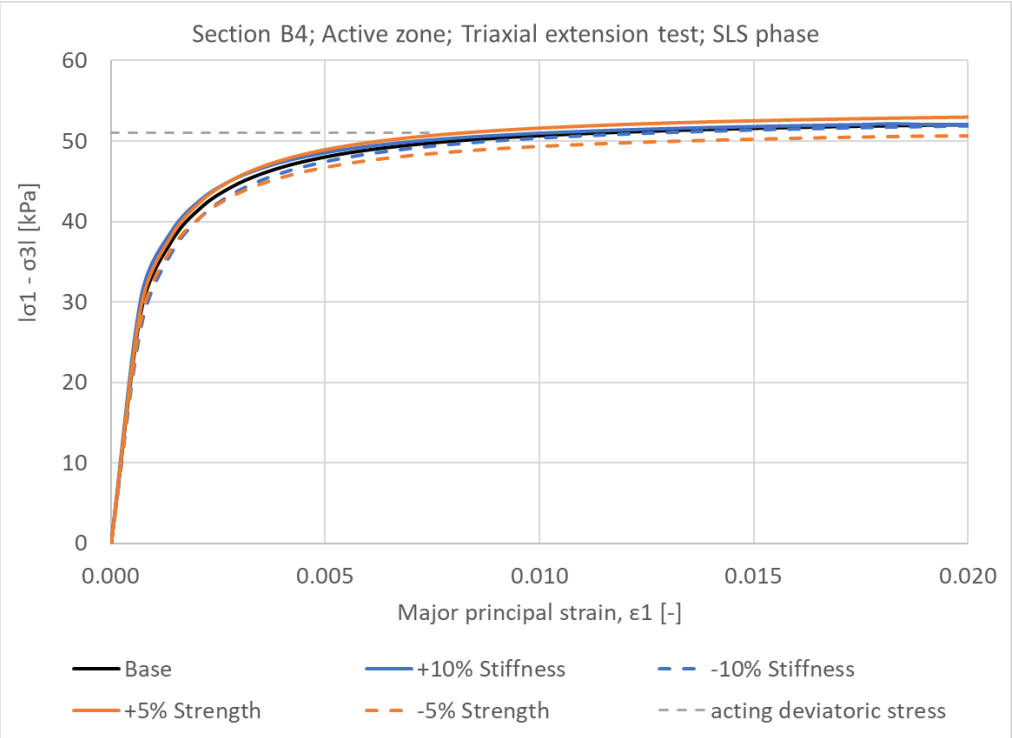

Figure E.5: Results triaxial extension tests section B4 for the active zone during SLS phase

E.2. Results laboratory tests section D1

The results of the laboratory tests of section D1 are presented. First the stress point on the active side is examined and then the stress point on the passive side. The base model parameters for layers 5 (active zone) and 6 (passive zone) are presented in Figure E.6.

Property	Value	Unit
Material set		
Identification	5	
Material model	Hardening soil	
Stiffness		
E_{50}^{ref}	45.00E3	kN/m²
E_{oed}^{ref}	45.00E3	kN/m²
E_{ur}^{ref}	135.0E3	kN/m²
power (m)	0.5000	
ν'_{ur}	0.2000	
K_0^{nc}	0.3500	
p_{ref}	100.0	kN/m²
Strength		
c'_{ref}	1.000	kN/m²
φ' (phi)	47.50	°
ψ (psi)	7.000	°
R_f	0.9000	
Tension cut-off	☑	
Tensile strength	0.000	kN/m²

Property	Value	Unit
Material set		
Identification	6	
Material model	Hardening soil	
Stiffness		
E_{50}^{ref}	30.00E3	kN/m²
E_{oed}^{ref}	30.00E3	kN/m²
E_{ur}^{ref}	90.00E3	kN/m²
power (m)	0.5500	
ν'_{ur}	0.2000	
K_0^{nc}	0.4323	
p_{ref}	100.0	kN/m²
Strength		
c'_{ref}	1.000	kN/m²
φ' (phi)	35.00	°
ψ (psi)	3.500	°
R_f	0.9000	
Tension cut-off	☑	
Tensile strength	0.000	kN/m²

Figure E.6: Base parameters layers 5 and 6 section D1

Stress point passive side

To simulate the increase of the major principle effective stress a compression triaxial test is performed. The input for the triaxial compression test is shown in Table E.3. The initial cell pressure is set equal to the minor principle stress that acts in the FE model.

Input	Test Final Construction phase	Test SLS phase
Type of test	Drained	
Direction	Compression	
Consolidation	Isotropic	
Initial cell pressure $\lvert\sigma'_{xx}\rvert$ [kPa]	34	24

Table E.3: Input triaxial compression tests

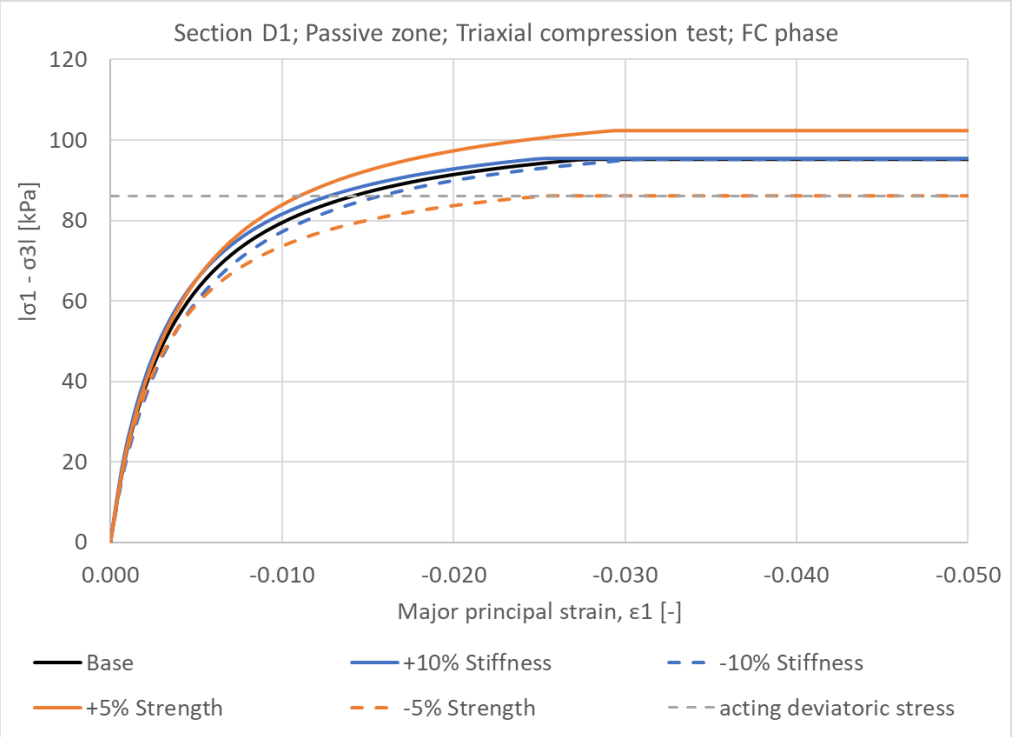

Figure E.7: Results triaxial compression tests section D1 for the passive zone during Final construction phase

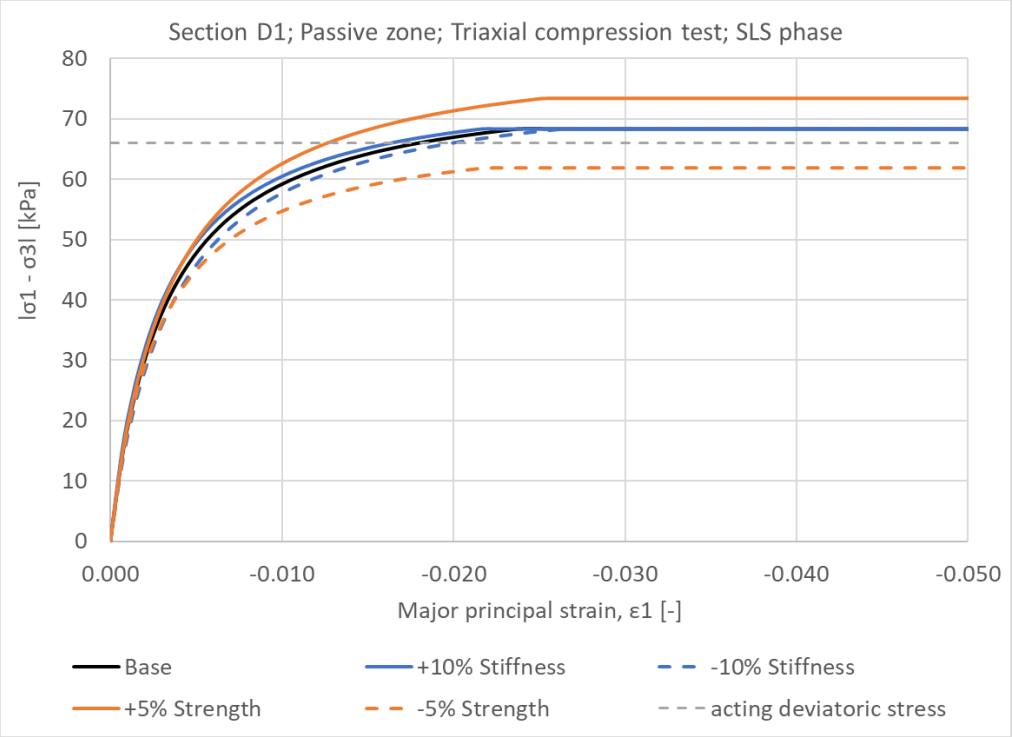

Figure E.8: Results triaxial compression tests section D1 for the passive zone during SLS phase

Stress point active side

To simulate the decrease of the minor principle effective stress a extension triaxial test is performed. The input for the triaxial extension test is shown in Table E.4. The initial cell pressure is set equal to the major principle stress that acts in the FE model.

Input	Test Final Construction phase	Test SLS phase
Type of test	Drained	
Direction	Extension	
Consolidation	Isotropic	
Initial cell pressure $\lvert\sigma'_{xx}\rvert$ [kPa]	125	122

Table E.4: Input triaxial extension tests

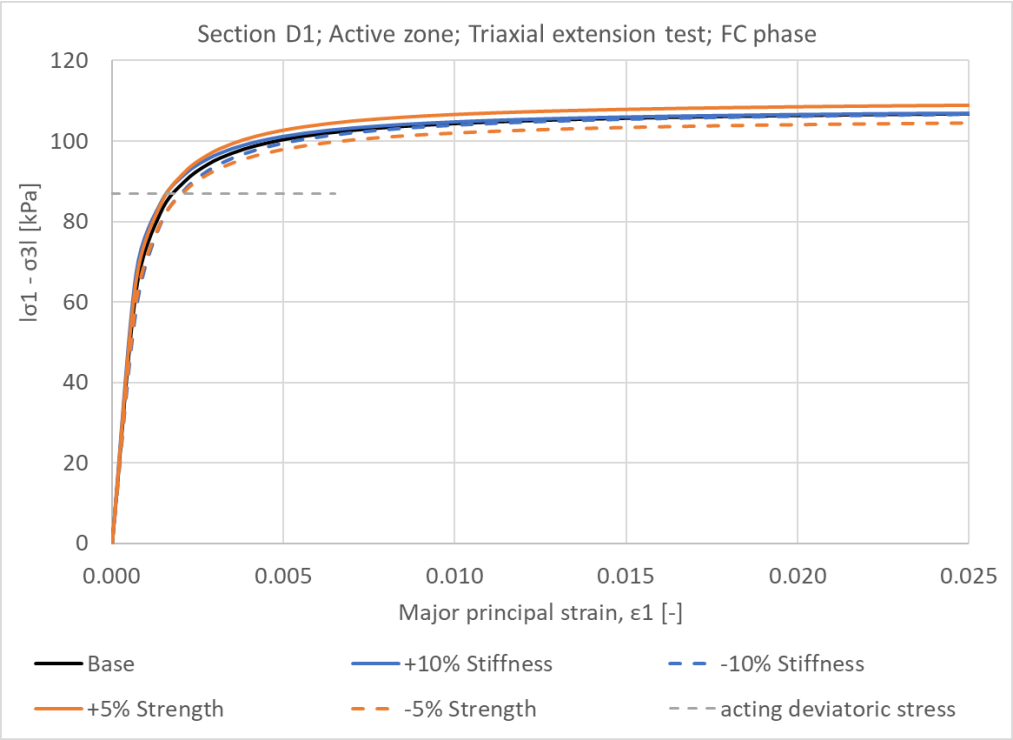

Figure E.9: Results triaxial extension tests section D1 for the active zone during Final construction phase

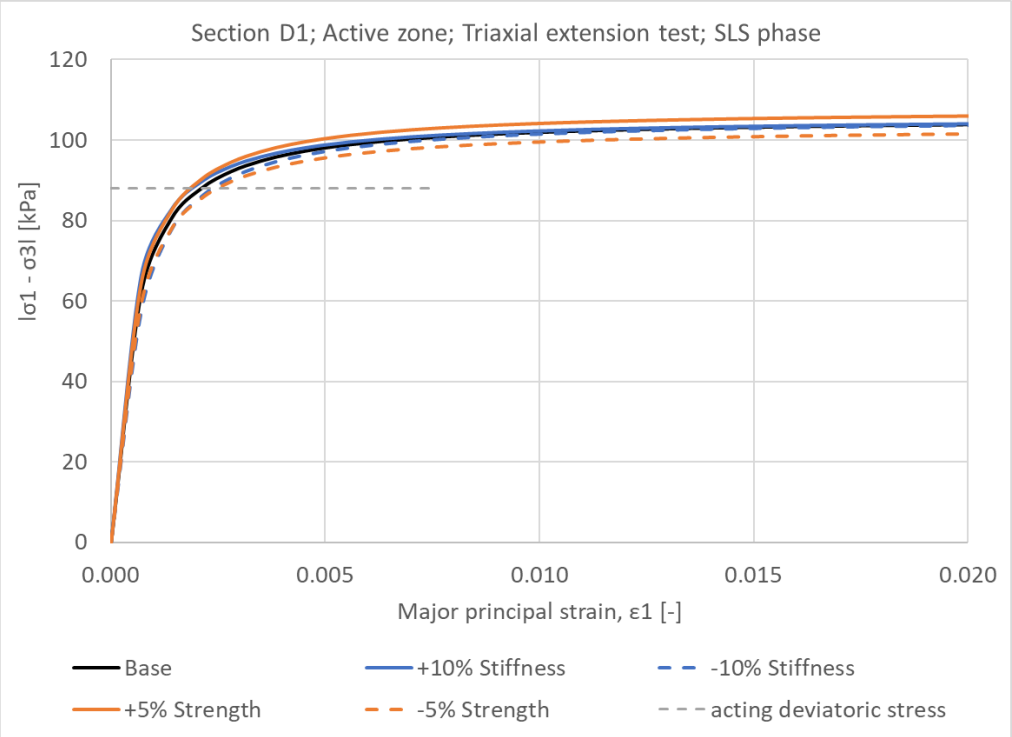

Figure E.10: Results triaxial extension tests section D1 for the active zone during SLS phase

F

Representative Cone Penetration Tests

In this appendix 4 CPT’s are presented which are representative for the soil conditions at the project location.

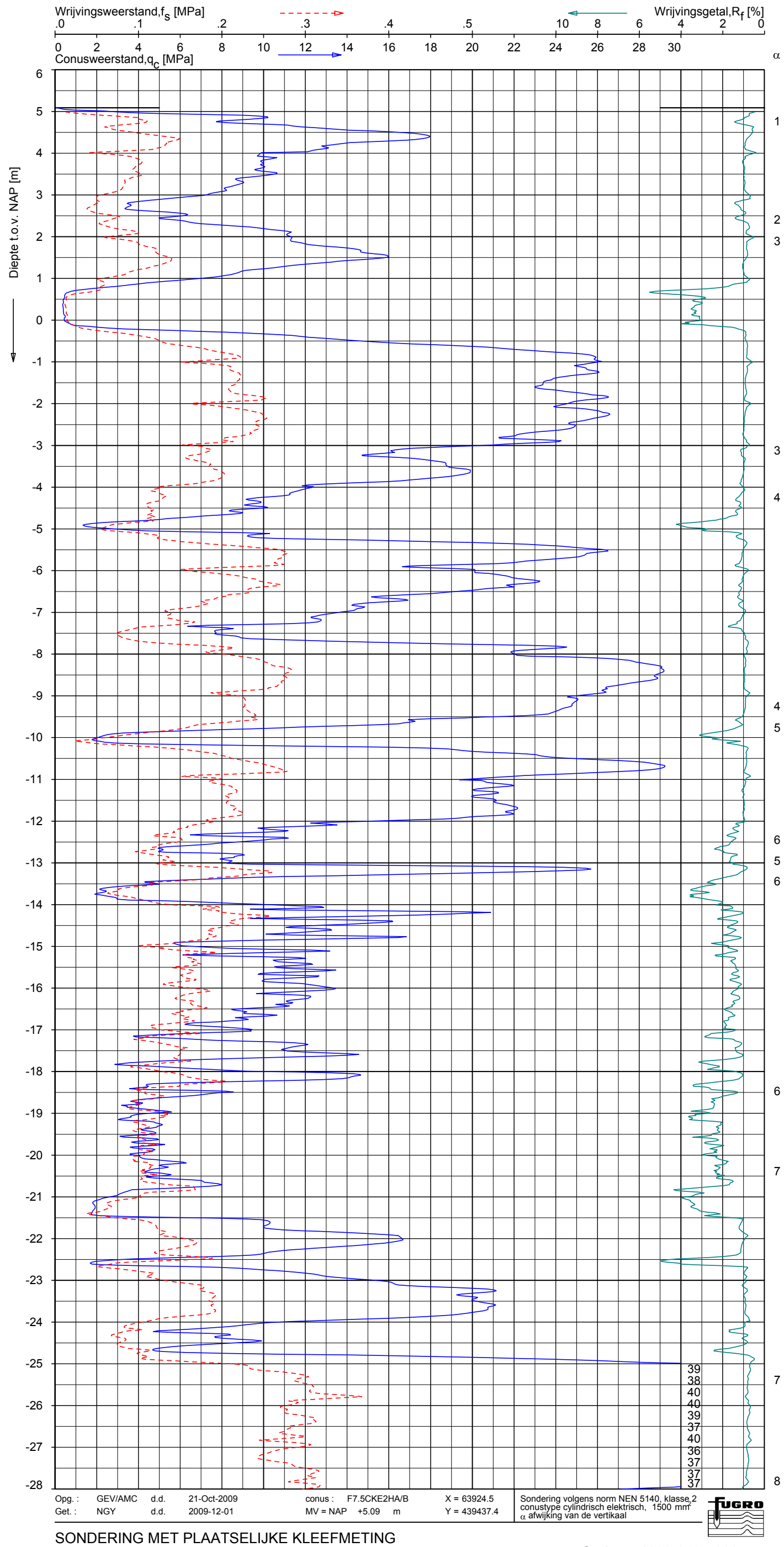

CPT data classificatie - indicatief

Classificatie gebaseerd op genormaliseerde conusweerstand en wrijvingsgetal. (Robertson 1990, NL corr.)
Geldig onder grondwaterpeil.

- (7) ZAND tot ZAND, grindig
- (7) ZAND tot ZAND, grindig
- (7) ZAND tot ZAND, grindig
- (6) ZAND, zwak siltig tot siltig
- (6) ZAND, zwak siltig tot siltig
- (6) ZAND, zwak siltig tot siltig
- (3) KLEI, zwak siltig tot siltig
- (6) ZAND, zwak siltig tot siltig
- (7) ZAND tot ZAND, grindig
- (6) ZAND, zwak siltig tot siltig
- (6) ZAND, zwak siltig tot siltig
- (6) ZAND, zwak siltig tot siltig
- (4) KLEI, siltig / LEEM
- (6) ZAND, zwak siltig tot siltig
- (6) ZAND, zwak siltig tot siltig
- (4) KLEI, siltig / LEEM
- (6) ZAND, zwak siltig tot siltig
- (6) ZAND, zwak siltig tot siltig
- (6) ZAND, zwak siltig tot siltig
- (4) KLEI, siltig / LEEM
- (4) KLEI, siltig / LEEM
- (4) KLEI, siltig / LEEM
- (4) KLEI, siltig / LEEM
- (3) KLEI, zwak siltig tot siltig
- (6) ZAND, zwak siltig tot siltig
- (6) ZAND, zwak siltig tot siltig
- (6) ZAND, zwak siltig tot siltig

Opg. : GEV/AMC d.d. 21-Oct-2009
Get. : NGY d.d. 2009-12-01

conus : F7.5CKE2HA/B X = 63924.5
MV = NAP +5.09 m Y = 439437.4

Sondering volgens norm NEN 5140, klasse 2
conustype cylindrisch elektrisch, 1500 mm²
α afwijking van de vertikaal

SONDERING MET PLAATSELIJKE KLEEFMETING

GRONDONDERZOEK VAN UDEN STEVEDORING MAASVLAKTE ROTTERDAM

Opdr. 1009-0135-000
Sond. DKM25

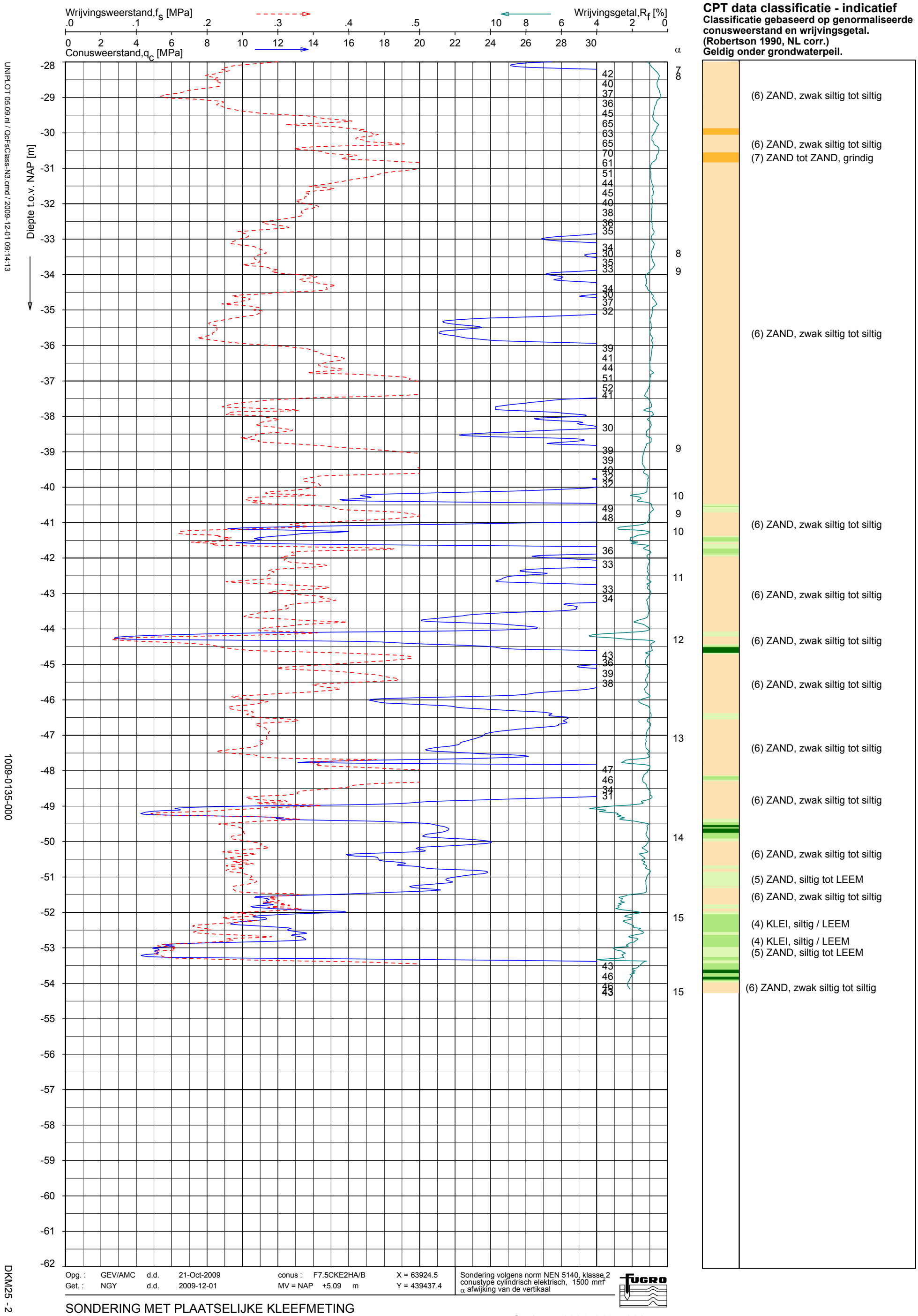

CPT data classificatie - indicatief

Classificatie gebaseerd op genormaliseerde conusweerstand en wrijvingsgetal. (Robertson 1990, NL corr.)
Geldig onder grondwaterpeil.

SONDERING MET PLAATSELIJKE KLEEFMETING

GRONDONDERZOEK VAN UDEN STEVEDORING MAASVLAKTE ROTTERDAM

Opdr. 1009-0135-000
Sond. DKM25

UNIPLOT 05.09.nl / QcFsClass-N3.cmd / 2009-12-01 09:14:13

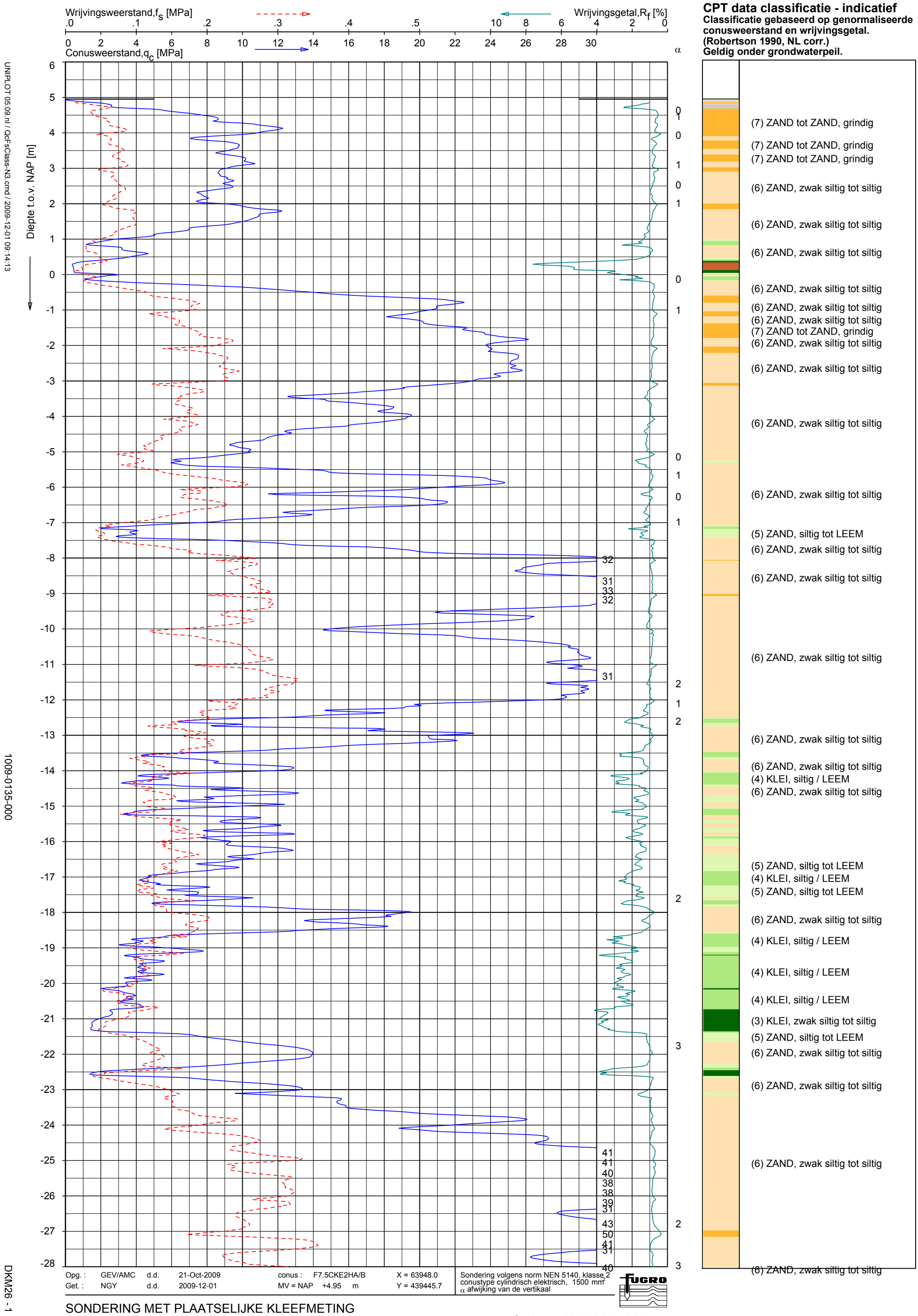

CPT data classificatie - indicatief
Classificatie gebaseerd op genormaliseerde conusweerstand en wrijvingsgetal. (Robertson 1990, NL corr.)
Geldig onder grondwaterpeil.

SONDERING MET PLAATSELIJKE KLEEFMETING

GRONDONDERZOEK VAN UDEN STEVEDORING MAASVLAKTE ROTTERDAM

Opdr. 1009-0135-000
Sond. DKM26

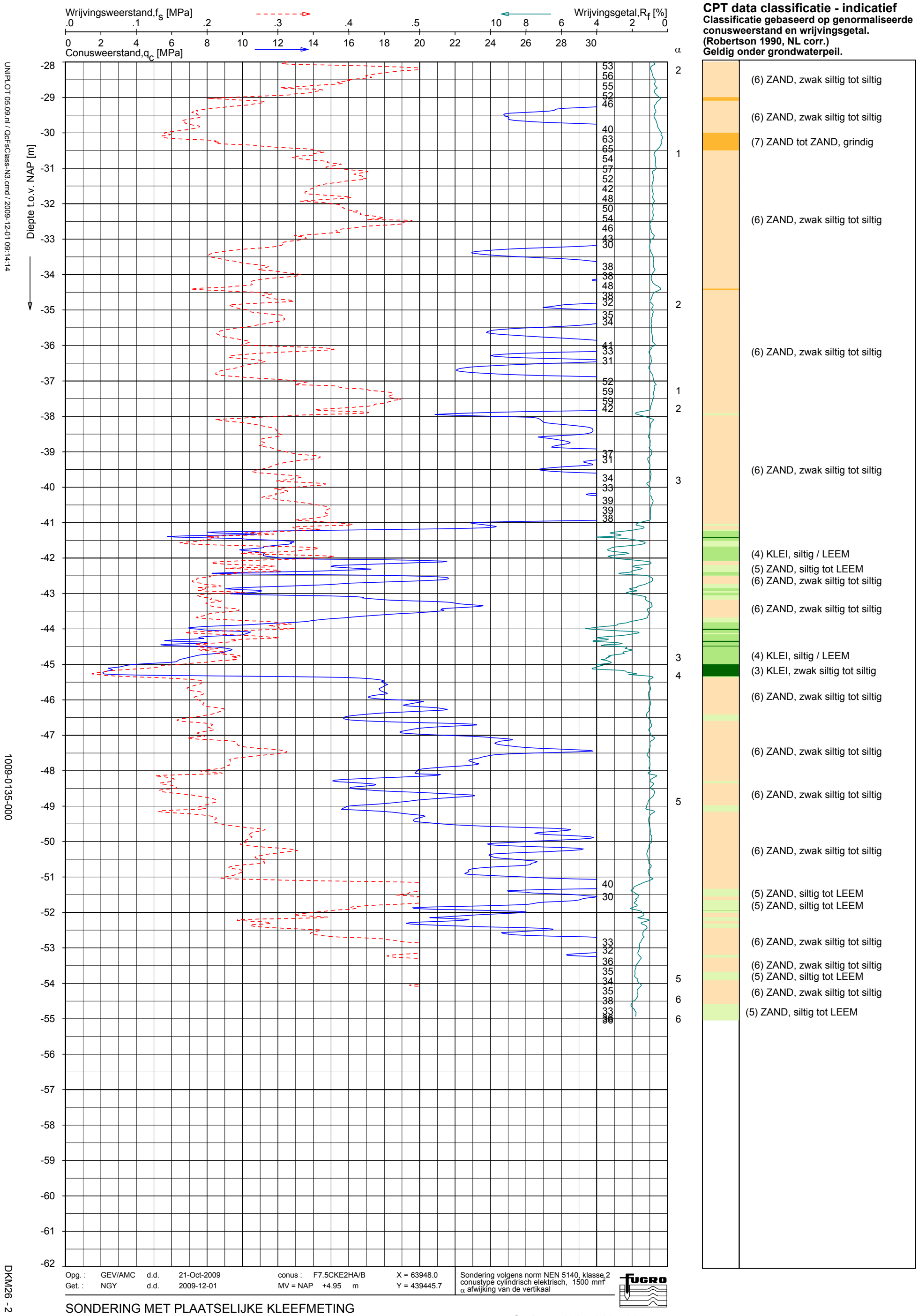

CPT data classificatie - indicatief

Classificatie gebaseerd op genormaliseerde conusweerstand en wrijvingsgetal. (Robertson 1990, NL corr.)
Geldig onder grondwaterpeil.

- (6) ZAND, zwak siltig tot siltig
- (6) ZAND, zwak siltig tot siltig
- (7) ZAND tot ZAND, grindig
- (6) ZAND, zwak siltig tot siltig
- (6) ZAND, zwak siltig tot siltig
- (6) ZAND, zwak siltig tot siltig
- (4) KLEI, siltig / LEEM
- (5) ZAND, siltig tot LEEM
- (6) ZAND, zwak siltig tot siltig
- (6) ZAND, zwak siltig tot siltig
- (4) KLEI, siltig / LEEM
- (3) KLEI, zwak siltig tot siltig
- (6) ZAND, zwak siltig tot siltig
- (6) ZAND, zwak siltig tot siltig
- (6) ZAND, zwak siltig tot siltig
- (6) ZAND, zwak siltig tot siltig
- (5) ZAND, siltig tot LEEM
- (5) ZAND, siltig tot LEEM
- (6) ZAND, zwak siltig tot siltig
- (6) ZAND, zwak siltig tot siltig
- (5) ZAND, siltig tot LEEM
- (6) ZAND, zwak siltig tot siltig
- (5) ZAND, siltig tot LEEM

Opg. :	GEV/AMC	d.d.	21-Oct-2009	conus :	F7.5CKE2HA/B	X = 63948.0	
Get. :	NGY	d.d.	2009-12-01	MV = NAP	+4.95 m	Y = 439445.7	

Sondering volgens norm NEN 5140, klasse 2
conustype cylindrisch elektrisch, 1500 mm²
α afwijking van de vertikaal

SONDERING MET PLAATSELIJKE KLEEFMETING

GRONDONDERZOEK VAN UDEN STEVEDORING MAASVLAKTE ROTTERDAM

Opdr. 1009-0135-000
Sond. DKM26

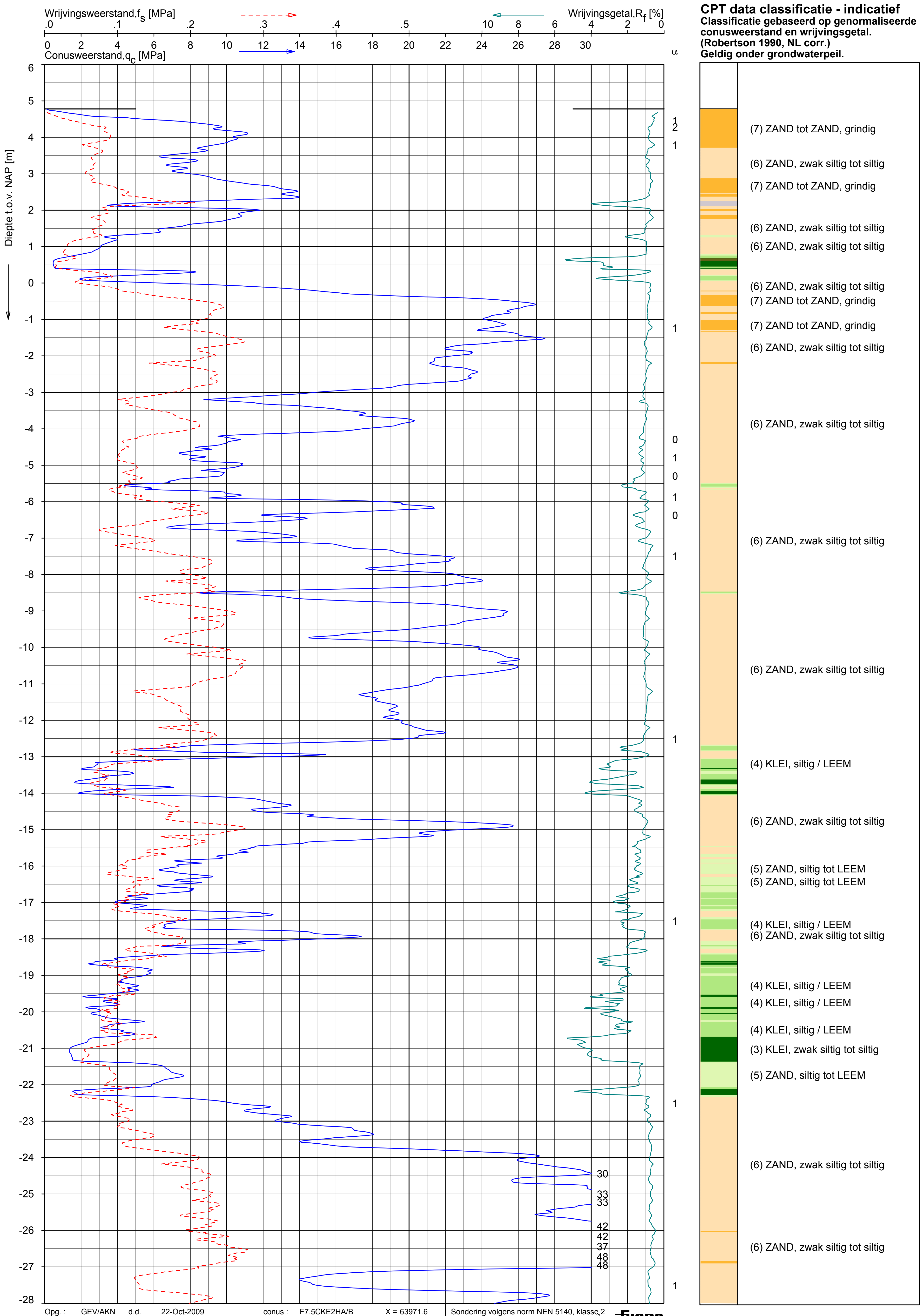

UNIPLOT 05.09.nl / QcFsClass-N3.cmd / 2009-12-01 09:14:14

1009-0135-000

Opg. :	GEV/AKN	d.d.	22-Oct-2009	conus :	F7.5CKE2HA/B	X = 63971.6	Sondering volgens norm NEN 5140, klasse 2	
Get. :	NGY	d.d.	2009-12-01	MV = NAP	+4.78 m	Y = 439447.1	conustype cylindrisch elektrisch, 1500 mm²	
							α afwijking van de vertikaal	

SONDERING MET PLAATSELIJKE KLEEFMETING

GRONDONDERZOEK VAN UDEN STEVEDORING MAASVLAKTE ROTTERDAM

Opdr. 1009-0135-000
Sond. DKM27

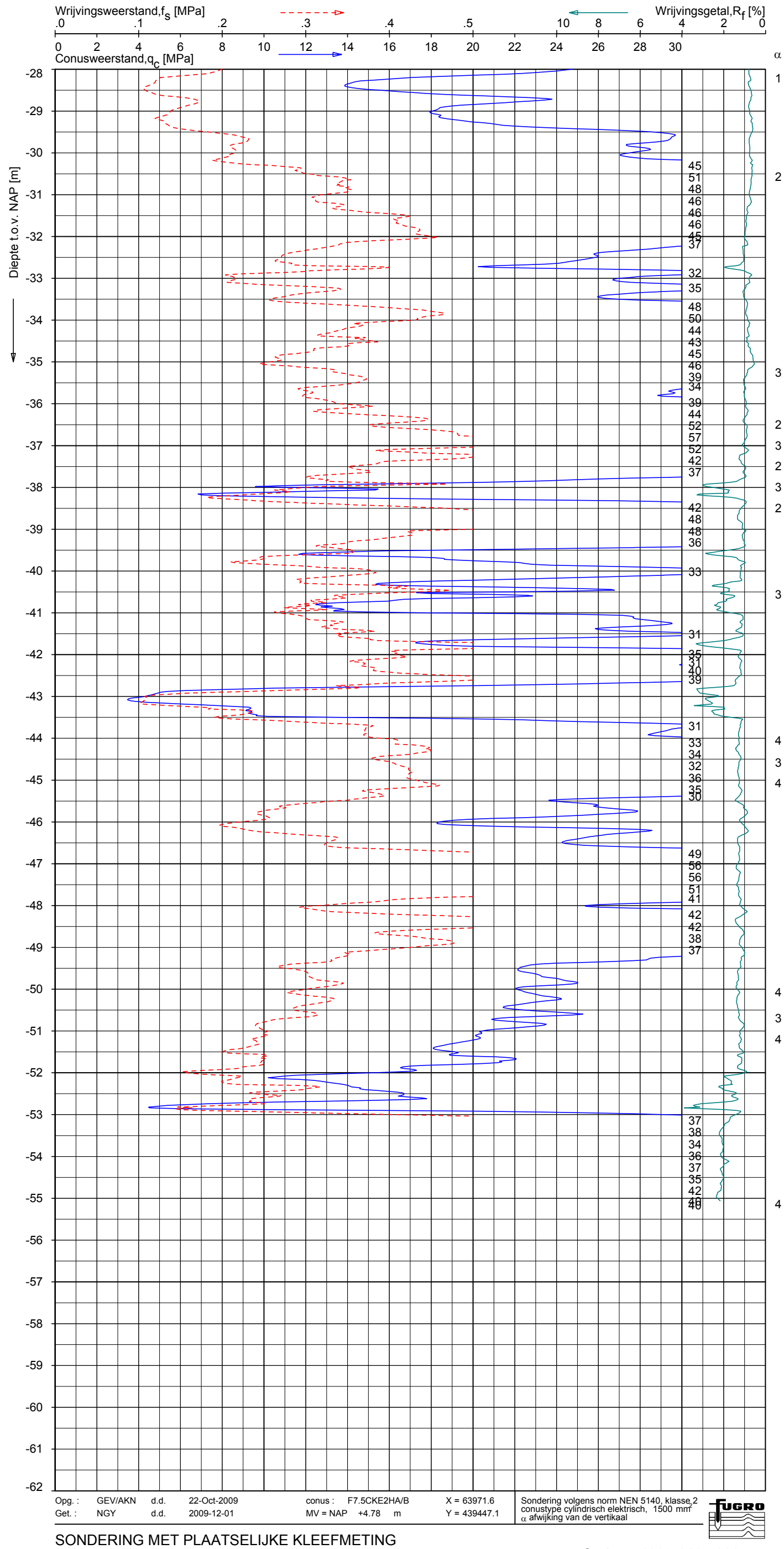

CPT data classificatie - indicatief

Classificatie gebaseerd op genormaliseerde conusweerstand en wrijvingsgetal. (Robertson 1990, NL corr.)
Geldig onder grondwaterpeil.

(6) ZAND, zwak siltig tot siltig
(6) ZAND, zwak siltig tot siltig
(6) ZAND, zwak siltig tot siltig
(6) ZAND, zwak siltig tot siltig
(4) KLEI, siltig / LEEM
(6) ZAND, zwak siltig tot siltig
(6) ZAND, zwak siltig tot siltig
(4) KLEI, siltig / LEEM
(6) ZAND, zwak siltig tot siltig
(6) ZAND, zwak siltig tot siltig
(6) ZAND, zwak siltig tot siltig
(6) ZAND, zwak siltig tot siltig
(5) ZAND, siltig tot LEEM
(5) ZAND, siltig tot LEEM
(6) ZAND, zwak siltig tot siltig
(5) ZAND, siltig tot LEEM
(5) ZAND, siltig tot LEEM

SONDERING MET PLAATSELIJKE KLEEFMETING

GRONDONDERZOEK VAN UDEN STEVEDORING MAASVLAKTE ROTTERDAM

Opdr. 1009-0135-000
Sond. DKM27

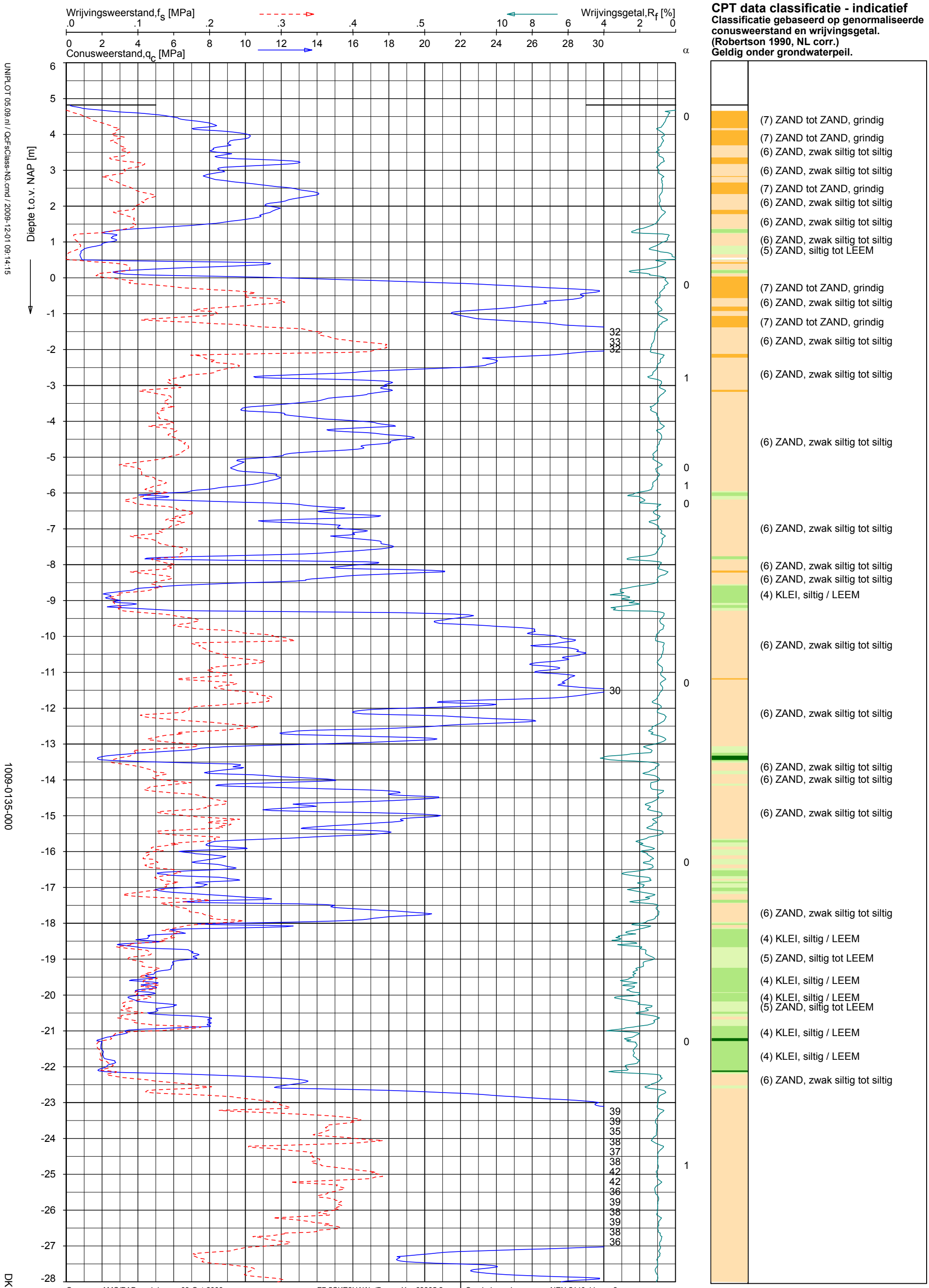

CPT data classificatie - indicatief

Classificatie gebaseerd op genormaliseerde conusweerstand en wrijvingsgetal. (Robertson 1990, NL corr.)
Geldig onder grondwaterpeil.

(7) ZAND tot ZAND, grindig
(7) ZAND tot ZAND, grindig
(6) ZAND, zwak siltig tot siltig
(6) ZAND, zwak siltig tot siltig
(7) ZAND tot ZAND, grindig
(6) ZAND, zwak siltig tot siltig
(6) ZAND, zwak siltig tot siltig
(6) ZAND, zwak siltig tot siltig
(5) ZAND, siltig tot LEEM
(7) ZAND tot ZAND, grindig
(6) ZAND, zwak siltig tot siltig
(7) ZAND tot ZAND, grindig
(6) ZAND, zwak siltig tot siltig
(6) ZAND, zwak siltig tot siltig
(6) ZAND, zwak siltig tot siltig
(6) ZAND, zwak siltig tot siltig
(4) KLEI, siltig / LEEM
(6) ZAND, zwak siltig tot siltig
(6) ZAND, zwak siltig tot siltig
(6) ZAND, zwak siltig tot siltig
(6) ZAND, zwak siltig tot siltig
(6) ZAND, zwak siltig tot siltig
(6) ZAND, zwak siltig tot siltig
(6) ZAND, zwak siltig tot siltig
(4) KLEI, siltig / LEEM
(5) ZAND, siltig tot LEEM
(4) KLEI, siltig / LEEM
(4) KLEI, siltig / LEEM
(5) ZAND, siltig tot LEEM
(4) KLEI, siltig / LEEM
(4) KLEI, siltig / LEEM
(6) ZAND, zwak siltig tot siltig

Opg. : AMC/PAD d.d. 09-Oct-2009
Get. : NGY d.d. 2009-12-01

conus : F7.5CKE2HAW 1/B
MV = NAP +4.82 m

X = 63995.2
Y = 439455.4

Sondering volgens norm NEN 5140, klasse 2
conustype cylindrisch elektrisch, 1500 mm²
α afwijking van de vertikaal

SONDERING MET PLAATSELIJKE KLEEFMETING

GRONDONDERZOEK VAN UDEN STEVEDORING MAASVLAKTE ROTTERDAM

Opdr. 1009-0135-000
Sond. DKMP28

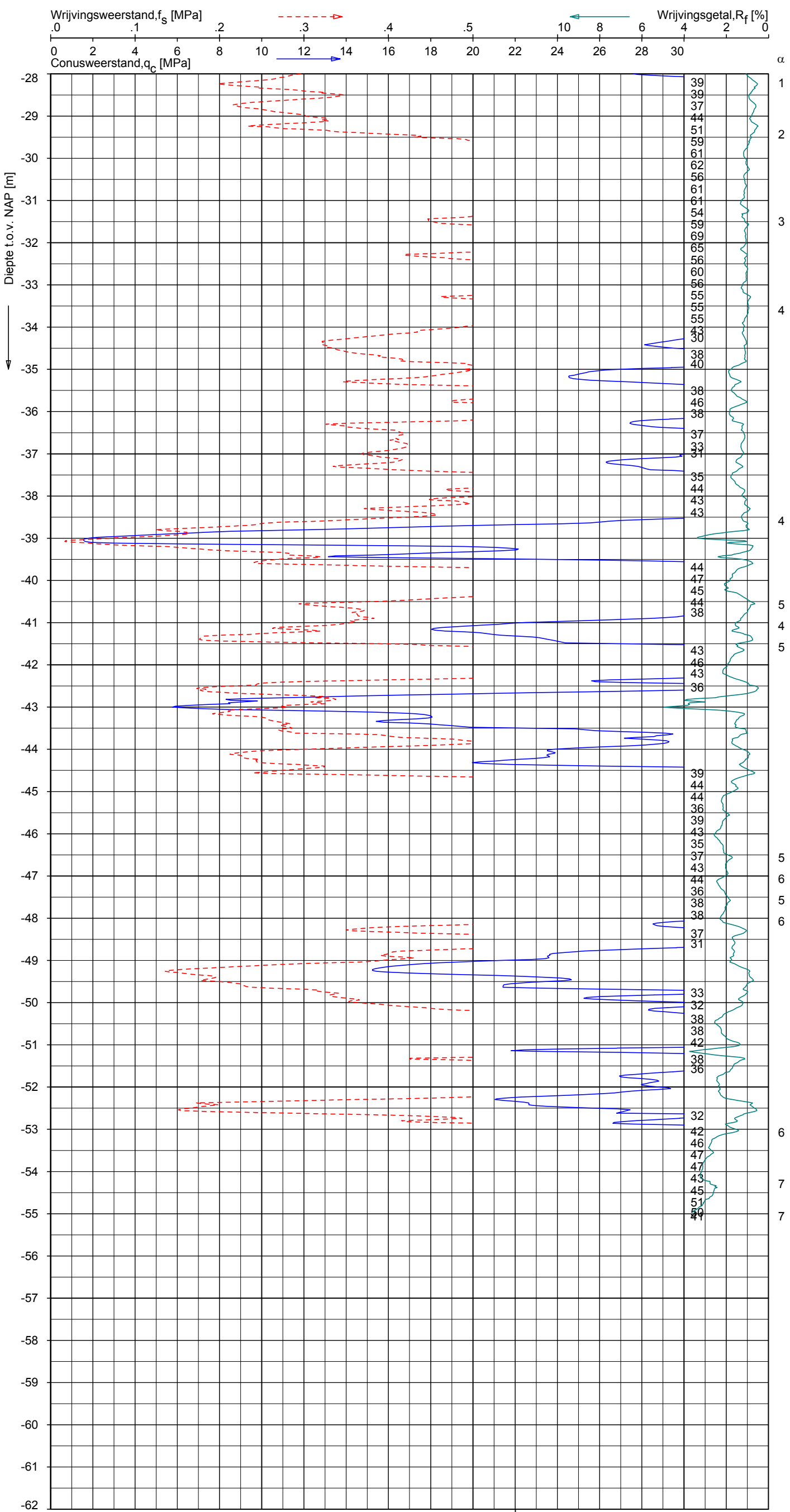

CPT data classificatie - indicatief

Classificatie gebaseerd op genormaliseerde conusweerstand en wrijvingsgetal. (Robertson 1990, NL corr.)
Geldig onder grondwaterpeil.

- (6) ZAND, zwak siltig tot siltig
- (6) ZAND, zwak siltig tot siltig
- (5) ZAND, siltig tot LEEM
- (6) ZAND, zwak siltig tot siltig
- (6) ZAND, zwak siltig tot siltig
- (4) KLEI, siltig / LEEM
- (5) ZAND, siltig tot LEEM
- (6) ZAND, zwak siltig tot siltig
- (5) ZAND, siltig tot LEEM
- (6) ZAND, zwak siltig tot siltig
- (4) KLEI, siltig / LEEM
- (5) ZAND, siltig tot LEEM
- (6) ZAND, zwak siltig tot siltig
- (6) ZAND, zwak siltig tot siltig
- (6) ZAND, zwak siltig tot siltig
- (5) ZAND, siltig tot LEEM
- (6) ZAND, zwak siltig tot siltig
- (4) KLEI, siltig / LEEM
- (5) ZAND, siltig tot LEEM
- (6) ZAND, zwak siltig tot siltig
- (6) ZAND, zwak siltig tot siltig
- (4) KLEI, siltig / LEEM
- (8) ZAND, vast / ZAND, kleiig
- (4) KLEI, siltig / LEEM
- (8) ZAND, vast / ZAND, kleiig

Opg. : AMC/PAD d.d. 09-Oct-2009
Get. : NGY d.d. 2009-12-01

conus : F7.5CKE2HAW$_1$/B X = 63995.2
MV = NAP +4.82 m Y = 439455.4

Sondering volgens norm NEN 5140, klasse 2
conustype cylindrisch elektrisch, 1500 mm²
α afwijking van de vertikaal

SONDERING MET PLAATSELIJKE KLEEFMETING

GRONDONDERZOEK VAN UDEN STEVEDORING MAASVLAKTE ROTTERDAM

Opdr. 1009-0135-000
Sond. DKMP28